

# FOG

## Freiberg Online Geoscience

FOG is an electronic journal registered under ISSN 1434-7512



2016, Volume 45



Anna Seither

### Isotopic and geomicrobial investigation of Darzila karst cave, NE Iraq

150 pages, 50 figures, 11 tables, 168 references

---

## Acknowledgements

Writing a thesis often seems a solitary undertaking. However, it is impossible to complete without help and support of many people.

First of all, I would like to thank my supervisor Prof. Dr. Broder Merkel, who offered this amazing topic. Thanks for organizing the journey and the finances, arranging all the chemicals and materials I asked for, revising my thesis within no time, and always being there for answering questions – even on vacation. Thank you for constructive critique and recommendations.

Also, I'm very grateful to my Kurdish advisors Dr. Polla Azad Khanaqa and Dr. Diyar Ali Al-Manmi. Thanks for organizing a place to stay in the beautiful old city centre of Sulaimaniyah, organizing the fieldtrips, supervising our work, and showing us your amazing country. Thank you for your support and your recommendations. Your expertise in local geology was very valuable for me.

My special thank is addressed to my fellow student Karin Heiland, who was a great companion during the whole trip. Thank you, Karin for your assistance, support, and for proofreading my thesis.

I want to thank Dr. Frank Haubrich for his advice with respect to sample preparation techniques and for his assistance during the interpretation of the isotope data. Thank you, Frank for sharing your knowledge with me. The discussions have proven invaluable for me.

I want to express my gratitude to Dr. Sascha Kummer, Karina Taupadel and Hans-Joachim Peter, who were amazingly patient with me. Thank you for your kind advice and assistance in countless occasions.

Apart from the department of hydrogeology, several other institutes and laboratories of this university were involved into my work. Therefore, I want to thank Daniela Bauer, Katharina Strecker and Caroline Seidel from the Institute of Analytical chemistry for evaluating the feasibility of procedures with me. I also want to thank Franziska Gottwald and Brunhilde Süßner from the Institute of Organic chemistry for their advice and support. Thanks for letting me use the facilities of the laboratory and for assisting me with the procedures. Also, I want to thank Beate Erler from the Microbiology department for her advice and spontaneity. Furthermore, I want to thank the team of the *Stable Isotope Geochemistry Laboratory* of the

---

TUBAF. I'm especially grateful for Mrs Meinhard`s advice with respect to the preparation of necessary solutions during the procedures.

Furthermore, I want to thank the team of the *Kurdistan Institution for Strategic Studies & Scientific Research* in Sulaimaniyah, for their support and advice, as well as for taking us to fascinating places in the city we would not have seen otherwise. I would like to thank Dr. Jan Küver, Steffen Böhm and the rest of the involved team from the MPA Bremen Institute for Materials Testing, for the laborious gene analyses of my biological samples and for their counsel. Moreover, I would like to thank Dr. Kay Knöller from the Helmholtz-Centre for Environmental Research in Halle, for measuring the isotopes of sulphur species in his laboratories and for his advice.

I sincerely like to thank the DAAD for their generous financial support during the trip. I'm also very grateful to the German National Academic Foundation, who greatly supported me financially as well as personally during the last two years of my studies.

I also want to express my gratitude to Prof. Arthur Palmer, Dr. Markus Ostermann, Prof. Adina Paytan, and Dr. Fadhil Lawa, who kindly responded to my email requests and supported me with publications, data and advice.

Furthermore, I would like to thank Mandy Hoyer, Judith Heinrich and Einar Gustaffson for taking the time to correct and comment my work.

Last but not least, I would like to thank my family and friends for all their love and faithful support. Thank you!

## Abstract

Darzila cave, located near Sulaimaniyah in Northern Iraq, offers remarkable opportunities to investigate an active karst system of sulphuric acid origin. Although previous hydrogeochemical studies could resolve many of the underlying mechanisms, uncertainties remained about the provenance of the waters emerging in the cave. Thus, the principal purpose of this study was to trace the origin of the fluids and the aqueous sulphur species.

For this purpose, isotopic analyses ( $\delta\text{D}$ ,  $\delta^{18}\text{O}$ ,  $\delta^{34}\text{S}$ ) were conducted on water, crude oil, primary gypsum, secondary cave minerals, cave sediments and host rock limestone. Furthermore, dominant microorganisms in cave sediments and biofilms were determined by 16S rRNA gene analyses.

The isotopic composition of dissolved sulphate and sulphide exhibited large differences. Subsequent evaluation of these values showed, that sulphur originates from at least two sources:  $\text{H}_2\text{S}$  affluxes from hydrocarbons ( $\delta^{34}\text{S} \approx -9 \text{‰ VCDT}$ ), gypsum from the Lower Fars Formation ( $\delta^{34}\text{S} \approx 22 \text{‰ VCDT}$ ), and possibly also from the Sagirma Formation.

Two isolated, acidic cave pools were clearly influenced by ascending  $\text{H}_2\text{S}$ . Evidence was given by strongly  $^{34}\text{S}$  and  $^{18}\text{O}$  depleted sulphate, small differences between the sulphur isotopic signature of sulphate and sulphide, as well as elevated  $\delta\text{D}$  values in ambient water. In contrast, sulphur species in water rising at the main groundwater inlet, showed distinct signs of bacterial sulphate reduction. Main indications were a  $\delta^{34}\text{S}_{\text{SO}_4}$  value above 22 ‰ VCDT and strongly  $^{34}\text{S}$  depleted sulphide. However, it appears that sulphate reduction was superimposed by several secondary transformation processes. The main springs of Awa Spi River and the reservoir of the well nearby show similar characteristics. This suggests that all these waters are influenced by one large subterranean reservoir.

Filamentous, rock-attached biofilms at the main groundwater inlet were dominated by sulphur-oxidizing bacteria of the genus *Acidithiobacillus* and of the family *Halothiobacillaceae*. Biofilms at the acidic cave sites were inhabited by a variety of *Acidithiobacilli*, including *Acidithiobacillus ferrooxidans*. Considering their close proximity to carbonate surfaces, it can be suggested that they play a decisive role in the development and enlargement of Darzila cave.

## Zusammenfassung

Die Karsthöhle Darzila befindet sich im Norden des Iraks, nahe der Stadt Sulaimaniyah. Da sie nicht durch Kohlensäure, sondern hauptsächlich durch Schwefelsäure gebildet wird, stellt sie eine geologische Besonderheit dar. Hydrogeochemische Untersuchungen vorheriger Studien konnten bereits einige zugrunde liegende Prozesse aufdecken. Über den Ursprung der Wässer, die die Höhle formen, ist allerdings nur wenig bekannt. Das Hauptziel dieser Arbeit war daher, die Herkunft der Wässer und der darin enthaltenen Schwefelspezies zurück zu verfolgen.

Hierzu wurden verschiedene Arten von Proben, namentlich Wasser, Rohöl, primärer Gips, sekundäre Höhlenminerale, Höhlensedimente sowie das umgebende Carbonatgestein, auf ihre stabile Isotopenzusammensetzung ( $\delta D$ ,  $\delta^{18}O$ ,  $\delta^{34}S$ ) untersucht. Außerdem wurden die in Sedimenten und Biofilmen vorherrschenden Mikroorganismen mittels 16S rRNA Gen-Analyse bestimmt.

Die isotopische Zusammensetzung der gelösten Sulfate und Sulfide der verschiedenen Proben wies große Unterschiede auf. Es konnte gezeigt werden, dass Schwefel von mindestens zwei verschiedenen Quellen stammt: aufsteigendes  $H_2S$  aus Erdöl ( $\delta^{34}S \approx -9 \text{ ‰ VCDT}$ ), Gips der Lower Fars Formation ( $\delta^{34}S \approx 22 \text{ ‰ VCDT}$ ), und unter Umständen auch Gips der Sagirma Formation.

Zwei saure Wasserpools waren deutlich von aufsteigendem  $H_2S$  beeinflusst. Stark  $^{34}S$ - und  $^{18}O$ -abgereichertes Sulfat, geringe Unterschiede zwischen der Isotopensignatur des Schwefels im Sulfat und im Sulfid, sowie erhöhte  $\delta D$ -Werte im umgebenden Wasser konnten dies belegen. Die Schwefelspezies im Wasser des Hauptzuflusses gaben dagegen deutliche Hinweise auf bakterielle Sulfatreduktion. Die wichtigsten Anzeichen hierfür waren ein  $\delta^{34}S_{SO_4}$ -Wert größer als  $22 \text{ ‰ VCDT}$  und stark  $^{34}S$ -abgereichertes Sulfid. Die Sulfatreduktion scheint jedoch von mehreren sekundären Transformationsprozessen überlagert zu sein. Die Hauptzuflüsse des Flusses Awa Spi und das Reservoir des nahegelegenen Brunnens weisen ähnliche Eigenschaften auf. Das legt die Vermutung nahe, dass alle diese Wässer von einem großen unterirdischen Reservoir beeinflusst werden.

Die faserartigen Biofilme, welche in der Nähe des großen Grundwasserzutritts am Gestein hafteten, waren dominiert von Schwefel-oxidierenden Bakterien der Gattung *Acidithiobacillus* und der Familie *Halothiobacillaceae*. Die Biofilme an den sauren Stellen enthielten verschiedene *Acidithiobacilli*, unter anderem *Acidithiobacillus ferrooxidans*. In Anbetracht der Tatsache, dass diese Mikroorganismen in sehr engem Kontakt zu Carbonat-Oberflächen leben, wird ihnen eine entscheidende Rolle in der Entwicklung und Vergrößerung der Höhle zugesprochen.

---

## Table of Contents

<b>STATUTORY DECLARATION</b> .....	<b>I</b>
<b>ACKNOWLEDGEMENTS</b> .....	<b>II</b>
<b>ABSTRACT</b> .....	<b>IV</b>
<b>ZUSAMMENFASSUNG</b> .....	<b>V</b>
<b>TABLE OF CONTENTS</b> .....	<b>VI</b>
<b>LIST OF FIGURES</b> .....	<b>IX</b>
<b>LIST OF TABLES</b> .....	<b>XIV</b>
<b>SYMBOLS AND ABBREVIATIONS</b> .....	<b>XV</b>
<b>NOMENCLATURE</b> .....	<b>XVII</b>
<b>1 INTRODUCTION</b> .....	<b>1</b>
1.1 Motivation and Objectives .....	1
1.2 Collaboration with Karin Heiland.....	2
1.3 GRI Project.....	3
<b>2 STUDY AREA</b> .....	<b>4</b>
2.1 Location of the Study Area.....	4
2.2 Geological Description .....	5
2.3 Hydrogeological and Hydrological Setting.....	9
2.4 Climate Conditions .....	11

---

<b>2.5</b>	<b>Description of Cave Pattern .....</b>	<b>13</b>
2.5.1	Setting and Dimensions of Darzila Cave .....	13
2.5.2	Hydrogeochemistry and Location of Sampling Sites .....	16
<b>3</b>	<b>FUNDAMENTALS .....</b>	<b>18</b>
<b>3.1</b>	<b>Biogeochemistry of Sulphur .....</b>	<b>18</b>
3.1.1	Fundamental Aspects of Sulphur Isotope Geochemistry .....	18
3.1.2	Sulphur Species and the Microbial Sulphur Cycle .....	19
3.1.2.1	Assimilatory sulphate reduction .....	21
3.1.2.2	Dissimilatory sulphate reduction .....	21
3.1.2.3	Sulphide oxidation .....	22
<b>3.2</b>	<b>Sulphuric Acid Speleogenesis .....</b>	<b>24</b>
<b>4</b>	<b>METHODS .....</b>	<b>28</b>
<b>4.1</b>	<b>Sampling and Storage .....</b>	<b>28</b>
4.1.1	Water and Gas Samples, In-Situ Parameters and Photometry .....	28
4.1.2	Water Sampling for Isotopic Analysis .....	28
4.1.3	Rock and Mineral Sampling .....	29
4.1.4	Oil Sampling .....	30
4.1.5	Sediment Sampling .....	30
4.1.6	Microbiological Sampling .....	30
<b>4.2</b>	<b>Geochemical and Mineralogical Analyses .....</b>	<b>32</b>
4.2.1	X-ray Fluorescence Spectroscopy (XRF) .....	32
4.2.2	Imaging .....	32
4.2.3	X-ray Diffraction (XRD) .....	32
4.2.4	CHNS Composition of Crude Oil .....	32
<b>4.3</b>	<b>Isotopic Analyses .....</b>	<b>33</b>
4.3.1	Hydrogen and Oxygen Isotopes of Water .....	33
4.3.2	Sulphur and Sulphate Oxygen Isotopes .....	34
4.3.2.1	Sample Preparation .....	34
4.3.2.2	Analysis .....	41
<b>4.4</b>	<b>Data Processing, Calculations and Statistics .....</b>	<b>43</b>
4.4.1	Processing of XRD Data .....	43
4.4.2	General Yield Calculations .....	43
4.4.3	Calculation of the Total Sulphur Isotopic Composition of Water .....	43

---

4.4.4	Calculation of Total Sulphur Concentration and $\delta^{34}\text{S}$ Composition of Sediments .....	44
4.4.5	Statistical Analyses .....	45
<b>4.5</b>	<b>16S rRNA Gene Analysis.....</b>	<b>46</b>
4.5.1	DNA Extraction .....	46
4.5.2	PCR-DGGE.....	47
4.5.3	Sequencing .....	48
4.5.4	Alignment of the Sequences .....	49
<b>5</b>	<b>RESULTS AND INTERPRETATION.....</b>	<b>50</b>
<b>5.1</b>	<b>Evaluation of Methods and Errors .....</b>	<b>50</b>
5.1.1	Microbiological Analyses .....	50
5.1.2	X-ray Fluorescence Spectroscopy Data .....	51
5.1.3	Stable Isotopes of Water .....	51
5.1.4	Preparation of Gypsum for $\delta^{34}\text{S}$ and $\delta^{18}\text{O}$ Analysis .....	52
5.1.5	Preparation of Dissolved Sulphate $\delta^{34}\text{S}$ and $\delta^{18}\text{O}$ Analysis.....	52
5.1.6	Preparation of Mono- and Disulphides for $\delta^{34}\text{S}$ Analysis .....	52
5.1.6.1	Reference materials.....	52
5.1.6.2	Dissolved sulphide .....	53
5.1.7	Elemental, Mineralogical and $\delta^{34}\text{S}$ Analyses of Sediments .....	55
5.1.7.1	Total sulphur concentration and $\delta^{34}\text{S}$ composition .....	55
5.1.7.2	Evaluation of the sequential extraction.....	57
5.1.7.3	Evaluation of the Eschka extraction .....	58
5.1.8	Sulphur Isotope Measurements at TUBAF and UFZ .....	59
<b>5.2</b>	<b>Mineralogy of the Cave.....</b>	<b>61</b>
<b>5.3</b>	<b>The Microbial Community of the Cave and Awa Spi River.....</b>	<b>65</b>
5.3.1	Cave Sediments .....	65
5.3.2	Biofilms.....	68
5.3.2.1	Crystal chamber.....	68
5.3.2.2	Acidic cave sites .....	68
5.3.2.3	Main floor feeder.....	69
5.3.2.4	Awa Spi River .....	70
5.3.3	Comparison to Earlier Microbial Investigations of Darzila Cave .....	71
<b>5.4</b>	<b>Stable Isotopes .....</b>	<b>72</b>
5.4.1	Hydrogen and Oxygen Isotopes .....	72
5.4.2	Sulphur Isotopic Composition .....	75

---

5.4.2.1	Sulphur and sulphate oxygen isotopes in water.....	75
5.4.2.2	Gypsum and limestone.....	79
5.4.2.3	Elemental sulphur.....	81
5.4.2.4	Sedimentary sulphur species.....	82
5.4.2.5	Crude oil.....	83
<b>5.5</b>	<b>Constraints on Cave-Forming Processes.....</b>	<b>84</b>
5.5.1	Estimation of the Cave Age.....	84
5.5.2	The Origin of the Fluids.....	86
5.5.2.1	Lower Fars gypsum as endmember.....	88
5.5.2.2	Reduced sulphur in crude oil as endmember.....	92
5.5.2.3	Individual sampling sites and mixing processes.....	94
5.5.3	The Origin of Sulphate Oxygen.....	105
5.5.4	Formation of Secondary Cave Minerals.....	108
<b>6</b>	<b>SUMMARY OF THE MAIN RESULTS.....</b>	<b>112</b>
<b>7</b>	<b>RECOMMENDATIONS.....</b>	<b>115</b>
<b>8</b>	<b>REFERENCES.....</b>	<b>117</b>
<b>9</b>	<b>APPENDIX.....</b>	<b>127</b>
9.1	Appendix A - Tables.....	129
9.2	Appendix B - Figures.....	148
9.3	Appendix C – Spreadsheet.....	150

## List of figures

Figure 1: Location of Sangaw region (modified after Khanaqa and Al-Manmi 2011).....	4
Figure 2: Geological map and location of the study area (modified after Maala 2001).....	5
Figure 3: Cross sectional view of lithographic units from southwest to northeast. The sketch is not to scale. Groundwater flow direction is indicated by blue arrows. Patterns and symbols were used according to the recommendations of the Federal Geographic Data Committee (2006).....	6
Figure 4: Awa Spi River and Darzila village .....	10
Figure 5: Average temperature graph for Sangaw District (World Weather Online 2011).....	12
Figure 6: Great sinkhole providing access to Darzila cave .....	13
Figure 7: Cross sectional view of Darzila cave. Sketch modified after Heiland (2016).....	14
Figure 8: Map view of Darzila cave, including sampling locations (blue numbers). Karst symbols according to UIS guidelines (Häuselmann and Neumann 1999).....	15
Figure 9: Location of sampling points in the surrounding of Darzila cave depicted in an aerial photo of Google earth. DW-W-1, DR-W-1, DR-W-2, and DR-W-8 are water samples, DR-O-4 is a sample of crude oil, and DR-B-6 is a biofilm sample.....	17
Figure 10: The microbial sulphur cycle (adapted from Canfield 2001a; Tang <i>et al.</i> 2009).....	20
Figure 11: A typical setting for sulphuric acid caves (after Palmer and Palmer 2004).....	25
Figure 12: Early assumptions about the formation of elemental sulphur. Roughly: “It [elemental sulphur] is most common in the gypsum ranges. Therefore, the largest part of elemental sulphur in nature must arise from a mysterious reduction process that occurs when lime and sulphuric acid combine”. Source: Steffens, H. (1819) <i>Vollständiges Handbuch der Oryktognosie</i> , Halle p. 133. ....	27
Figure 13: Distillation unit for the extraction of mono- and disulfides.....	35
Figure 14: Sequential extraction of sulphur species from cave sediments.....	38
Figure 15: Chromium chloride solutions before (left) and after (right) reduction. ....	39
Figure 16: Flow diagram showing the different steps in the analysis of the microbial community structure by PCR-DGGE. At first, DNA was extracted from environmental samples. This DNA was then used to amplify 16S rRNA encoding genes by polymerase chain reaction (PCR). These amplified fragments were separated by denaturing gradient gel electrophoresis (DGGE). Individual,	

- separated bands were excised from the gel and sequenced to identify community members. Diagram based on Muyzer 1999. ....46
- Figure 17: Dissolved sulphide concentration – determined by photometry (blue) and by mass balance calculations from  $\text{Ag}_2\text{S}$  precipitates (beige). Due to significantly higher concentrations that would change the scale, data from the well (DW-W-1) are not included. ....54
- Figure 18: Comparison of  $\delta^{34}\text{S}$  values for total sedimentary sulphur, obtained by two different methods. With the Eschka-method, all sulphur was extracted at once – regardless of the species. The prepared  $\text{BaSO}_4$  was analyzed for its sulphur isotopic composition. In contrast, sequential extraction targeted individual species, namely sulphate, elemental sulphur, and pyrite. Each species was analysed separately. Based on individual extraction yields and  $\delta^{34}\text{S}$  values, the theoretical  $\delta^{34}\text{S}$  value of total sulphur was calculated. ....56
- Figure 19: Total sulphur content in sediments determined with different methods: Concentrations were analysed by X-ray fluorescence spectroscopy (XRF), calculated from mineral contents determined by X-ray diffraction (XRD), and weight out from precipitates of wet chemical extraction procedures.....56
- Figure 20: Comparison of 24  $\delta^{34}\text{S}$  measurements at the TUBAF with measurements at the UFZ. The dashed line shows a regression line ( $R^2 = 0.999$ ), and the continuous line depicts the bisecting line.....60
- Figure 21: Bland – Altman – plot of  $\delta^{34}\text{S}$  data from the TUBAF and the UFZ. Depicted is the isotopic difference of the measurements against the average value of the two laboratories. The red lines show the mean difference and the “limits of agreement” (mean  $\pm 2 \cdot s$ )......60
- Figure 22: Variations of gypsum in the cave. (Upper left) DC-SG-15 was collected from the entrance of the cave. The mineral has distinct and stable crystals. (Upper right) DC-SG-14a was collected from the outermost gypsum layer at the narrow passage to the crystal chamber. The mineral has a rough and firm surface, composed of gypsum needles. (Lower left) DC-SG-9c was collected from the crystal chamber. Like the samples depicted in the upper photos, it presents the outermost gypsum layer of the sampling site. In contrast to the others, it is a relatively loose, brittle accumulation of small, young gypsum needles. (Lower right) Sample DC-SG-9b, a soft, homogeneous, and chalky gypsum from the layer underneath DC-SG-9c. ....61
- Figure 23: Large gypsum crystals with sulphur blooms on their surface. (Bottom) Gypsum crystal DC-SG-13c. (Upper Left) Gypsum crystal DC-SG-13d with the corresponding sulphur bloom DC-ES-13d (Right).....62
- Figure 24: Coating of elemental sulphur on the cave wall. The crusts are approximately 3 mm thick and have convex, broccoli-like surfaces. ....62

Figure 25: (Left) Calcite crystals in between gypsum crystals on sample DC-SG-14a. (Right) Dissolving limestone on the cave floor (DC-PL-16).....	63
Figure 26: Mineral composition of cave sediments. In order to highlight sulphur containing minerals, other minerals are summarized into groups. The only exception to this rule is the titanium dioxide anatase, which failed to be part of a group. DC-S-1 and DC-S-9 belong to the sediments from the same waterbody. DC-S-2 is a sediment sample from the upper course of the main cave river. DC-S-3 is sediment from an isolated, acidic pool. DC-S-5 was sampled from the rear part of the cave. ....	64
Figure 27: Phylogenetic tree based on 16S rRNA gene sequences - calculated using the Parsimony method. Up to date data bases and the program ARB were used to fit the DGGE sequences into the tree and to optimize their positions (Ludwig <i>et al.</i> 2004). The families Enterobacteriaceae, Thiotrichaceae, Pseudomonadaceae, Halothiobacillaceae and Acidothiobacillaceae belong to the class of gamma-Proteobacteria. The Bradyrhizobiaceae belong to the alpha-Proteobacteria, whereas the Leptospiraceae are part of the Phylum Spirochaetes and the order Oscillatoriales to the Cyanobacteria. The depicted bar shows a 10% sequence divergence. Methanopyrus kandleri served as outgroup. ....	67
Figure 28: Suspected biofilm DC-B-9 in the crystal room.....	68
Figure 29: Left: Biofilm DC-B-4 on a pair of tweezers. Right: DC-B-12, a biofilm covering a tiny puddle.....	69
Figure 30: Filamentous biofilm next to the main floor feeder (sample DC-B-7).....	69
Figure 31: Filamentous biofilm in Awa Spi River (sample DR-B-6) .....	70
Figure 32: Isotopic composition of water samples from cave water (black symbols), from inlets of Awa Spi river (red symbols) and from a well nearby (green symbol). Samples were taken in September and October 2011 at the end of the dry season. The global meteoric water line (GMWL) as well as two local meteoric water lines (LMWL) and the Eastern Mediterranean meteoric water line (EMWL) are given for reference. The error bars show the standard deviation of the data points.....	73
Figure 33: The sulphur isotopic composition of dissolved sulphide and sulphate in cave waters (black symbols), springs (red symbols), and well water (green symbol). Bars in the right corner depict the analytical error ( $\pm 0.4 \text{ ‰}$ ) of the respective sulphur species. ....	76
Figure 34: The sulphur isotopic difference $\Delta$ between dissolved sulphate and sulphide.....	77
Figure 35: Total sulphur concentration in water samples combined with the relative proportions of sulphur in dissolved sulphide and sulphate. Note that the %-scale is only depicted until 16%. Of course, in reality it goes up to 100% but due to the overwhelming dominance of dissolved sulphate, the relative proportions of sulphide sulphur would be difficult to see. ....	78

- Figure 36: The sulphur and oxygen isotopic composition of dissolved sulphate in cave waters (black symbols), springs (red symbols), and well water (green symbol). .....79
- Figure 37:  $\delta^{18}\text{O}$  and  $\delta^{34}\text{S}$  measurements of gypsum and limestone samples. The depicted analytical error applies to all data points of the respective isotope species ( $\pm 0.4\text{‰}$  VCDT for sulphur,  $\pm 0.6\text{‰}$  VSMOW for oxygen). .....80
- Figure 38: Sulphur isotopic composition of elemental sulphur (yellow bars) in comparison to secondary gypsum (grey bars). .....81
- Figure 39: Bars: Sulphur isotopic composition of different sulphur extracts from sediments. Sedimentary sulphate was extracted as  $\text{BaSO}_4$ ,  $\text{S}^0$  was recovered as  $\text{S}^0$ , pyrite was recovered as  $\text{Ag}_2\text{S}$ . Analytical precision was typically  $\pm 0.4\text{‰}$  VCDT, but there were two exceptions:  $\pm 2.1\text{‰}$  (DC-S-5,  $\text{BaSO}_4$ ) and  $\pm 2.2\text{‰}$  (DC-S-9,  $\text{Ag}_2\text{S}$ ).  $\delta^{34}\text{S}_{\text{total,Eschka}}$  is based on a single measurement. Data points: Total sulphur concentration based on yield calculations – either from sequential (green) or Eschka (blue) extraction. ....82
- Figure 40: Oil infrastructure of Northern Iraq and sulphur isotopic data for selected oil fields (map modified after CIA 2003;  $\delta^{34}\text{S}$  values from Thode and Monster, 1970). .....83
- Figure 41: Dissolution of calcite caused by oxidation of  $\text{H}_2\text{S}$  to sulphuric acid in a system at  $25^\circ\text{C}$  and an initial  $\text{CO}_2$  concentration of 0.001 M. Lower line = calcite saturation in the initial system prior oxidation. Upper line = calcite saturation after complete oxidation of dissolved  $\text{H}_2\text{S}$ . Dashed lines in between reflect that dissolution diminishes on  $\text{CO}_2$  outgassing. After Palmer (1991). .....85
- Figure 42: First ideas about the origin of dissolved sulphur species in individual water samples. More specifically, the graph shows the isotopic composition of sulphate oxygen and sulphide against that of sulphate sulphur. The symbols that were used in the previous chapter (black = cave water, red = inlets of Awa Spi, green = well) are used to depict the isotopic composition of sulphate ( $\delta^{34}\text{S}_{\text{SO}_4}$  and  $\delta^{18}\text{O}_{\text{SO}_4}$ ). As indicated by the dashed lines, the orange diamonds show the respective sulphur isotopic composition of sulphide ( $\delta^{34}\text{S}_{\text{HS}}$ ). The sulphate isotopic composition of Lower Fars gypsum (mean  $\delta^{34}\text{S}$  and  $\delta^{18}\text{O}$ ) is shown for comparison. ....87
- Figure 43: Stable sulphur and oxygen isotope ratios of remaining, unconsumed  $\text{SO}_4^{2-}$  and of produced hydrogen sulphide. Samples DC-W-6 and DC-W-4 were excluded.  $R^2$  of the logarithmic fit: 0.52. ....88
- Figure 44: Stable sulphur and oxygen isotope ratios of remaining, unconsumed  $\text{SO}_4^{2-}$  and of produced hydrogen sulphide. Only samples DC-W-7, DR-W-1, DR-W-2, DR-W-8, and DW-W-1 were included. ....89
- Figure 45: Sulphur isotopic evolution of sulphur species derived from Lower Fars gypsum as endmember. Enrichment factors: <sup>1</sup> Böttcher and Usdowski 1993; <sup>2</sup> Habicht and Canfield 1997b; <sup>3</sup> Ohmoto and Rye

- 1979; <sup>4</sup>Böttcher *et al.* 1998; <sup>5</sup>Wilkin and Barnes 1996; <sup>6</sup>Knöller and Schubert 2007; <sup>7</sup>Balci *et al.* 2007. ....91
- Figure 46: Sulphur isotopic evolution of sulphur species derived from sulphur in crude oil as endmember. Enrichment factors: <sup>1</sup> Thode and Monster 1970, Thode and Rees 1970, Vredenburg and Cheney 1971, Orr 1974; <sup>2</sup>Knöller and Schubert 2007; <sup>3</sup>Böttcher *et al.* 1998; <sup>4</sup>Wilkin and Barnes 1996; <sup>5</sup>Balci *et al.* 2007.....93
- Figure 47:  $\delta^{34}\text{S}$  values of dissolved sulphate versus the reciprocal sulphate concentration. The straight line that can be drawn through the acidic pools and the neutral creek indicates mixture of respective waters.....96
- Figure 48:  $\delta^{34}\text{S}$  values of dissolved sulphate versus the reciprocal sulphate concentration. Dashed line: suggests that the cave stream presents a mixture of water from site 8 and site 1. Note that DC-W-8 has not been analyzed for its sulphur isotopic composition. Its  $\delta^{34}\text{S}$  value has been taken from the nearby floor feeder DC-W-7. See text for further explanations.....100
- Figure 49:  $\delta^{34}\text{S}$  values of dissolved sulphate versus the reciprocal sulphate concentration. The sloped line through the data points of the initial solution ( $\delta^{34}\text{S} = 22.2\text{‰}$ ,  $[\text{SO}_4^{2-}] \approx 2000\text{ mg/L}$ ), the main floor feeder DC-W-7, the well DW-W-1, the spring DR-W-1, and the spring DR-W-2 indicates mixture. The horizontal line highlights the phenomenon, that the floor feeder, the well, and the spring ultimately have the same  $\delta^{34}\text{S}$  values but differ in sulphate concentration.....103
- Figure 50: Oxygen isotopic composition of dissolved sulphate and ambient water. Cave waters are depicted with black symbols, springs with red symbols, and well water with a green symbol.....105

---

## List of tables

Table 1: Characteristics of the main geological formations occurring in the study area (modified after Iurkiewicz and Stevanovic 2010, Kharajiany 2008, and Nairn and Alsharhan 1997). .....	8
Table 2: Geomicrobially important forms of sulphur (after Ehrlich 2002). .....	20
Table 3: Purpose and preparation of solutions required during sampling. ....	29
Table 4: Preparation of peptone water. ....	31
Table 5: Microwave digestion conditions .....	37
Table 6: Methodological details of IRMS analysis of $\delta^{34}\text{S}$ and $\delta^{18}\text{O}$ ratios in different sulphur species and laboratories. ....	41
Table 7: DGGE primers. ....	47
Table 8: Stock solutions for preparing a denaturing gradient in the DGGE gel. ....	48
Table 9: Sequencing primers for the 16S gene fragment .....	48
Table 10: Analysis of sphalerite and pyrite as reference materials. ....	53
Table 11: $\delta^{34}\text{S}$ analysis of elemental sulphur. ....	81

## Symbols and Abbreviations

<b><u>Symbol</u></b>	<b><u>Denotation</u></b>	<b><u>Unit</u></b>
asl	Above sea level	-
AVS	Acid volatile sulphide	-
BSR	Bacterial Sulphate Reduction	-
c	Concentration	mg/L
CDT	Cañon Diablo Troilite	-
CRS	Chromium reducible sulphide	-
D	Deuterium ( $^2\text{H}$ )	-
DGGE	Denaturing gradient gel electrophoresis	-
DOC	Dissolved organic carbon	mg/L
EC	Electrical conductivity	$\mu\text{S/cm}$
EH	Redox potential at 25°C referred to standard hydrogen electrode	V
GMWL	Global Meteoric Water Line	-
GPS	Geographical Positioning System	-
GRI	Geoscience Resources Iraq	-
IC	Ion chromatography	-
ICP-MS	Inductive coupled plasma mass spectrometry	-
IRMS	Isotope ratio mass spectrometry	-
LGR	Los Gatos Research	-
LMWL	Local Meteoric Water Line	-
M	Molar mass	g/mol
MPA	Bremen Institute for Material Testing	-
n	Sample size	-
nm	Not measured	-
p.a.	Per analysis	-
PCR	Polymerase chain reaction	-
rRNA	Ribosomal RNA	-
SAS	Sulphuric acid speleogenesis	-
SOP	Sulphur oxidizing prokaryotes	-

---

<b><u>Symbol</u></b>	<b><u>Denotation</u></b>	<b><u>Unit</u></b>
TDS	Total dissolved solids	mg/L
TSR	Thermochemical Sulphate Reduction	-
TUBAF	Technische Universität Bergakademie Freiberg	-
UFZ	Helmholtz-Centre for Environmental Research in Halle / Saale	-
VCDT	Vienna Cañon Diablo Troilite	-
VSMOW	Vienna Standard Mean Ocean Water	-
XRD	X-ray diffraction	-
XRF	X-ray fluorescence spectroscopy	-
$\delta^{18}\text{O}$	The ratio of $^{18}\text{O}/^{16}\text{O}$ relative to VSMOW	‰
$\delta^{34}\text{S}$	The ratio of $^{34}\text{S}/^{32}\text{S}$ relative to VCDT	‰
$\delta\text{D}$	The ratio of $^2\text{H}/^1\text{H}$ relative to VSMOW	‰
$\varepsilon$	Isotope enrichment factor	‰

---

## Nomenclature

	<u>Nomenclature</u>	<u>Denotation</u>
General	D	Darzila
Location	C	Cave
	R	River
	W	Well
	S	Surrounding
Type of sample	W	Water
	O	Oil
	PG	Primary gypsum
	SG	Secondary gypsum
	PL	Primary limestone
Location number	1, 2, 3, etc.	
Additional remarks	a, b, c, etc.	

*Example: DC-W-1 = Darzila Cave-Water sample-at location 1*

# 1 Introduction

## 1.1 Motivation and Objectives

Darzila cave offers remarkable opportunities to study an active cave system that is formed by sulphuric acid dissolution of carbonate rocks. Comparable caves in New Mexico, Italy, or Romania have been studied extensively already, but little is known about the karstic caves in the Kurdish region of Northern Iraq. Iurkiewicz and Stevanovic (2010), who surveyed active sulphide springs and karst phenomena in the investigation area, provided a first outline about the dominant karstic processes. However, they did not investigate the cave itself. Khanaqa and Al-Manmi (2011) were the first who specifically studied the cave and its surroundings. Still, little is known about the complexity and interaction of relevant karstification processes in that area.

The investigation of Darzila cave in September and October 2011 was carried out in collaboration with Karin Heiland. While Karin Heiland (2016) examined the hydrogeochemistry of Darzila cave and the nearby river Awa Spi, this thesis is concerned with stable isotopic (O, H, S) and microbiological analyses.

All previous workers speculated about the origin of sulphur in the cave waters. They suggested gypsum from Lower Fars Formation as main sulphur source and pointed towards a potential influence of nearby petroleum fields.

The main deliverable of this thesis was to resolve these speculations and to trace back the origin of cave waters by hydrogen, oxygen and sulphur isotopic analyses. Furthermore, the occurrence of individual sulphur species was evaluated in dependence on the local setting and on sulphur and sulphate oxygen isotopic data. Last but not least, DNA analysis of biofilms and cave sediments was conducted and possible microbial contributions to redox processes were evaluated.

---

## 1.2 Collaboration with Karin Heiland

This work is based on a close cooperation with Karin Heiland. Exploration of the cave, planning of the fieldwork, sampling, photometrical measurements etc. were conducted as a team. Accordingly, there are also some *shared chapters* that can be found in both theses.

Three chapters from this work have previously been printed in Heiland (2016):

- GRI Project
- Sulphur Species and the Microbial Sulphur Cycle
- Sulphuric Acid Speleogenesis

Similarly, four chapters from Karin Heiland were included into this thesis as well:

- Location of the Study Area
- Hydrogeological and Hydrological Setting
- Climate Conditions
- Settings and Dimensions of Darzila cave

Own text passages that were used by Karin Heiland are marked with “*Previously printed in Heiland (2016)*”. Text passages from Heiland (2016) used for this thesis are marked with “*Co-author: Karin Heiland*”. The chapters “Hydrogeological and Hydrological Setting” and “Settings and Dimensions of Darzila cave” are based on the corresponding text passage by Karin Heiland, but had to be modified, in order to include new information.

---

### 1.3 GRI Project

*Previously printed in Heiland (2016)*

Three decades of war have severely damaged Iraq's infrastructure and the loss of qualified personnel slows down the reconstruction of the country. In order to support the rebuilding of the Iraqi university system, the DAAD initiated cooperations between German and Iraqi universities. In 2009, altogether five academic programs at four German universities were selected for funding.

The *Geoscience Resources Iraq* (GRI) project of the TU Bergakademie Freiberg is one of these. The project outlines were compiled by Prof. Merkel, the head of the Geology department of the TU Bergakademie Freiberg. The goal of GRI is capacity building at several Iraqi universities in Baghdad, Basrah, Erbil, and Sulaimaniyah, and to establish a joint master course.

Last but not least GRI aims on initiating joint research programs, which facilitated the investigation of Darzila cave. The research was carried out as a cooperation between the TU Bergakademie Freiberg, the University of Sulaimaniyah and the *Kurdistan Institution for Strategic Studies and Scientific Research*.

## 2 Study Area

### 2.1 Location of the Study Area

*Co-author: Karin Heiland*

The study area is located in the southern part of the Sulaimaniyah Governorate in Kurdistan Region, NE Iraq. Administratively, this area belongs to the Sangaw District, but is commonly also called Garmian area (“Garmian” means very hot in Kurdish) (Figure 1). Sangaw region is located to the west of the Sagirma Mountains, representing the southeastern segment of the Iraqi Zagros Mountains (Jurkiewicz and Stevanovic 2010).

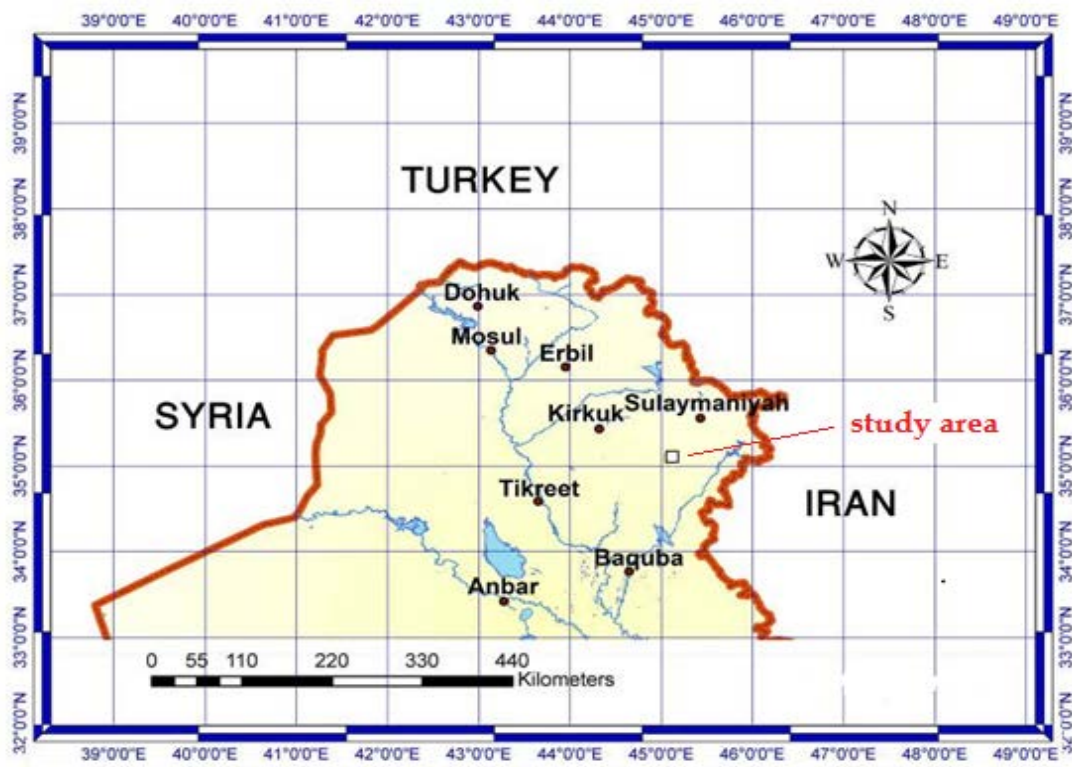


Figure 1: Location of Sangaw region (modified after Khanaqa and Al-Manmi 2011)

## 2.2 Geological Description

The study area is situated at the structurally highest part of the Foothill Zone (Low Folded), which is a subzone of the Unstable Shelf. This specific zone is called Butmah-Chamchamal Subzone, and is characterized by long, medium-sized anticlines as well as long, deep synclines (Jassim and Buday 2006). More precisely, Darzila cave is located at the southern limb of the Azhdagh Mountain. As depicted in the geological map (Figure 2), this mountain is an anticline structure.

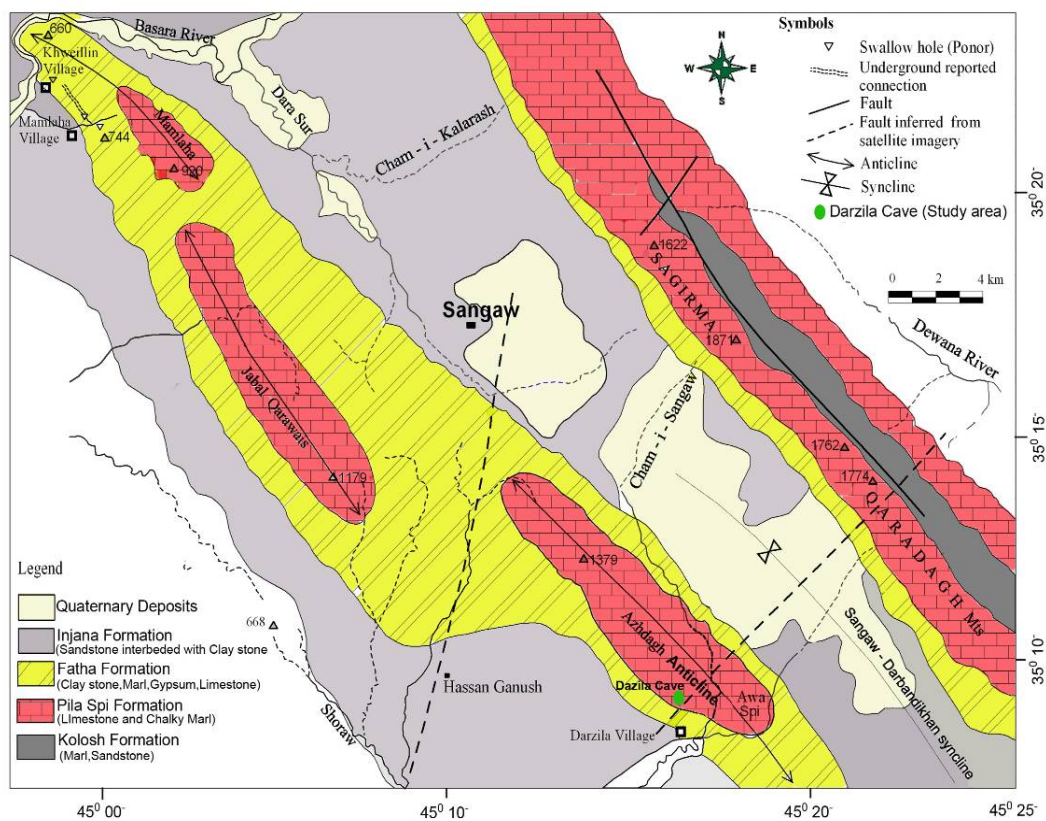


Figure 2: Geological map and location of the study area (modified after Maala 2001)

In order to get a better understanding of the processes investigated in this thesis, a cross sectional view of the local stratigraphy is additionally provided in Figure 3. The figure is not claimed to be accurate and complete in every detail. It can be assumed that the area was studied extensively by oil companies, but these data are confidential and not accessible for scientific purposes. Accordingly, the scheme had to be derived based on a conceptual model of Iurkiewicz and Stevanovic (2010), descriptions given by Khanaqa and Al-Manmi (2011), Khanaqa (Khanaqa 2011), Al-Manmi (2012), personal field observations, and on Lawa (2012).

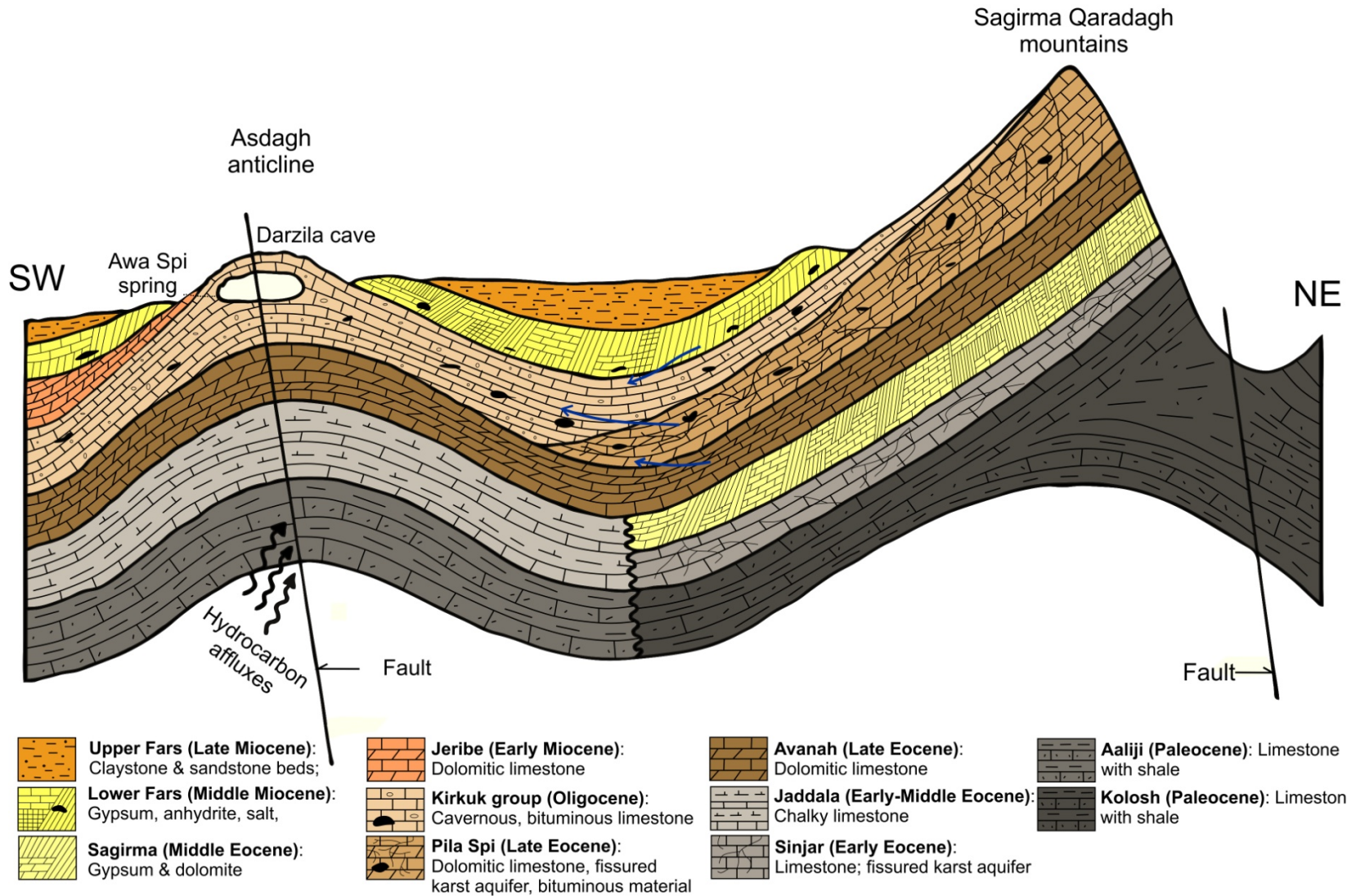


Figure 3: Cross sectional view of lithographic units from southwest to northeast. The sketch is not to scale. Groundwater flow direction is indicated by blue arrows. Patterns and symbols were used according to the recommendations of the Federal Geographic Data Committee (2006).

A good observant might notice that the two figures give conflictive information about the host rock of the cave. While the geological map suggests that the cave is embedded in Pila Spi Formation, the cross section depicts the cave in Oligocene Formation instead. This is due to the fact, that the local stratigraphy is not entirely resolved yet. While Khanaqa and Al-Manmi (2011) wrote in their publication, that the cave is situated in Pila Spi Formation, stratigraphers who conducted geological surveys of that area, argued that the cave is situated in rocks of the Kirkuk group (Oligocene) instead (e.g. Kharanjany 2008, Lawa 2012). However, Khanaqa (2011) clearly identified some of the cave walls to be Pila Spi limestone. He proposed, that Pila Spi Formation does not thin out somewhere between the Sagirma Quaradagh mountains and the Azdagh Anticline, but continues all the way to the fault going through the cave. As can be seen from this discussion, further studies are required to clarify the subject. But until then, the conceptual model depicted in Figure 3 is considered to give a clear, comprehensive outline of the study area.

As shown in the cross section, the order of stratigraphic layers in Sagirma anticline from the bottom to the top is: Kolosh (oldest), Sinjar, Sagirma, Pila Spi, Kirkuk Group, Lower Fars (Fatha) and Upper Fars (Injana) (youngest). In Azdagh anticline, the stratigraphic column was found to be Aliji (oldest), Jaddala, Avanah, Kirkuk Group, Jeribe, Lower Fars, and Upper Fars (youngest), respectively (Kharanjany 2008). Characteristics of these formations are given in Table 1. Something that is not depicted in the cross section but shown in the geological map is the NE-SW striking lineament crossing the SE plunge of the Azhdagh anticline. The associated weakened zone is considered to have a major impact on the surface and underground water flow (Iurkiewicz and Stevanovic 2010).

Table 1: Characteristics of the main geological formations occurring in the study area (modified after Iurkiewicz and Stevanovic 2010, Kharajiany 2008, and Nairn and Alsharhan 1997).

<b>Formation</b>	<b>Age</b>	<b>Lithology</b>	<b>Hydrogeological function</b>
Upper Fars (Injana)	Late Miocene	Massive beds of red claystone, silty & clayey sandstone	Very low productive aquifer (aquitard)
Lower Fars (Fatha)	Middle Miocene	Alternation of gypsum, anhydrite, salt, green marl, limestone, sandstone, red claystone; bituminous & sulphuric components to the lower part	Low to medium productive aquifer to the base
Jeribe	Early Miocene	Dolomitic limestone	
Oligocene	Late Oligocene	Limestone with bituminous material	Porous, fractured, and cavernous aquifer
Pila Spi	Middle-Late Eocene	Lower part: dolomitic limestone; Upper part: crystalline chalky limestone with thin beds of calcareous marl & chert nodules	Fissured-karst aquifer
Avanah	Late Eocene	Dolomitized and recrystallized limestone of shoal type	
Sagirma	Middle-Upper Eocene	Gypsum, dolomite (extends laterally over 50 km)	Probably aquifer
Jaddala	Early-Middle Eocene	Marly and microporous (chalky) limestone and marl	
Sinjar	Paleocene- Early Eocene	Limestone	Fissured-karst aquifer
Kolosh	Paleocene- Early Eocene	Typical flysch: shale limestone, sandstone, conglomerate	Aquitard
Aaliji	Upper Paleocene – lower Eocene	Marl, marly limestone and shale with fine-grained chert	

## 2.3 Hydrogeological and Hydrological Setting

*Co-author: Karin Heiland (first paragraph modified)*

Hydrologically, the study area is located in the Chamchamal-Sangaw basin. The main aquifer system in the area of interest was proposed to be the Pila Spi fractured karst aquifer that extends in NW-SE direction in the central and southern area of northern Iraq. Pila Spi consists of Eocene limestone, sometimes up to 200 m thick, and represents a typical heterogeneous anisotropic aquifer that is fractured and intensively karstified (Stevanovic and Markovic 2003b). It must be kept in mind that the local lithology is not entirely resolved yet (see previous chapter), and that Stevanovic and Marcovic (2003b) did not evaluate the role of Oligocene formation. According to Kharajiany (2008), Oligocene strata are highly porous, karstified and cavernous, but its role as aquifer was not evaluated. Considering the overall confusion about the affiliation of rock units, the following presentation about the characteristics of Pila Spi aquifer, might equally apply to the Oligocene aquifer.

The aquifer contains medium to large groundwater reserves strongly varying in space and time. As a result of general aquifer anisotropy and the presence of many fissures, the aquifer is generally characterised by a very high permeability (Stevanovic and Markovic 2003b). Values of transmissivity are in the range of 3.5 to 42000 m<sup>2</sup>/day (Jassim and Goff 2006).

Another characteristic of the Pila Spi aquifer is a turbulent water-flow regime. A highly fractured karst aquifer system such as Pila Spi combined with a lack of vegetation result in a highly effective infiltration capacity. According to Stevanovic and Markovic (2003b), estimated recharge coefficients of the Pila Spi aquifer amounts to about 30%, in particular cases up to 50% of the total rainfall. Compared to the Bekhma aquifer, which covers large areas in the northern part of northern Iraq, pure limestone outcrops are present to a less extent, resulting in lower values of aquifer recharge for the Pila Spi aquifer. Furthermore, sequences of marly and clayed components reduce the absorption capacity and contribute to secondary filling of existing fractures (secondary permeability).

Since Pila Spi Formation is largely overlain by the Lower and Upper Fars (Injana) Formation, which represent aquitards, confined conditions are created in the Pila Spi aquifer.

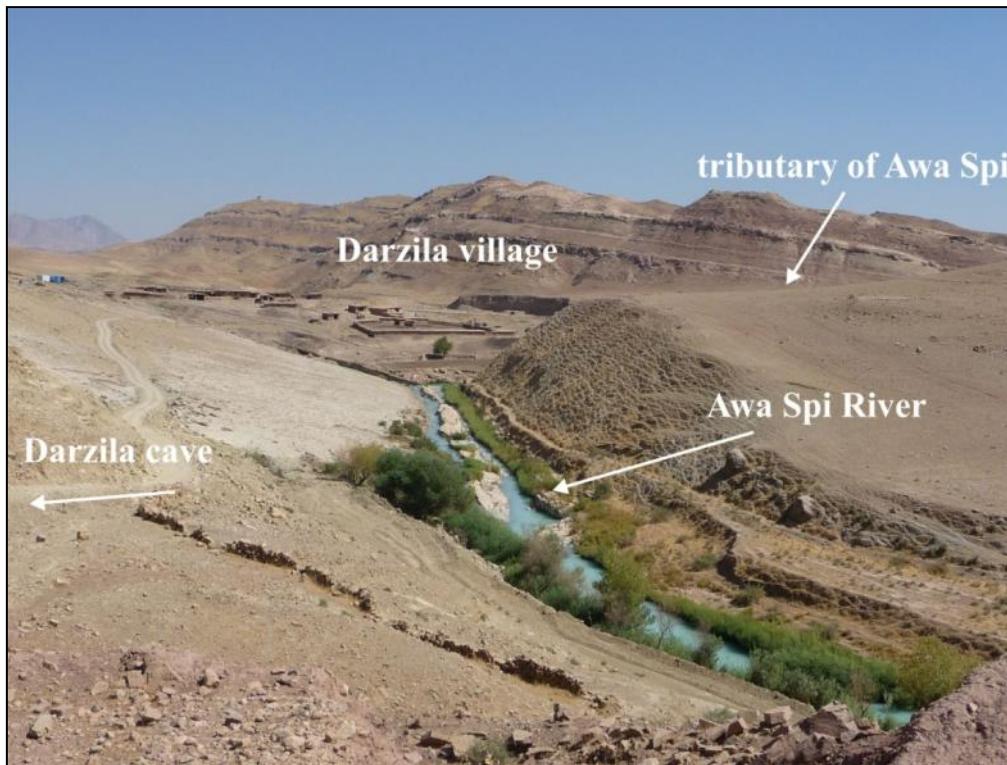


Figure 4: Awa Spi River and Darzila village

Nearby Darzila cave, the perennial river Awa Spi is located (Figure 4). The river has cut the limestone deeper and deeper and nowadays forms a canyon of about 50-60 m depth and 5-10 m width in the river upper course. The river initially flows parallel to the Azhdagh anticline towards SE and then changes towards SW at the anticline plunge. As sampling was carried out at the end of the dry season flow rates were low.

## 2.4 Climate Conditions

*Co-author: Karin Heiland*

Due to unstable political situations and periods of war in the past, the network of meteorological stations is relatively underdeveloped in northern Iraq. Long periods of rainfall observation exist only for the three stations: Sulaimaniyah (since 1941), Dokan dam (since 1958) and Darbandikhan dam (since 1962). However, approximate rainfall analyses have been conducted by Stevanovic & Markovic (2003a) based on data from 23 meteorological stations. The distribution of rainfall varies strongly over the year. The average annual rainfall rate amounts to about 675 mm (Sulaimaniyah station, 1941-2002) of which the highest precipitations occur in January (115 mm, Sulaimaniyah station, 1941-2002) whereas there is a long dry period between June and September. As the topography strongly influences the rainfall distribution, precipitation rates decrease from NE to SW direction. In the Sangaw District, average annual rainfall rates amounts to about 600 mm (isohyets maps in Stevanovic and Markovic, 2003a). Precipitation usually occurs in bursts and thus wadies drain quickly restricting recharge of groundwater aquifers (Jassim, Goff 2006).

The Sangaw District is one of the warmest regions of Kurdistan within the Iraq (Stevanovic *et al.* 2009). However, longterm data about monthly and annual variations of air temperatures are only rarely available. Data exist for Diana (two-hourly recorded data in the period from November 1957 to January 1959) (HAZRA Engineering Company 1963) and for Erbil city (average monthly temperatures for the period from 1959 to 1972) (Haddad and Smoor 1973). In order to give an overview of the monthly variations in air temperatures in the Sangaw District a temperature graph provided by World Weather Online (2011) is depicted in Figure 5.

Moreover, average monthly air temperatures and several other meteorological parameters were recorded during the year 2002 at the FAO stations Qaradagh, Mawat, Degala, Gopal, Qadish and Jelan, which are distributed throughout northern Iraq. According to these data, average annual relative humidity ranges from 44.5% (Jelan) up to 52% (Mawat) whereupon the monthly average minimum is in June (Gopal, 18%) and the monthly maximum in December (Qaradagh, 84%) (Stevanovic and Markovic, 2003a).

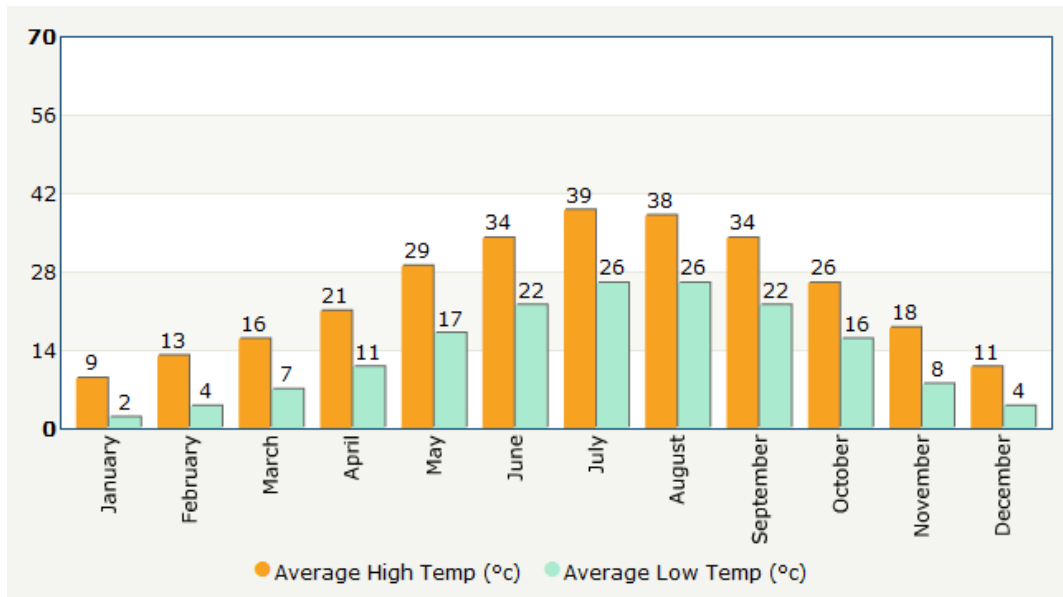


Figure 5: Average temperature graph for Sangaw District (World Weather Online 2011)<sup>1</sup>

In the year 2002, the rates of reference evapotranspiration ( $ET_o$ )<sup>2</sup> varied from 920 mm/year (Qaradagh) to 1506 mm/year (Gopal). Highest rates occurred during the summer. Monthly variations ranged from 17 mm/month in January (Gopal) to 274 mm/month in July (Gopal) in 2002. In mountainous areas,  $ET_o$  rates are much lower (Stevanovic and Markovic 2003a).

Due to the direct influence of Zagros Mts. in the Sulaimaniyah Governorate, northern winds are dominant throughout the year (Stevanovic and Markovic 2003a). Beyond that, Aziz (2001) mentions the influence of Mediterranean anticyclones in the summer moving from (south-) west to north and developing dust storms. Mediterranean cyclones moving from (north-) east are responsible for high rainfall rates in the winter period (Aziz 2001).

In summary, the climate of Sangaw region can be described as continental arid to semiarid climate with very hot and dry summers and cold and wet winters. Due to the given climate conditions vegetation and fertile soils are generally absent (Iurkiewicz and Stevanovic 2010).

<sup>1</sup> any information about period of measurements are not provided

<sup>2</sup> Calculations are based on Penmen-Monteith formula (Cropwat 5.7 Programme)

## 2.5 Description of Cave Pattern

### 2.5.1 Setting and Dimensions of Darzila Cave

*Co-author: Karin Heiland (modified)*

Darzila cave is located approximately 25 km road-distance from Sangaw in the Garmian area. More specifically, the cave can be accessed via a large sinkhole (photo in Figure 6) that is located at 35°08'770''N, 45°16'740''E and 688 m asl, in about 1 km distance of Darzila village. The sinkhole has probably formed by breakdown of instable parts of the cave (Figure 6). Those so-called collapse dolines are characterised by almost vertical rock walls and a debris floor sloping down into an open cave passage (Bell *et al.* 2005). The cave is embedded in limestone of Oligocene Formation, and possibly also from Pila Spi Formation.



Figure 6: Great sinkhole providing access to Darzila cave

The sinkhole has a diameter of approximately 30 m and a mean depth of around 15 m (Figure 6). From the base of the sinkhole, a narrow and steep passage leads down into the open cave passage. The cave floor lies approximately 38 m below terrain surface, about 650 m asl (Figure 6). It has to be kept in mind that these values are only approximations because precise measurement could not be performed. Total explored length of the cave is about 200 m (Figure 8). Further exploration in easterly direction had to be interrupted due to

bad air quality, increased danger of rock fall, and the subsequent enlargement of the main cave stream. Thus, the end of the cave could not be reached yet.

In order to get a better idea about the dimension of the cave a map view as well as a cross sectional view were set up based on the surveying that has been conducted during field work (Figure 7, Figure 8). Karst symbols are used according to the official UIS list (Häuselmann and Neumann 1999). An overview of the location of sampling points inside of Darzila cave is provided in Figure 9.

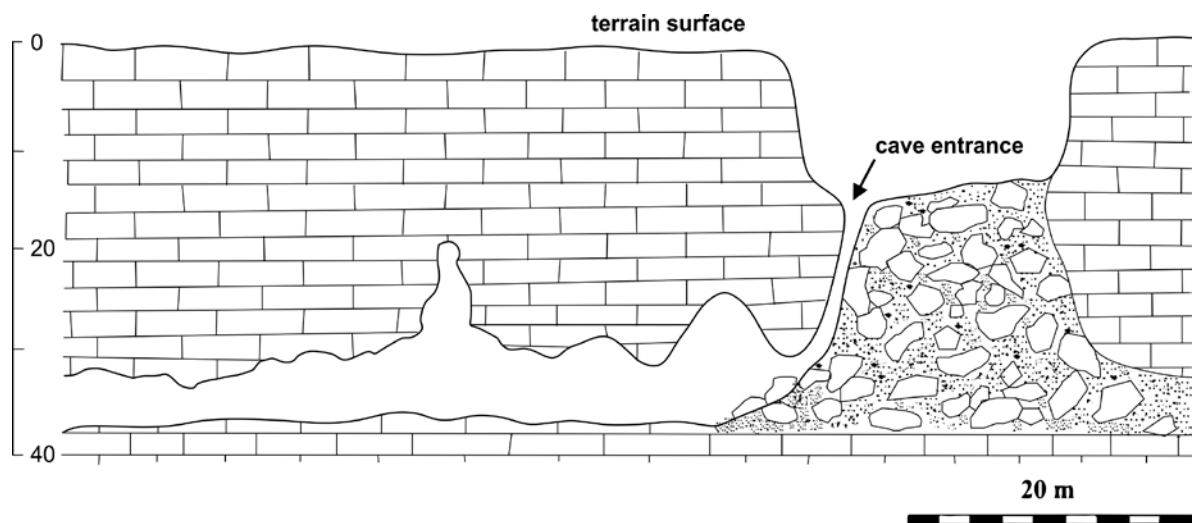


Figure 7: Cross sectional view of Darzila cave. Sketch modified after Heiland (2016).

As it is depicted in Figure 7, the cave shows an irregular profile with vaulted ceilings. Although they are not included in the cross sectional view, small skylights are present in the passage of ceilings nearby the entrance. The floor is nearly flat over a large area.

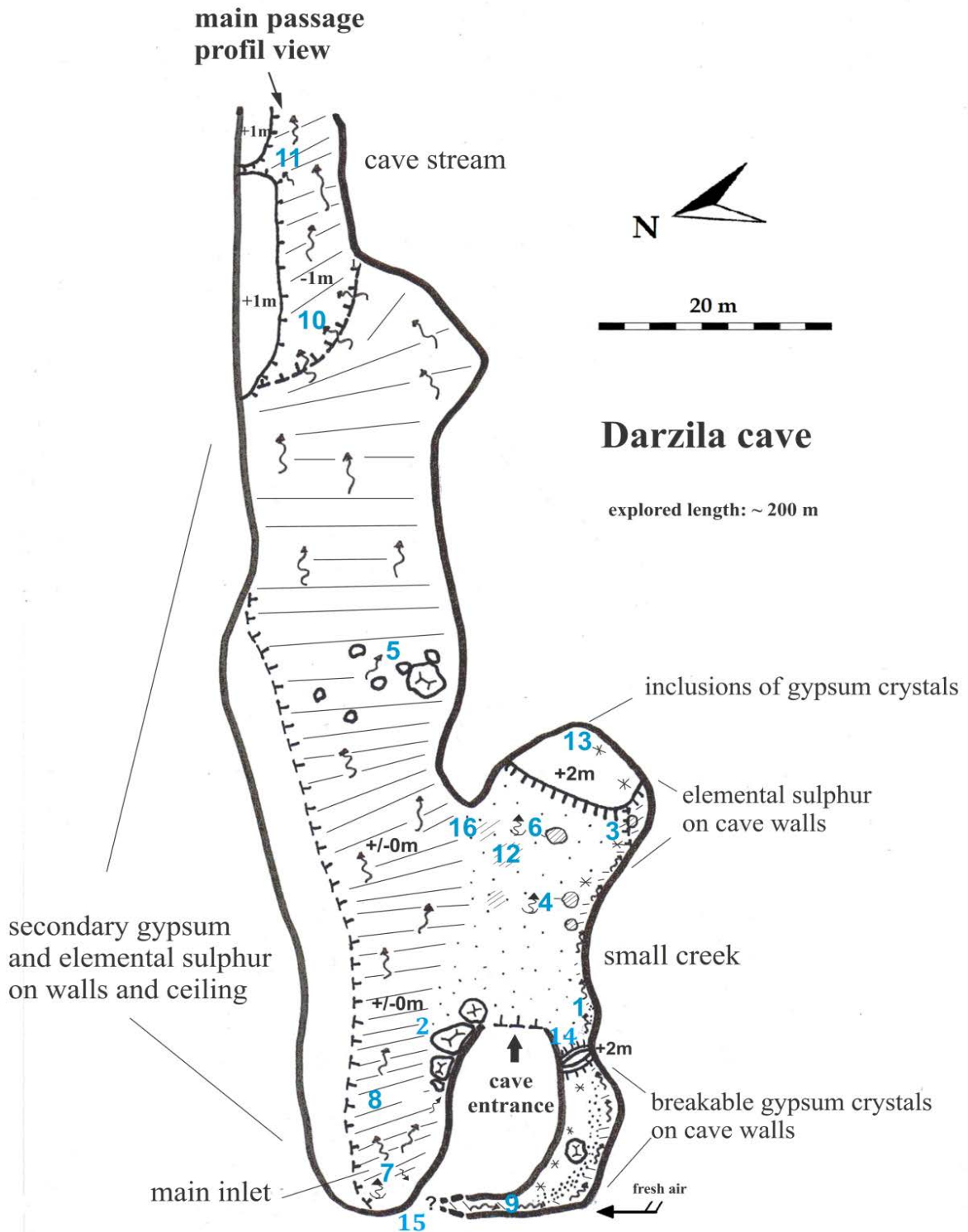


Figure 8: Map view of Darzila cave, including sampling locations (blue numbers). Karst symbols according to UIS guidelines (Häuselmann and Neumann 1999).

## 2.5.2 Hydrogeochemistry and Location of Sampling Sites

Darzila cave is fed by several groundwater inlets, most of which are present as floor feeders. Khanaqa and Al-Manmi (2011) were the first who studied the hydrogeochemistry of these waters. Furthermore, an extensive analysis of water and gas samples was carried out by Heiland (2016). Due to close collaboration with the latter, choice of sampling sites (Figure 8) and naming of the samples were generally the same.

Large parts of the cave floor are covered by a shallow (a few cm to dm) stream of low velocity. In the rear part of the cave, the water forms a distinct stream in a narrow bed. Most of these waters arise from the floor feeder at site 7, located in the north of the cave entrance. Here waters emerge from a deep, steeply inclined fault. Heiland (2016) demonstrated that the hydrogeochemistry of this inlet presents the main influence on the composition of the cave stream. The vicinity of site 7 is colonized by filamentous biofilms.

On the other side of the cave, a small creek (site 1) was identified. Before emerging into the main part of the cave, it flows through a small, neighbouring room, which is only accessible via a narrow passage. Due to an overwhelming presence of gypsum crystals at the cave walls and the ceiling, this outstanding part of the cave was named *crystal room*, corresponding to sampling site 9. While the rest of the cave atmosphere is characterized by warm (22 °C), humid air and a strong smell of hydrogen sulphide, the *crystal room* was supplied by fresh air that was several degrees colder (17.5 °C). It was not possible to follow the creek any further, so its primary source remained unidentified. Creek water, represented by DC-W-1 and DC-W-9, was characterized by neutral pH, partly reducing redox conditions, high content of dissolved oxygen and low sulphide concentrations (Heiland 2016).

Apart from the flowing cave waters, there were several small, isolated pools (site 3, 4, and 6) and puddles (site 12). All of them were characterized by highly acidic waters, ranging from pH 1.0 for DC-W-6 to a pH of 3.3 for DC-W-3. Heiland demonstrated that DC-W-3 is largely influenced by the nearby creek, whereas DC-W-4 and DC-W-6 were found to be fed by ascending water. Both pools contained saline waters with high concentrations of dissolved organic carbon. In contrast to the pools, the puddles were only a temporary phenomenon. DC-W-4 and some of the puddles were covered by white, slimy biofilms. The cave walls were covered by gypsum crystals and crusts of elemental sulphur. The crusts were thickest near the acidic sites.

In the rear part of the cave, water from different sources assembles and forms the main cave stream. Heiland (2016), who investigated three sites along the flow path of the stream (site 5, 10, 11), described the water as brackish, milky in colour, with neutral to alkaline pH conditions (pH = 6.6- 8.0). Khanaqa and Al-Manmi (2011) proposed, that the discharge rate typically varies between 40 L/s (dry season, June) and 60 L/s (wet season, April). Discharge rates were not measured, but since sampling was carried out at the very end of the dry season (September and October), lower values can be assumed. The stream continued in easterly direction.

Water sampling was also carried out at three springs that feed Awa Spi River. Hydrogeochemical investigations of Heiland (2016) revealed a hydraulic connection between Darzila cave and the river Awa Spi. DR-W-1, the first subterranean feeder of Awa Spi, was found to be the main outlet of cave waters. Further up the valley, there was another outlet, but the discharge was too low to be sampled. Approximately 200 m downstream, a second subterranean stream (DR-W-2) discharged into Awa Spi. The second spring has no hydraulic connection to the cave (Heiland 2016). A small spring (DR-W-8), located approximately 1 km downstream from the first spring, was sampled too.

Water sampling was also conducted at a well (DW-W-1) nearby the entrance of the cave. According to the locals, the depth to the water table is about 30 m (657 m asl). Water of the well possessed very high sulphide concentrations (about 50 mg/L) (Heiland 2016). Accordingly, the water was neither suitable as drinking water nor for irrigation purposes.

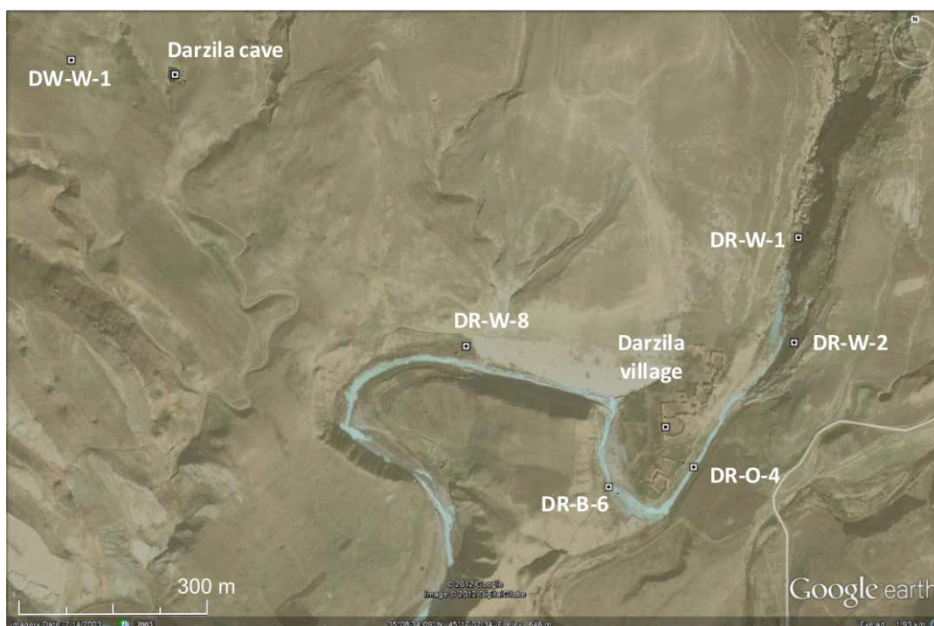


Figure 9: Location of sampling points in the surrounding of Darzila cave depicted in an aerial photo of Google earth. DW-W-1, DR-W-1, DR-W-2, and DR-W-8 are water samples, DR-O-4 is a sample of crude oil, and DR-B-6 is a biofilm sample.

## 3 Fundamentals

### 3.1 Biogeochemistry of Sulphur

#### 3.1.1 Fundamental Aspects of Sulphur Isotope Geochemistry

Natural sulphur is composed of four stable isotopes ( $^{32}\text{S}$ ,  $^{33}\text{S}$ ,  $^{34}\text{S}$ ,  $^{36}\text{S}$ ). By far the most abundant of these is  $^{32}\text{S}$ , which represents 95.04% of all sulphur. The second most abundant isotope is  $^{34}\text{S}$  (4.2%) followed by  $^{33}\text{S}$  (0.75%) and  $^{36}\text{S}$  (0.015%) (Berglund and Wieser 2011). These values reflect the average composition of terrestrial material.

Stable sulphur isotopic compositions are reported as  $\delta^{34}\text{S}$ , the ratio R of  $^{34}\text{S}/^{32}\text{S}$  in per mill (‰) relative to a standard (Thode 1991):

$$\delta^{34}\text{S} (\text{‰}) = \left[ \frac{R_{\text{sample}}}{R_{\text{standard}}} - 1 \right] \cdot 1000 = \left[ \frac{\left( \frac{^{34}\text{S}}{^{32}\text{S}} \right)_{\text{sample}}}{\left( \frac{^{34}\text{S}}{^{32}\text{S}} \right)_{\text{standard}}} - 1 \right] \cdot 1000 \quad [1]$$

Originally, the agreed upon reference material for reporting sulphur isotopic abundances was troilite (FeS) from the Cañon Diablo meteorite (CDT) with  $\delta^{34}\text{S} = 0.0\text{‰}$  by definition (Jensen and Nakai 1962). Unfortunately, CDT became more and more difficult to obtain and turned out to be not sufficiently homogeneous for being used as a reference (Beaudoin *et al.* 1994). As a consequence, the CDT scale was replaced with the VCDT (Vienna-CDT) scale which is currently defined relative to a silver sulphide reference material (IAEA-S-1) with  $\delta^{34}\text{S}_{\text{VCDT}} = -0.3\text{‰}$  (Ding 2001).

With respect to the study of the sulphur cycle oxygen and hydrogen isotopes are of concern, as well. Hydrogen ( $Z = 1$ ) has two stable isotopes:  $^1\text{H}$  and  $^2\text{H}$  (deuterium = D), with approximate terrestrial abundances of 99.99 and 0.015 percent, respectively (Berglund and Wieser 2011). Oxygen ( $Z = 8$ ) is composed of three stable isotopes:  $^{16}\text{O}$ ,  $^{17}\text{O}$ , and  $^{18}\text{O}$ , with approximate terrestrial abundances of 99.763, 0.0375, and 0.1995 %, respectively (Garlick 1969). Analogically to equation [1], oxygen and hydrogen isotopes are defined relative to *Vienna Standard Mean Ocean Water* (VSMOW), a hypothetical water that resembles the oxygen and hydrogen isotopic composition of average ocean water.  $\delta^{18}\text{O}$  and  $\delta\text{D}$  are 0.0‰ by definition.

Stable isotope geochemistry primarily deals with the relative partitioning of stable isotopes among substances, rather than with their absolute abundances. Variations in the relative proportions of  $^{34}\text{S}$  and  $^{32}\text{S}$  occur as a result of fractionation due to isotopic exchange or unidirectional reaction processes (Bottrel and Raiswell 2000). Generally spoken, the heavier  $^{34}\text{S}$  isotope forms more stable bonds. Accordingly,  $^{34}\text{S}$  and  $^{32}\text{S}$ -bearing molecules react at different rates leading to subsequent partition of the isotopes (Seal 2006).

Sakai (1982) and Bachinski (1969) emphasized that the importance of the oxidation state of sulphur is of major importance. The higher oxidation states of sulphur are enriched in the heavier isotopes relative to lower oxidation states. Therefore,  $^{34}\text{S}$  enrichment follows the general trend  $\text{SO}_4^{2-} > \text{SO}_3^{2-} > \text{S}_x^0 > \text{S}^{2-}$ .

The stable isotope fractionation can be quantified in terms of the kinetic fractionation factor ( $\alpha$ ) or the isotope enrichment factor ( $\epsilon$ , in ‰) (e.g. Hoefs 2004). The expressions are directly related by  $\epsilon = (\alpha - 1) \cdot 1000$ . The kinetic fractionation factor is calculated using the following equation (Clark and Fritz 1997):

$$\alpha_{(A-B)} = \frac{R_A}{R_B} = \frac{1000 + \delta_A}{1000 + \delta_B} \quad [2]$$

### 3.1.2 Sulphur Species and the Microbial Sulphur Cycle

*Previously printed in Heiland (2016)*

Sulphur is one of the most abundant elements in nature. It is present in various minerals (e.g. elemental sulphur, gypsum, metal sulphides), gases (e.g.  $\text{SO}_2$ ,  $\text{H}_2\text{S}$ ), aqueous species (e.g.  $\text{SO}_4^{2-}$ ,  $\text{H}_2\text{S}_{\text{aq}}$ ), as well as organic compounds (e.g. humic matter, oil, coal, dimethyl sulphoxide). Furthermore, sulphur is highly redox sensitive, occurring in oxidation states from -2 in sulphides to +6 in sulphate. The latter species commonly are the dominant forms of sulphur. Species with intermediate or mixed oxidation states occur as well, though in lesser amounts (Kaasalainen and Stefánsson 2011). Transformations between different sulphur species can occur through chemical or biological pathways. However, the abiotic route usually is significantly slower (Ehrlich 2002). Table 1 lists geomicrobially important forms of sulphur and their oxidation states.

Table 1: Geomicrobially important forms of sulphur (after Ehrlich 2002).

Species	Formula	Oxidation state(s) of Sulphur
Sulphide	$S^{2-}$ , $HS^-$ , $H_2S$	-2
Polysulphides	$S_n^{2-}$	-2 and 0
Elemental sulphur	$S_8$ (usually written $S^0$ )	0
Sulphite	$SO_3^{2-}$	+4
Thiosulphate	$S_2O_3^{2-}$	-1 and +5
Polythionates	$S_nO_6^{2-}$ ( $n \geq 2$ )	+4 with $n = 2$ ; -2 and +6 with $n > 2$
Sulphate	$SO_4^{2-}$ , $HSO_4^-$	+6

The microbial metabolism comprises a major portion of the global sulphur cycle (Trüper 1984). A simplified scheme of the microbial sulphur cycle is presented in Figure 10.

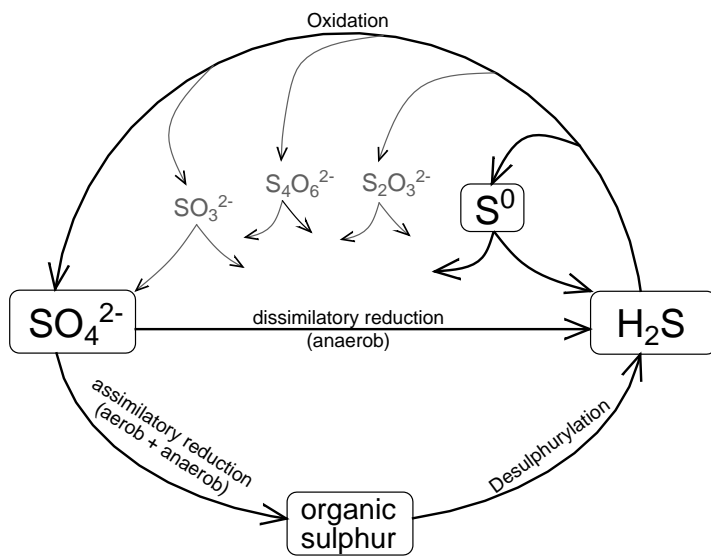


Figure 10: The microbial sulphur cycle (adapted from Canfield 2001a; Tang *et al.* 2009).

### 3.1.2.1 Assimilatory sulphate reduction

Sulphur is an essential element for living cells. Most commonly in the form of sulphate, it is assimilated, reduced, and incorporated into amino acids, vitamins, and various other components of the cell (Le Faou 1990). Associated isotopic fractionations are very small. According to Thode (1991),  $\delta^{34}\text{S}$  values of reduced organic sulphur, range from +0.5 to -4.4 ‰, relative to the sulphate in the surrounding environment.

### 3.1.2.2 Dissimilatory sulphate reduction

Some prokaryotes can use sulphate or elemental sulphur as electron acceptor (dissimilatory sulphate reduction) instead of oxygen. Sulphate-reducing bacteria such as *Desulfomonas* gain energy by coupling anaerobic oxidation of organic matter or  $\text{H}_2$  gas to the reduction of sulphate, which results in the formation of hydrogen sulphide. A comprehensive review of the metabolism, the ecology and diversity of sulphate reducing bacteria is given by Muyzer and Stams (2008). Dissimilatory sulphate reduction involves several steps, but it can be simplified to the equations (Rees 1973):



where  $\text{CH}_2\text{O}$  symbolically stands for an organic compound. The bonding energy of  $^{32}\text{S}-\text{O}$  is smaller and therefore easier to break than that of  $^{34}\text{S}-\text{O}$ . Consequently,  $^{32}\text{S}$  tends to react faster than  $^{34}\text{S}$ , and the expelled  $\text{H}_2\text{S}$  is enriched in  $^{32}\text{S}$  relative to the sulphur in the environment (Shen and Buick 2004). In natural populations that use organic electron donors, there appears to be fractionations between 10 and 42 ‰ VCDT (Habicht and Canfield 1997a).

Bacterial sulphate reduction typically leads to a progressive sulphur isotopic composition of unconsumed sulphate. Under closed system conditions, this process follows a Rayleigh distillation equation (Mariotti *et al.* 1981), where  $\epsilon$  is the respective enrichment factor for sulphur and  $f$  stands for the fraction of residual sulphate ( $[\text{SO}_4^{2-}]/[\text{SO}_4^{2-}]_0$ ).

$$\delta^{34}\text{S}_{\text{SO}_4} = \delta^{34}\text{S}_{\text{SO}_{4,0}} + \epsilon \ln f \quad [5]$$

$\delta^{34}\text{S}_{\text{SO}_4}$  stands for the measured sulphur isotopic composition of dissolved sulphate [‰ VCDT], and  $\delta^{34}\text{S}_{\text{SO}_{4,0}}$  stands for the initial sulphur isotopic composition of dissolved sulphate [‰ VCDT], before bacterial reduction.

### 3.1.2.3 Sulphide oxidation

In oxic environments, hydrogen sulphide oxidizes quickly and spontaneously without any microbial mediation (Kaasalainen and Stefánsson 2011). However, numerous prokaryotes are not only able to compete with this process - reaction rates are often significantly higher than abiotic rates (Luther III *et al.* 2011). For these so-called sulphur-oxidizing prokaryotes (SOP), reduced forms of sulphur, serve as sources of energy or reducing power (Janssen *et al.* 2009). The SOP are phylogenetically diverse. In the domain *Bacteria*, members can be divided into two major subgroups – *photoautotrophic* and (mostly) *chemolithotrophic* sulphur-oxidizing organisms (Friedrich *et al.* 2001). Due to their great variability, individual mechanisms are not presented here.

Arguably the most interesting sulphur-oxidizing bacteria belong to the genus *Acidithiobacillus*. This genus currently comprises four recognized bacterial species, namely *A. thiooxidans*, *A. caldus*, *A. ferrooxidans*, *A. ferrivorans*, and one (*A. albertensis*) whose status is uncertain. All of them are extremely acidophilic bacteria that have the ability to grow autotrophically using  $S^0$  and several reduced forms of sulphur as sole energy source (Kelly and Wood 2000, Hallberg *et al.* 2010). *A. ferrooxidans* is furthermore able to utilize ferrous-iron and can degrade pyrite as well as various other sulphide minerals (Kelly and Wood 2000).

Aerobic sulphide oxidizers have to live where oxygen and sulphide coexist. Because the organisms compete with abiotic oxidation processes, their presence is generally limited to areas where gaseous sulphide rises from the anoxic zone and meets oxygenated water (Madigan and Brock 2009). Planctonic life as individual cells in these waters is only one of the possible life styles. The more typical strategy is the formation of a biofilm (Korber *et al.* 1999). According to Wimpenny (2000), a biofilm can be described as microbial community that forms at a phase boundary, most often at a liquid-solid interface. It is a spatially and temporally heterogeneous system that generates extracellular polymeric substances (EPS) for adhesion, protection and to facilitate interactions of individual members of the community.

The isotopic effects that are associated with sulphide oxidation have not been studied as thorough as for sulphate reduction. Accordingly, available data are scarce, mostly several decades old, and partly conflictive. However, the general conclusion is that microbial sulphur oxidation yields only small or negligible sulphur isotope fractionations (see for example Fry *et al.* 1988; Kaplan and Rittenberg 1964). Oxidation of pyrite probably presents the oxidation pathway that is studied best. Here, the isotopic effects are influenced by the

oxidant, the time of exposure, grain size, pH conditions and the involvement of microorganisms (e.g. Balci *et al.* 2007, Balci *et al.* 2012, Heidel and Tichomirowa 2010, Heidel *et al.* 2009). Balci *et al.* (2007) reported an enrichment factor  $\epsilon^{34}\text{S}_{\text{SO}_4\text{-FeS}_2}$  of around -0.7 ‰ for both the biological and the abiotic anaerobic oxidation of pyrite. Under aerobic conditions, no significant oxidation was observed.

The oxidation of dissolved sulphide or metal sulphides to sulphate involves the incorporation of oxygen. And depending on the mode of oxidation, sulphate oxygen may come from either atmospheric oxygen or from water. In contrast to sulphur, oxygen isotopic effects can be significant. Balci *et al.* (2007) conducted a series of experiments concerning abiotic and biological pyrite oxidation, and determined associated enrichment factors. They found, that the enrichment factor  $\epsilon^{18}\text{O}_{\text{SO}_4\text{-H}_2\text{O}}$  was the same for abiotic and biotic experiments (~ 3.5 ‰). The enrichment factor  $\epsilon^{18}\text{O}_{\text{SO}_4\text{-O}_2}$  between sulphate and dissolved oxygen was -10.8 ‰ for the long-term biological experiments.

The relative proportions of oxygen in sulphate from molecular oxygen and water can be calculated by means of the following equation from Lloyd (1967):

$$\delta^{18}\text{O}_{\text{SO}_4} = \text{X}(\delta^{18}\text{O}_{\text{H}_2\text{O}} + \epsilon_{\text{SO}_4\text{-H}_2\text{O}}) + (1 - \text{X}) \cdot (\delta^{18}\text{O}_{\text{O}_2} + \epsilon_{\text{SO}_4\text{-O}_2}) \quad [6]$$

$\delta^{18}\text{O}_{\text{SO}_4}$ ,  $\delta^{18}\text{O}_{\text{H}_2\text{O}}$ , and  $\delta^{18}\text{O}_{\text{O}_2}$  are the oxygen isotopic compositions of sulphate, water, and molecular oxygen ( $\delta^{18}\text{O} = 23.5$  ‰, Kroopnick and Craig 1972), respectively. X stands for the proportion of water-derived oxygen, whereas (1-X) is the corresponding proportion that is derived from molecular oxygen.  $\epsilon_{\text{SO}_4\text{-H}_2\text{O}}$  and  $\epsilon_{\text{SO}_4\text{-O}_2}$  are the respective oxygen isotope enrichment factors between sulphate and water or molecular oxygen.

## 3.2 Sulphuric Acid Speleogenesis

*Previously printed in Heiland (2016)*

In cave science, the term *speleogenesis* refers to the origin as well as the development of caves (Gunn 2004). Unfortunately, expressions used by cave scientists are not always consistent with the terminology of geosciences. In order to avoid confusions, cave science nomenclature was avoided in this thesis. The terms *epigene* and *hypogene* karst were replaced by *phytokarst* and *unconventional karst* or *karst of deep-seated origin*, respectively.

Most accessible karstic caves are phytokarst caves that are formed by dissolution of limestone by infiltrating shallow, meteoric water enriched in CO<sub>2</sub> (Palmer 2011). However, the expression karst is a much wider concept. Ford (2006) defines karst as a terrain with distinctive hydrology and landforms that is formed due to the combination of high rock solubility and a well-developed secondary porosity underground.

The typical difference between phytokarst and unconventional karst caves is the direction of the water or gas flow, namely descending in the former and ascending in the latter (Ford 2006, Klimchouk 2007).

Like phytokarst caves, uncommon karst caves can be formed by carbonic acid dissolution. However, Klimchouk (2007) lists a variety of other processes that are relevant for the formation of the latter. Possibly the most interesting among these is the dissolution by sulphuric acid. Typically, these caves consist of a central area or passage with irregular rooms, ascending blind passages, abundant gypsum deposits and floor feeders (Palmer and Hill 2012). Egemeier (1973, 1981) was the first who systematically studied such features and proposed the sulphuric acid speleogenesis (SAS) model to explain the origin and evolution of Lower Kane Cave in Wyoming: When H<sub>2</sub>S-bearing water enters the oxygenated, subaerial cave environment, hydrogen sulphide reacts with oxygen to produce sulphuric acid. Adjacent limestone dissolves and is partly replaced by gypsum precipitation.

The SAS model was later recognised to explain the development of some major cave systems, such as la Cueva de Villa Luz in Mexico (Hose and Pisarowicz 1999), Carlsbad Cavern and Lechuguilla Cave in New Mexico (Hill 1990; Hose *et al.* 2000; Engel *et al.* 2004), the Frasassi Cave System in Italy (Galdenzi and Menichetti 1995; Galdenzi and Maruoka 2000) and the caves in the Cerna Valley in Romania (Onac *et al.* 2011). A typical setting for SAS is shown in Figure 11.

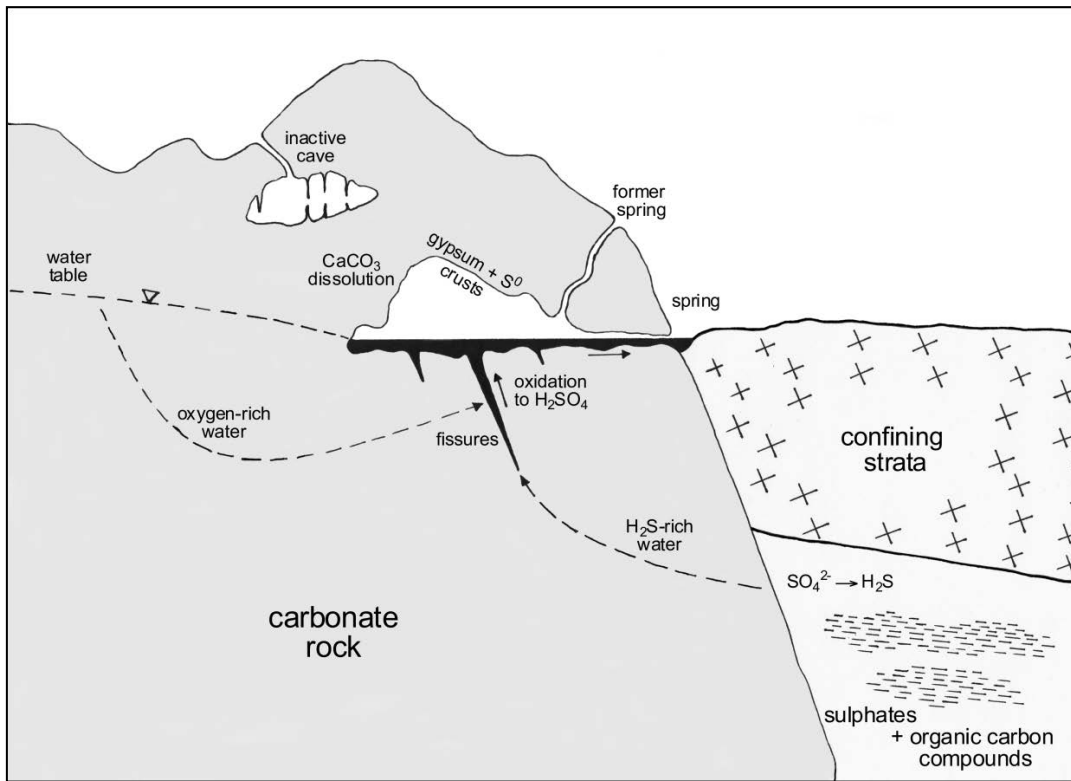


Figure 11: A typical setting for sulphuric acid caves (after Palmer and Palmer 2004)

Cave-forming hydrogen sulphide typically originates either from oil-rich reservoirs directly or from the reduction of sulphates by organic matter (Palmer and Palmer 2004), as shown in equation [3]. Theoretically, thermochemical sulphate reduction (TSR) without any microbiological support may occur at temperatures as low as 25 °C (Worden and Smalley 1996). However, only at temperatures above 100-140 °C reaction rates appear to be high enough to be geologically significant. At temperatures less than about 80 °C the reaction requires bacterial mediation (Machel 2001).

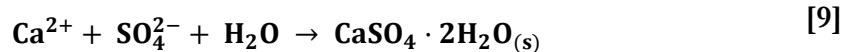
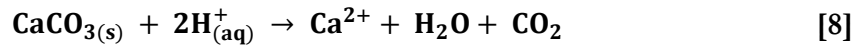
When H<sub>2</sub>S-bearing water encounters oxygenated groundwater, ascends to the water table, or volatiles into the cave atmosphere and adsorbs to moist cave wall surfaces, sulphuric acid is produced; either in a single or, more commonly, in several intermediate steps (Palmer and Palmer 2004):



Polysulphides (S<sub>n</sub><sup>2-</sup>), elemental sulphur (S<sup>0</sup>), sulphite (SO<sub>3</sub><sup>2-</sup>), thiosulphate (S<sub>2</sub>O<sub>3</sub><sup>2-</sup>), and polythionates (S<sub>n</sub>O<sub>6</sub><sup>2-</sup>) are possible intermediate sulphur species of the reaction (Kaasalainen and Stefánsson 2011).

In the first SAS model, sulphuric acid production was completely ascribed to chemical oxidation. Later studies (especially Angert *et al.* 1998, Hose *et al.* 2000, Engel *et al.* 2004, and Barton and Luiszer 2005) demonstrated that microbial mediation by sulphur oxidizing bacteria like *Thiobacillus* can enhance this process substantially.

The sulphuric acid dissolves the carbonate rock of the limestone, and calcium ions ( $\text{Ca}^{2+}$ ) may combine with the sulphate ions to form gypsum:



These secondary gypsum precipitates tend to be blistered and poorly bonded to the carbonate rock (Palmer and Palmer 2004). When they become too heavy to support their own weight, they fall to the cave floor and are carried away by cave rivers. The net result is the removal of mass from the host rock and the enlargement of void volume.

Furthermore, elemental sulphur crusts can occur in close proximity to gypsum and carbonate rocks. This was already observed by the mineralogist Steffens (1819). However, at that time it was a phenomenon that could not be explained yet. It was described as a “mysterious reduction process that occurs when lime and sulphuric acid react” (Figure 12). The author was a good observant, but couldn’t put the pieces together. The occurrence of elemental sulphur in such unconventional karstic caves can be attributed to incomplete oxidation  $\text{H}_2\text{S}$  according to equation [10] (Hose and Pizarowicz 1999):



At places where thick gypsum precipitates coat adjacent carbonate rock, sulphuric acid is not neutralised. As the acid concentration increases, the pH drops to fairly low levels. Below about pH 2, gypsum dissolution becomes pH dependent and beforehand precipitated gypsum might dissolve again. At this low pH  $\text{HSO}_4^-$  becomes the dominant sulphate species. Under reducing conditions (Osseo-Asare 1998), elemental sulphur might precipitate on the gypsum crust (Palmer and Palmer 2000).

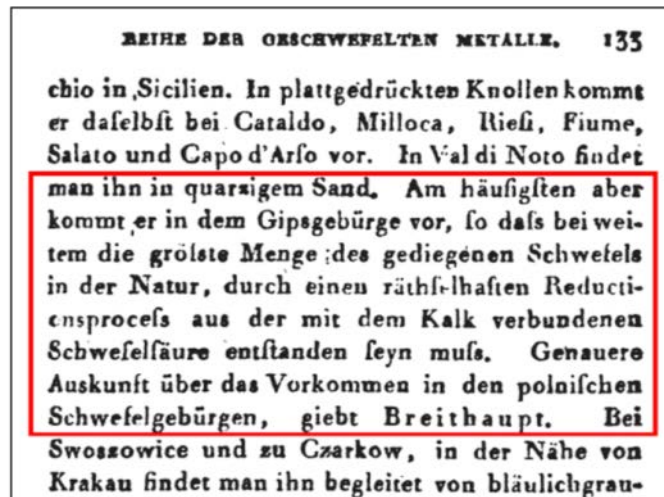


Figure 12: Early assumptions about the formation of elemental sulphur. Roughly: “It [elemental sulphur] is most common in the gypsum ranges. Therefore, the largest part of elemental sulphur in nature must arise from a mysterious reduction process that occurs when lime and sulphuric acid combine”. Source: Steffens, H. (1819) Vollständiges Handbuch der Oryktognosie, Halle p. 133.

Darzila cave has been proposed to enlarge by the same dissolution mechanisms (Iurkiewicz and Stevanovic 2010, Khanaqa and Al-Manmi 2011, Heiland 2016). Cave sulphur is thought to originate from petroleum fields, or from gypsum of Lower Fars Formation (Iurkiewicz and Stevanovic 2010). A small natural oil spill into Awa Spi River confirms the general presence of hydrocarbons and pathways where oil can rise from deep reservoirs to the surface. The occurrence of substantial oil reservoirs in the vicinity of the cave is not yet documented in the literature. However, only about 5 km from the cave, confidential test drillings are performed. Furthermore, the Chamchamal and the Khor Mor gas-condensate field, as well as the famous Kirkuk oil field are located within a few tens of km distance from the study area.

## 4 Methods

### 4.1 Sampling and Storage

Sampling of water, sediment, rocks & minerals, crude oil, and biofilms was conducted in the period from September, 15<sup>th</sup> to October, 6<sup>th</sup> 2011 at the end of the dry season. GPS data of sampling points are given in the Appendix (Table A 1 and Table A 2).

#### 4.1.1 Water and Gas Samples, In-Situ Parameters and Photometry

The parameters pH, electrical conductivity, temperature, redox potential, turbidity and oxygen content were measured in-situ. Photometrical analysis of redox-sensitive species such as dissolved sulphide, ammonia, nitrate and phosphate was conducted immediately after return from the fieldwork. Water samples for various parameters (IC, ICP-MS, DOC, dissolved gases, etc) were collected at 19 locations. Detailed information about used instruments, stabilisation methods, analytical procedures, data processing, as well as an extensive evaluation of the results is given in Heiland (2016). Corrected results of in situ measurements as well as photometrical data are given in Table A 9, results of IC and ICP-MS analyses are given in Table A 10 and Table A 11, respectively.

#### 4.1.2 Water Sampling for Isotopic Analysis

Water sampling for stable isotope analyses of water ( $\delta\text{D}$  and  $\delta^{18}\text{O}$ ) and of dissolved sulphate ( $\delta^{34}\text{S}_{\text{SO}_4}$ ;  $\delta^{18}\text{O}_{\text{SO}_4}$ ) and sulphide ( $\delta^{34}\text{S}_{\text{HS}^-}$ ) was performed at 11 locations. Seven of these samples were taken within the cave (code DC-W), three from springs that discharge into Awa Spi (code DR-W) and one from the inactive well nearby (code DW-W).

##### ➤ Water sampling for $\delta\text{D}$ and $\delta^{18}\text{O}$ analysis

Water from 12 locations was filled directly in 100 mL HDPE bottles. In order to avoid a gas phase above the water, bottles were filled entirely. During transport from the investigation area to the local laboratory, samples were stored on ice. Samples were kept refrigerated until measured.

##### ➤ Water sampling for $\delta^{34}\text{S}$ and $\delta^{18}\text{O}$ analysis

Sampling was accomplished by filling foldable plastic containers of 10 L volume with water. At two sites, smaller containers had to be used instead. Here, sample volume amounted to 6 L only. In order to minimize sulphide oxidation and degassing of dissolved  $\text{H}_2\text{S}$ , containers were filled completely and as quick as possible.

A series of steps which aim for the extraction of sulphide and sulphate followed. Immediately after sampling, 50 mL 0.169 M ammonium Zn-acetate solution was added, in order to precipitate sulphide as ZnS. After one day, about 2L of sulphide free excess solution was decanted into a plastic bottle for later treatment. The remains of the solution and the ZnS precipitate in the container were filtrated. The filters were left to air dry and finally stored in zipper-bags.

The pH of the remaining water was adjusted to 4 by using 6 M HCl. The purpose of this was to prevent co-precipitation of CaCO<sub>3</sub>. Then, 10-20 mL 1.7 M BaCl<sub>2</sub> solution was added for BaSO<sub>4</sub> precipitation. After one day, the BaSO<sub>4</sub> precipitate was separated from the excess solution by filtration. As before, the filters were left to air dry and transferred into zipper-bags were they were stored until further treatment.

Table 2: Purpose and preparation of solutions required during sampling.

<b>Solution</b>	<b>Purpose</b>	<b>Preparation</b>
0.169 M ammonia zinc acetate solution	Precipitation of sulphide	100 mL of 25% ammonia (Prolabo VWR) and 35 g Zn(CO <sub>3</sub> COO) <sub>2</sub> · 2H <sub>2</sub> O (Merck, p.a.) are dissolved in 900 mL deionised water
1.7 M barium chloride solution	Precipitation of sulphate	41.7 g BaCl <sub>2</sub> · 2H <sub>2</sub> O (Isocomerz, p.a.) were dissolved in 100 mL deionised water

### 4.1.3 Rock and Mineral Sampling

Sampling of rocks and minerals was accomplished with the objective to analyze different materials for their sulphur isotopic composition. The materials were stored in zipper bags.

Elemental sulphur (code DC-ES) was collected directly from the crust covering gypsum incrustations on the cave wall.

Secondary gypsum (code DC-SG), present as single large crystals and easily breakable crusts, was sampled from numerous locations in the cave. It was intended to analyze only a few representative samples, and to refine the grid if significant differences occur. Primary gypsum of Lower Fars Formation (code DS-PG) presents a likely source of cave sulphur. Accordingly, it was sampled at three locations of the Chamchamal-Sangaw-basin, where the formation was accessible from the surface. Two samples were taken in approximately 3 km distance from the cave. The third sample was taken at the foot of the Sagirma Quaradagh

Mountains, approximately 35 km from the cave. The sampling locations were too far out to be depicted in Figure 9, but their GPS coordinates are listed in the Appendix (Table A 2).

Rock material from the host rock limestone (Kirkuk group, Oligocene) was collected from the terrain surface above Darzila cave (DC-PL-15), from the fault near the cave (DS-PL-1), as well as from the cave floor. Secondary limestone in Darzila cave could not be found during fieldwork.

#### **4.1.4 Oil Sampling**

A distinctive feature of Awa Spi River is the presence of crude oil on the water surface. At one location, crude oil obviously rises from the subsurface and seeps into the river. Here, one oil sample (DR-O-4) for sulphur isotopic analysis was collected. Glass vials of various sizes were used as sample containers.

#### **4.1.5 Sediment Sampling**

At five locations within the cave (DC-S-1, -2, -3, -5, -9), sediment samples were collected and stored in 1 L zipper-bags without any preservation.

#### **4.1.6 Microbiological Sampling**

Biofilms, sediments, crude oil and material from the cave wall were sampled for microbiological cultivation and analyses. To minimize the risk of contamination and to ensure sample integrity, several precautions were taken to obtain representative samples:

- Any handling of material intended for microbiological analysis was accomplished with disposable lab gloves
- Sampling tubes were either new and sterile, or autoclaved prior usage
- Small instrument like tweezers were flame-sterilized directly before handling
- Treatments in the lab before and after the field day were conducted next to a Bunsen burner or under a hood, both of which create an updraft of air and thus prevent airborne contamination
- Any solutions needed during the procedures were autoclaved and stored refrigerated
- If not stated otherwise, samples were kept on ice during transport from the field and then stored refrigerated until further treatment

➤ **Crude Oil**

One sample of crude oil was collected at the location where it seeps into Awa Spi. A 25 mL glass vial was used as sample container. In order to keep the sample milieu anoxic, the vial was filled completely.

➤ **Cave wall**

Loose material from the cave wall, mainly consisting of gypsum and elemental sulphur, was collected into a zipper-bag. The sample was kept at room temperature until DNA extraction.

➤ **Sediments**

Six cave sediments (D-S-1, -4, -5, -9, -12a, -12b) were sampled for microbiological analysis. They were transferred into sterile 15 mL PE tubes and kept cool until further treatment.

➤ **Biofilms**

When there is a delay in the analysis of a microbiological sample, many microorganisms may not survive the transport. For DNA analysis this is not a problem but cultivation requires viable organisms. Therefore, 0.1% peptone water (Table 3) was used as a transport media to maintain the viability of the microbes. Peptone water was filled into the sterile 15 mL PE tubes, which were intended for sampling. The tubes were stored refrigerated until the next day. Biofilms were gathered at four cave sites (DC-B-4, -7, -9, -12) and one river site (DR-B-6). Sampling was accomplished with the help of flame-sterilized tweezers.

Table 3: Preparation of peptone water.

<b>Solution</b>	<b>Purpose</b>	<b>Preparation</b>
0.1% peptone-water	Transport media	10 g buffered peptone (ROTH, p.a.) was dissolved in 1000 mL deionised H <sub>2</sub> O. The solution was sterilized for 45 min at 121 °C and 1.1 bar in the autoclave CertoClav CV-EL.

## 4.2 Geochemical and Mineralogical Analyses

### 4.2.1 X-ray Fluorescence Spectroscopy (XRF)

Altogether 19 rock and mineral samples as well as 5 sediment samples were analysed for their elemental composition by X-ray fluorescence spectroscopy (XRF) with the instrument *SPECTRO XEPOS* in the water chemistry lab of the Hydrogeology department of TU BAF.

Prior analysis, rock and mineral samples were crushed, dried and subsequently pulverized to about 20 µm by using the planetary mill *Pulverisette 5*. Sediment samples were dried, pestled and sieved. Only the grain fraction < 80 µm was analysed for its elemental composition. Approximately 4 g pulverized sample material was used for analysis.

### 4.2.2 Imaging

Selected mineral samples were subject to high-resolution imaging at the Institute of Geology (Dr. M. Magnus) at TUBAF using a stereomicroscope *SteREO Discovery.V12* from Zeiss.

### 4.2.3 X-ray Diffraction (XRD)

Mineralogical analysis of five sediment samples was conducted at the mineralogical laboratory of the Institute of Mineralogy (Dr. R. Kleeberg) of TUBAF, using the diffractometer URD-6 (Seifert-FPM) equipped with automatic divergence aperture and semiconductor detector Meteor DT. Prior analysis, sediment samples were dried at 40° C, pestled and sieved to a grain size < 35 µm. Evaluation of results was accomplished using the software “Analyze” (database: pdf4+, 2011). The Rietveld program BGMN and Autoquant were used for quantifying the peaks. Due to the high content of silicate minerals, which impede an accurate determination of sulphur bearing minerals, results are only semi-quantitative.

### 4.2.4 CHNS Composition of Crude Oil

The elemental composition regarding carbon, hydrogen, nitrogen and sulphur of crude oil was analysed at the Institute of Organic Chemistry at the TU Bergakademie Freiberg, using a vario MICRO cube from *ELEMENTAR Analysensysteme*. The sample was combusted at 1150° C (shortly increased to approximately 1700° C). In a second furnace, combustion gases were reduced to the gases N<sub>2</sub>, CO<sub>2</sub>, H<sub>2</sub>O and SO<sub>2</sub>. Helium gas served as carrier to transport the gas mixture through a temperature programmed desorption column. The separated gases were detected with a thermal conductivity detector.

### 4.3 Isotopic Analyses

Stable isotopes of water were analysed at the chair of Hydrogeology at the TU Bergakademie Freiberg.

The sulphur and sulphate oxygen isotopic composition of several sample materials (water, sediment, raw-oil, rocks and minerals) was analysed at the Helmholtz-Centre for Environmental Research (UFZ) in Halle. Some materials (dissolved sulphate, gypsum and elemental sulphur) have additionally been analysed at the chair of Mineralogy at the TUBAF. Prior isotopic analysis, elaborate extraction and purification routines had to be accomplished.

#### 4.3.1 Hydrogen and Oxygen Isotopes of Water

Water samples from three springs that feed Awa Spi river, a selection of eight cave waters and the water from the well were subject to  $^{18}\text{O}/^{16}\text{O}$  and D/H analysis.

Simultaneous measurement of these ratios was conducted using a *Liquid Water Isotope Analyzer* (Los Gatos model 908-0008-3001) coupled to a CTC LC-PAL auto-injector. The measurement strategy of the analyser is based on high-resolution laser absorption spectroscopy. Compared to previous laser gas instruments, the employed *Liquid Water Analyzer* uses *Off-Axis integrated Cavity Output Spectroscopy* (OA-ICOS). High reflectivity off-axis mirrors, installed within an optical cavity, increase the optical path length from commonly less than 200 m to several kilometres (Baer *et al.* 2002). This leads to increased absorption, and thereby allows the use of more economical near-infrared diode lasers that can be operated at room temperature. The laser wavelength is tuned to fit the absorption spectra of H<sub>2</sub>O. Cavity temperature and pressure, laser path length, and absorption are recorded during the measurement. Based on Beer-Lambert's law, these records are used to calculate the concentrations of the individual isotopologues of H<sub>2</sub>O and the corresponding absolute isotope ratios (Lis *et al.* 2008).

Compared to the conventional method IRMS, OA-ICOS has numerous advantages (see Lis *et al.* 2008). Instead of time- and labour-intensive sample preparations prior analysis, the samples were simply filtered to remove any particulates that could clog the syringe or contaminate the instrument. Note that there is a threshold of 4 g/L of total dissolved solids in the fluids. Above this value, it becomes necessary to dilute or distillate the samples. Reverse osmosis is another promising method to reduce the salinity of the samples.

Los Gatos Research (LGR) recommends an “interleaved” analysis pattern, where a set of three samples is run after each standard. In the applied routine, five standards (see appendix Table A 7) were measured in rotating order, starting with standard 2. Every interleaved sample set was composed of two unknown samples from the investigation area, followed by deionised water to prevent salt deposition in the syringe. Each vial was sampled 20 times, and the first five measurements were discarded to reduce memory effects. Hence, the final values are based on the average of the last 15 injections.

The final results are reported as  $\delta D$  and  $\delta^{18}O$  values in ‰ relative to VSMOW (Vienna Standard Mean Ocean Water).

### **4.3.2 Sulphur and Sulphate Oxygen Isotopes**

#### **4.3.2.1 Sample Preparation**

Various procedures were necessary to extract the sulphur species of interest from the different sample materials. Table A 4 in the Appendix summarizes the applied procedures. The methodologies were adapted from various different institutes and researches. The respective references are given in the individual sections. In general, procedures were designed to avoid fractionation of the isotopes and to give high yields of analyzable materials. If not stated otherwise, samples were prepared at the chair of Hydrogeology at the TU Bergakademie Freiberg.

Various solutions were needed during the procedures. Table A 5 gives a list of necessary materials and a brief description of the preparation procedures.

##### **a) Aquatic sulphides**

In the field, aquatic sulphide was extracted from the water by precipitation of ZnS. Unfortunately, co-precipitation of other substances must have occurred. The colour of the salts ranged from white to brownish and black. Consequently, the precipitates had to be re-dissolved and precipitated again to form pure ZnS. The procedure was conducted with a distillation unit. A scheme of the device is given in Figure 13. Installation of the device and the execution of the procedure were conducted analogically to the lab routines at the UFZ.

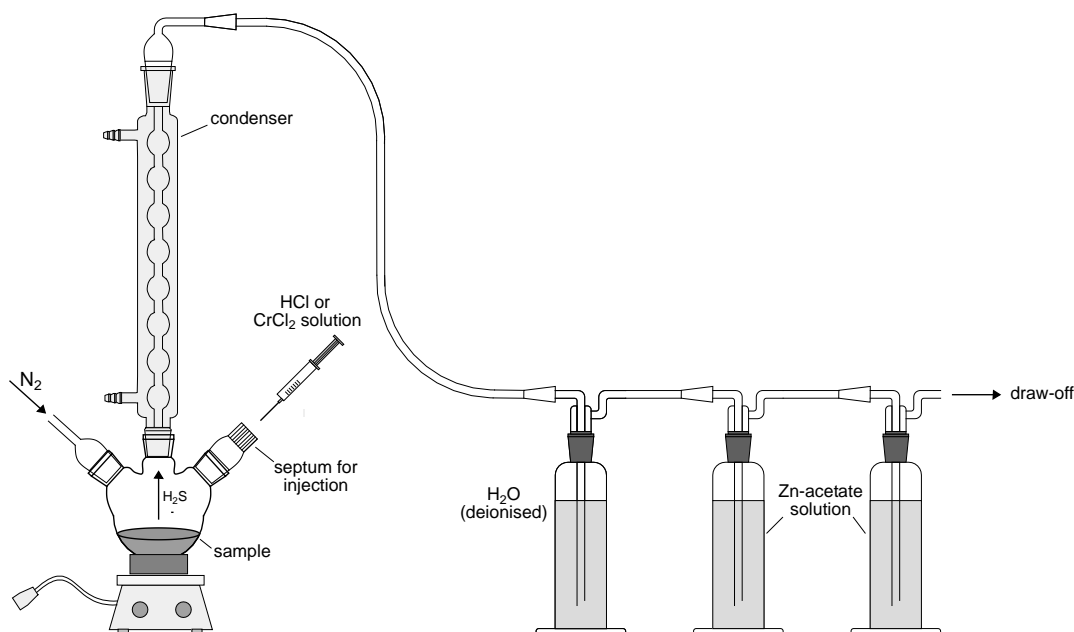


Figure 13: Distillation unit for the extraction of mono- and disulfides.

Generally, it can be differentiated between sulphur species that are soluble in hydrochloric acid (acid-volatile sulphur, AVS) and those that are soluble in chromium-(II) solution (chromium reducible sulphur, CRS) (Billon *et al.* 2001). The ZnS precipitates from water samples were treated with HCl only.

Filters containing ZnS were placed into a three-neck round-bottom flask. The device was sealed and flushed with nitrogen (PRAXAIR, product quality 5.0) for several minutes to remove all oxygen from the system. The gas flow rate was adjusted to 2-4 bubbles per second. At next, 20-40 mL 6 N HCl was added through a septum in steps of 5 mL. The objective of this step is, to convert ZnS into dissolved, volatile hydrogen sulphide. The flasks were heated for about one hour. With nitrogen as carrier, emerging H<sub>2</sub>S was flushed into a glass bottle containing 3 % ammonia zinc acetate solution, where it precipitated as ZnS. The solution was transferred into beakers and 20-30 mL 0.1 M silver nitrate solution was added to convert ZnS to Ag<sub>2</sub>S. For better coagulation of the precipitate, the mixture was boiled shortly. The precipitate was collected on a 0.45 µm filter and washed with 25% ammonia solution until the filtrate was free of chlorine. Simultaneously, co-precipitated AgOH and Ag<sub>2</sub>O were dissolved. The remaining Ag<sub>2</sub>S precipitate was air-dried.

**b) Aquatic sulphate**

Based on recommendations of Haubrich (2011), about 10 mg BaSO<sub>4</sub> precipitate were stirred into deionised water and collected on a 0.47 µm filter paper. It was then washed until all residual chlorine from the acidification routine was removed. Whether the precipitate is free of chlorine was tested by adding 10% AgNO<sub>3</sub> solution to the filtrate. When chlorine is present in the filtrate, AgCl forms, and a white cloudiness can be observed. The precipitate was dried over night at 40 °C. For δ<sup>18</sup>O analysis, no further preparations were required. For δ<sup>34</sup>S analysis, BaSO<sub>4</sub> samples were glowed at 600 °C in a muffle furnace for about one hour.

**c) Gypsum**

Various types of gypsum samples were gathered during fieldwork. Their preparation resembles the treatment of sulphate dissolved in water (Haubrich 2011). At first, 100-150 mg gypsum was pulverized and stirred in about 200 mL deionised water until it dissolved completely. Insoluble components were removed by filtration. The filtrate was treated like any other water sample that is subject to δ<sup>34</sup>S analysis in aqueous sulphate. Accordingly, HCl was added until the solution reached pH 4. Then, 1-2 mL of 1.5 M BaCl<sub>2</sub>·2H<sub>2</sub>O solution was added for BaSO<sub>4</sub> precipitation. The precipitate was collected on a filter, washed to remove chlorine and dried at 40 °C. It was continued as described in paragraph b.

**d) Sulphate in carbonate rocks**

Kampschulte *et al.* (2001) suggest a two step extraction procedure of sulphate from carbonate rocks. At first, the rock powder is treated with NaCl to extract discrete sulphate minerals. The remaining powder is then treated with HCl to gather sulphate that is bound to calcite crystals. However, the limestone samples from Oligocene Formation contain very little sulphur (0.07 – 4.9 mg/g). It was therefore decided to disregard the different bonding types and to extract all present sulphate in only one step.

Depending on their expected sulphur content (based on XRF values), 3-25 g rock powder was dissolved in 10% HCl. About 200 mL deionised water were added to the resulting solution in order to dilute the acid. Insoluble components were removed by filtration. The filtrate was treated as described in section b.

### e) Elemental sulphur

The elemental sulphur which was sampled from the cave walls does not require extensive preparation (Haubrich 2011). It was simply washed with deionised water, in order to remove all sulphate and chlorine before analysis. The sulphur was dried and homogenized.

### f) Sulphur in crude oil

Traditionally, sulphur extraction from crude oil is conducted using the Parr bomb oxidation method first described by Siegfried *et al.* (1951). However, it involves expensive apertures and a dangerous procedure, so an alternative method was needed. Based on the procedures given in Hearn *et al.* (2005) and Ostermann *et al.* (2003), and on personal recommendation of the latter, digestion of crude oil was performed using an *MLS Start 1500* microwave oven. Details of the microwave program are given in Table 4.

0.15 – 0.2 g untreated crude oil were weighed into Teflon vessels and covered by nitric acid and H<sub>2</sub>O<sub>2</sub>. This way, altogether 1.65 g oil was digested. One vessel was filled with the digestion acids only, to obtain a blind value. A thermometer was installed in one of the oil containing vessels to monitor the temperature during the procedure.

Table 4: Microwave digestion conditions

Sample weight	0.15 – 0.18 g
Digestion acids	8 mL HNO <sub>3</sub> (65%, p. A.) + 1 mL H <sub>2</sub> O <sub>2</sub> (30%, suprapure)
Maximum temperature	210 °C
Settings: Stage 1	Heat to 90 °C in 10 min; Constant for 5 min
Settings: Stage 2	Heat to 150 °C in 10 min; Constant for 5 min
Settings: Stage 3	Heat to 210 °C in 10 min; Constant for 15 min; Cool down

The digestion resulted in a clear, yellowish solution. Any sulphur present in solution should now be fully oxidised to SO<sub>4</sub><sup>2-</sup>. In case, some sulphur did not reach the highest oxidation state yet, a few mL of bromine water was added to the solution. Also, the pH was elevated to about 3 by the addition of 6 M NaOH (FISHER CHEMICAL, p.a.). Then, the solution was filtrated and 2 mL of 1.5 M BaCl<sub>2</sub>·2H<sub>2</sub>O solution was added and left for reaction. At the next day, precipitated BaSO<sub>4</sub> was gathered by filtration, washed with deionised water and air dried for analysis.

### g) Cave sediments: Sequential extraction of sulphur species

In order to determine the necessary extraction steps, sediments were analysed for their mineral composition by *X-ray diffraction* (see chapter 4.2.3 for details). The sediments were found to contain sulphate minerals, elemental sulphur and pyrite in differing amounts. The species were sequentially extracted by the procedure outlined in Figure 14 (adapted from Rees and Holt 1991, Knöller and Schubert 2010, and de Groot 2009).

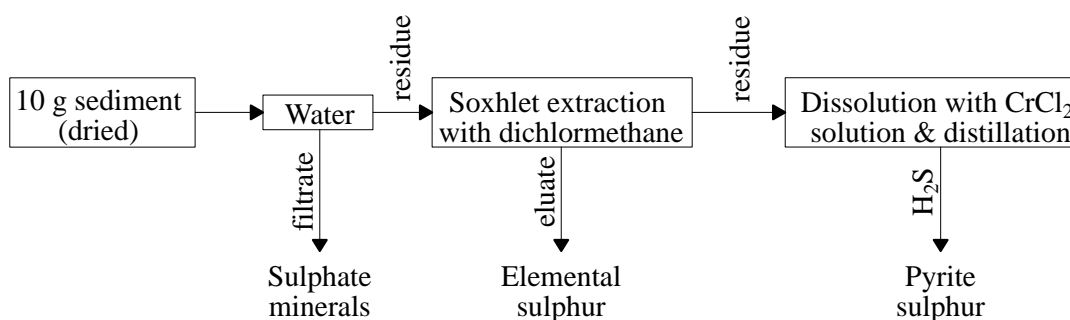


Figure 14: Sequential extraction of sulphur species from cave sediments

**Sulphate sulphur:** 10 g dried (at 40 °C), homogenized sediment was stirred in 1 L deionised water for 1 h. The insoluble, sulphate-free portion was collected on a 0.47 µm filter paper and dried in an evacuated exsiccator. BaSO<sub>4</sub> was precipitated from the filtrate as outlined in paragraph a and c.

**Elemental sulphur:** A Soxhlet extractor was used for the recovery of elemental sulphur from the sediment residues. 250 mL dichloromethane (Merck, ≥ 99.8%) served as solvent. The continuous distillation process was conducted for 11 hours. The procedure was followed by solvent regeneration (at room temperature, supported by vacuum), which led to oversaturation and subsequent crystallization of sulphur. The crystals were washed with deionised water and dried at room temperature.

**Pyrite sulphur:** Pyrite belongs to the Cr<sup>2+</sup> reducible sulphides (Carmody *et al.* 1998). Accordingly, 30-40 mL freshly prepared CrCl<sub>2</sub> solution was added step-wise to the residual sample and the solution was boiled for about three hours. As before, produced H<sub>2</sub>S was trapped in Zn-acetate solution. Produced ZnS was re-precipitated as Ag<sub>2</sub>S as described in paragraph b.

The preparation of most solutions is very straight forward, and the information in Table A 5 is sufficient. However, this is not the case for chromium-(II) solution, which is necessary for the reduction of pyrite. Accordingly, a detailed description of the preparation procedure is given in the following section.

### Preparation of chromium-(II) solution

Chromium-(II) solution was prepared on the basis of the procedures described in Canfield *et al.* (1986) and Tuttle (1986) and on the lab routine of the *Stable Isotope Geochemistry Laboratory* of the TUBAF.

At first, 194 g  $\text{CrCl}_3 \cdot 2 \text{H}_2\text{O}$  (VEB Laborchemie Apolda, p.a.) were dissolved in 1 L 0.1 M HCl to produce  $\text{CrCl}_3$  solution. A dark-green solution formed.

Zinc was employed to reduce  $\text{Cr}^{3+}$  to  $\text{Cr}^{2+}$ . In order to avoid the simultaneous formation of metal hydroxides, the pH of the solution must be kept low. Unfortunately, zinc does not only reduce  $\text{Cr}^{3+}$ , but also  $\text{H}_3\text{O}^+$  to form  $\text{H}_2$ . However, the latter reaction can be repressed by a thin amalgam layer on the surface of the zinc. Small zinc plates (Roth and Aldrich, both  $\geq 99.99\%$ , p.a.) were washed with deionised water. They were transferred into a separation funnel until they accounted for about two thirds of the funnel's volume. The granules were covered with 1 M HCl (p.a.) for about one minute. Then, about 100 mL 0.25 M mercury(II) chloride solution was added to the zinc and the funnel was shaken thoroughly until the zinc plates became a polished-silvery appearance.

The solution was drained and about 120 mL  $\text{CrCl}_3$  solution (ca. 2 cm excess above zinc plates) as well as 15 mL concentrated hydrochloric acid was added. The mixture was shaken and evacuated every 10-15 min for several hours. This led to reduction of the initial solution. The colour changed from dark-green to turquoise-blue (see Figure 15), reflecting the valence change from chromic(III) to chromous(II) ion.



Figure 15: Chromium chloride solutions before (left) and after (right) reduction.

The solution was gathered from the funnel under a stream of nitrogen. Due to atmospheric oxidation of  $\text{CrCl}_2$  solution, extracted portions were used immediately.

---

**h) Cave sediments: Total sulphur extraction using the Eschka method**

Except cooling, no other method of preservation had been applied to the sediments after sampling. Hence, the relative abundances of sulphur species may have shifted due to oxidation reactions, and accordingly, isotopic fractionations may have occurred. However, the  $\delta^{34}\text{S}$  value of the entire sulphur in specific samples should remain constant and reflect the combined results of all three sequentially extracted sulphur species.

The extraction of sulphur was conducted as described by Kester *et al.* (2001) and ISO 334 (1999-12). 2 g of dry sediment was mixed with three times the weight of Eschka's mixture (two parts MgO + one part anhydrous  $\text{Na}_2\text{CO}_3$  by weight) in a ceramic crucible, and covered with an additional 3 g Eschka's mixture. The crucible was placed in a muffle furnace, slowly heated to 820 °C, and kept at this temperature for 6 hours. After cooling, the mixture was dissolved in 200 mL deionised water, heated for 30 minutes and filtrated. Then, the filtrate was adjusted to pH ~ 4 with 6 M HCl. 5-10 mL of bromine water was added to oxidize all sulphur species to sulphate. The solution was boiled to expel excess bromine and 1-2 mL of 1.5 M  $\text{BaCl}_2 \cdot 2\text{H}_2\text{O}$  solution was added for  $\text{BaSO}_4$  precipitation. The solution was boiled for another 10 minutes and left to digest for several hours. The  $\text{BaSO}_4$  precipitate was collected on a filter, rinsed, dried and further prepared for analysis as described in paragraph b.

### 4.3.2.2 Analysis

The relative abundances of sulphur and sulphate oxygen isotopes of prepared materials were determined at the UFZ Halle, and in parts additionally at the chair of Mineralogy at the TU Bergakademie Freiberg.

For  $\delta^{18}\text{O}$  analysis at the UFZ Halle, 425  $\mu\text{g}$  ( $\pm 25 \mu\text{g}$ ) homogenized  $\text{BaSO}_4$  was weighed into silver capsules. Prior sealing of the capsule, a small spatula C+Ni mixture (10:1) was added. Per sample, two capsules were prepared.

For  $\delta^{34}\text{S}$  analysis, homogenized  $\text{BaSO}_4$ ,  $\text{Ag}_2\text{S}$ ,  $\text{ZnS}$ ,  $\text{FeS}_2$  and  $\text{S}^0$  were weighed into tin capsules. The oxidizing agent vanadium pentoxide ( $\text{V}_2\text{O}_5$ ) was added prior sealing of the capsule. The weighed masses vary between materials and institutes (see Table 5 for details).

Table 5: Methodological details of IRMS analysis of  $\delta^{34}\text{S}$  and  $\delta^{18}\text{O}$  ratios in different sulphur species and laboratories.

Material	Isotope ratio of interest	Lab	Amount taken for analysis [ $\mu\text{g}$ ]	Oxidizing agent / catalyst added	Capsule material	Capsules per sample	Analytical precision
$\text{Ag}_2\text{S}$	$\delta^{34}\text{S}$	UFZ	300 - 320	Spatula $\text{V}_2\text{O}_5$	Tin	2	$\pm 0.4 \text{ ‰}$ VCDT
$\text{ZnS}$	$\delta^{34}\text{S}$	UFZ	120 - 150	Spatula $\text{V}_2\text{O}_5$	Tin	2	$\pm 0.4 \text{ ‰}$ VCDT
$\text{FeS}_2$	$\delta^{34}\text{S}$	UFZ	75 - 95	Spatula $\text{V}_2\text{O}_5$	Tin	2	$\pm 0.4 \text{ ‰}$ VCDT
$\text{S}^0$	$\delta^{34}\text{S}$	UFZ	40 - 50	Spatula $\text{V}_2\text{O}_5$	Tin	2	$\pm 0.4 \text{ ‰}$ VCDT
		TUBAF	35-40	35-40 $\mu\text{g}$ $\text{V}_2\text{O}_5$	Tin	3	$\pm 0.3 \text{ ‰}$ VCDT
$\text{BaSO}_4$	$\delta^{34}\text{S}$	UFZ	350 - 370	Spatula $\text{V}_2\text{O}_5$	Tin	2	$\pm 0.4 \text{ ‰}$ VCDT
		TUBAF	260 - 300	260 - 300 $\mu\text{g}$ $\text{V}_2\text{O}_5$	Tin	3	$\pm 0.3 \text{ ‰}$ VCDT
	$\delta^{18}\text{O}$	UFZ	400 - 450	Spatula C+Ni (10:1)	Silver	2	$\pm 0.6 \text{ ‰}$ VSMOW

### ➤ Analysis at the UFZ

For determination of the sulphur isotope composition of  $S^0$ ,  $BaSO_4$ ,  $Ag_2S$ ,  $ZnS$ , and  $FeS_2$  the materials had to be converted to pure  $SO_2$  to permit analysis by isotope ratio mass spectrometry (IRMS). An elemental analyzer from HEKAtech (model CAP 4012) was employed to combust the sulphur samples together with  $V_2O_2$  and  $O_2$ . The sulphur isotopic composition of produced  $SO_2$  was determined on a continuous flow II IRMS delta S from Finnigan MAT. All samples were measured in duplicates.

$SO_2$  was produced by combusting the sulphur samples with  $V_2O_5$  and  $O_2$  in an elemental analyzer from HEKAtech. The sulphur isotope ratios of resulting  $SO_2$  were measured on a continuous-flow IRMS Delta Plus from ThermoQuest Finnigan.

Analysis of oxygen isotopes in sulphates started with high temperature ( $1450^\circ C$ ) pyrolysis of  $BaSO_4$  in a glassy-carbon-tube of an elemental analyzer from HEKAtech. There, sulphate oxygen reacted to CO. The final measurement of  $^{18}O/^{16}O$  ratios was carried out with a continuous-flow III IRMS delta S from Finnigan MAT. Samples were measured in duplicates.

The values were calibrated using internal standards for  $SO_2$  and  $BaSO_4$ , as well as several international reference standards for  $BaSO_4$  and  $Ag_2S$  (see appendix Table A 7) The results are reported as  $\delta^{34}S$  and  $\delta^{18}O$  values in per mill relative to the VCDT (Vienna Cañon Diablo Troilite) and VSMOW (Vienna Standard Mean Ocean Water) standard, respectively.

### ➤ Analysis at the TUBAF

Determination of sulphur isotopes in  $S^0$  and  $BaSO_4$  resembled the analysed at the UFZ. The materials were combusted in an elemental analyzer from HEKAtech (model: EA 1110 CHN). The sulphur isotope ratio of produced  $SO_2$  was then measured on a continuous-flow IRMS Delta Plus from ThermoQuest Finnigan. All samples were analyzed in triplicate. The values were calibrated using internal and international reference standards (see Table A 7). The results are reported in per mill  $\delta$ -deviation from VCDT, with an overall analytical precision of better than  $\pm 0.3 \text{ ‰}$ .

## 4.4 Data Processing, Calculations and Statistics

### 4.4.1 Processing of XRD Data

Raw data were checked for missing values, outliers and concentrations below the detection limit. Prior usage of the data, values below the detection limit were replaced by  $0.3 \cdot$  detection limit.

### 4.4.2 General Yield Calculations

An important aspect of method evaluations is a thorough examination of product yields. In this thesis, such calculations were necessary for several problems, for example:

- Evaluating, how much  $\text{H}_2\text{S}$  can be precipitated with the Zn-acetate solution
- Relating  $\text{Ag}_2\text{S}$  yields to the  $\text{H}_2\text{S}$  concentration in water prior extraction
- Determining the theoretical  $\text{BaSO}_4$  yield from gypsum preparations
- Relating  $\text{BaSO}_4$  and  $\text{Ag}_2\text{S}$  yields from sediments to gypsum and pyrite contents

The calculations were based on the stoichiometry of the respective, balanced reactions, and the basic equations used for the calculations, were:

$$\frac{m_1}{M_1} = \frac{m_2}{M_2} \quad [11]$$

$$\frac{\text{actual yield [g]}}{\text{theoretical yield [g]}} \cdot 100\% = \text{percent yield} \quad [12]$$

With  $m_{1,2}$  = mass of the respective species [g]

$M_{1,2}$  = Molar mass of respective species [g/mol]

### 4.4.3 Calculation of the Total Sulphur Isotopic Composition of Water

The total sulphur isotopic composition of water was computed by the following equation:

$$\delta^{34}\text{S}_{\text{total}} = \frac{(\delta^{34}\text{S}_{\text{SO}_4} \cdot \text{S}_{\text{SO}_4}) + (\delta^{34}\text{S}_{\text{HS}^-} \cdot \text{S}_{\text{HS}^-})}{\text{S}_{\text{total}}} \quad [13]$$

With  $\text{S}_{\text{total}}$  = total sulphur concentration in water [mg/L]

$\text{S}_{\text{SO}_4, \text{HS}^-}$  = sulphur concentration of the respective sulphur species [mg/L].

#### 4.4.4 Calculation of Total Sulphur Concentration and $\delta^{34}\text{S}$ Composition of Sediments

Theoretically, total (Eschka) extraction and sequential extraction of sedimentary sulphur species should result in the same total sulphur concentration and  $\delta^{34}\text{S}$  composition. The first step towards a comparison of methods was the calculation of the respective values:

Total sulphur extraction with the Eschka method gave  $\text{BaSO}_4$  as final precipitate. Sulphur content was calculated from  $\text{BaSO}_4$  yields and related to the mass of the sediment, it was extracted from.

Sulphate sulphur (gypsum, bassanite, anhydrite), elemental sulphur, and pyrite have been extracted stepwise. Total sulphur content of sediments was calculated based on the yields of extracted specimen. While  $\text{BaSO}_4$  precipitates represent the sulphate species and  $\text{Ag}_2\text{S}$  precipitates represents pyrite, elemental sulphur remained the same. Equation [14] summarizes the overall concept and equation [15] gives more detailed information about the calculation of the total sulphur concentration. Equation [16] was used to calculate the total sulphur isotopic composition, as it should be in theory.

$$S_{\text{total}} = S_{\text{S}^0} + S_{\text{FeS}_2} + S_{\text{SO}_4} \quad [14]$$

$$S_{\text{total}} = M_{\text{S}} \left( \frac{m_{\text{S}^0}}{M_{\text{S}^0}} + \frac{m_{\text{Ag}_2\text{S}}}{M_{\text{Ag}_2\text{S}}} + \frac{m_{\text{BaSO}_4}}{M_{\text{BaSO}_4}} \right) \quad [15]$$

$$\delta^{34}\text{S}_{\text{total}} = \frac{\delta^{34}\text{S}_{\text{S}^0} \cdot S_{\text{S}^0} + \delta^{34}\text{S}_{\text{Ag}_2\text{S}} \cdot S_{\text{Ag}_2\text{S}} + \delta^{34}\text{S}_{\text{BaSO}_4} \cdot S_{\text{BaSO}_4}}{S_{\text{total}}} \quad [16]$$

With: $S_{\text{total}}$	= total sulphur concentration in sediments [mg/g]
$S_{\text{S}^0, \text{Ag}_2\text{S}, \text{FeS}_2, \text{SO}_4}$	= sulphur concentration with respect to a particular sulphur species (e.g. sulphate sulphur), in relation to sediment mass [mg/g]
$m_{\text{S}^0, \text{Ag}_2\text{S}, \text{BaSO}_4}$	= mass of sulphur species (e.g. $\text{BaSO}_4$ ) obtained by sequential extraction, related to the sediment mass [mg/g]
$M_{\text{S}^0, \text{Ag}_2\text{S}, \text{BaSO}_4}$	= Molar mass of sulphur species [g/mol]
$\delta^{34}\text{S}_{\text{S}^0, \text{Ag}_2\text{S}, \text{BaSO}_4}$	= $\delta^{34}\text{S}$ values of individual sulphur species in ‰ vs. VCDT
$\delta^{34}\text{S}_{\text{total}}$	= theoretical $\delta^{34}\text{S}$ value of all sulphur species combined [‰ VCDT]

#### 4.4.5 Statistical Analyses

The data sets were too small and inhomogeneous to conduct major statistical analyses. However, because several samples were analyzed at the UFZ and at the TUBAF, an appropriate tool was needed to compare the two data sets. Bland and Altman (1986) argued that the correlation coefficient is an inappropriate tool to assess the agreement between methods or instruments. And Grouven *et al.* (2007) demonstrated that a paired t-test can lead to paradox results. Accordingly, an alternative approach suggested by Bland and Altmann (1986) was used: The data were plotted as difference of the values from the laboratories against the mean value. Using this plot, dimensions and pattern of individual deviations between measurements can be better assessed than with simple scatter plots (Grouven *et al.* 2007). The lack of agreement was summarized by calculating the bias, which was estimated by the mean difference  $d$  and the standard deviation  $s$  of the differences. Beforehand, a Kolmogorov-Smirnov test was conducted using program Statgraphics Centurion XVI, in order to check for normal distribution of the differences. The test could not reject normal distribution. Therefore, 95 % of the differences are expected to fall between  $d + 2 \cdot s$  and  $d - 2 \cdot s$  (after Bland and Altmann 1986).

## 4.5 16S rRNA Gene Analysis

Traditionally, microorganisms are analyzed by light microscopic observation and cultivation of microbial colonies. Unfortunately, only a small fraction of microorganisms is actually cultivable on standard laboratory media. In order to obtain culture-independent information about the microbial communities, a selection of molecular biological techniques was employed. The flow chart in Figure 16 and the associated text summarize the overall procedure.

### 4.5.1 DNA Extraction

DNA extraction from biofilms, sediments and cave wall material was carried out at the *Kurdistan Institution for Strategic Studies and Scientific Research* by using the *PowerSoil DNA Isolation Kit* from MOBIO Laboratories. The procedure was conducted as explained in the accompanying manual. At first, extracted DNA was stored in a buffer solution at  $-20^{\circ}\text{C}$ . However, due to the upcoming transport to Germany, and the associated risk of freeze-thaw cycles that might damage the DNA, another method of preservation was applied later on. In a nearby hospital, the DNA was dried at  $30^{\circ}\text{C}$  by the instrument *Concentrator plus* from Eppendorf. During spinning like a centrifuge, a vacuum was created and the buffer solution was carried away, leaving the DNA behind.

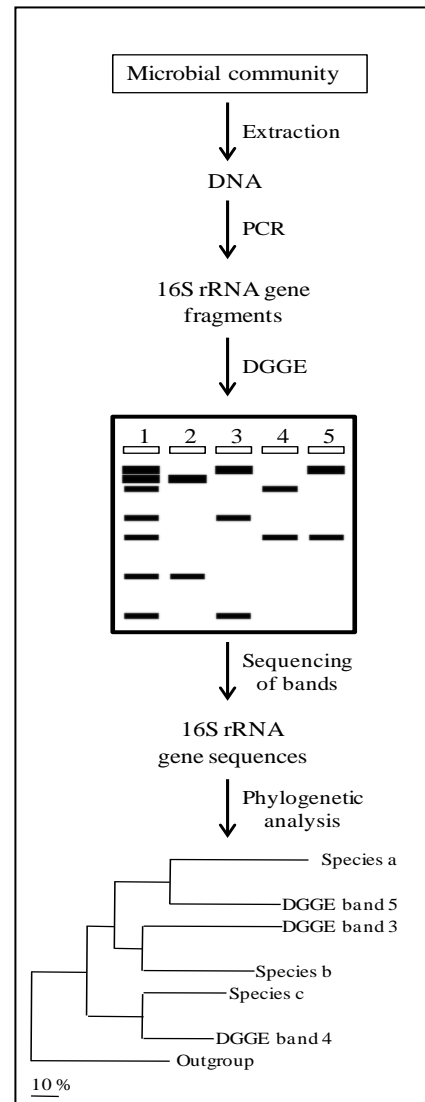


Figure 16: Flow diagram showing the different steps in the analysis of the microbial community structure by PCR-DGGE. At first, DNA was extracted from environmental samples. This DNA was then used to amplify 16S rRNA encoding genes by polymerase chain reaction (PCR). These amplified fragments were separated by denaturing gradient gel electrophoresis (DGGE). Individual, separated bands were excised from the gel and sequenced to identify community members. Diagram based on Muyzer 1999.

### 4.5.2 PCR-DGGE

DNA extracts were analyzed at the *Microbiology Department of the Bremen Institute for Material Testing* (MPA) by combining the advantages of *polymerase chain reaction* (PCR) and *denaturing gradient gel electrophoresis* (DGGE).

PCR is a powerful method used for repetitive in vitro copying of a specific section of double stranded DNA. Depending on the target sequence, different sets of specific oligonucleotide primers are required. The MPA used the DGGE-primers in Table 6, which target the 16S rRNA gene.

Table 6: DGGE primers

Name	Direction	Base pairs	Sequence	Conc. [pMol/ $\mu$ l]
Ba101f-GC	Forward	58	CGCCCGCCGCGCCCCGCGCCCGTCCCGCC GCCCCCGCCCGTGGCGGACGGGTGAGTAA	100
BA518f	Reverse	20	CGTATTACCGCGGCTGCTGG	100

The applied temperature program of the PCR was as follows:

- 1) **Initial denaturation:** The two strands of the DNA were separated by heating (95 °C for 3 minutes).
- 2) **Denaturation:** 94 °C for 45 sec
- 3) **Annealing:** The strands were cooled down. The primers annealed to the template DNA and served as starting points for DNA replication by Tag DNA polymerase (62 °C for 20 seconds).
- 4) **Elongation:** The temperature was raised again, in order to let the Tag DNA polymerase bind the primers and synthesize a new DNA strand. Individual deoxynucleotides were used as raw material (72 °C for 20 sec).
- 5) **Final elongation:** 72 °C for 3 min
- 6) **Storage:** 10 °C

Steps 2-4 were repeated rapidly 40 times to obtain a sufficient quantity of the gene.

Afterwards, PCR products were separated by DGGE. The principle of DGGE relies on electrophoretic separation of DNA fragments that are identical in length but differ in sequence. The main difference to conventional gel electrophoresis is that the polyacrylamide gel contains a gradient of increasing DNA denaturants, namely urea and formamide. The technique takes advantage of the fact, that guanine-cytosine pairs (GC) are more stable than adenosine-thymine pairs. Accordingly, DNA fragments richer in GC, denature further down the gel. Denatured DNA molecules become effectively larger and therefore less mobile until they finally stop in the gel (Green *et al.* 2010). Detailed and

comprehensive information about underlying principles are for instance given in Muyzer (1999) and Ercolini (2004).

Two stock solutions (Table 7) of different denaturing strength were used to create a continuous gradient in the gel. The DGGE chamber was prepared according to the specifications of the manufacturer (BioRad). Depending on the yield of the PCR, 8-25  $\mu\text{L}$  DNA was loaded onto the gel. The electrophoresis was run at 58 °C for 16 hours, at a voltage of 100 V.

Table 7: Stock solutions for preparing a denaturing gradient in the DGGE gel.

Solution	Denaturing strength	Preparation
6 % Acrylamide	0 %	15 mL of 40 % acrylamide (37.5:1, acrylamide : bis-acrylamide), add 2 mL of 50X TAE and fill up with $\text{H}_2\text{O}_{\text{bidest}}$ to 100 mL. Shortly before usage: addition of 25 $\mu\text{L}$ freshly prepared APS (10% in $\text{H}_2\text{O}_{\text{bidest}}$ ) and 5 $\mu\text{L}$ TEMED (N,N,N',N'-tetramethylethylenediamine).
8 % Acrylamide	80 %	18 mL of 40 % acrylamide (37.5:1, acrylamide : bis-acrylamide), add 2 mL of 50X TAE, 32 mL formamide, a few mL $\text{H}_2\text{O}_{\text{bidest}}$ , add 33.6 g urea, and fill up with $\text{H}_2\text{O}_{\text{bidest}}$ to 100 mL. Shortly before usage: addition of 25 $\mu\text{L}$ freshly prepared APS and 10 $\mu\text{L}$ TEMED.

The gel was stained using a GelRed<sup>TM</sup>-bath (0.5-fold in 100mM NaCl, initial concentration 10,000-fold in DMSO). Visualized bands were excised from the gel and placed in a bath of 10  $\mu\text{L}$   $\text{H}_2\text{O}_{\text{bidest}}$  over night, to allow the diffusion of DNA from the gel to the water. In order to obtain a higher yield of the individual sequences, PCR was run a second time. The amplified fragments were sent to *LGC Genomics* for analysis of the sequences.

### 4.5.3 Sequencing

Determination of DNA sequences was accomplished by *LGC Genomics*, using the traditional Sanger approach. The primers used for sequencing the 16S gene fragment are given in Table 8. For detailed information about the methodology, the reader is referred to Sanger's original research paper (1977) and to comprehensive reviews such as Sterky and Lundeberg (2000).

Table 8: Sequencing primers for the 16S gene fragment

Name	Direction	Base pairs	Sequence	Conc. [pMol/ $\mu\text{L}$ ]
515f	Forward	20	GTGCCAGCMGCCGCGGTAA	100
907rc	Reverse	19	CCGTCAATTCCTTTRAGTTT	100

Wobbles: R = A+C and M = A+G; used to compensate for variability in the target sequence

Two different services of *LGC Genomics* were tested, namely *Ready2Run* as well as the current offer *Microtiter plate* (MTP) sequencing. *Ready2Run* is the basic service of *LGC Genomics*, and primers were added to purified templates by MPA prior transport. For MTP sequencing, the PCR product was pipetted directly into microtiter plates. In this case, DNA purification and addition of primers was undertaken by *LGC Genomics*.

#### 4.5.4 Alignment of the Sequences

Sequencing of the 16S rRNA encoding gene fragments gives separate results for forward- and reverse-sequences. The MPA used the software *BioEdit*<sup>3</sup> to trim off untrustworthy sequences at the ends and to align the fragmental sequences to form complete “consensus-sequences”. A distance matrix was used to compute similarities between the aligned sequences. The approximate positions of these sequences in the phylogenetic tree were determined with the webservices *nt-BLAST*<sup>4</sup> and *SepsiTest-BLAST*<sup>5</sup> (16S-rRNA).

In *BioEdit*, alignment of the sequences is merely based on the primary structure ( $\triangleq$  sequence of bases) of the DNA. In order to obtain better results, the program *Arb*<sup>6</sup> was used for re-aligning the sequences. The program includes information about the secondary structure ( $\triangleq$  basepair interactions) of the DNA and can thus refine the preliminary results. Aligned sequences were compared to those of catalogued species in the database LTP-102 – provided by the *Living-Tree-Project*<sup>7</sup> of *Arb* and several international partners. *Arb* was then used to refine previously determined positions of sequences in the phylogenetic tree using the maximum parsimony method. With this method, a tree is constructed that requires the minimum number of mutations.

---

<sup>3</sup> <http://www.mbio.ncsu.edu/bioedit/bioedit.html>

<sup>4</sup> [blast.ncbi.nlm.nih.gov](http://blast.ncbi.nlm.nih.gov)

<sup>5</sup> [www.sepsitest-blast.de](http://www.sepsitest-blast.de)

<sup>6</sup> [www.arb-home.de](http://www.arb-home.de)

<sup>7</sup> [www.arb-silva.de/projects/living-tree/](http://www.arb-silva.de/projects/living-tree/)

## 5 Results and Interpretation

This chapter is divided in several sub-chapters. The first deals with the evaluation of methods and errors. The chapter is followed by a presentation of mineralogical and geochemical results, microbiological findings, and stable isotopic results.

### 5.1 Evaluation of Methods and Errors

#### 5.1.1 Microbiological Analyses

It is critical to keep in mind, that the 16S rRNA gene analysis does not detect all organisms. More recent technologies, such as pyrosequencing, would give a fingerprint of the whole community, but DNA extraction combined with PCR amplification and DGGE separation merely allows the identification of dominant populations. Several DNA extracts from Darzila samples gave only one or two distinct bands on the DGGE gel – some extractions were not successful at all. The main reason for this is thought to be non-exhaustive DNA extraction. Especially soils and sediments are known for being problematic substances.

One of the very first steps during DNA extraction with the PowerSoil DNA Isolation Kit from MOBIO was bead-beating of the samples. The samples were vortexed together with small beads for 10 minutes at maximum speed, in order to rupture the microbial cells and to liberate their DNA. Obviously, this is a critical step. It might have been appropriate, to modify protocol instructions by prolonging bead-beating for several more minutes. Firm biofilm structures or sediments with stable mineral aggregates might need more processing. Except for simply extending bead-beating, it could be favourable to include freeze-thaw cycles into the extraction procedure. Liphay *et al.* (2004), who systematically tested the impact of the chosen DNA extraction method on the measured bacterial community composition, found that including freeze-thaw cycles can increase DNA yields significantly. Yet, their main findings were, that each extraction method resulted in unique community patterns, and that the efficiency differed with soil type.

After extraction and DGGE analysis, DNA was amplified via PCR. Theoretically, all replicated molecules are the exact copies of the original ones and the number of molecules is doubled after each replication cycle. In the real PCR, sequence artifacts and bias can impair DNA quality. These problems are well documented in publications, such as Kanagawa (2003) or Acinas *et al.* (2005). However, the impact of such problems is expected to be considerably smaller than that of DNA extraction.

In DGGE, gene sequences move through a gel that contains a gradient of increasing DNA denaturants. Depending on the melting domain, DNA denatures and moves more slowly, until it finally stops. Adding too much DNA leads to smears on the gel – then, overall resolution is low and it can be difficult to excise individual bands without contamination. DNA from complex communities can cause similar effects. In contrast, adding only a little DNA can make some bands too small to be clearly identified. So, even though DGGE analysis was done with great care, some organisms might have been missed.

Additionally to gene analyses, cultivation of microorganisms in crude oil was attempted. Crude oil components are generally difficult to degrade and microbial growth is very slow. The samples were incubated for around six months, but up to date, no degradation of complex organic matter could be observed. It may take years before there is clear evidence of microbial degradation.

### **5.1.2 X-ray Fluorescence Spectroscopy Data**

The analytical results are given in the Appendix (Table A 16). Data of gypsum samples were checked for their plausibility by stoichiometrically comparing their calcium and sulphur content. For most samples, calcium content was a little higher than sulphur content. However, sample DC-SG-13a and DC-SG-13b, which were taken from different layers of the wall, had elevated sulphur concentrations. Accordingly, elemental sulphur must be present in addition to gypsum.

### **5.1.3 Stable Isotopes of Water**

The analytical results are given in the appendix (Table A 19). The LWIA Post Analysis Software was used to assess measurement performance (temperature, pressure, number density of water molecules), to correct the measurements of standard solutions based on their actual compositions, to remove problematic data, to relate individual measurements to corrected standards, and to calculate mean values of the repetitions. The measurements were generally good and most data could be used for processing. Not a single injection of these samples was flagged to be problematic of any kind. Also, all sample data were initially checked with the LWIA Spectral Contamination Identifier Software, and for none of them, spectral interferences due to contaminations could be detected.

According to the manufacturer's instructions, water with more than 4 g/L total dissolved solids (TDS) should be subject to further treatment prior analysis. Because the instrument was new and not routinely used yet, this remark was overlooked and two samples with

elevated TDS values were measured despite of the given limitation. However, according to the manufacturer, this did neither damage the instrument nor deteriorate data quality (LGR 2012). The upper limit of 4 g/L is given to avoid salt accumulations in the syringe or the injector.

#### **5.1.4 Preparation of Gypsum for $\delta^{34}\text{S}$ and $\delta^{18}\text{O}$ Analysis**

Gypsum samples were pulverized, dissolved in deionised water, and filtrated. The filtrate was treated with  $\text{BaCl}_2$  to precipitate dissolved sulphate as  $\text{BaSO}_4$ . Accordingly,  $\text{BaSO}_4$  yields must reflect the prepared mass of gypsum that was prepared. When excluding the samples DC-SG-13a and -13b, which are not only composed of gypsum, sulphate recovery from gypsum ranged from 94.5 to 98.7 %.

#### **5.1.5 Preparation of Dissolved Sulphate $\delta^{34}\text{S}$ and $\delta^{18}\text{O}$ Analysis**

The addition of 10-20 mL 1.7 M  $\text{BaCl}_2 \cdot \text{H}_2\text{O}$  solution allows for a precipitation of about 1600 to 3300 mg sulphate. Based on IC analysis conducted by Heiland (2016), sulphate concentrations in the acidic puddles DC-W-4 and DC-W-6 were higher than 3300 mg/L (see appendix Table A 10). Accordingly, sulphate precipitation as  $\text{BaSO}_4$  was incomplete at these sites. However, since the reaction does not involve the breakage of S-O bonds, fractionations were expected to be small to negligible. This was confirmed by Knöller (2012), who conducted systematic tests on this issue and did not find any fractionation effects.

#### **5.1.6 Preparation of Mono- and Disulphides for $\delta^{34}\text{S}$ Analysis**

##### **5.1.6.1 Reference materials**

Apart from the samples of interest, sphalerite ( $(\text{Zn,Fe})\text{S}$ ) and pyrite ( $\text{FeS}_2$ ) isolates were prepared and analysed using the same methods. While sphalerite was dissolved using HCl, the pyrite isolate had to be treated with  $\text{CrCl}_2$  solution in order to produce hydrogen sulphide.  $\text{H}_2\text{S}$  was forced through a zink-acetate solution. The  $\text{ZnS}$  precipitate was re-precipitated as  $\text{Ag}_2\text{S}$  and analyzed together with the other samples. Sphalerite and pyrite were also analyzed directly, without any species conversion. Table 9 lists the relevant data. Due to small impurities of the initial substances and the unknown share of iron in sphalerite, it is not possible to determine, whether the low  $\text{Ag}_2\text{S}$  yield is caused by losses during preparation or predetermined by the initial composition. However, sulphur isotopic results can be compared. For both substances,  $\delta^{34}\text{S}$  of the prepared species is 0.4 ‰ vs. VCDT higher than of the original compounds. This could indicate a minor fractionation process –

caused by preferential volatilization of the lighter isotope. However, as the corresponding values are within the range of analytical precision, it can be stated that the preparation procedures did not cause a relevant fractionation of sulphur isotopes.

Table 9: Analysis of sphalerite and pyrite as reference materials.

	<b>Sphalerite, (Zn,Fe)S</b>		<b>Pyrite, FeS<sub>2</sub></b>	
	(Zn,Fe)S	Ag <sub>2</sub> S	FeS <sub>2</sub>	Ag <sub>2</sub> S
Analyzed as	(Zn,Fe)S	Ag <sub>2</sub> S	FeS <sub>2</sub>	Ag <sub>2</sub> S
Sample weight, initial [g]	-	0.1	-	0.1
Maximum possible yield [g]	-	0.25	-	0.41
Actual yield [g]	-	0.12	-	0.37
$\delta^{34}\text{S}$ [‰ VCDT]	$-0.8 \pm 0.4$	$-0.4 \pm 0.4$	$1.2 \pm 0.4$	$1.6 \pm 0.4$

### 5.1.6.2 Dissolved sulphide

In order to minimize sulphide oxidation and degassing, dissolved sulphide was precipitated as ZnS immediately after sampling. Also, the solution was left to react for about one day. Some of the precipitates were obviously contaminated with other reaction products. Accordingly, ZnS precipitates had to be re-dissolved and re-precipitated as described in the method section. By mass balance, it could be calculated how much of the theoretical sulphide content from the water that was recovered as Ag<sub>2</sub>S. Most of the yields were significantly different from those expected by photometrical data (Figure 17, Table A 9). Photometrical analysis was conducted for a few mL only. In contrast, the precipitates were gathered from 6 L or 10 L of water. The quality of photometrical data of dissolved sulphide was already questioned and discussed by Heiland (2016). Accordingly, sulphide concentrations determined by mass balance calculations are thought to be more reliable than photometrical data. Therefore, sulphide data used in the following chapters are based on these calculations.

The largest deviations from theoretical values were found in the samples DC-W-6 (acidic pool), DC-W-7 (floor feeder) and DW-W-1 (well). Based on the Ag<sub>2</sub>S precipitate, DC-W-6 contained around 200 times more sulphide than detected by photometry (10.04 mg/L instead of 0.05 mg/L). Similarly, DC-W-7 contained around 70 times more sulphide than expected (4.79 mg/L instead of 0.07 mg/L). In contrast, the recovered precipitate from well water (DW-W-1) accounted for considerably less sulphide than determined by photometry (11.9 mg/L instead of 49.92 mg/L). It could be suspected, that the added Zn-acetate solution was not sufficient to precipitate all dissolved sulphide. However, even if the photometrical

value was correct, in 50 ml of 0.169 M Zn-acetate solution,  $Zn^{2+}$  ions would still be present in excess to bind all sulphide present.

As described by Heiland (2016), the photometrical determination of sulphide in water is very error prone. Strongly reducing ions, such as sulphite, can interfere with the procedure by preventing the formation of the blue colour during photometry. Because no stabilisation technique was applied to preserve sulphite in the water, the effect cannot be quantified. However, considering that water from floor feeders are more heavily affected than creek or stream water, the initial presence of this species is very likely. Upon contact with the oxygenated cave atmosphere, it is oxidized quickly. In consequence, the content of interfering substances diminishes, too.

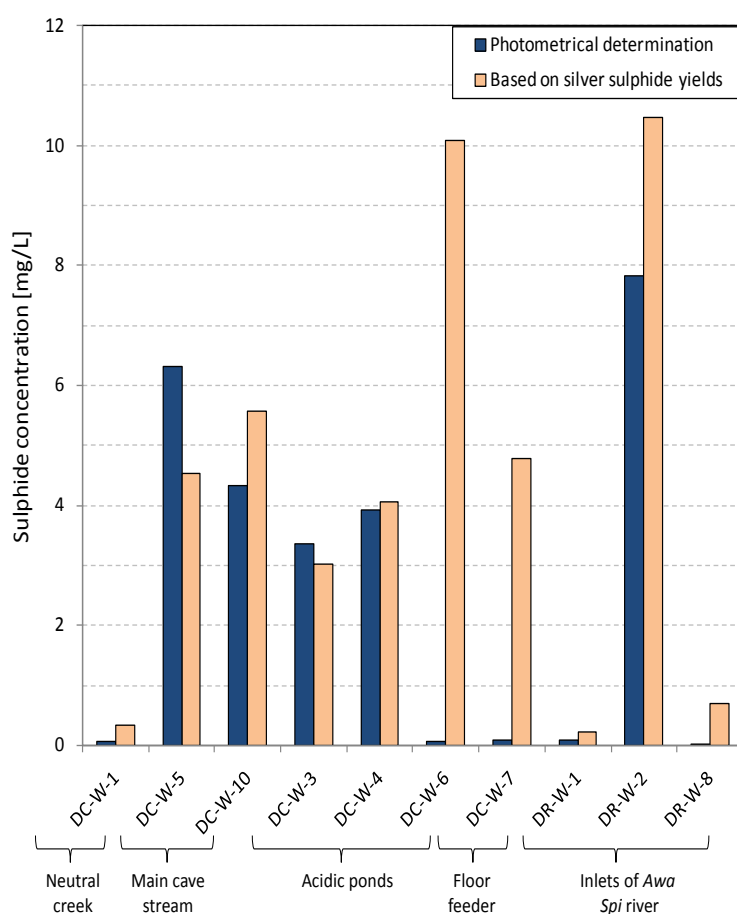


Figure 17: Dissolved sulphide concentration – determined by photometry (blue) and by mass balance calculations from  $Ag_2S$  precipitates (beige). Due to significantly higher concentrations that would change the scale, data from the well (DW-W-1) are not included.

### 5.1.7 Elemental, Mineralogical and $\delta^{34}\text{S}$ Analyses of Sediments

Sediments have been analysed by various methods. Their elemental and mineralogical composition was determined by X-ray fluorescence spectroscopy and X-ray diffraction, respectively. Furthermore, sediments were subject to total and sequential extraction of sulphur specimen for  $\delta^{34}\text{S}$  analysis.

#### 5.1.7.1 Total sulphur concentration and $\delta^{34}\text{S}$ composition

Theoretically, total (Eschka) extraction and sequential extraction of sedimentary sulphur species should result in the same total sulphur concentration and  $\delta^{34}\text{S}$  composition. The respective species were calculated as described in chapter 4.4.4. All sequential extractions gave lower sulphur yields than corresponding extractions with the Eschka method. Differences ranged from 2.2 mg to 4.7 mg. Considering that sequential extraction comprises several steps, in each of which sulphur can get lost, this result is expected. Differences in measured and calculated  $\delta^{34}\text{S}$  range from 0.3 to 0.96 ‰ vs. VCDT (Figure 18). Except for DC-S-9, calculated values from sequential extraction were all lower than measured values from total extraction. Most of these  $\delta^{34}\text{S}$  values were determined with an analytical precision of  $\pm 0.4$  ‰ VCDT, but there were exceptions: For DC-S-5,  $\delta^{34}\text{S}_{\text{total}}$  is based on a single measurement only. Accordingly, depicted error bars for this sample are only indicative. For the double determination of sulphate in DC-S-5 and pyrite in DC-S-9, analytical precision was not within the accepted range of  $\pm 0.4$  ‰. Instead, values had a difference of 2.1 ‰ and 2.2 ‰, respectively. These variations were accounted for when calculating the total sulphur isotopic composition of the sediments. Even though small differences could be observed, the two methods agreed very well.

The discrepancies between the total-S concentrations calculated from extraction yields and determined by XRF and XRD analyses are greater (see Figure 19 or Table A 24), but this can be attributed to a lack of homogeneity in the prepared sediment samples.

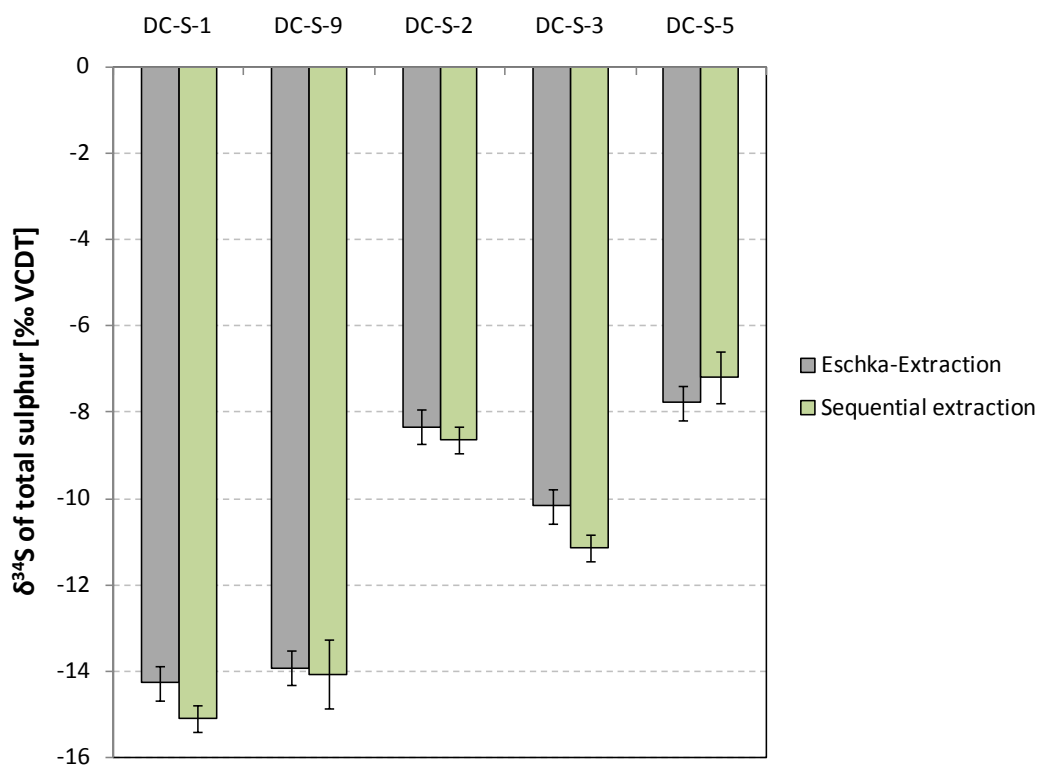


Figure 18: Comparison of  $\delta^{34}\text{S}$  values for total sedimentary sulphur, obtained by two different methods. With the Eschka-method, all sulphur was extracted at once – regardless of the species. The prepared  $\text{BaSO}_4$  was analyzed for its sulphur isotopic composition. In contrast, sequential extraction targeted individual species, namely sulphate, elemental sulphur, and pyrite. Each species was analysed separately. Based on individual extraction yields and  $\delta^{34}\text{S}$  values, the theoretical  $\delta^{34}\text{S}$  value of total sulphur was calculated.

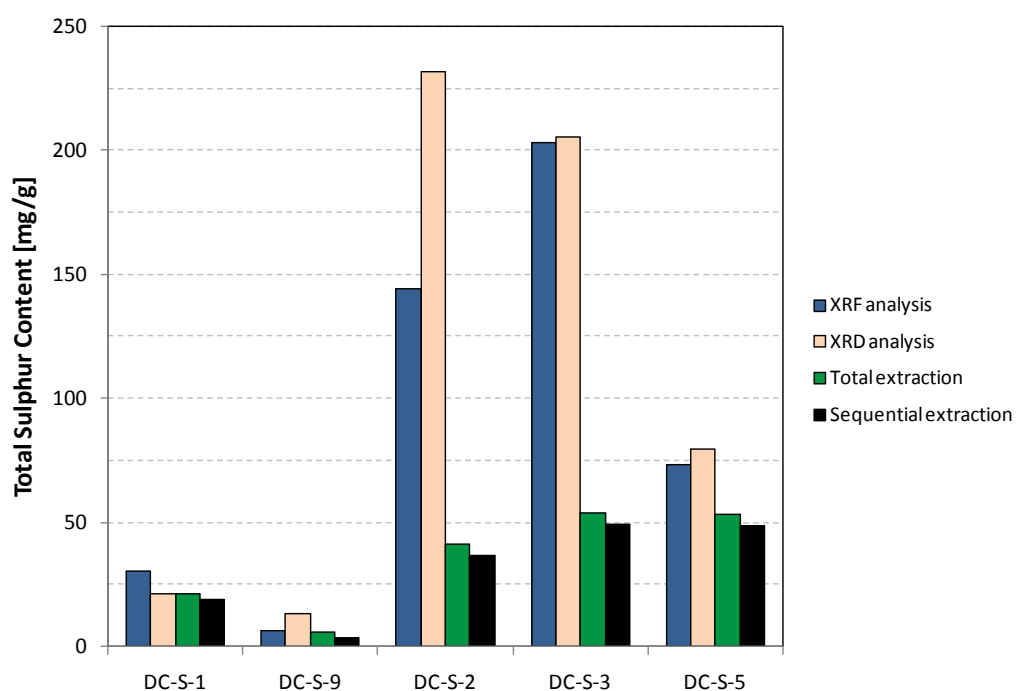


Figure 19: Total sulphur content in sediments determined with different methods: Concentrations were analysed by X-ray fluorescence spectroscopy (XRF), calculated from mineral contents determined by X-ray diffraction (XRD), and weight out from precipitates of wet chemical extraction procedures.

### 5.1.7.2 Evaluation of the sequential extraction

According to XRD analyses, sediments contained sulphate species, elemental sulphur, and pyrite in varying concentrations. The conducted sequence of extraction steps was planned based on these mineralogical results. Pyrite had to be dissolved with  $\text{CrCl}_2$  solution (Canfield *et al.* 1986). However, elemental sulphur is chromium reducible as well and if the species must be separated, elemental sulphur must be extracted first. Dichlormethane was used to leach elemental sulphur from the sediments. As there was no record in the literature about the solubility of sulphate in dichlormethane, sulphate was the first sulphur species to be extracted. All sediment samples were subject to all three extraction procedures – regardless of individual mineralogical compositions determined by XRD. Because sediments are highly inhomogeneous materials, it is conceivable that the sediment portions used for sequential extraction contain other sulphur species in addition to the ones determined by XRD. In that case, acid-soluble sulphate would have been lost. Acid-soluble sulphides such as sphalerite would have been reduced upon contact with  $\text{CrCl}_2$  solution, form  $\text{H}_2\text{S}$  and precipitated as  $\text{ZnS}$  together with the pyrite fraction. The recovery of pyrite is discussed together with the recovery of other sulphide species in chapter 5.1.6.

Extraction and further preparation of elemental sulphur from sediments was complicated by methodological problems. Initially, the eluent of the Soxhlet extraction was treated as described by Lauerwald (2004) and Knöller (2012): Copper swarfs were treated with concentrated  $\text{HNO}_3$ , in order to remove the oxide layer (activation), and added to the eluent of the Soxhlet extraction. This led to the formation of  $\text{CuS}$ . In order to enhance the reaction, the beaker was placed in an ultrasound bath for around 20 minutes.  $\text{CuS}$  was loaded into the distillation apparatus and treated with 6 M  $\text{HCl}$  to dissolve  $\text{CuS}$  and to liberate  $\text{H}_2\text{S}$ . However, even after excessive addition of the acid and 5 hours of boiling,  $\text{CuS}$  did not dissolve. The described method failed to deliver a sulphur compound that is analyzable by IRMS. Subsequent search for alternative methods showed that hot, concentrated  $\text{HNO}_3$  must be used instead of  $\text{HCl}$  to dissolve  $\text{CuS}$  (Cooper and Morse 1998; Whitten *et al.* 2009). Cooper *et al.* systematically tested the extractability of metal sulphide minerals in acidic solutions and found that  $\text{HCl}$  gives considerably lower yields than  $\text{HNO}_3$ . Zaback and Pratt (1992) chose to eliminate the dissolution step by direct combustion of  $\text{CuS}$  and analysis of generated sulphur dioxide. And according to De Groot (2009), the solvent can simply be evaporated to deposit the sulphur. The latter method seemed to be the easiest and least error prone procedure, so it was used for Darzila sediments. According to Steudel (1998), elemental sulphur vaporizes at  $100\text{ }^\circ\text{C}$  under high vacuum conditions. As evaporation was

performed at room temperature, supported by vacuum, it can be expected that all elemental sulphur was recovered from the solution.

As the sequential extraction comprises multiple steps, errors can add up easily. For future preparations it should be considered to spike the sediment with enriched  $^{34}\text{S}$  species, in order to evaluate individual extractions.

### 5.1.7.3 Evaluation of the Eschka extraction

All sedimentary sulphur was extracted at once – regardless of the species – in order to control sulphur yields and isotopic composition of individually extracted species. Even though the Eschka method is a reliable and approved technique for extracting all sulphur from sediments, there is one aspect that is not mentioned in the literature but can be of major importance when it comes to the application for sulphur isotopic analysis: During the procedure, silicates are cracked, and adsorbed ions, such as  $\text{Ba}^{2+}$  are released (Haubrich 2012). When dissolving the mixture in deionised water, released  $\text{Ba}^{2+}$  and  $\text{SO}_4^{2-}$  might form  $\text{BaSO}_4$ . Unfortunately, the following filtration step would remove this precipitate along with other solid residues. The eluent, which is treated with  $\text{BaCl}_2$  to precipitate  $\text{BaSO}_4$  for analysis, would therefore contain less sulphate than originally present and the sulphur content would be underestimated.

XRF measurement detected low barium concentrations in sediments (0.11 – 0.34 mg/g). Considering the discrepancies between the methods, these barium concentrations should not be used for calculating sulphate loss via  $\text{BaSO}_4$  formation. However, the relevance of such losses can also be evaluated by examining the overall sulphur content.  $\text{BaSO}_4$  yields ranged from 42 to 391 mg/g sediment. Considering a hypothetical barium concentration of 1 mg/g, this could react to 1.7 mg  $\text{BaSO}_4$  per gram sediment. None of the prepared sediments would be significantly affected by this process.

The procedure would be more reliable when conducted together with a standard. Spiking the sediment with enriched  $^{34}\text{S}$  would make the success or failure of the preparation more transparent.

### 5.1.8 Sulphur Isotope Measurements at TUBAF and UFZ

Due to instrumental difficulties at the Isotope Geochemistry Lab of the TUBAF, sample analysis was continued at the UFZ in Halle. Samples that had been analyzed already, were analyzed a second time, for obtaining a data set that was gathered under equal conditions. However, from the two elemental sulphur blooms on gypsum crystals, there was no material left to repeat the measurement. Except for these two samples, all sulphur isotopic results that are presented in the following chapters belong to the UFZ data set.

Figure 20 shows how the  $\delta^{34}\text{S}$  measurements of the two laboratories relate to each other. The correlation coefficient of the regression line was found to be very high ( $R^2 = 0.999$ ). Still, a systematic deviation between each pair of samples could be detected. All  $\delta^{34}\text{S}$  values from the TUBAF were slightly higher (Mean: +0.7 ‰ VCDT) than those from the UFZ. Also, the deviation to the bisecting line becomes higher with higher  $\delta^{34}\text{S}$  values. The data were plotted as the difference between analytical results of the laboratories against the mean value (Figure 21). The graph indicates that the deviation between  $\delta^{34}\text{S}$  values from different laboratories depends on the proportion of the heavy isotope. Except for sample DC-W-6, samples with low  $\delta^{34}\text{S}$  values show a better agreement between the laboratories than those with higher  $\delta^{34}\text{S}$  values. The overall analytical precision was  $\leq 0.4$  ‰ VCDT for the double determination at the UFZ, and  $\leq 0.3$  ‰ VCDT for the triple analysis at the TUBAF. Hence, all samples with differences of  $\leq 0.7$  ‰ agree well with each other. For others, a small deviation is visible.

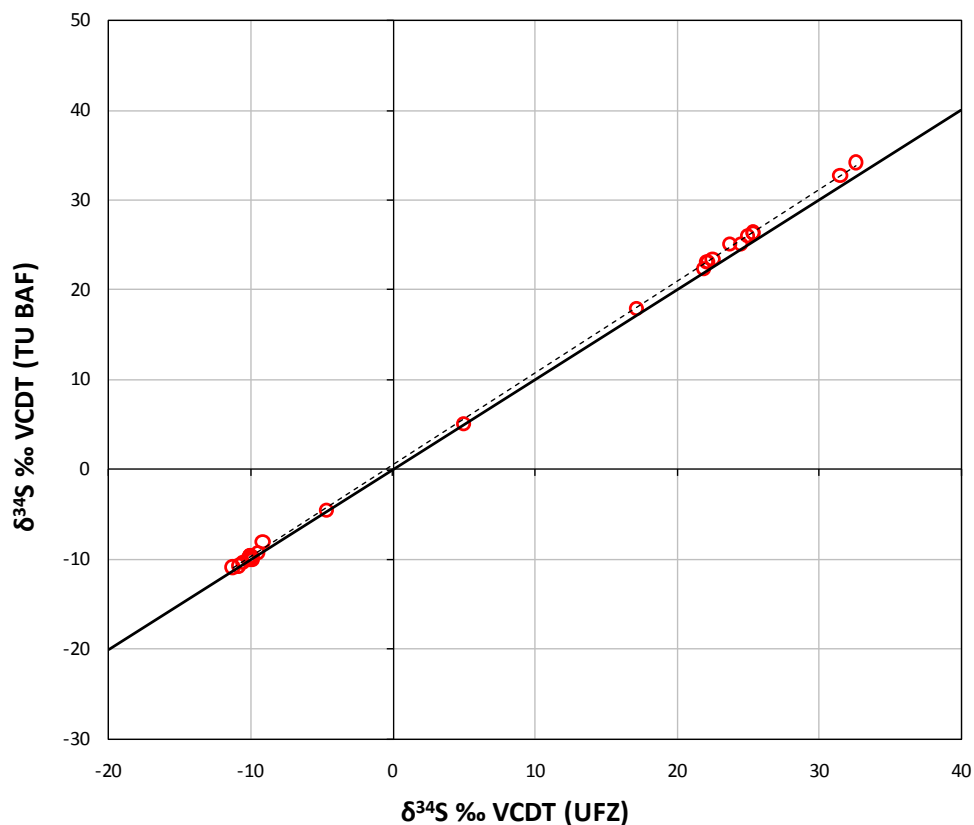


Figure 20: Comparison of 24  $\delta^{34}\text{S}$  measurements at the TUBAF with measurements at the UFZ. The dashed line shows a regression line ( $R^2 = 0.999$ ), and the continuous line depicts the bisecting line.

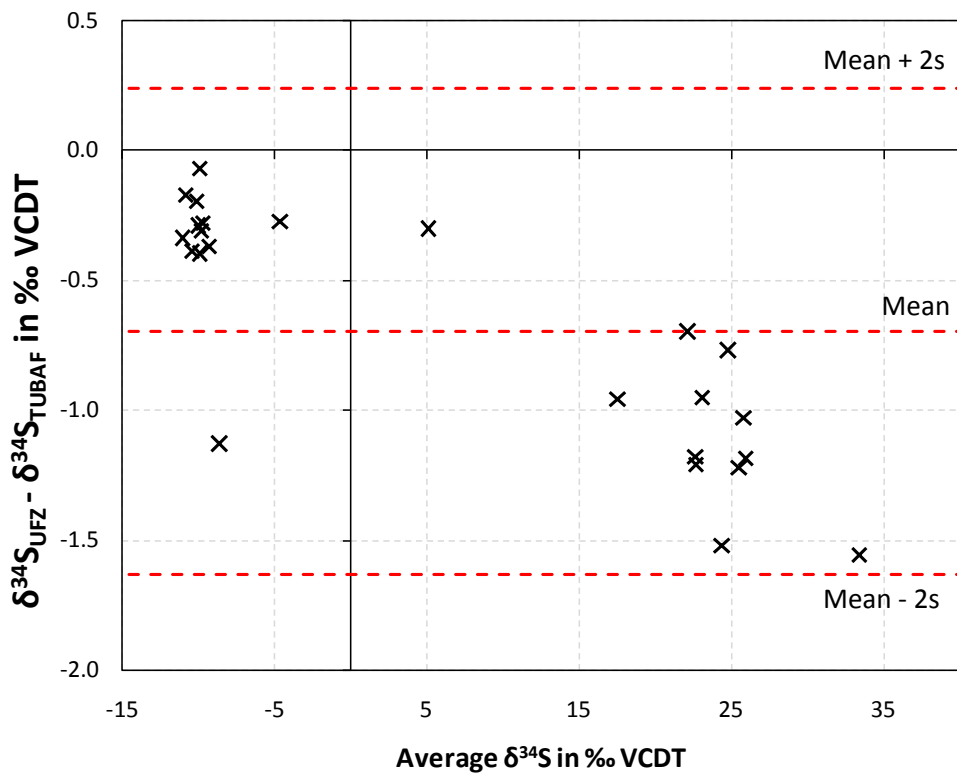


Figure 21: Bland – Altman – plot of  $\delta^{34}\text{S}$  data from the TUBAF and the UFZ. Depicted is the isotopic difference of the measurements against the average value of the two laboratories. The red lines show the mean difference and the “limits of agreement” ( $\text{mean} \pm 2 \cdot s$ ).

## 5.2 Mineralogy of the Cave

Gypsum is the most abundant mineral in Darzila cave, forming extensive crusts along the walls and on the ceiling. Especially in the *crystal room* and along the passage that leads into this chamber, an overwhelming presence of gypsum crystals could be found. In the rear part of the cave, massive blocks of fallen gypsum lie on the cave floor. The appearance of the mineral varied greatly from one location to another. Figure 22 depicts photographs of some selected and representative samples of gypsum incrustations on the cave wall. These coatings are the result of the interaction of sulphuric acid with the host rock and are a typical feature of non-conventional karst caves (Palmer and Palmer 2004). At the outermost layer of the wall gypsum was generally present as distinct crystals. In contrast, gypsum underneath was rather soft and chalky, with crystals that could only be seen with a magnifier.



Figure 22: Variations of gypsum in the cave. (Upper left) DC-SG-15 was collected from the entrance of the cave. The mineral has distinct and stable crystals. (Upper right) DC-SG-14a was collected from the outermost gypsum layer at the narrow passage to the crystal chamber. The mineral has a rough and firm surface, composed of gypsum needles. (Lower left) DC-SG-9c was collected from the crystal chamber. Like the samples depicted in the upper photos, it presents the outermost gypsum layer of the sampling site. In contrast to the others, it is a relatively loose, brittle accumulation of small, young gypsum needles. (Lower right) Sample DC-SG-9b, a soft, homogeneous, and chalky gypsum from the layer underneath DC-SG-9c.

Besides those coatings, a few large gypsum crystals (Figure 23) were found embedded in the wall. Single knobs of elemental sulphur could be observed on their surfaces. However, the largest portion of elemental sulphur in Darzila cave was present as extensive, dense crusts on the walls (Figure 24), covering gypsum incrustations. The coatings were typically around

3 mm thick and of microcrystalline structure. Magnification of the crystals showed that cave sulphur is present as orthorhombic cyclooctasulphur ( $S_8$ ). According to Steudel and Eckert (2003), this is the only stable form of elemental sulphur at standard conditions. The occurrence of elemental sulphur in Darzila cave can be attributed to incomplete oxidation of  $H_2S$ .



Figure 23: Large gypsum crystals with sulphur blooms on their surface. (Bottom) Gypsum crystal DC-SG-13c. (Upper Left) Gypsum crystal DC-SG-13d with the corresponding sulphur bloom DC-ES-13d (Right)



Figure 24: Coating of elemental sulphur on the cave wall. The crusts are approximately 3 mm thick and have convex, broccoli-like surfaces.

Secondary carbonate formations, such as stalactites or cave pearls were not present in the explored part of the cave. However, when examining gypsum crystal with a magnifier, a few small crystals (Figure 25, left) were found that were suspected to be calcite or dolomite (trigonal crystal system), instead of gypsum (monoclinic crystal system). The acid test confirmed the hypothesis.

Calcite is also present in terms of primary limestone. As shown in Figure 25 (right photo), limestone at the cave floor is highly altered - most likely due to sulphuric-acid attack near the water table. This was also reflected by its sulphur content. Elemental analysis of cave floor limestone DC-PL-16 and the corresponding, unaltered Oligocene limestone, gave considerably higher sulphur concentrations ( $\sim 4.97$  mg/g) than the unaltered limestone ( $\sim 1.77$  mg/g).

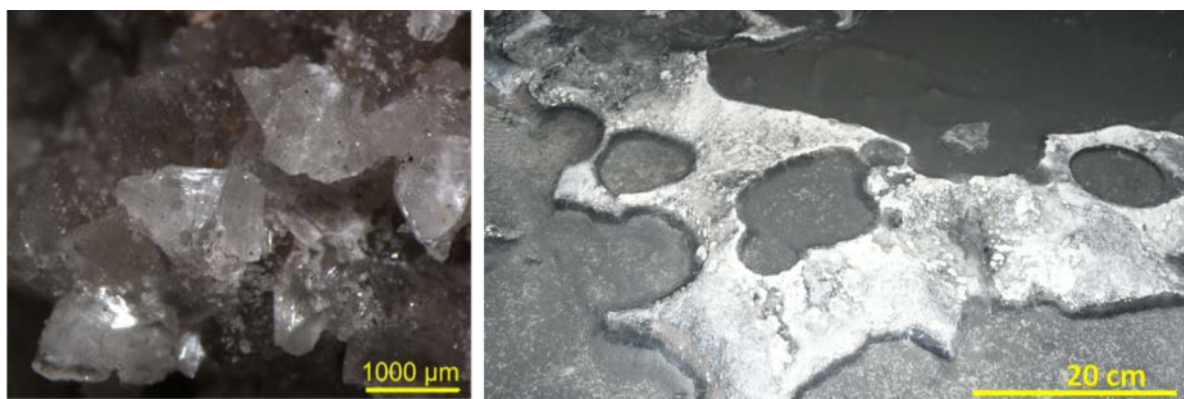


Figure 25: (Left) Calcite crystals in between gypsum crystals on sample DC-SG-14a. (Right) Dissolving limestone on the cave floor (DC-PL-16).

Five sediment samples were analyzed using XRD and a total of 20 different minerals was identified (Appendix Table A 15). Eleven of these were silicate minerals. Figure 26 displays the mineralogical composition of the samples. The initial motivation for mineralogical analysis of the sediments was to choose adequate extraction methods for sulphur species. For simplification reasons, only sulphur containing species are displayed individually. Others are grouped to allow a quicker survey of the data.

Except for sediment DC-S-3 from the isolated, acidic pool at cave site 3, silicate minerals such as quartz, smectite, or muscovite account for up to 80 wt% (in sum) of the sediment sample. Except for sample DC-S-3, all sediments contained an appreciable portion (12 - 21 wt%) of carbonate minerals, mostly in form of calcite. For DC-S-3, gypsum is the dominant mineral. It accounts for approximately 60 wt% of the analysed sample. No carbonate mineral could be found in this sediment.

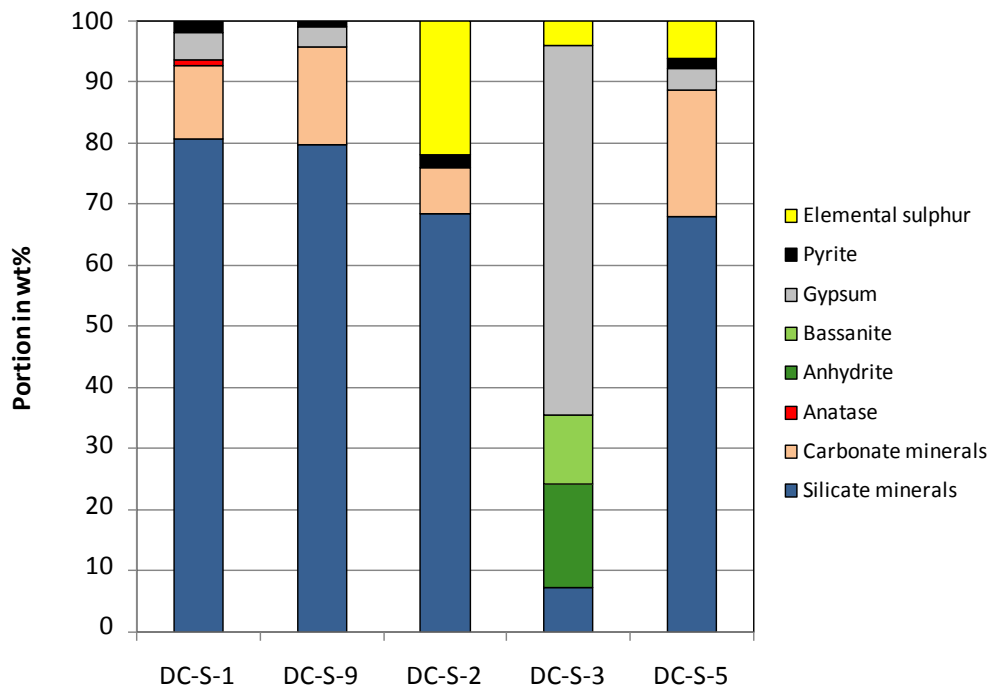


Figure 26: Mineral composition of cave sediments. In order to highlight sulphur containing minerals, other minerals are summarized into groups. The only exception to this rule is the titanium dioxide anatase, which failed to be part of a group. DC-S-1 and DC-S-9 belong to the sediments from the same waterbody. DC-S-2 is a sediment sample from the upper course of the main cave river. DC-S-3 is sediment from an isolated, acidic pool. DC-S-5 was sampled from the rear part of the cave.

### 5.3 The Microbial Community of the Cave and Awa Spi River

Six sediment samples, five biofilms and one DNA extract from cave wall material (containing gypsum and elemental sulphur) were subject to phylogenetic analysis based on their 16S rRNA gene sequences. The extract from wall material and from two sediment samples did not yield enough DNA to finish the procedures. In the following sections, the term “isolates” will refer to DNA from individual bands in the DGGE gel.

The results of the sequential analyses are shown as phylogenetic tree in Figure 27. It can be seen, that the isolates are affiliated with various microbial families. Some of these, such as the *Enterobacteriaceae*, are indicators for anthropogenic contamination. Others, such as the family *Acidithiobacillaceae*, are typical sulphur-oxidizing bacteria.

#### 5.3.1 Cave Sediments

It was expected to find a variety of sulphate-reducing bacteria – this however was not the case. From the acidic site 12 (shallow, temporary puddles), two different sediment samples were taken. DC-S-12a is, strictly speaking, both sediment and biofilm sample. It was taken from a thin (< 1 mm), white biofilm layer approximately 5 cm below the water surface. However, the film was very fragile and instantly disintegrated on contact. It was impossible to sample the biofilm without simultaneously sampling some associated sediment. Due to this, the sample was grouped with sediments instead of biofilms. The difficulty to obtain entirely separated samples for the biofilm and for the associated sediment (DC-S-12b) is reflected by the overlap of identified microorganisms. DC-S-12b was dominated by species that belong to the Enterobacteria. The isolates were strongly related to the species *Citrobacter freundii*, *Klebsiella oxytoca*, and *Yokenella regensburgei*, all of which belong to the group of coliform bacteria. Bacteria from this group are commonly used as an indicator of faecal contamination of drinking water. The mentioned species do not necessarily originate from human or animal faeces – however, the presence of these genera generally suggest anthropogenic input via skin, hairs, intestinal and/or the respiratory tract (Farmer III and Brenner 2005, Bitton 2005). The detection of such bacteria in cave sediments can be attributed to the fact, that the cave is regularly visited by people from neighbouring villages and towns to take recreational baths and to bottle cave water for skin treatment.

One isolate from each DC-S-12 sample, was closely related to species of the genus *Acidithiobacillus*, which are typical sulphur-oxidizing bacteria. These organisms will be presented in more detail in the following chapter, where biofilm communities are discussed.

DC-S-9, a sediment sample from the “crystal room”, contained Enterobacteria species as well as isolates that can be placed among the genus *Pseudomonas*. This genus is one of the most diverse and ubiquitous bacterial genera and its species have been isolated from all kinds of environments (Peix *et al.* 2009). Even though they possess some interesting traits, for the work on hand they are not particularly relevant.

Sediment from the acidic pool at site 4 (DC-S-4) was found to contain microorganisms closely related to *Bosea thiooxidans*, a chemolithoheterotroph<sup>8</sup> that is able to obtain energy from the oxidation of reduced sulphur species in the presence of organic carbon. Yet, as it is also found in cultivated soils (Das 2005), its presence should not be overrated. *Bosea thiooxidans* grows at pH values between 6 and 9 (Das 2005). Unfortunately, pH in the sediment pore water was not measured. Yet considering the pH of 1.6 of the overlying water column, their presence is rather astonishing. Apparently, pH conditions change rapidly at the sediment-water interface.

---

<sup>8</sup> Organisms that obtain energy by oxidation of inorganic substances and that use organic compounds as carbon source

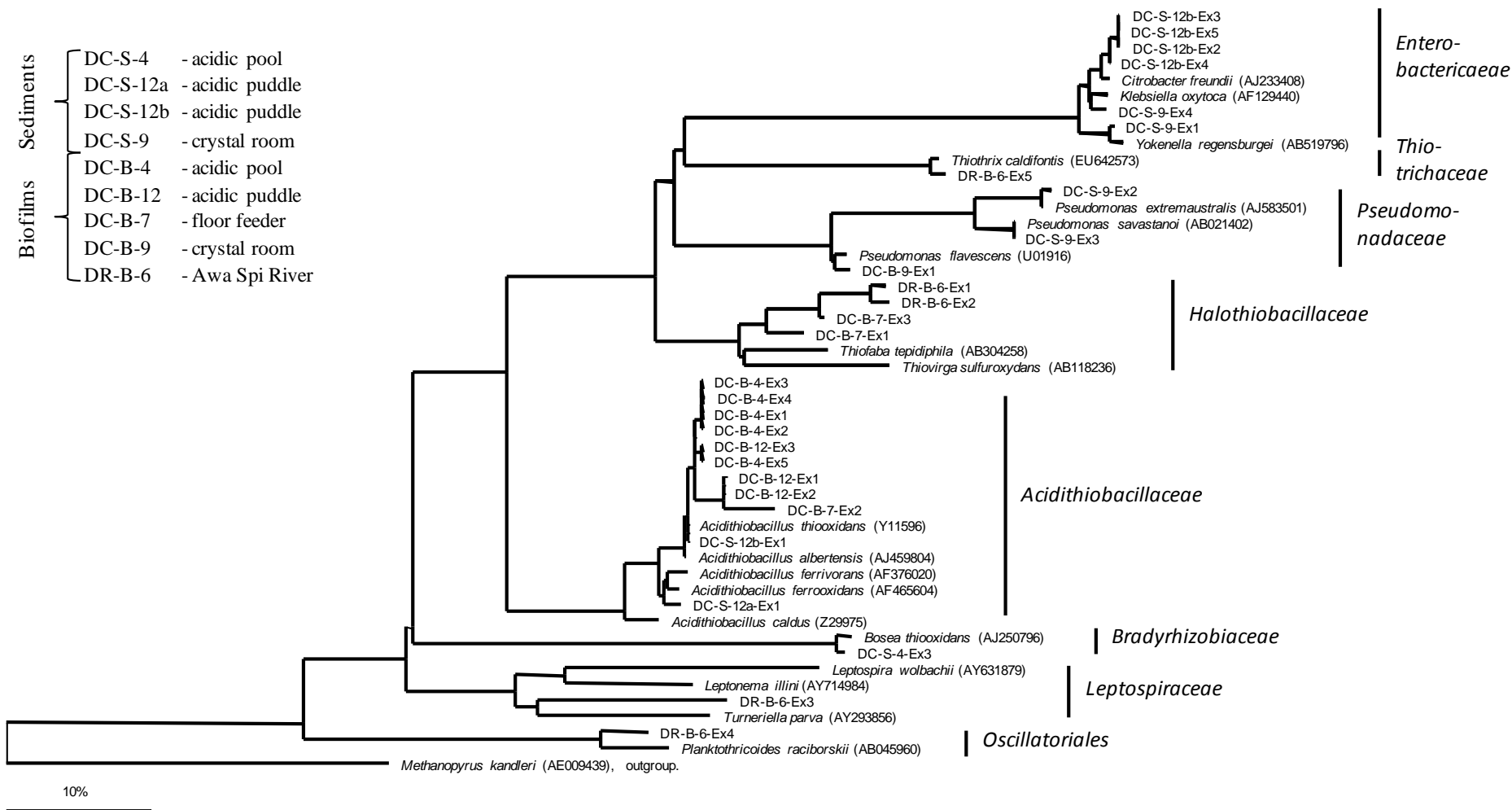


Figure 27: Phylogenetic tree based on 16S rRNA gene sequences - calculated using the Parsimony method. Up to date data bases and the program ARB were used to fit the DGGE sequences into the tree and to optimize their positions (Ludwig *et al.* 2004). The families Enterobacteriaceae, Thiotrichaceae, Pseudomonadaceae, Halothiobacillaceae and Acidithiobacillaceae belong to the class of gamma-Proteobacteria. The Bradyrhizobiaceae belong to the alpha-Proteobacteria, whereas the Leptospiraceae are part of the Phylum Spirochaetes and the order Oscillatoriales to the Cyanobacteria. The depicted bar shows a 10% sequence divergence. *Methanopyrus kandleri* served as outgroup.

### 5.3.2 Biofilms

Darzila cave and the river *Awa Spi* host a variety of biofilms. In small, calm puddles white films loosely cover the sediments. At the main floor feeder and in the river *Awa Spi*, where strong currents prevail, such a biofilm-architecture cannot exist. Instead, these sites were colonized by strong, filamentous, rock-attached streamers. Another distinctive type was found floating on the water surface of an acidic pool (site 4) and of several small puddles (site 12). The following section will give deeper insights into the appearance and the microbial communities of the sampled biofilms.

#### 5.3.2.1 Crystal chamber

Most biofilms were instantly recognized as such. In the case of DC-B-9, a red film on sediments in the crystal room, this was not so clear. Assuming, that it might just be a ferric iron precipitate, a sample for DNA analysis was taken. After all, microorganisms could be intimately involved in iron cycling processes in the cave. Yet, the only organism found by 16S rRNA gene sequence analysis was *Pseudomonas flavescens* (96.5% sequence similarity). With respect to microbial inhabitants, the suspected “biofilm” was therefore not very different from nearby sediments (see previous chapter) and thought to be not especially relevant to karstic processes.



Figure 28: Suspected biofilm DC-B-9 in the crystal room

#### 5.3.2.2 Acidic cave sites

The overwhelming presence of microorganisms as well as their ability to occupy available niches could be clearly observed during fieldwork. During the period of the fieldwork, the water level of the main cave stream dropped a few cm which led to the formation of temporary puddles at cave site 12 (pH 1.3). A few days later, the puddles were already covered by white, floating, elastic, and slimy biofilms – similar to that on the acidic pool at cave site 4 (pH 1.6). Photos of these films are shown in Figure 29.

16S rRNA gene sequence analysis of DC-B-4 and DC-B-12 showed that all DNA isolates belong to the genus *Acidithiobacillus*. At both sites, analyzed DNA isolates agree best with that of *Acidithiobacillus thiooxidans* and *Acidithiobacillus albertensis*. With respect to the latter, isolates from site 12 had 97.6-98.7% 16S rRNA gene sequence similarity. And

isolates from site 4 had 99.0-99.2 % similarity, respectively. Sequence similarities with *A. thiooxidans* were 98.1-99.2% for site 12, and 99.5-99.7 % for site 4. Sequence similarities with *A. ferrooxidans* were 93.6-94.5 % for site 12 and 94.7-95.0 % for site 4.



Figure 29: Left: Biofilm DC-B-4 on a pair of tweezers. Right: DC-B-12, a biofilm covering a tiny puddle.

### 5.3.2.3 Main floor feeder

The vicinity of floor feeder (site 7) was characterized by abundant, white, slimy, and filamentous biofilms that were drifting in the current. The filaments were attached to bare rocks at the cave floor and had a typical length of 3-5 cm (Figure 30). Based on 16S rRNA gene analysis, DNA can be assigned to the genus *Acidithiobacillus* and to the *Halothiobacillaceae* family. With respect to the latter, *Thiofaba teptiphilia*, an aerobic, sulphur-oxidizing bacterium (Mori and Suzuki 2008), was the closest relative that could be identified (94.3-95.5 % 16S rRNA gene sequence similarity).



Figure 30: Filamentous biofilm next to the main floor feeder (sample DC-B-7).

Site 7 offers a constant supply of dissolved sulphide, and features a pH of 6.6, as well as lukewarm water temperatures (26 °C), which makes it a favourable habitat for this organism. Macalady *et al.* (2008), who studied the niche differentiation among sulphur-oxidizing bacteria in the Frasassi cave system in Italy, identified very similar (95.1%) 16S rRNA gene sequences among their clones from sulphur-oxidizing biofilms.

One of the isolates could be assigned to the genus *Acidithiobacillus*, being most closely related to the species *At. thiooxidans* (95.1%) and *At. albertensis* (94.8%).

#### 5.3.2.4 Awa Spi River

*Awa Spi* River was characterized by an overwhelming quantity of filamentous biofilms. They were firmly attached to pebbles, had a pale, green-greyish colour, and were up to 10 cm long. The microbial community of biofilm from river site 6 (DR-B-6) was found to be dominated by a strain of *Thiothrix caldifontis*, cyanobacteria, and representatives of the genera *Leptospira* and *Thiofaba*.



Figure 31: Filamentous biofilm in Awa Spi River (sample DR-B-6)

One of the isolates could be positioned within the *Leptospiraceae* family. Its closest identified relative was *Turneriella parva*, a chemoorganotrophic organism (Levett 2005), which was probably introduced to the habitat by anthropogenic activities. More relevant for understanding the microbial community are the two isolates, which showed high 16S rRNA gene sequence similarity (92.5 and 92.7%) with *Thiofaba teptiphilia* – the same organism that was found in the biofilm at the floor feeder in Darzila cave.

One isolate shared practically 100% sequence similarity with the sulphur-oxidizing species *Thiothrix caldifontis*, which was previously discovered by Chernousova *et al.* (2009). Another important member of the microbial community is an organism that shares 98.7% sequence similarity with the filamentous cyanobacterium *Planktothricoides raciborskii* (Suda *et al.* 2002) of the order *Oscillatoriales*.

### 5.3.3 Comparison to Earlier Microbial Investigations of Darzila Cave

Khanaqa and Al-Manmi (2011) were the first to study the hydrogeochemistry and the geomicrobiology of the cave. Altogether five cave waters were analyzed bacteriologically. Three *Thiobacillus* species, namely *T. thiooxidans*, *T. ferrooxidans*, and *T. acidophilus* could be identified. Considering that *T. thiooxidans* and *T. ferrooxidans* have been reclassified to the genus *Acidithiobacillus* (Kelly and Wood 2000), 16S rRNA gene sequence analyses of cave biofilms could confirm the presence of these organisms in the cave. The presence of *Thiobacillus acidophilus* was not detected via DGGE. However, it must be kept in mind that DGGE does not capture all organisms. It is merely a snap-shot of dominant species in the community.

Furthermore, the authors mentioned the preliminary identification of green sulphur bacteria, growing in the apparent total absence of light. Many bacteria are opportunists – switching between energy sources if they have to. But for green sulphur bacteria there is no other option than using light for food production from CO<sub>2</sub>. However, they grow at extremely low light intensities. Even from deep-sea hydrothermal vents, where the only source of light with suitable wavelengths is geothermal radiation, green sulphur bacteria could be found (Beatty *et al.* 2005). Hence, presence of green sulphur bacteria in Darzila cave is conceivable, but during field work for the current study, no such films could be detected.

## 5.4 Stable Isotopes

In this chapter, results of stable isotope analyses of water, dissolved sulphate and sulphide, primary and secondary gypsum, host rock limestone, elemental sulphur and various sedimentary sulphur species are presented and evaluated. The expressions used in stable isotope analyses are often bulky, which hampers both writing and reading. In order to counteract this phenomenon, expressions were shortened most of the time. The complete and formal expressions are defined in the beginning of the following chapters. Afterwards, the respective reference materials were left out.

Samples with higher  $\delta$  values are relatively enriched in the heavy isotope compared to the standard material and are therefore “heavier”. Thus in this thesis, the terms “heavier” and “enriched” refer to samples that have higher  $\delta$  values, whereas “lighter” and “depleted” refer to samples that have lower  $\delta$  values.

### 5.4.1 Hydrogen and Oxygen Isotopes

The isotopic composition regarding  $\delta D$  ( $\delta^2H$ ) and  $\delta^{18}O$  of twelve water samples ranges from -31.85 to -24.57 ‰ vs. VSMOW for  $\delta D$  and from -6.62 to -5.53 ‰ vs. VSMOW for  $\delta^{18}O$ , respectively (Table A 19, Figure 32). The overall precision of the determination was 0.04 ‰ for  $^{18}O$  and 0.13 ‰ for deuterium.

For evaluation of the data, four reference lines were plotted into the same graph. One of these lines, the “global meteoric water line” (GMWL), is based on numerous precipitation data from locations around the globe. The equation  $\delta D = 8.13 \cdot \delta^{18}O + 10.8 \text{ ‰ VSMOW}$ , published by Rozanski *et al.* (1993), is the updated version of Craig’s (1961) original findings.

The two “local meteoric water lines” (LMWL) are derived from isotopic data of two different areas in Northern Iraq. LMWL 2 ( $\delta D = 7.7 \cdot \delta^{18}O + 14.4 \text{ ‰ VSMOW}$ ) is derived from 55 precipitation events during the period December 2009 to June 2010 at the Bazian Meteorological Station in the Basara basin. It is located approximately 25 km west of Sulaimaniyah city (Hamamin and Ali 2012), and represents a neighbouring region of the Chamchamal-Sangaw basin (study area). Accordingly it was expected, that samples from Darzila plot near that line, but LMWL 1 ( $\delta D = 8 \cdot \delta^{18}O + 20 \text{ ‰ VSMOW}$ ) appears to be a better fit for the data. LMWL 1 is not based on precipitation data, but on isotopic analysis of water samples from 12 springs and 10 wells in the Erbil province, collected in July and August 2001 as well as on data from other studies in neighbouring countries (Mawlood

2003). Unfortunately, this PhD thesis is not published and only partly accessible. Accordingly, the underlying data set could not be evaluated.

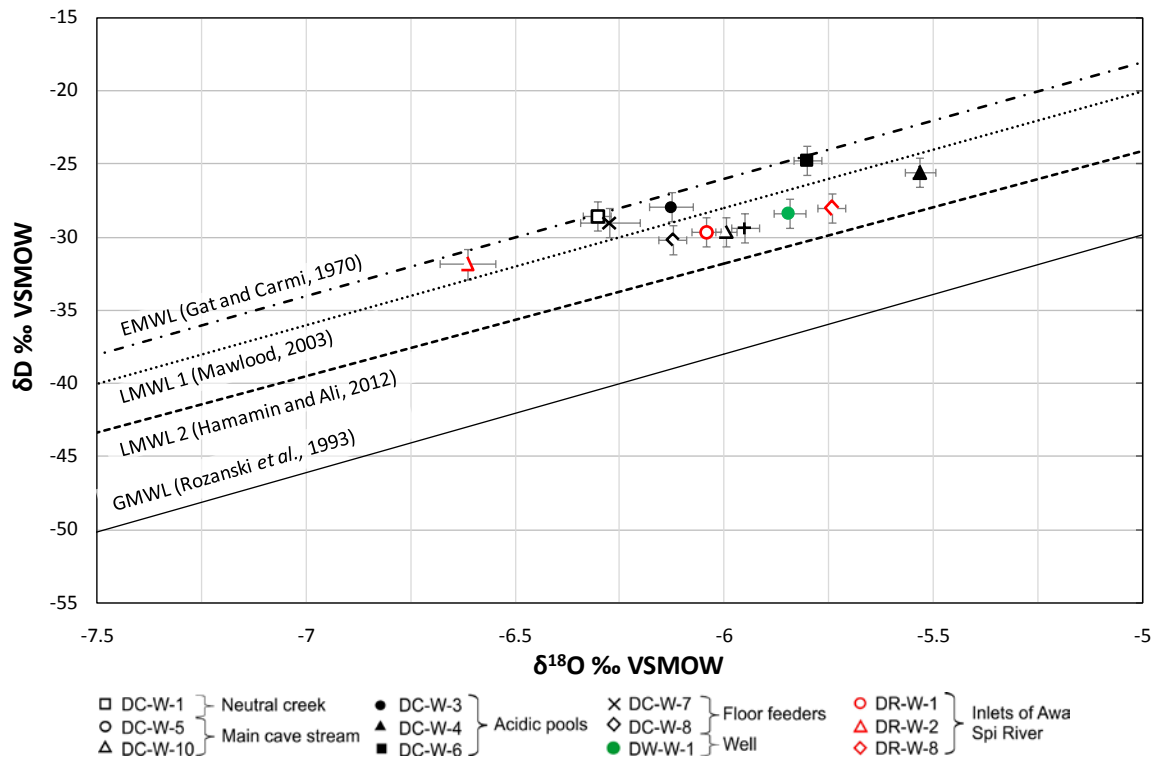


Figure 32: Isotopic composition of water samples from cave water (black symbols), from inlets of Awa Spi river (red symbols) and from a well nearby (green symbol). Samples were taken in September and October 2011 at the end of the dry season. The global meteoric water line (GMWL) as well as two local meteoric water lines (LMWL) and the Eastern Mediterranean meteoric water line (EMWL) are given for reference. The error bars show the standard deviation of the data points.

All samples plot on or slightly below the Eastern Mediterranean meteoric water line ( $\delta D = 8 \cdot \delta^{18}O + 22 \text{ ‰ VSMOW}$ ) of Gat and Carmi (1970). This indicates that precipitation in the research area is primarily Mediterranean, and that the dry, hot air caused an evaporative loss of light molecules prior infiltration.

Alternatively, water-rock interactions may have changed the isotopic signature of the water. Especially dissolution of Oligocene limestone could have significant impacts. No record of  $\delta^{18}O$  values in calcite of the study area was found in the literature, but Poore and Matthews (1984) systematically studied the carbon and oxygen isotopic composition of calcite from Eocene and Oligocene age. Based on their stable isotope record, a  $\delta^{18}O$  value of around +1.5 ‰ vs. PDB was derived. Conversion to the VSMOW scale via equation [17] from Coplen *et al.* (1983) yielded a  $\delta^{18}O$  value of around 32.5 ‰ VSMOW.

---

$$\delta^{18}\text{O}(\text{VSMOW}) = 1.03091 \cdot \delta^{18}\text{O}(\text{PDB}) + 30.91 \quad [17]$$

Dissolution of the host-rock may therefore cause a shift of  $\delta^{18}\text{O}$  values in water to heavier values. Because hydrogen is not contained in considerable amounts in minerals,  $\delta\text{D}$  values are not affected. Instead, deuterium enrichment may arise through exchange with ascending  $\text{H}_2\text{S}$ . At around  $50^\circ\text{C}$ , partitioning of deuterium into the water reservoir is associated with an enrichment factor  $\varepsilon_{\text{D}_{\text{H}_2\text{O}-\text{H}_2\text{S}}}$  of 2.2 ‰ (Clark and Fritz 1997). With respect to Figure 32, water-rock interaction and exchange with ascending  $\text{H}_2\text{S}$  may be especially relevant for the two acidic sites DC-W-4 and DC-W-6.

## 5.4.2 Sulphur Isotopic Composition

Altogether 36 samples of different materials were analysed for their sulphur and (when relevant) sulphate oxygen isotopic composition. The results are reported as  $\delta^{34}\text{S}$  and  $\delta^{18}\text{O}$  values in per mill relative to the VCDT (Vienna Cañon Diablo Troilite) and VSMOW (Vienna Standard Mean Ocean Water) standard, respectively. A complete list of analytical results is given in the Appendix (Table A 20, Table A 21, Table A 22, and Table A 23).

It is important to note, that in this thesis all sulphur isotopic data are reported relative to VCDT, including historical data that were initially reported relative to CDT.

Both sulphur and oxygen show wide variations in  $\delta$ -values:  $\delta^{34}\text{S}$  ratios of dissolved sulphide ranged from -20.7 ‰ to +9.6 ‰ VCDT. The  $\delta^{34}\text{S}$  and  $\delta^{18}\text{O}$  values of dissolved sulphate varied from -9.1 ‰ to +32.6 ‰ VCDT and from -2.4 ‰ to 14.5 ‰ VSMOW, respectively. The isotopic composition of gypsum samples ranged from  $\delta^{34}\text{S} = -10.9$  to 22.5 ‰ VCDT and from  $\delta^{18}\text{O} = -7.0$  to 15.2 ‰ VSMOW. The  $\delta^{34}\text{S}$  and  $\delta^{18}\text{O}$  values of limestone ranged from -13.7 ‰ to +24.7 ‰ VCDT and from 1.3 ‰ to 1.4 ‰ VSMOW, respectively. Crude oil had a sulphur isotopic composition of -9.05 ‰ VCDT. Total sulphur extracts of sediment samples showed  $\delta^{34}\text{S}$  ratios of -14.3 ‰ to -7.8 ‰ VCDT. A detailed presentation of analytical results is given in the following sections.

### 5.4.2.1 Sulphur and sulphate oxygen isotopes in water

Isotopic analysis of dissolved sulphur species from cave waters, springs and the nearby well revealed large differences in both sulphur and oxygen isotope ratios. Dissolved sulphide showed a remarkable spread of  $\delta^{34}\text{S}$  values, ranging from -20.7 ‰ to 9.6 ‰. With -9.1 ‰ to +32.6 ‰,  $\delta^{34}\text{S}$  ratios of dissolved sulphate had an even larger range.  $\delta^{18}\text{O}$  ratios of dissolved sulphate ranged from -2.4 ‰ to 14.5 ‰.

Figure 33 displays the relationship of sulphur isotopes in sulphides and sulphates. All except one sulphide sample were depleted in  $^{34}\text{S}$ . The only sample having  $^{34}\text{S}$  enriched sulphide (+9.6 ‰) is DR-W-2, a spring that discharges into the river *Awa Spi*. Simultaneously, it was the sample with the highest  $\delta^{34}\text{S}$  value of dissolved sulphate (+32.6 ‰). In contrast, the acidic cave pools DC-W-4 and DC-W-6 were depleted with respect to  $^{34}\text{S}$  in both sulphur species. With  $\delta^{34}\text{S}_{\text{SO}_4} = -9.1$  ‰, DC-W-6 had the lightest sulphate sulphur of all analysed water samples. The acidic pool DC-W-3 is similar with respect to sulphide sulphur, but dissolved sulphate was slightly enriched in  $^{34}\text{S}$ . This might be due to an occasional connection to the small, neutral creek DC-W-1. This creek featured the lowest (-20.7 ‰)

$\delta^{34}\text{S}_{\text{HS-}}$  ratio of water samples, whereas sulphate sulphur was enriched in  $^{34}\text{S}$  by 17.1 ‰. The residual samples, namely the floor feeder DC-W-7, the main cave stream DC-W-5 and DC-W-10, the spring waters DR-W-1 and DR-W-8 as well as the well water DW-W-1, form a relatively homogeneous group. The mean values are  $\delta^{34}\text{S}_{\text{SO}_4} = 24.2$  ‰ and  $\delta^{34}\text{S}_{\text{H}_2\text{S}} = -8.8$  ‰, with a standard deviation of 1.3 and 1.6 ‰, respectively.

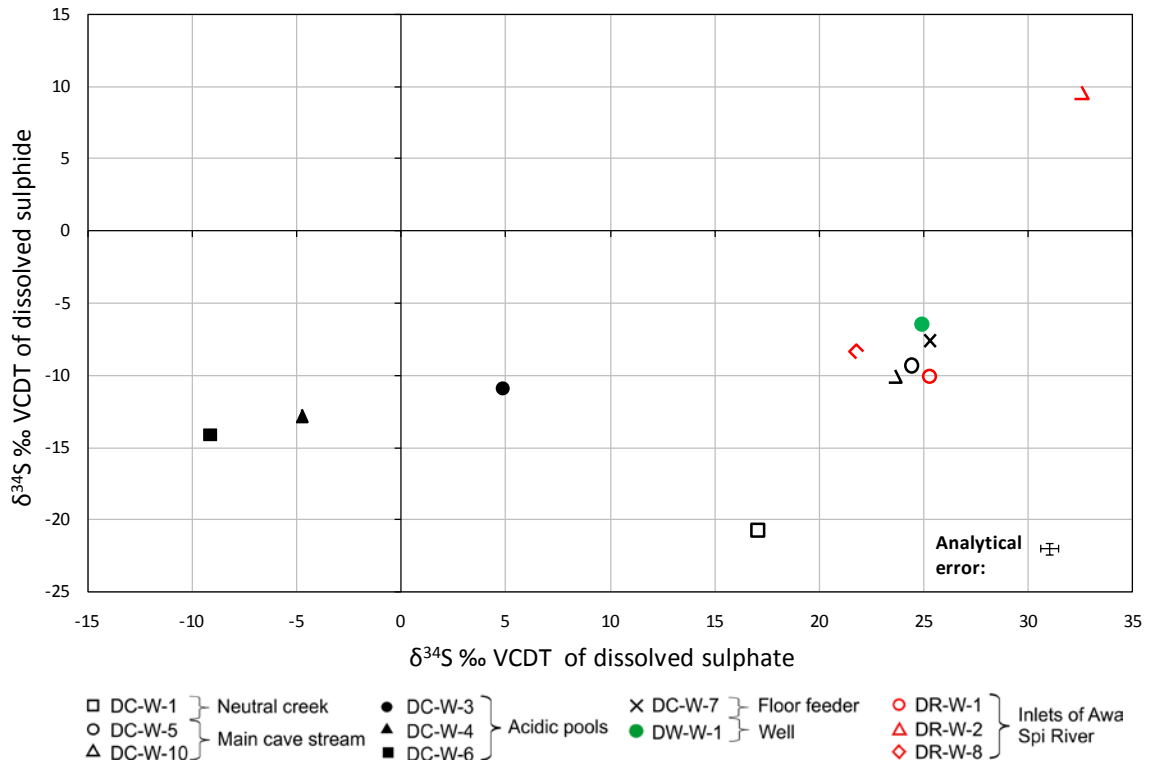


Figure 33: The sulphur isotopic composition of dissolved sulphide and sulphate in cave waters (black symbols), springs (red symbols), and well water (green symbol). Bars in the right corner depict the analytical error ( $\pm 0.4$  ‰) of the respective sulphur species.

With some imagination, various trends can be identified. However, the small number of samples does not allow for any rash conclusions. Relationships between samples will be discussed thoroughly in chapter 5.5.2 (Origin of the fluids).

In order to evaluate the underlying processes, it is not only necessary to know the  $\delta^{34}\text{S}$  values of the sulphur species. Valuable information can also be gained by computing the isotopic difference between the respective species. It is already apparent from Figure 33 that some samples have very different  $\delta^{34}\text{S}$  values for sulphate and sulphide, but it is easier to grasp in Figure 34, where the isotopic differences of the respective species are depicted. The isolated pools DC-W-6, -4, and -3 had relatively similar  $\delta^{34}\text{S}$  values for the species. This is reflected by  $\Delta_{\text{SO}_4\text{-HS}}$  values of 5 ‰, ~ 8 ‰, and 15.8 ‰, respectively. The largest isotopic separation between dissolved sulphur species was found in the small creek DC-W-1 (~ 37.8 ‰). The

implications of these differences will be discussed in the chapter *Constraints on Cave Forming Processes* (chapter 5.5).

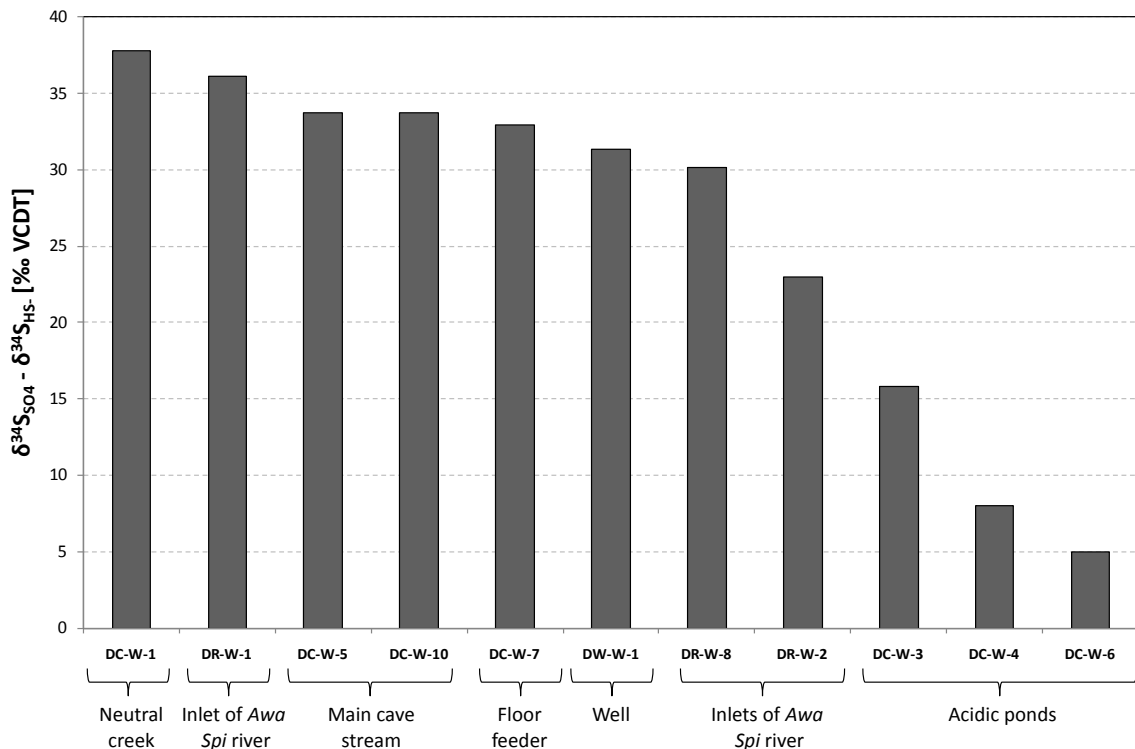


Figure 34: The sulphur isotopic difference  $\Delta$  between dissolved sulphate and sulphide.

Plots like Figure 33 or Figure 34 can be very misleading because they treat dissolved sulphate and sulphide as equally important species. It is crucial to keep in mind that the concentrations of the respective species vary considerably from each other. Even though dissolved sulphide is a major sulphur species, sulphate was dominant in all samples. With two exceptions (DR-W-2 and DW-W-1), sulphide sulphur presented less than 2 % of the total sulphur concentration (Figure 35). Computation of  $\delta^{34}\text{S}_{\text{total}}$  by equation [13] showed that  $\delta^{34}\text{S}$  values of sulphate clearly dominate the overall sulphur isotopic signature of all waters.

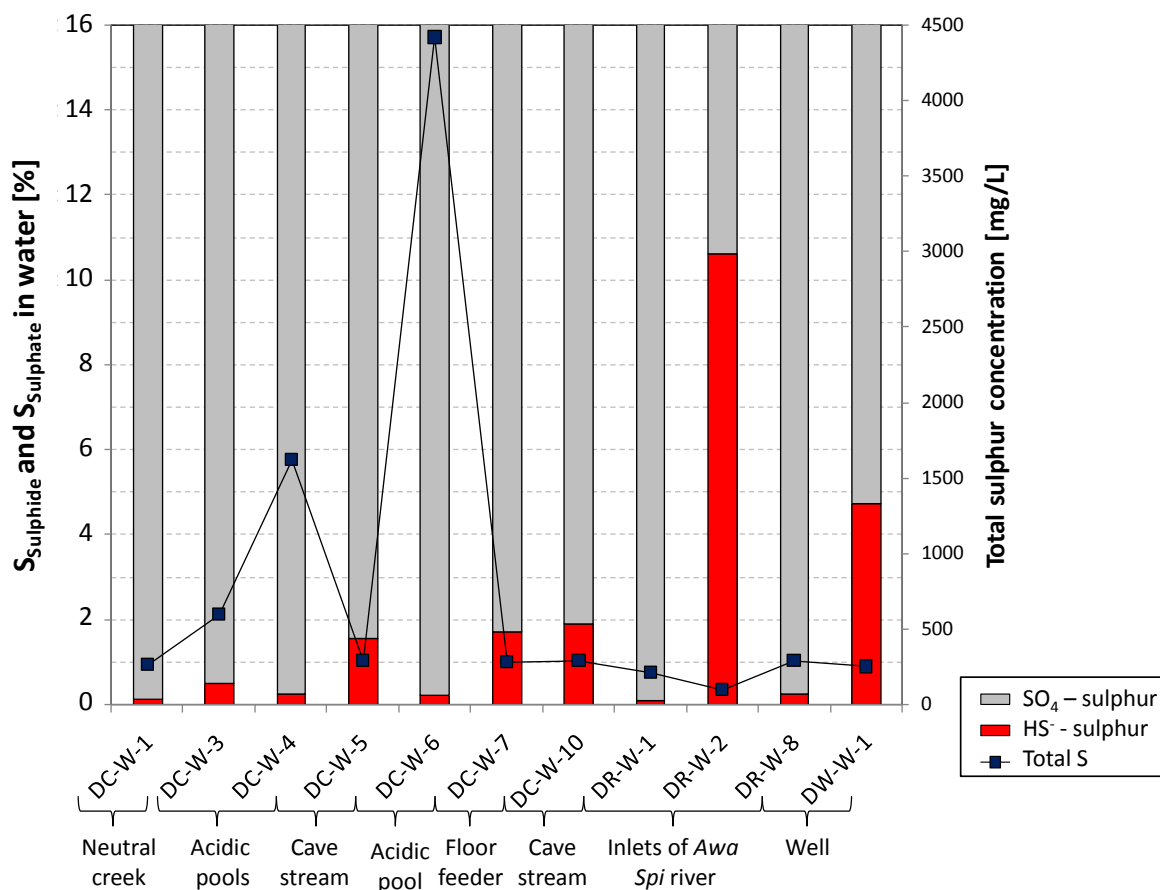


Figure 35: Total sulphur concentration in water samples combined with the relative proportions of sulphur in dissolved sulphide and sulphate. Note that the %-scale is only depicted until 16%. Of course, in reality it goes up to 100% but due to the overwhelming dominance of dissolved sulphate, the relative proportions of sulphide sulphur would be difficult to see.

The relationship of sulphur and oxygen isotopes in dissolved sulphate is presented in Figure 36. As before, the acidic pools DC-W-4 and DC-W-6 form a distinct group. They are depleted in both  $^{34}\text{S}$  as well as  $^{18}\text{O}$ . The sulphide rich spring DR-W-2 is located at the other end of the scale. A line fitted through all samples gives an  $R^2$  of 0.99. It appears that the different waters are somehow related, possibly by a mixing process. This subject will be discussed extensively in the chapter *The Origin of the Fluids* (chapter 5.5.2).

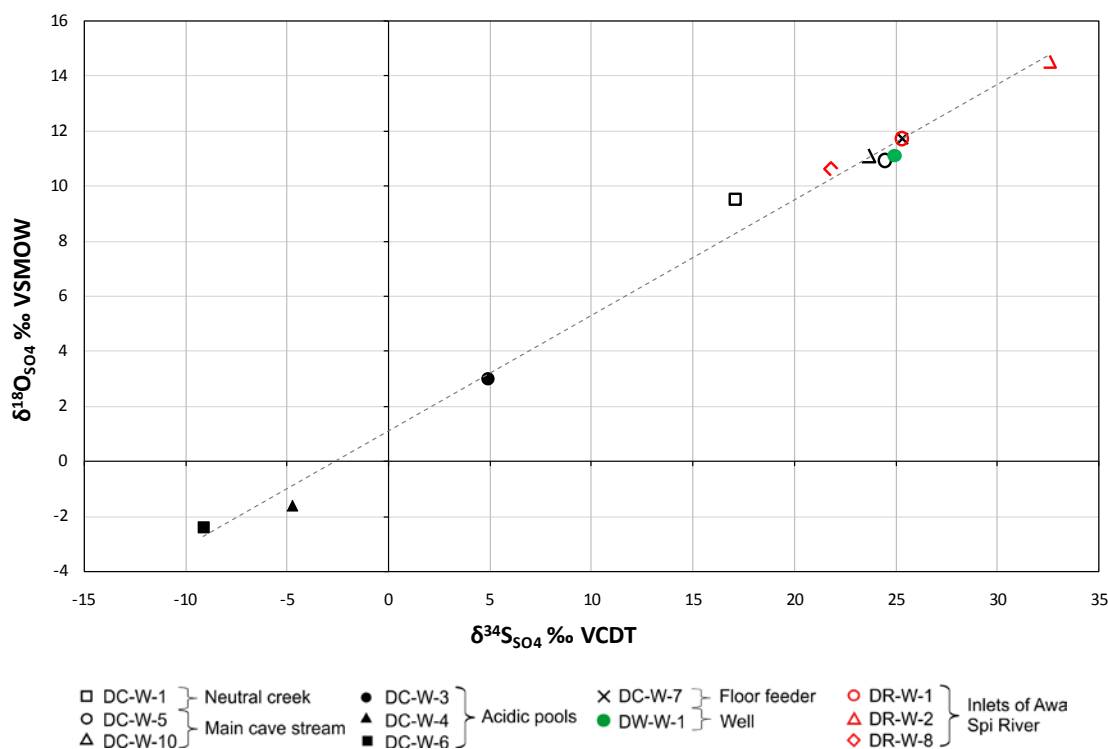


Figure 36: The sulphur and oxygen isotopic composition of dissolved sulphate in cave waters (black symbols), springs (red symbols), and well water (green symbol).

#### 5.4.2.2 Gypsum and limestone

$\delta^{34}\text{S}$  data for analyzed gypsum can be divided into two distinct groups, namely primary and secondary gypsum (Figure 37). The primary gypsum of Lower Fars Formation, a possible source of cave sulphur, had mean  $\delta^{34}\text{S}$  and  $\delta^{18}\text{O}$  values of 22.2 ‰ and 13.6 ‰, respectively (based on three samples). The sulphur isotopic results correspond very well to data from Thode and Monster (1970). They analyzed 19 gypsum samples from Lower Fars in Northern Iraq and found a  $\delta^{34}\text{S}$  range of +20.8 to 23.2 ‰.

The second group is composed of 9 secondary gypsum samples. The  $\delta^{34}\text{S}$  values are remarkably uniform (-10.9 to -9.6 ‰). On the contrary,  $\delta$  values of oxygen isotopes have a range of 10.3 ‰, with -7.0 ‰ being the lowest and +3.3 ‰ being the highest  $\delta^{18}\text{O}$  value. This is further evaluated in chapter 5.5.3.

Two samples of Oligocene limestone were prepared for sulphur isotopic analysis. Yet, sample DS-PL-1 contained very little sulphur (~0.07 mg/g, XRF analysis) and even though 25 g limestone powder was taken for the procedure, no  $\text{BaSO}_4$  precipitate could be recovered from the filter paper. Accordingly, only one single sample of Oligocene Formation could be

further analyzed. Its sulphur isotopic composition was very low (-13.7 ‰) – even lower than values of analyzed secondary gypsum.

Technically speaking, sample DC-PL-16 is a third sample from Oligocene Formation, but in contrast to the original limestone, it was taken from the cave floor and shows clear signs of alteration. Compared to the unaltered rock, DC-PL-16 shows elevated sulphur contents, as well as a  $\delta^{34}\text{S}$  value that is around 10 ‰ higher. Interestingly, the  $\delta^{18}\text{O}$  value remained at around 1.3 ‰.

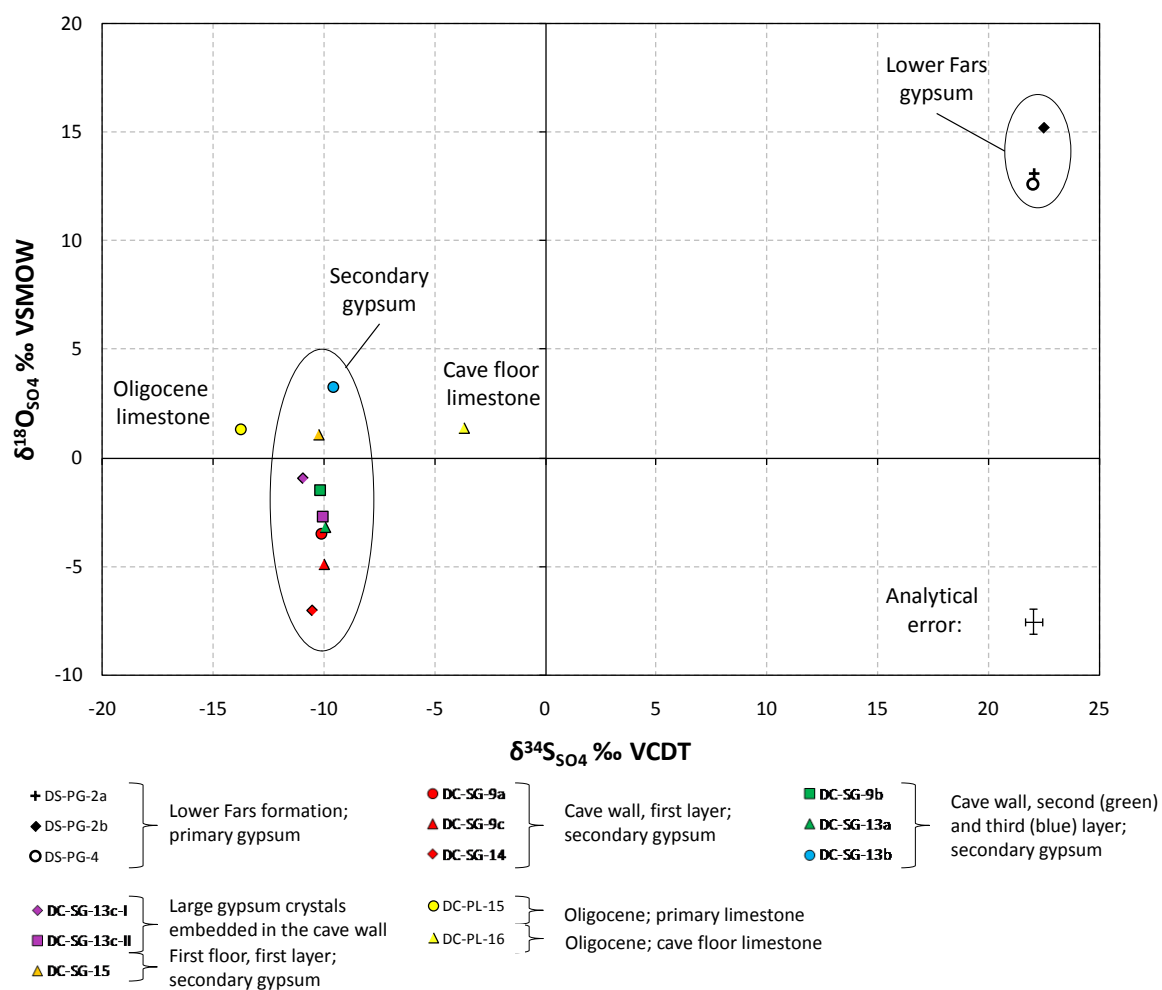


Figure 37:  $\delta^{18}\text{O}$  and  $\delta^{34}\text{S}$  measurements of gypsum and limestone samples. The depicted analytical error applies to all data points of the respective isotope species ( $\pm 0.4$  ‰ VCDT for sulphur,  $\pm 0.6$  ‰ VSMOW for oxygen).

### 5.4.2.3 Elemental sulphur

As described earlier, several parts of the cave wall are covered by a crust of elemental sulphur. Two such sulphur samples were analyzed for their  $\delta^{34}\text{S}$  ratios. Furthermore, the sulphur isotopic composition of small sulphur blooms, growing on the surface of large gypsum crystals (see chapter 5.2 for detailed description), was determined for two samples. Unfortunately, there was not enough material left to analyze these blooms in both laboratories. Hence, in contrast to all other sulphur isotopic results, the presented  $\delta^{34}\text{S}$  values of the sulphur blooms were determined at the TUBAF instead of the UFZ. Because  $\delta^{34}\text{S}$  measurements of  $^{34}\text{S}$  depleted samples agree well between the laboratories (see chapter 0), the analytical results listed in Table A 23 and Table 10 are thought to be comparable. A graphical comparison of the measurements with the results of associated secondary gypsum samples is presented in Figure 38.

Table 10:  $\delta^{34}\text{S}$  analysis of elemental sulphur.

ID	Description	$\delta^{34}\text{S}$ in ‰ vs VCDT	Lab
DC-ES-1	Elemental sulphur crust at cave site 1	-10.7	UFZ
DC-ES-13a	Elemental sulphur crust at cave site 13	-11.3	UFZ
DC-ES-13c	Sulphur bloom on gypsum crystal DC-SG-13c	-15.2	TUBAF
DC-ES-13d	Sulphur bloom on gypsum crystal DC-SG-13d	-10.1	TUBAF

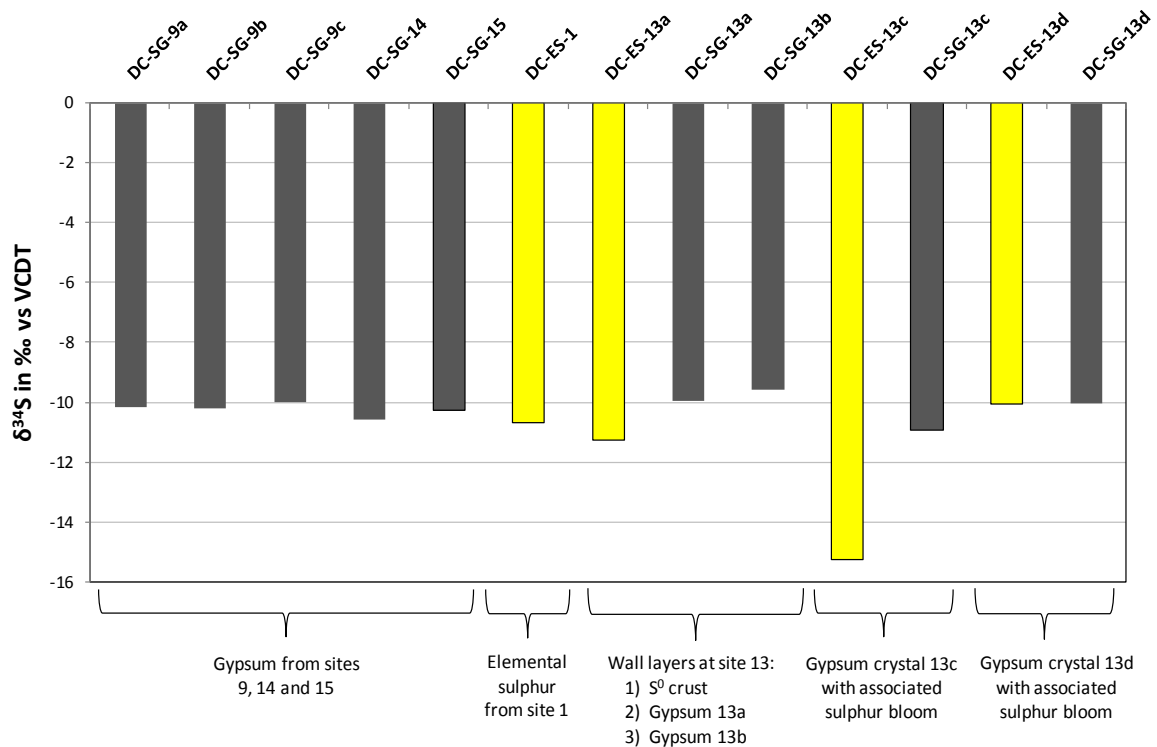


Figure 38: Sulphur isotopic composition of elemental sulphur (yellow bars) in comparison to secondary gypsum (grey bars).

### 5.4.2.4 Sedimentary sulphur species

Altogether five cave sediments were analyzed for the sulphur isotopic composition of sedimentary sulphur species. Figure 39 depicts the analytical results. A more detailed compilation of the data is given in the Appendix (Table A 22). If not stated otherwise, analytical precision was  $\pm 0.4$  ‰. Four of five sediments contained pyrite, ranging from a  $\delta^{34}\text{S}$  value of -22.9 to -11.8 ‰. Elemental sulphur had  $\delta^{34}\text{S}$  values of -11.9 to -7.5 ‰, and sedimentary sulphate species (mainly gypsum) ranged from -11.9 to  $4.1 \pm 2.1$  ‰. The total sulphur extracts gave  $\delta^{34}\text{S}$  values ranging from -14.3 to -7.8 ‰.

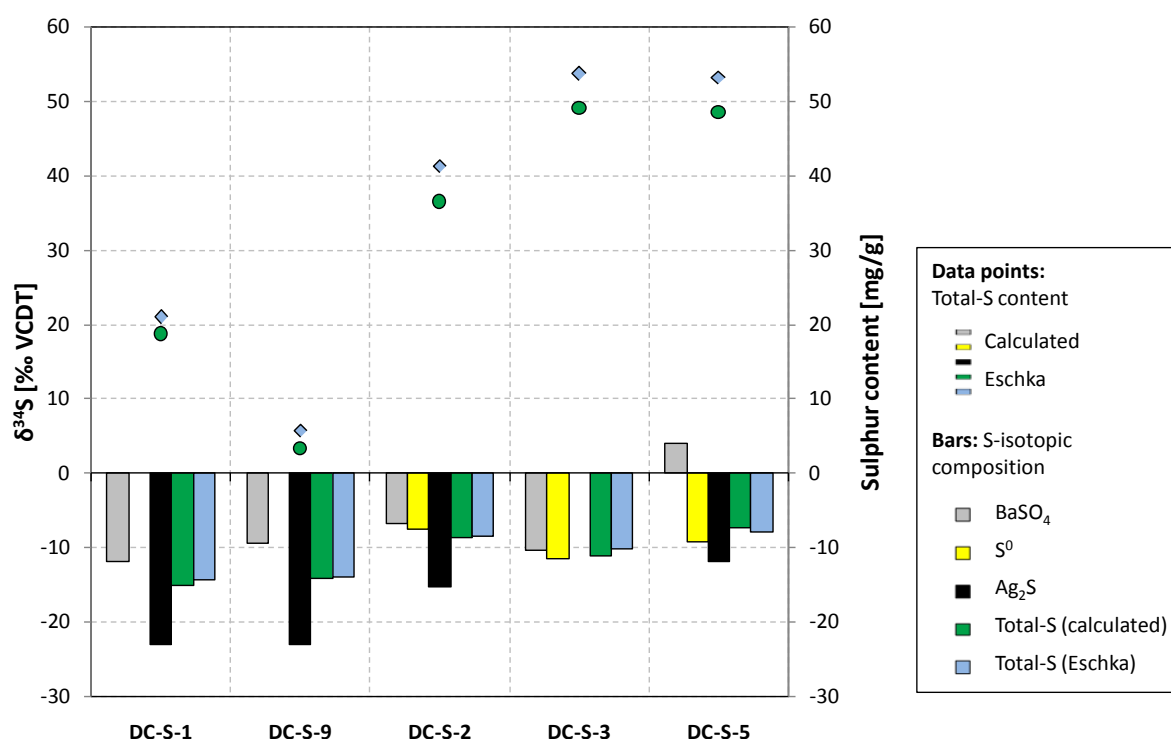


Figure 39: Bars: Sulphur isotopic composition of different sulphur extracts from sediments. Sedimentary sulphate was extracted as  $\text{BaSO}_4$ ,  $\text{S}^0$  was recovered as  $\text{S}^0$ , pyrite was recovered as  $\text{Ag}_2\text{S}$ . Analytical precision was typically  $\pm 0.4$  ‰ VCDT, but there were two exceptions:  $\pm 2.1$  ‰ (DC-S-5,  $\text{BaSO}_4$ ) and  $\pm 2.2$  ‰ (DC-S-9,  $\text{Ag}_2\text{S}$ ).  $\delta^{34}\text{S}_{\text{total, Eschka}}$  is based on a single measurement. Data points: Total sulphur concentration based on yield calculations – either from sequential (green) or Eschka (blue) extraction.

### 5.4.2.5 Crude oil

Crude oil, seeping from the subsurface into *Awa Spi* River, contained 0.14 wt% sulphur (see Table A 6 for concentrations of H, C, and N) with a  $\delta^{34}\text{S}$  value of -9.05 ‰ relative to VCDT. According to Faure (1986),  $\delta^{34}\text{S}$  values of petroleum typically vary between -8 and +32 ‰. Thus, oil from Darzila can be placed at the very bottom of the scale. Unfortunately, this one sample was the only oil discharge found in the vicinity of the cave, so there were no additional measurements. It is thus not possible to verify that this  $\delta^{34}\text{S}$  value is representative for local oil accumulations. However, compared to the findings of Thode and Monster (1970) as well as Thode and Rees (1970), the result appears reasonable (Figure 40). These authors studied the source and migration of oil fields of northern Iraq. Altogether 42 crude oil samples from Cretaceous and Tertiary oil reservoirs were analyzed for their sulphur isotopic composition. The results were remarkably uniform. The lowest  $\delta^{34}\text{S}$  value found (-8.7 ‰) came from one of the *Bay Hassan* field samples; the overall mean for all these oils was  $\delta^{34}\text{S} = -5.4$  ‰.

Several authors (e.g. Khanaqa and Al-Manmi 2011, Iurkiewicz and Stevanovic 2010, Heiland 2016) mentioned that hydrocarbon affluxes could present a source of cave sulphur. This will be discussed in chapter 5.5.2 (Origin of the fluids).

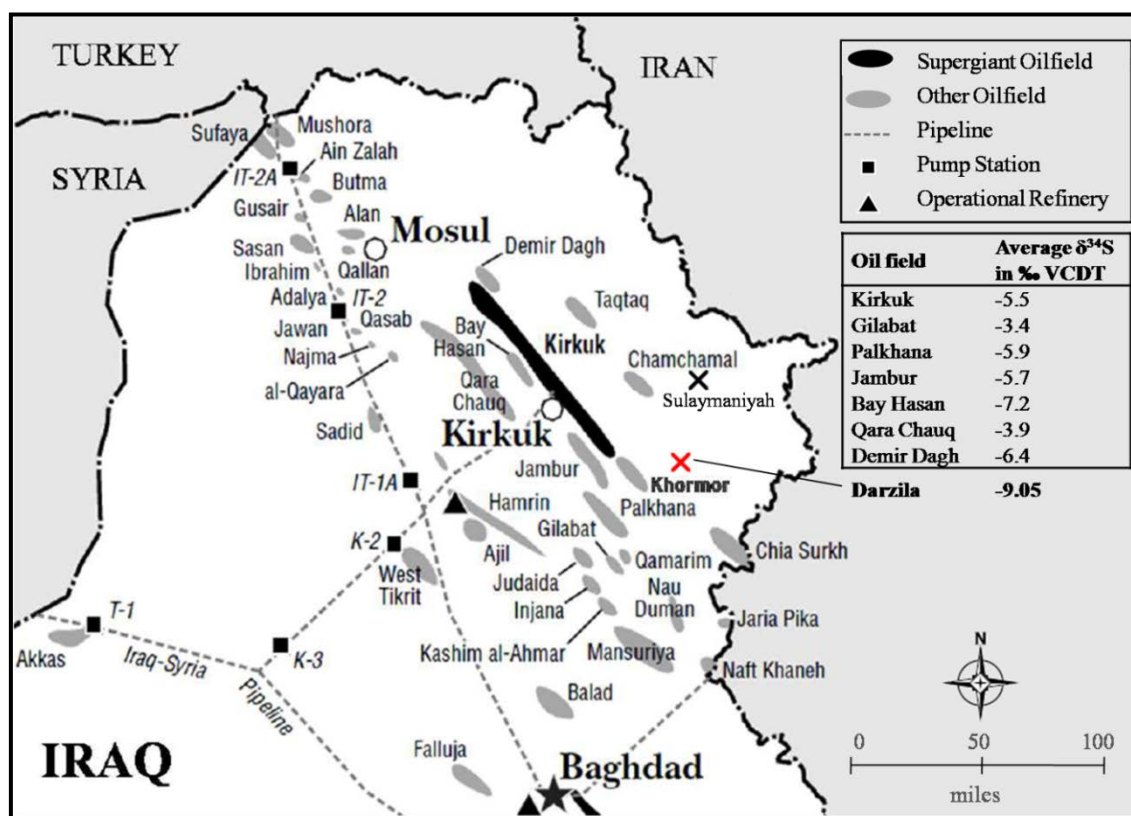
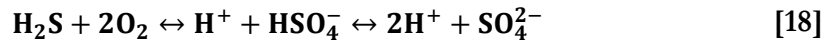


Figure 40: Oil infrastructure of Northern Iraq and sulphur isotopic data for selected oil fields (map modified after CIA 2003;  $\delta^{34}\text{S}$  values from Thode and Monster, 1970).

## 5.5 Constraints on Cave-Forming Processes

### 5.5.1 Estimation of the Cave Age

It is a major challenge to reconstruct the exact condition of cave formation through time. Still, it should be possible to assess the limits on the processes and their rates. During fieldwork, only about 200 m of the cave could be explored. Accordingly, the total size of Darzila cave is still unknown. However, with a few assumptions, it is not difficult to estimate the mass of H<sub>2</sub>S needed to produce the investigated part of the cave. Simplifying the explored cave void to a body of 200 m length, 15 m width and 10 m height, the produced room has an approximate volume of 30000 m<sup>3</sup>. If the host rock is assumed to be pure calcite (density = 2.7 g/cm<sup>3</sup>), 1 m<sup>3</sup> of host rock weighs 2700 kg. It is furthermore assumed that all H<sub>2</sub>S entering the cave is consumed according to the equations (Palmer and Palmer 2000):



In that case, one mole of H<sub>2</sub>S (34 g/mol) would dissolve one mole of calcite (100 g/mol) and 2 mol of O<sub>2</sub>. Accordingly, 9.18 · 10<sup>5</sup> g of H<sub>2</sub>S would be necessary to dissolve 1 m<sup>3</sup> of calcite. Since the prevailing conditions in the cave have changed over time, it is difficult to relate this mass of H<sub>2</sub>S to the time span that was needed for dissolution. The dissolution rate greatly depends on the production of sulphuric acid. In turn, dissolution rate depends on H<sub>2</sub>S flux, discharge rate, availability of oxygen (see equation 1), and CO<sub>2</sub> partial pressure (Palmer and Palmer 2000). Due to all these uncertain variables, any calculations must be regarded as rough estimations only. According to Khanaqa and Al-Manmi (2011), the discharge rate in the cave varies between 40 L/s (dry season) and 60 L/s (wet season). During fieldwork at the end of the dry season, the discharge rate appeared to be even lower. Therefore, a very conservative value of 10 L/s discharge rate was applied for the calculation. The initial value of dissolved H<sub>2</sub>S was set to 0.001 mol/L (34 mg/L). This is around seven times higher than the determined concentration in water at the main floor feeder (DC-W-7), but it is significantly lower than the concentration of ascending H<sub>2</sub>S (prior oxidation to SO<sub>4</sub><sup>2-</sup>) at the acidic pool DC-W-6. With these basic assumptions, the simple dissolution model of Palmer (1991) can be applied. Figure 41 shows the saturation concentration of calcite in H<sub>2</sub>S and H<sub>2</sub>SO<sub>4</sub> solutions at 25° C. It is assumed, that the water is saturated with calcite (prior sulphuric acid formation) and contains 0.001 mol/L (44 mg/L) CO<sub>2</sub>. When the water reaches the water table, all H<sub>2</sub>S oxidizes to H<sub>2</sub>SO<sub>4</sub>, which facilitates calcite dissolution. The

prevailing temperature of DC-W-7 is around 26° C, so it agrees rather well to the model. According to Heiland (2016), DC-W-7 is slightly undersaturated with respect to calcite and contains around 60 mg/L CO<sub>2</sub> (based on TIC values and PhreeqC modelling). Accordingly, the conditions are not exactly met, but they will be used as approximations. Heiland (2016) detected a decrease of total inorganic carbon in water along the flow path as well as a change of the saturation indices of carbonates and proposed that this is due to CO<sub>2</sub> degassing. Since CO<sub>2</sub> degassing leads to a decrease of dissolution, this is a very important observation.

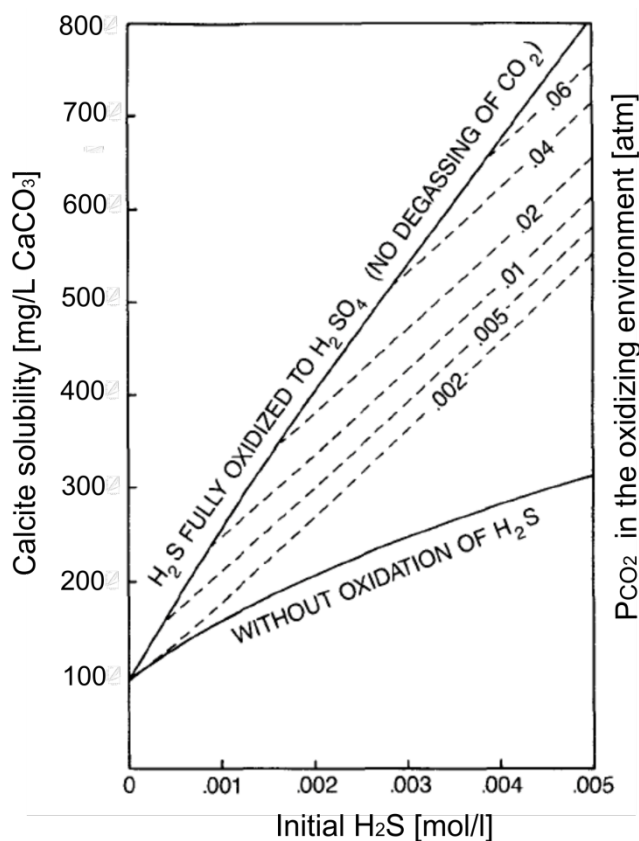


Figure 41: Dissolution of calcite caused by oxidation of H<sub>2</sub>S to sulphuric acid in a system at 25° C and an initial CO<sub>2</sub> concentration of 0.001 M. Lower line = calcite saturation in the initial system prior oxidation. Upper line = calcite saturation after complete oxidation of dissolved H<sub>2</sub>S. Dashed lines in between reflect that dissolution diminishes on CO<sub>2</sub> outgassing. After Palmer (1991).

According to Figure 41, a solution containing 0.001 mole/L H<sub>2</sub>S which completely oxidizes to sulphuric acid, but is subject to CO<sub>2</sub> degassing (ambient CO<sub>2</sub> in cave air ≈ 0.01 atm), around 100 mg/L of additional calcite could be dissolved. Applying a discharge rate of 10 L/s and a calcite density of 2.7 g/cm<sup>3</sup>, approximately 12 m<sup>3</sup> host rock could be dissolved each year. At that rate it would take only around 2500 years to dissolve the explored part of Darzila cave. However, this value is thought underestimate the actual age considerably. Most importantly, not all H<sub>2</sub>S converts to sulphuric acid. At the very end of the explored passage, the cave river still contained considerable amounts of dissolved sulphide. Also, due to a

strong smell of rotten eggs, it is evident, that H<sub>2</sub>S degasses from the water. The smell was strong and persistent, led to irritations of the eyes, the nose and the throat, but it was possible to work in the cave for several hours without getting headache or losing the sense of smell. Accordingly, the concentration of H<sub>2</sub>S in the cave atmosphere could have been approximately 5 ppm (Safety Directory 2004). Based on an equation ( $c[\text{mg}/\text{m}^3] = 0.0409 \cdot c[\text{ppm}]/M(\text{H}_2\text{S})$ , at 25° C) of Boguski (2008), this equals around 180 mg

hydrogen sulphide in the cave void. While a portion of this  $\text{H}_2\text{S}$  oxidizes to  $\text{H}_2\text{SO}_4$  or elemental sulphur, another portion degasses from the cave and is lost from the system.

A more simple approach to estimate the age of the cave, is to use the  $\text{Ca}^{2+}$  concentration of the water and relate it to the volume of water per time. Because precipitation water is distilled water, it can be assumed that all calcite present in cave waters originates from calcite dissolution. Using the simplifications from above (discharge = 10 L/s, host rock = pure calcite), and the  $\text{Ca}^{2+}$  concentration in stream water of the rear part of the cave (~305 mg/L), an even younger age can be computed. Only 340 years would be necessary to dissolve 30000  $\text{m}^3$  of calcite. However, the  $\text{Ca}^{2+}$  concentration at the main floor feeder was 300 mg/L already. Thus, dissolution of calcite starts well below the cave floor. Using the 5 mg/L difference between inlet and outlet as  $\text{Ca}^{2+}$  concentration, the age would be around 20000 years. Unfortunately, the situation is complicated by the fact that much of the reaction of sulphuric acid with limestone produces gypsum. Although gypsum blocks fall to the floor and dissolve - the removal of  $\text{Ca}^{2+}$  from the cave is delayed, and the age estimation becomes afflicted with extra uncertainties. Nevertheless, an age of around 20000 years appears plausible.

### 5.5.2 The Origin of the Fluids

The sulphur isotopic signature of dissolved sulphur species varies considerably between the different sampling sites, and there is reason to believe that the waters are influenced by different sulphur sources.

One possible source is outgassing sulphur from the host rock formation. However, the sulphur content is negligibly small and a major impact on cave sulphur is unlikely. Therefore, host rock sulphur will not be considered in the following sections. A more likely source is isotopically light hydrogen sulphide ( $\delta^{34}\text{S} = -9.05 \text{ ‰}$ ) from crude oil. The similarity of  $\delta^{34}\text{S}$  values in the isolated pools (Figure 42) with that of crude oil indicates a potential influence. Another possible source of cave sulphur is gypsum from Lower Fars Formation. Based on three samples, an average  $\delta^{34}\text{S}$  value of 22.2 ‰ VCDT could be determined. This value lies relatively close to those of the spring waters, flowing cave waters, and the well. The isolated pool DC-W-3 is located somewhere in between and appears to be a mixture.

According to Iurkiewicz and Stevanovic (2010), Sagirma gypsum layers could present a third sulphur source. Unfortunately, gypsum from Sagirma Formation was not sampled and no isotopic data are available for that formation. However, an approximate value can be

derived from the literature. Paytan *et al.* (1998) extensively studied the sulphur isotopic composition of Cenozoic seawater sulphate and generated a continuous  $\delta^{34}\text{S}$  curve for this geological era. Based on the underlying data set (Paytan 2012), Sagirma Formation, which is of middle to upper Eocene age, should have a sulphur isotopic composition of about 22.3 ‰ VCDT. This value is basically identical to that of Lower Fars Formation. All considerations and calculations in the following sections are based on Lower Fars data. However, most likely they apply to Sagirma Formation as well.

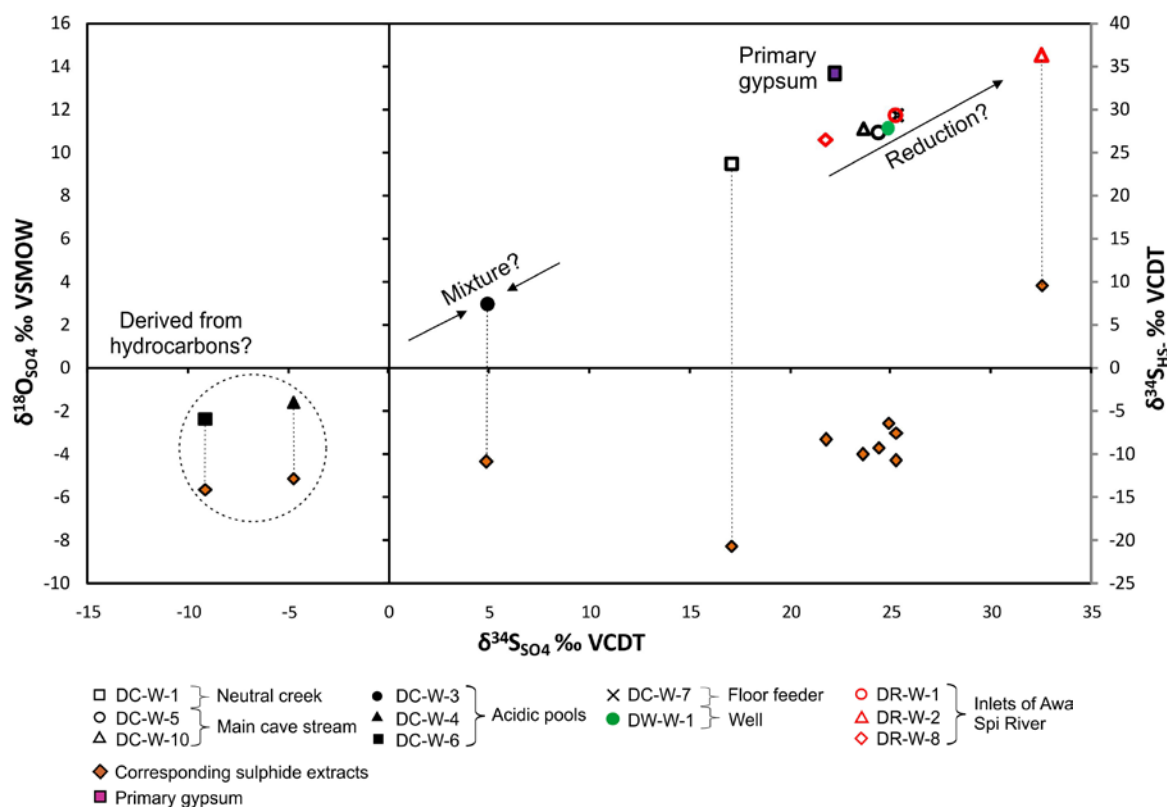


Figure 42: First ideas about the origin of dissolved sulphur species in individual water samples. More specifically, the graph shows the isotopic composition of sulphate oxygen and sulphide against that of sulphate sulphur. The symbols that were used in the previous chapter (black = cave water, red = inlets of Awa Spi, green = well) are used to depict the isotopic composition of sulphate ( $\delta^{34}\text{S}_{\text{SO}_4}$  and  $\delta^{18}\text{O}_{\text{SO}_4}$ ). As indicated by the dashed lines, the orange diamonds show the respective sulphur isotopic composition of sulphide ( $\delta^{34}\text{S}_{\text{HS}}$ ). The sulphate isotopic composition of Lower Fars gypsum (mean  $\delta^{34}\text{S}$  and  $\delta^{18}\text{O}$ ) is shown for comparison.

### 5.5.2.1 Lower Fars gypsum as endmember

The dissolution of gypsum from Lower Fars Formation ( $\delta^{34}\text{S} = 22.2\text{‰}$ ) occurs without sulphur isotopic fractionation (based on Böttcher and Usdowski 1993). In the aquifer, a certain fraction of dissolved sulphate may get reduced to  $\text{H}_2\text{S}$  due to bacterial mediation, which typically leads to a progressive sulphur isotopic composition of unconsumed sulphate. Under closed system conditions, this process follows a Rayleigh distillation equation as described in chapter 3.1.2.2. The fraction  $f$  of residual, unconsumed sulphate was computed using an initial sulphate concentration of 2001.7 mg/L. This value belongs to a well sample from Lower Fars Formation in the Chamachamal region, sampled in the dry season (Al-Manmi 2012). Values for  $f$  varied from -0.31 (DR-W-2) to 6.60 (DC-W-6). A complete list of values is given in Table A 25.

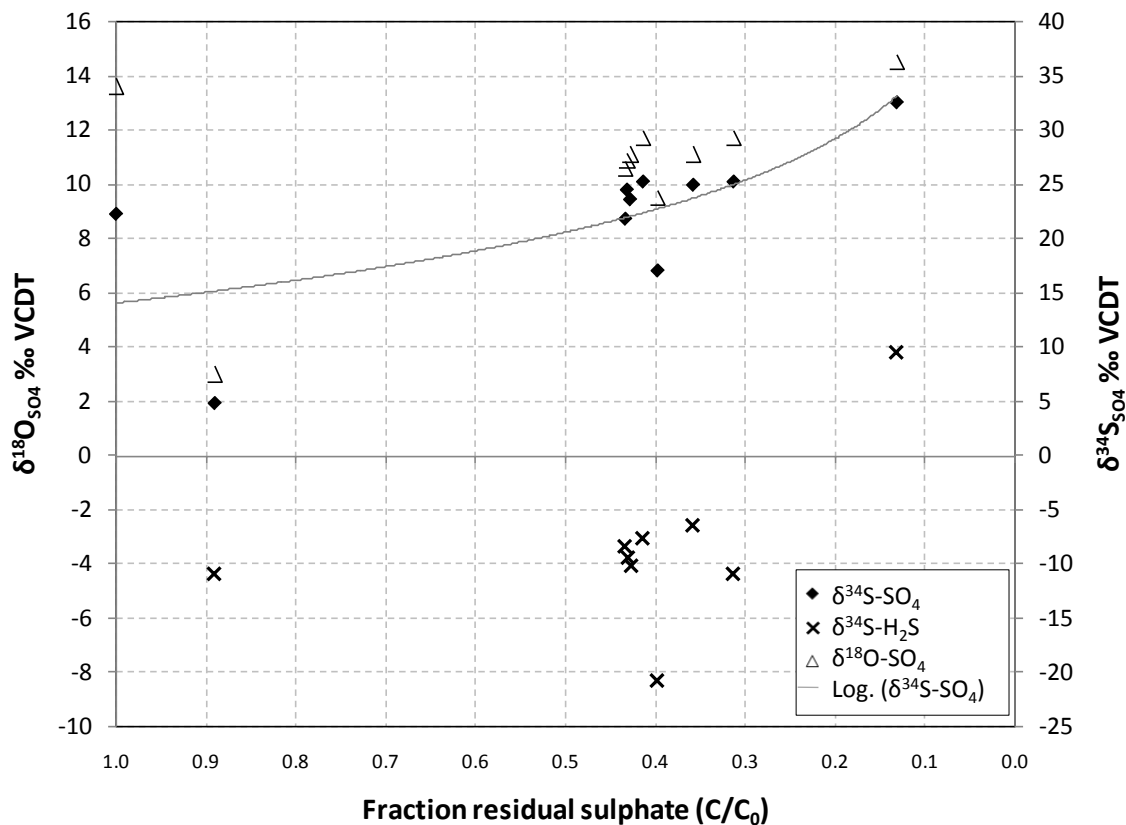


Figure 43: Stable sulphur and oxygen isotope ratios of remaining, unconsumed  $\text{SO}_4^{2-}$  and of produced hydrogen sulphide. Samples DC-W-6 and DC-W-4 were excluded.  $R^2$  of the logarithmic fit: 0.52.

If sulphate reduction was the controlling mechanism for the observed isotopic effects, the data points should be correlated. However, the logarithmic relationship of the plotted data (Figure 43) is not convincing, and a linear relationship cannot be detected either. Two of the samples, DC-W-6 and DC-W-4, were not even included into the graph, because they gave  $f$  values of 6.6 and 2.42, respectively. As described above,  $f$  stands for the fraction of

sulphates remaining. Accordingly, DC-W-6 and DC-W-4 have a higher sulphate concentration than possible, if Lower Fars gypsum was the only sulphur source. Because it is not entirely clear, if the sulphate concentration used as initial value is representative, the value was varied. However, the overall message of the graph did not change. Due to the inhomogeneous appearance of the samples, the Rayleigh distillation model is not applicable to the complete data set. Accordingly, the data set was reduced to those specific samples that are suspected to be derived from gypsum (see Figure 42): The main cave inlet DC-W-7, all three feeders of Awa Spi River, and the well. As before an initial solution with a sulphate concentration of approximately 2000 mg/l and a  $\delta^{34}\text{S}$  value of 22.2 ‰ was used.

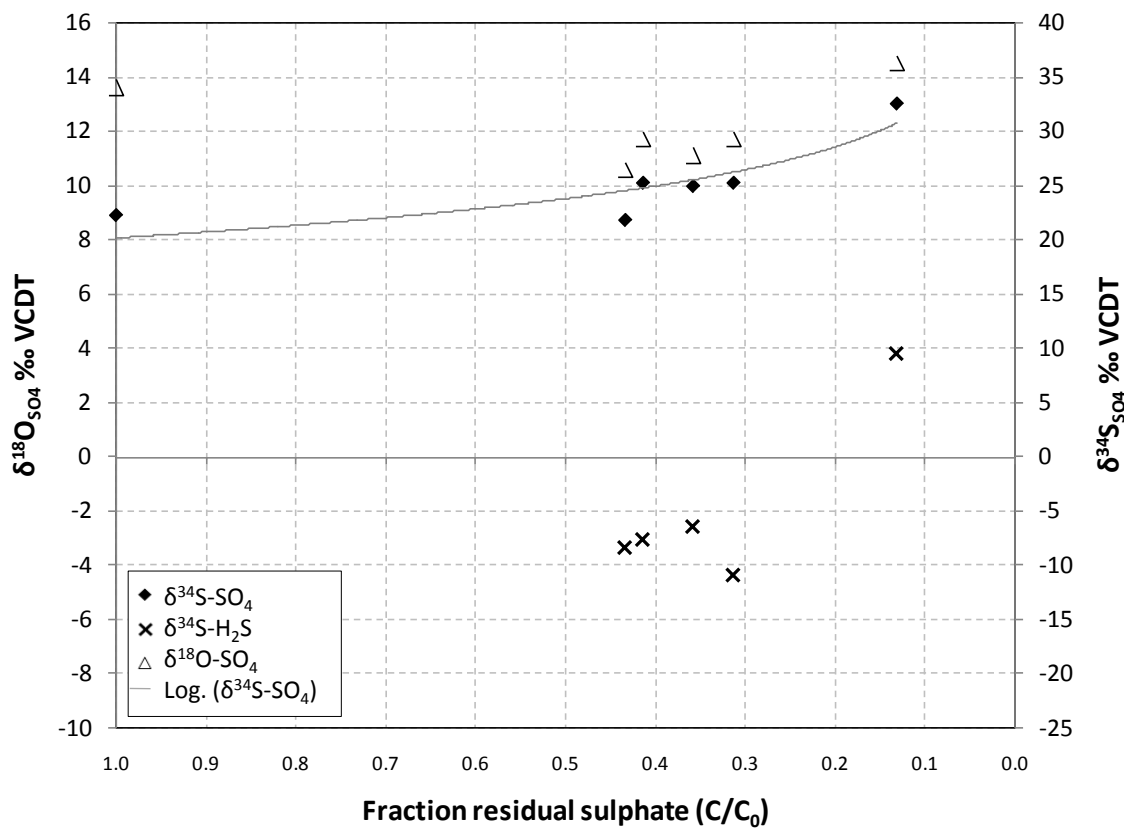


Figure 44: Stable sulphur and oxygen isotope ratios of remaining, unconsumed  $\text{SO}_4^{2-}$  and of produced hydrogen sulphide. Only samples DC-W-7, DR-W-1, DR-W-2, DR-W-8, and DW-W-1 were included.

This time, logarithmic regression analysis of  $\delta^{34}\text{S}_{\text{SO}_4}$  yielded an  $R^2$  of 0.78. This appears to be an improvement to the previous model but there are still more than 20 % of variation that are not explained by this model. Nevertheless, a preliminary enrichment factor  $\epsilon^{34}\text{S}_{\text{H}_2\text{S}-\text{SO}_4}$  of -5.34 ‰ was computed. This value does not agree with the range of values reported for bacterial sulphate reduction. Typically, the isotope fractionation should be considerably larger. Accordingly, bacterial sulphate reduction seems to be superimposed by other sulphur transformation processes.

The approach to model the evolution of the sulphur isotopic composition in the aquifer by Rayleigh distillation was not successful. Thus, a step-by-step analysis (Figure 45) of the systems and the associated processes seems necessary: Gypsum with the initial sulphur isotopic composition of 22.2 ‰ dissolves without measurable fractionation. In the aquifer, bacterial sulphate reduction occurs and leads to large fractionation effects. As the primary sulphate stock is virtually infinite, it can be expected that the system is open with respect to sulphides. Accordingly, there should be distinct fractionation effects for dissolved sulphide, while  $\delta^{34}\text{S}$  of dissolved sulphate could remain relatively constant at 22.2 ‰. At places, where the assumption of an infinite supply with freshly dissolved sulphate does not apply, unconsumed sulphate would get enriched in  $^{34}\text{S}$ . If these fluids would enter the cave at that instant, dissolved sulphides and sulphates would have a sulphur isotopic composition of -19 to +6 ‰ VCDT, and  $\geq 22.2$  ‰ VCDT, respectively.

However, this process might be complicated by removal of sulphides from the aquifer. Likely processes to withdraw produced sulphide are either precipitation of metal sulphides, upward transport of  $\text{H}_2\text{S}$  by degassing from the sites of BSR, or re-oxidation to elemental sulphur or sulphate. All these processes would affect the composition of the fluid:

Degassing of sulphide would cause only small ( $\sim 1.5$  ‰ at 22° C, Szaran 1996) to negligible (Ohmoto and Rye 1979) sulphur isotopic effects. Thus it was assumed, that degassing of  $\text{H}_2\text{S}$  merely diminishes the concentration of the dissolved species, but leaves its sulphur isotopic composition unchanged.

If reactive ferrous iron ( $\text{Fe}^{2+}$ ) is present in the aquifer, a certain part of formed sulphide may precipitate instantly as FeS. Based on the findings of Böttcher *et al.* (1998), FeS should be slightly depleted in  $^{34}\text{S}$  when compared to the parent sulphide ( $\epsilon^{34}\text{S}_{\text{FeS-HS}} = -1.2$  ‰; room temperature). Progressive sulphidation and conversion of FeS leads to the formation of pyrite, which inherits the sulphur isotopic composition of its precursor entirely (at 70 °C; Wilkin and Barnes 1996).

On contact with oxidizing compounds such as dissolved oxygen, nitrate or ferric iron, reduced sulphur species may get re-oxidized to sulphate. Generally spoken, sulphur isotopic effects during sulphide oxidation are small (see chapter 3.1.2.3 for detailed information). Accordingly, the residual sulphide pool will retain its isotopic composition with a characteristically light  $\delta^{34}\text{S}$  value. Produced sulphate will be isotopically light, too. If this

sulphate mixes with the original sulphate pool prior BSR, sulphate concentrations increase again. Simultaneously, its  $\delta^{34}\text{S}$  value will decrease and might fall back to 22.2 ‰.

Accordingly, the sulphur isotopic variations in analyzed samples could be ascribed to a varying degree of re-oxidation, degassing and precipitation.

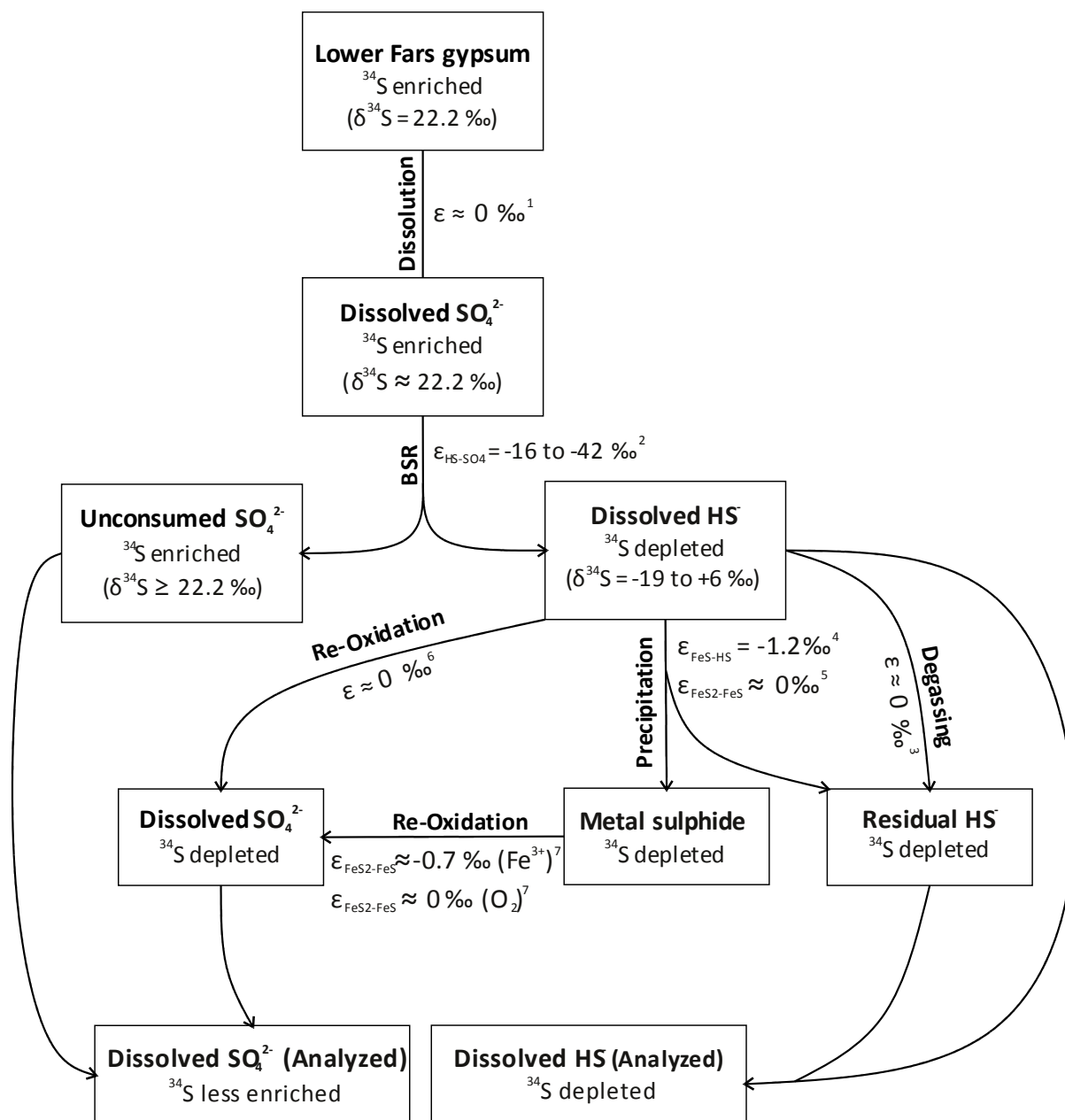


Figure 45: Sulphur isotopic evolution of sulphur species derived from Lower Fars gypsum as endmember. Enrichment factors: <sup>1</sup> Böttcher and Usdowski 1993; <sup>2</sup> Habicht and Canfield 1997b; <sup>3</sup> Ohmoto and Rye 1979; <sup>4</sup> Böttcher *et al.* 1998; <sup>5</sup> Wilkin and Barnes 1996; <sup>6</sup> Knöller and Schubert 2007; <sup>7</sup> Balci *et al.* 2007.

### 5.5.2.2 Reduced sulphur in crude oil as endmember

Similar considerations can be conducted for the evolution of sulphur that originates from crude oil (Figure 46). The  $\delta^{34}\text{S}$  value of sulphur species in crude oil was -9.05 ‰. Because this value agrees well with literature values for oil fields from Northern Iraq (Thode and Monster 1970), it will be used as the initial value for sulphur in hydrocarbons. Several authors (Thode and Monster 1979, Thode and Rees 1970, Vredenburg and Cheney 1971, Orr 1974) independently discovered that migration and maturation of oil, as well as degassing of  $\text{H}_2\text{S}$  do not cause sulphur isotope fractionations. Accordingly, the first step in the evolution of sulphur from crude oil with  $\delta^{34}\text{S} \approx -9$  ‰ was assumed to occur without any fractionations. Outgassing  $\text{H}_2\text{S}$  may precipitate as mono- or disulphides as described in the previous chapter. When the sulphide ascends into oxygenated waters or gets in contact with ferric iron, it is oxidized to elemental sulphur and/or sulphate. If the oxidation is nearly complete (low  $\text{H}_2\text{S}:\text{SO}_4^{2-}$ ), little or no fractionation is evident between reactants and products – regardless of isotopic fractionations accompanying the oxidation. In this case, the initially low  $\delta^{34}\text{S}$  is evident between reactants and products and thus, the initially low  $\delta^{34}\text{S}$  values of the ascending sulphide are retained at around -9 ‰.

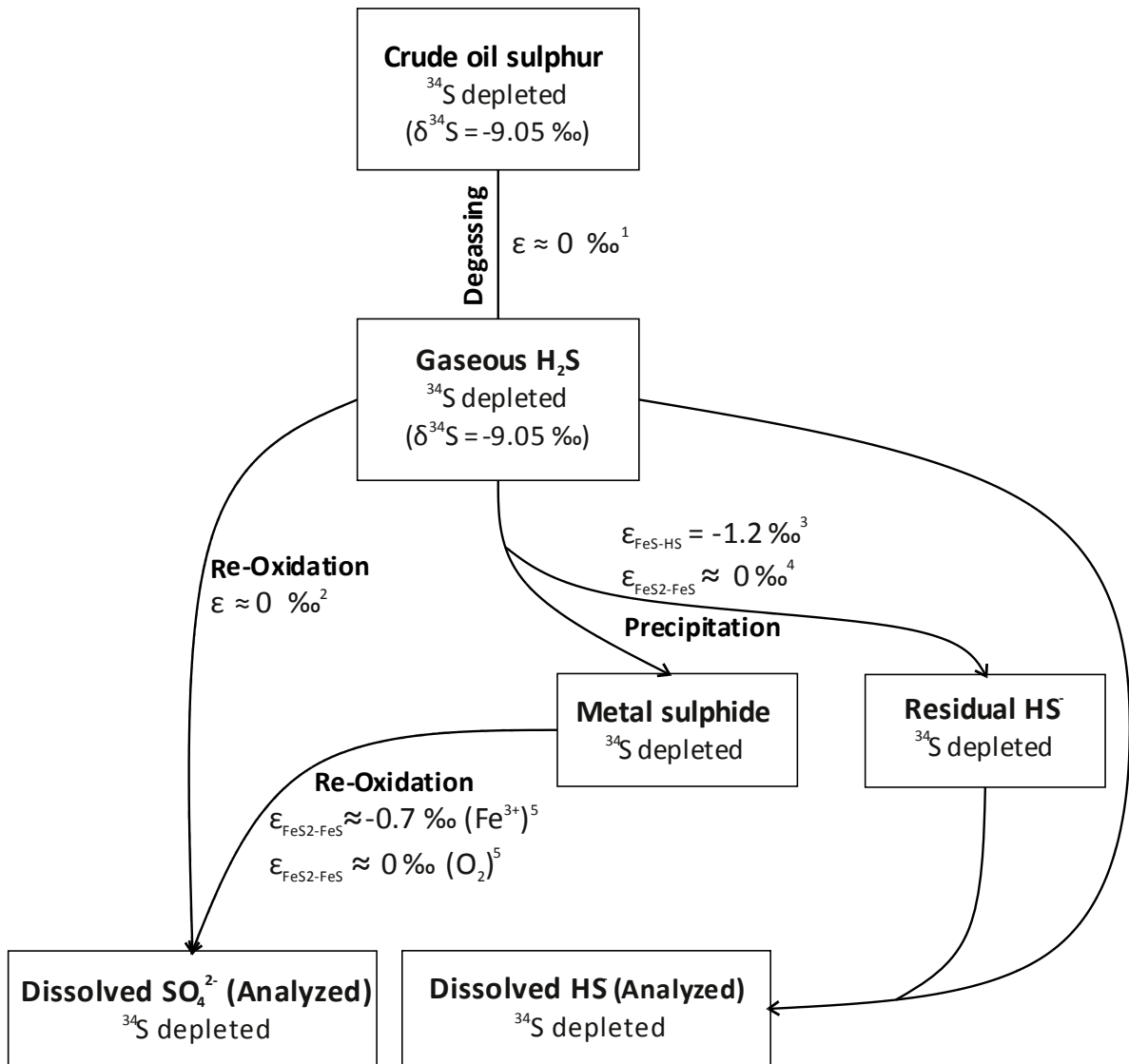


Figure 46: Sulphur isotopic evolution of sulphur species derived from sulphur in crude oil as endmember. Enrichment factors: <sup>1</sup>Thode and Monster 1970, Thode and Rees 1970, Vredenburg and Cheney 1971, Orr 1974; <sup>2</sup>Knöller and Schubert 2007; <sup>3</sup>Böttcher *et al.* 1998; <sup>4</sup>Wilkin and Barnes 1996; <sup>5</sup>Balci *et al.* 2007.

### 5.5.2.3 Individual sampling sites and mixing processes

As shown in Figure 42, water samples were suspected to be derived from hydrogen sulphide affluxes, primary gypsum, or a mixture of both. Due to the inhomogeneous appearance of the data and the complexity of possible influences, sampling sites will be evaluated individually.

#### ➤ Isolated pools

The isolated pool DC-W-6 is arguably the most extreme water found in the cave. Based on elevated concentrations of dissolved organic carbon, total dissolved solids, and relative enrichments of trace elements such as Cr, Be, Ga, and Ni, Heiland (2016) suspected a potential influence of hydrocarbon-related waters. The low  $\delta^{34}\text{S}$  values of sulphur species in water point towards the same direction. Yet, in order to challenge this thought, all these indications were disregarded, and it was tried to reconstruct the resulting sulphur isotopic composition by a combination of the processes depicted in Figure 45. It was not possible. To begin with, the sulphate concentration (13210 mg/L) is higher than expected from an initial concentration of around 2000 mg/L. The pool is regularly emptied by local visitors who use the water for treating skin problems. Therefore, evaporation of water in the cave and subsequent concentration of the fluid cannot explain this phenomenon. Secondly, bacterial sulphate reduction generally leads to high fractionations between residual sulphate and produced sulphide. Yet, the water had  $\delta^{34}\text{S}$  values of -14.1 ‰ for sulphide and -9.1 ‰ for sulphate. The isotopic difference amounts to around 5 ‰ only (Figure 34). Thirdly, even if the sulphate reducing bacteria would live under optimum conditions, where fractionation effects are typically smaller than otherwise (Canfield and Teske 1996), the measured  $\delta^{34}\text{S}$  values would not evolve the way they did - instead of being depleted with respect to  $^{34}\text{S}$ , both species should possess  $\delta^{34}\text{S}$  values close to 20 ‰. Even a substantial re-oxidation of sulphide, which would produce “light” sulphate, cannot lead to a  $\delta^{34}\text{S}_{\text{SO}_4}$  value of -9.1 ‰. After re-oxidation, the final  $\delta^{34}\text{S}_{\text{SO}_4}$  value would be a mixture of newly produced, light sulphate and unconsumed, heavy sulphate. Still,  $\delta^{34}\text{S}$  could only sink below 22.2 ‰, if basically all heavy sulphate is withdrawn from the system prior mixture. A small portion of sulphate might precipitate in pores of the aquifer, but it is unreasonable to expect major precipitations – especially when considering the high solubility of gypsum (2.531 g/L at 20°C, Klimchouk 1996) and the high concentrations of sulphate in the pool. It can be concluded, that sulphur in pool DC-W-6 does not originate from gypsum of Lower Fars Formation. Instead, the data are suddenly meaningful when linked to crude oil as endmember. By mass balance, the sulphur isotopic composition of dissolved sulphate and

sulphide combined was calculated to be -9.15 ‰. Considering an analytical precision of  $\pm 0.4$  ‰, this value is identical to that of crude oil (-9.05 ‰).  $\text{H}_2\text{S}$  with an initial  $\delta^{34}\text{S}$  value of -9.05 ‰ escapes from the crude oil and is subsequently oxidized to sulphate. Pool water has a sulphide concentration of about 10 mg/L, which presents only 0.23 % of dissolved sulphur species. Simultaneously,  $\delta^{34}\text{S}$  of sulphate equals the sulphur isotopic composition of the endmember. Any possible mixture with sulphur from Lower Fars would be masked by the overwhelming affluxes from hydrocarbon bearing layers. Accordingly it can be stated, that DC-W-6 is entirely controlled by the influence of hydrocarbons in the subsurface.

The controlling influence of the hydrocarbon affluxes can also be seen at pool DC-W-4. The sulphate and sulphide concentrations are lower than at site 6, but the relative concentrations are alike ( $[\text{SO}_4^{2-}] = 4840$  mg/L,  $[\text{HS}^-] = 4$  mg/L  $\approx 0.25$  % of total sulphur).

Based on hydrogeochemical similarities, Heiland (2016) proposed, that the pool at site 3 (DC-W-3) is influenced by the small creek from site 1 (DC-W-1). This can be confirmed with isotopic data. Figure 47 depicts  $\delta^{34}\text{S}$  values of sulphate against the reciprocal sulphate concentration in corresponding samples. In such a graph, straight lines indicate mixtures (Tichomirowa 2012). Based on this, pool water DC-W-3 can be described as mixture of creek water and ascending, hydrocarbon influenced waters.

Stable isotope data of water strengthen the discussions above: It can be seen in Figure 32 that  $\delta^{18}\text{O}_{\text{H}_2\text{O}}$  and  $\delta^{18}\text{O}_{\text{SO}_4}$  values of DC-W-3 lie between those of the creek and of DC-W-4. The same graph also shows that the pool DC-W-4 and DC-W-6 have the highest  $\delta\text{D}$  values of all samples. Considering that significant amounts of  $\text{H}_2\text{S}$  ascend at these sites, the positive shift of  $\delta\text{D}$  could be caused by strong partitioning of deuterium into ambient water. The elevated  $\delta^{18}\text{O}_{\text{H}_2\text{O}}$  values of DC-W-4 and DC-W-6 may be attributed to enhanced dissolution of the host rock and subsequent enrichment with liberated “heavy oxygen”. The oxygen isotopic composition of aqueous sulphate points towards hydrocarbon affluxes as well (see Figure 50 and chapter 5.5.3).

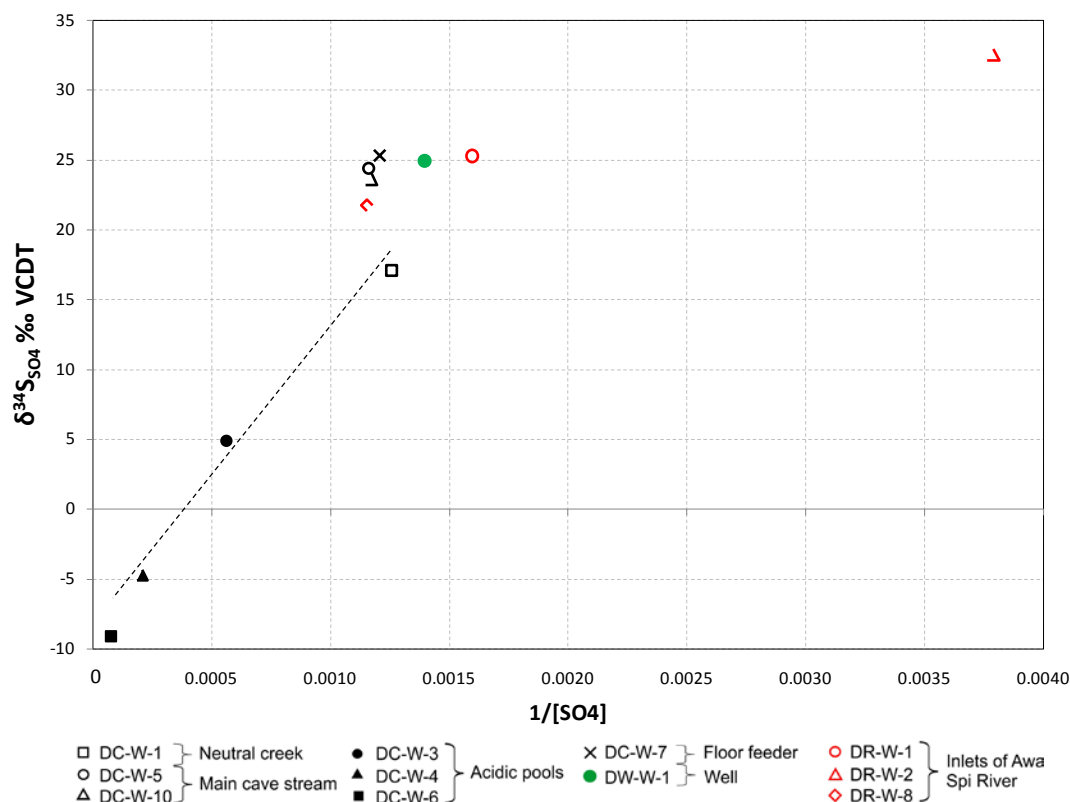


Figure 47:  $\delta^{34}\text{S}$  values of dissolved sulphate versus the reciprocal sulphate concentration. The straight line that can be drawn through the acidic pools and the neutral creek indicates mixture of respective waters.

### ➤ Flowing cave waters

The floor feeder DC-W-7 presents the main water discharge into the cave. In contrast to the isolated pools, the isotopic composition is best explained by bacterial sulphate reduction in the aquifer, followed by several secondary sulphur transformation processes. Possibly due to the high velocity of flowing waters at the discharge, no sediments were found directly at the sampling site. A few metres downstream, where irregularities of the cave floor reduced the velocity, sediment accumulation started. Here (DC-S-2), sedimentary pyrite, elemental sulphur, and sulphate was detected. Interestingly,  $\delta^{34}\text{S}$  of pyrite is  $-15.3\text{‰}$ , whereas dissolved sulphide has a  $\delta^{34}\text{S}$  value of  $-7.6\text{‰}$ . Based on the evaluation of isotope fractionations during sulphide precipitation in chapter 5.5.2.1, the  $\delta^{34}\text{S}$  value of pyrite could be expected to be around  $-8.8\text{‰}$  instead. Thus, the apparent sulphur isotope fractionation is much larger than commonly detected in other studies. This phenomenon might be explained by the following process: Bacterial sulphate reduction produced very light sulphide with a  $\delta^{34}\text{S}$  value of around  $-14\text{‰}$ . This sulphide precipitated almost instantly as  $\text{FeS}_2$  with a  $\delta^{34}\text{S}$  value of  $-15.3\text{‰}$ . Typically, the first sulphide produced from bacterial sulphate reduction is the “lightest”. If the sulphate pool does not get renewed, residual sulphate will get heavier and heavier. Simultaneously, produced sulphide will approach the initial  $\delta^{34}\text{S}$  value of

sulphate. Accordingly, a  $\delta^{34}\text{S}$  value of  $-15.3\text{‰}$  could reflect the first sulphide generation, whereas  $-7.6\text{‰}$  reflects the second sulphide generation. At some point, a proportion of dissolved sulphide was oxidized to elemental sulphur and/or directly to sulphate. This process is well reflected by the composition of the sediment DC-S-2, which contained considerable amounts of elemental sulphur with a  $\delta^{34}\text{S}$  value of  $-7.5\text{‰}$  – basically identical to that of dissolved sulphide. Sedimentary sulphate had a  $\delta^{34}\text{S}$  value of  $-6.8\text{‰}$ . Since sediments were sampled without proper preservation techniques, sedimentary sulphate may have formed after sampling.

Heavily enriched sulphate was diluted with the newly formed light sulphate. Accordingly, the sulphur isotopic difference between Lower Fars gypsum and DC-W-7 is lower than expected from bacterial sulphate reduction.

Filamentous biofilms thriving in the vicinity of the floor feeder were dominated by the sulphur oxidizing bacteria *Thiofaba teptiphilia*, *Acidithiobacillus thiooxidans* and *A. albertensis*. In certain community structures, *At. thiooxidans* may grow on pyrite (Kelly and Wood 2000), but the identified microbial community is considered to be unable to re-oxidize pyrite precipitates. However, the species are known to grow on various other reduced sulphur species. Considering that reaction rates of biotic sulphide oxidation typically are significantly higher than abiotic rates (Luther III *et al.* 2011), and that the biofilms flourish at that site, microbial mediation is thought to be the main driving force of sulphide oxidation. The microbial filaments were directly attached to the host rock on the cave floor. Such a close physical proximity to limestone material as well as their ability to consume sulphide before it comes into contact with high concentrations of dissolved oxygen (Engel *et al.* 2004) suggests that dissolution of the cave floor is mediated by these sulphur-oxidizing communities.

The small creek DC-W-1 presents the second largest discharge into the cave. Its isotopic signature clearly differs from that of DC-W-7. The large isotopic difference between dissolved sulphate ( $\delta^{34}\text{S}_{\text{SO}_4} = 17.07\text{‰}$ ) and dissolved sulphide ( $\delta^{34}\text{S}_{\text{HS}^-} = -20.74\text{‰}$ ) suggests that bacterial sulphate reduction has occurred. Pyrite in associated sediments (DC-S-1 and DC-S-9) had a  $\delta^{34}\text{S}$  value of around  $-23\text{‰}$ , which is very close to that of dissolved sulphide. Apparently, BSR diminished before the sulphate pool could be affected by isotopic fractionation. The high content of dissolved oxygen (4.23 mg/L) could have interfered with BSR. Almost all sulphur is present in its highest oxidation state – as sulphate. Only 0.12 % of dissolved sulphur is present as sulphide. Apart from a negligible content of polythionates

(Heiland 2016), no intermediate sulphur species were detected in the water (possibly due to inappropriate preservation techniques). This is also reflected in the associated sediments, which contained gypsum but no elemental sulphur. The  $\delta^{34}\text{S}$  value of sedimentary gypsum was around -10 ‰. This value is around 10 ‰ higher than that of dissolved sulphide and 17 ‰ lower than that of dissolved sulphate. Instead it agrees very well with the sulphur isotopic signature of gypsum crusts on the walls and the ceiling of the cave. Accordingly, sedimentary gypsum may not have formed in the water itself but above the water table and fell into the creek where it subsequently dissolves.

While most aspects of the neutral creek point towards Lower Fars gypsum as sulphur source, one value indicates that it may not be the only one. The isotopic signature of dissolved sulphate is around 5 ‰ lower than that of Lower Fars Formation. This deviation cannot be explained by sulphate reduction followed by a varying degree of degassing, precipitation and re-oxidation alone. However, the addition of light sulphur from another source would refresh the sulphur pool and dilute heavy sulphate to a value below 22.2 ‰. There are two possible scenarios: One explanation is the addition of light sulphur from hydrocarbon affluxes. Since  $\delta^{34}\text{S}$  values of pyrite and dissolved sulphide at site 1 agree so well with each other, it is likely that hydrogen sulphide from crude oil was already oxidized to sulphate when mixing with the solution. The second possible explanation is that the water is strongly influenced by falling and subsequently dissolving gypsum blocks. This would explain both the isotopic signature of sedimentary gypsum as well as the relatively low  $\delta^{34}\text{S}$  value of dissolved sulphate. Then again the question remains: Where does the sulphur in the gypsum crusts come from? The  $\delta^{34}\text{S}$  value of crude oil and gypsum crusts is basically identical, which points towards hydrocarbon affluxes as source. However, this will be discussed in chapter 5.5.3.

In the rear part of the cave, two additional water samples (DC-W-5, DC-W-10) and one sediment sample (DC-S-5) were analyzed for their sulphur isotopic composition. The close similarity to DC-W-7 clearly identifies the large floor feeder as main influence. However, a few minor deviations are noticeable: From site 7 to site 10, the  $\delta^{34}\text{S}_{\text{SO}_4}$ ,  $\delta^{18}\text{O}_{\text{SO}_4}$ , and  $\delta^{34}\text{S}_{\text{HS}}$ -values drop approximately 2 ‰, 1 ‰, and 3 ‰, respectively. Considering that the analytical precision of the oxygen isotopic analysis was  $\pm 0.6$  ‰, the supposedly falling trend of sulphate oxygen is not very convincing. Yet, since other isotope species are affected as well, a closer look seems to be necessary. In order to better understand the following section, it is recommended to review respective sampling locations on the cave map (Figure 8). Heiland

(2016) noticed a subsequent decrease of sulphate concentration along the flowpath (from the first to the last site: 8, 5, 10, 11) of the cave river. She suggested that sulphate may have precipitated, even though this was not reflected by calculated saturation indices. Sediment from site 5 contained gypsum with a  $\delta^{34}\text{S}$  value of +4.1 ‰ ( $\pm 2.1$  ‰). This is the only sulphur species in all cave sediments that was found to have a positive  $\delta^{34}\text{S}$  value. According to Claypool *et al.* (1980), precipitation of sulphate from aqueous sulphate is associated with an enrichment factor of 1.65 ‰, leading to a decrease in the  $\delta^{34}\text{S}$  of residual dissolved sulphate. This corresponds more or less to the 2 ‰ drop in  $\delta^{34}\text{S}_{\text{SO}_4}$  from the floor feeder to site 10. Simultaneously, it offers an explanation for  $^{34}\text{S}$  enriched sedimentary gypsum. However, a subsequent precipitation of sulphate minerals is not convincingly reflected in the amounts of sulphate extracted from the respective sediments (Table A 24).

An alternative explanation to sulphate precipitation is that the small creek emerges into the cave river at some point and changes its isotopic composition. The  $\delta^{34}\text{S}$  value of dissolved sulphate and sulphide in DC-W-1 lowers that of the main cave river. Since the values continue to drop from site 5 to site 10, it could be imposed that creek and river water were not entirely homogenized at site 5. If dilution occurs, it should be reflected not only by the sulphate concentration and stable isotopic values, but also by other components such as  $\text{Na}^+$ ,  $\text{K}^+$ , and  $\text{Cl}^-$ . When forming ratios between respective species from site 5 and site 7 (e.g.  $[\text{Na}^+]_5/[\text{Na}^+]_7$  or  $(\delta^{34}\text{S}_{\text{SO}_4})_5/(\delta^{34}\text{S}_{\text{SO}_4})_7$ ), values from 0.93 to 0.98 were obtained for sodium, potassium, chlorine,  $\delta^{34}\text{S}_{\text{SO}_4}$ ,  $\delta^{18}\text{O}_{\text{SO}_4}$ , and  $\delta^{18}\text{O}_{\text{H}_2\text{O}}$ . Due to the initial increase in sulphate concentration from the floor feeder to site 8, which is located a few metres downstream of the floor feeder, the respective ratio was above 1. Yet, substituting DC-W-7 with DC-W-8 when calculating the ratio  $[\text{SO}_4^{2-}]_5/[\text{SO}_4^{2-}]_7$  results in a value of 0.97. Even though obtained ratios are not exactly the same, they all point towards dilution with creek water. Assuming approximate contributions of 87 % from the river and 13 ‰ from the creek, a hypothetical water with similar characteristics to that of DC-W-5 can be computed. The straight line in Figure 48 connecting the respective samples, supports these findings.

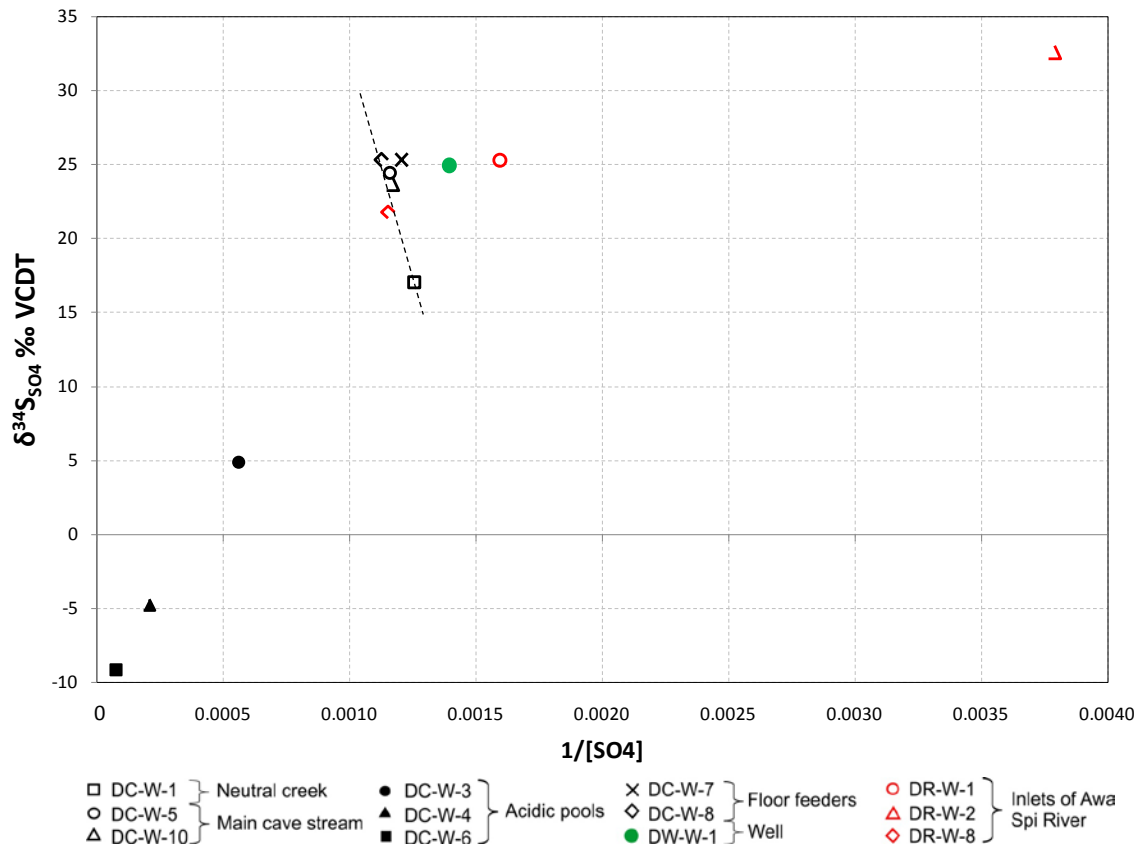


Figure 48:  $\delta^{34}\text{S}$  values of dissolved sulphate versus the reciprocal sulphate concentration. Dashed line: suggests that the cave stream presents a mixture of water from site 8 and site 1. Note that DC-W-8 has not been analyzed for its sulphur isotopic composition. Its  $\delta^{34}\text{S}$  value has been taken from the nearby floor feeder DC-W-7. See text for further explanations.

### ➤ Springs that feed Awa Spi River

The sulphide rich spring DR-W-2 that discharges into Awa Spi River has a very distinct sulphur and sulphate oxygen composition. Compared to the pool water DC-W-6, it is located at the very other end of the scale of measured  $\delta$  values (Figure 42). The water was characterized by a comparably low sulphate concentration (264 mg/L), a high proportion of dissolved sulphide (~10 % of dissolved sulphur species), heavily  $^{34}\text{S}$  and  $^{18}\text{O}$  enriched sulphate ( $\delta^{34}\text{S} = 32.55\text{‰}$ ,  $\delta^{18}\text{O} = 14.5\text{‰}$ ), and  $^{34}\text{S}$  enriched sulphide ( $\delta^{34}\text{S} = +9.6\text{‰}$ ). Imagine the following scenario: Sulphate from Lower Fars Formation gets reduced via dissimilatory bacterial sulphate reduction, leading to significant sulphur isotopic effects. Residual sulphate becomes  $^{34}\text{S}$  enriched, produced sulphide becomes  $^{34}\text{S}$  depleted. If large amounts of this sulphide are withdrawn from the system and the sulphate pool is not replenished quickly enough, both residual sulphate as well as produced sulphide get isotopically heavier and heavier. Re-oxidation of sulphide would lower the  $\delta^{34}\text{S}$  value of dissolved sulphate again. Accordingly, re-oxidation cannot explain the mentioned  $\delta$  values. Yet, there are two other processes that offer a plausible explanation for the phenomenon:

Precipitation and/or degassing of dissolved sulphide. Precipitation of FeS and subsequent conversion to FeS<sub>2</sub> would produce sedimentary sulphides that are slightly depleted (~1.2 ‰) in <sup>34</sup>S compared to the parent sulphide (Böttcher *et al.* 1998, Wilkin and Barnes 1996). Similarly, degassing of sulphide would cause small (~1.5 ‰ at 22° C, Szaran 1996) to negligible (Ohmoto and Rye 1979) sulphur isotopic effects. No sediment sample was analyzed from this site, so there are no data to back up the precipitation theory, yet there is an organoleptic confirmation of strong H<sub>2</sub>S effluxes from the water. The spring was draining another cave complex, and the attempt to go inside was anticipated by high concentrations of H<sub>2</sub>S in the atmosphere. Already in the vicinity of the entrance, effluxes were so strong and irritating, that they immediately caused a coughing reflex. Correspondingly, an approximate H<sub>2</sub>S concentration of 40 ppm in air can be assumed (SafetyDirectory 2004). Strong effluxes that continuously withdraw sulphide from the water subsequently remove “light sulphur” and cause a shift in the overall isotopic composition of the water.

Based on a cluster analysis, Heiland (2016) proposed a hydraulic connection between Darzila cave and Awa Spi, and suggested DR-W-1 as the main outlet of the cave. However, even though the water chemistry is very similar and can be grouped together, there appears to be a systematic deviation between the cave river and the outlet DR-W-1. Generally, concentrations of solutes decrease from the cave site 10 to this outlet. Ratios for sulphate, sodium, chlorine, and potassium concentrations between DR-W-1 and DC-W-10 led to the values 0.73, 0.74, 0.69, and 0.74, respectively. This is surprising. First of all, sulphate concentrations were expected to increase due to falling and subsequently dissolving gypsum blocks. Even if sulphate precipitates as sulphate minerals prior discharge at the spring - sodium, chlorine, and potassium are incompatible solutes and should not be affected by this. The similarity of the ratios rather suggests that cave water was diluted with water of similar, but generally less concentrated composition. The isotopic composition of the water behaves differently: The stable isotopic composition of the water molecules remains constant and the  $\delta^{34}\text{S}$  value of dissolved sulphate increases around 1.6 ‰. That  $\delta^{18}\text{O}_{\text{H}_2\text{O}}$  and  $\delta\text{D}$  values of cave and spring water are the same is not very informative, but an increase of heavy sulphur in dissolved sulphate is an interesting aspect. Precipitation of sulphate is associated with an enrichment factor of 1.65 ‰ (Claypool *et al.* 1980) and should cause a decreasing  $\delta^{34}\text{S}$  value of dissolved sulphate, and not the other way around. The effect of dissolving gypsum blocks (~ -10 ‰) would be even more dramatic. Accordingly, there must be a counteracting process. One explanation is bacterial sulphate reduction in the rear part of the cave. Unfortunately, gene analysis of cave sediments could not confirm the presence of sulphate

reducers. The more likely explanation points back to the hypothesis above, that the water was diluted with water of similar composition. Interestingly, the  $\delta^{34}\text{S}_{\text{SO}_4}$  and the  $\delta^{18}\text{O}_{\text{SO}_4}$  value of the spring coincide exactly with those of the main floor feeder inside the cave – an aspect that will be further evaluated at the end of this chapter.

DR-W-8, the third spring, plays only a minor role with respect to the water volume and hydrochemistry of Awa Spi River (Heiland 2016). Nevertheless, it presents an interesting site. The spring is situated around 1 km downstream of the first spring, and around 600 m southeast of the cave entrance. It is thus even closer to the cave than the spring DR-W-1 and a hydraulic connection to the cave is likely. This hypothesis is strengthened by the hydrogeochemistry of the water. Based on a cluster analysis, Heiland (2016) grouped the water with that of the cave river and with the spring DR-W-1. Like in the previous section, ratios were formed between solute concentrations at the spring and the cave site 10. Sulphate, sodium, chlorine, and potassium ratios gave the values 1.01, 1.00, 1.00, and 0.98, respectively. In contrast to spring 1, the concentrations almost exactly fit those of the cave river. This strongly suggests that at some point in the rear part of the cave, a small creek departs from the river and drains at the respective spring. The isotopic data are consistent with this hypothesis. There is a slight difference between the  $\delta^{18}\text{O}_{\text{H}_2\text{O}}$  and  $\delta\text{D}$  value of DC-W-10 and DR-W-8, respectively (Figure 32), which may be attributed to a minor evaporation process of isotopically light water molecules. Compared to the cave river, the  $\delta^{34}\text{S}$  value of dissolved sulphate at the spring is around 1.8 ‰ lower. This may be attributed to the dissolution of  $^{34}\text{S}$  depleted gypsum crystals.

➤ **The well and the subterranean reservoir**

With respect to the stable isotopic composition of water ( $\delta^{18}\text{O}_{\text{H}_2\text{O}}$ ,  $\delta\text{D}$ ) and dissolved sulphate ( $\delta^{34}\text{S}_{\text{SO}_4}$ ,  $\delta^{18}\text{O}_{\text{SO}_4}$ ), well water is practically identical to that of the large floor feeder in the cave (DC-W-7) and the first spring (DR-W-1) of Awa Spi River (Figure 32, Figure 36). This indicates that all these waters come from one large subterranean reservoir.

Figure 49 displays the sulphur isotopic composition of dissolved sulphates against the reciprocal value of sulphate concentration. A line was drawn through the samples under discussion (floor feeder DC-W-7, well DW-W-1, spring DR-W-1), through the spring DR-W-2 and the initial solution forming from dissolution of primary gypsum. The samples place very well on the line. Accordingly, all these waters may be derived from gypsum of Lower Fars Formation.

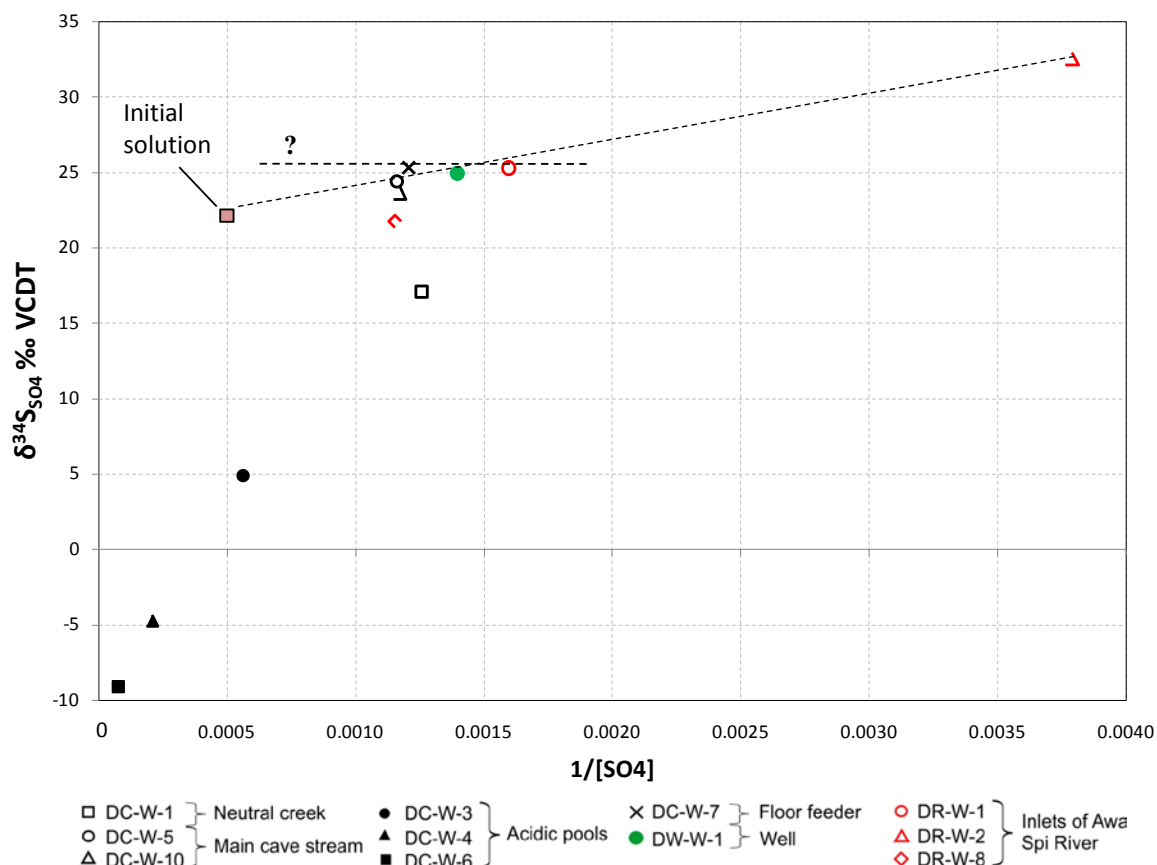


Figure 49:  $\delta^{34}\text{S}$  values of dissolved sulphate versus the reciprocal sulphate concentration. The sloped line through the data points of the initial solution ( $\delta^{34}\text{S} = 22.2\text{‰}$ ,  $[\text{SO}_4^{2-}] \approx 2000\text{ mg/L}$ ), the main floor feeder DC-W-7, the well DW-W-1, the spring DR-W-1, and the spring DR-W-2 indicates mixture. The horizontal line highlights the phenomenon, that the floor feeder, the well, and the spring ultimately have the same  $\delta^{34}\text{S}$  values but differ in sulphate concentration.

As noted above, the isotopic composition of the floor feeder, the well, and the spring DR-W-1, is almost identical. With a spread of 4.35 ‰, sulphide is the only species that clearly varies in its isotopic composition. However, considering the overall low concentrations of sulphide in these fluids, the sulphide pool is a lot more sensible to isotopic fractionation effects than the sulphate pool. That in mind, 4.35 ‰ difference between the samples is not so much after all, and the hypothesis of one large reservoir is not weakened. What puzzles more than the varying  $\delta^{34}\text{S}$  values of sulphide, are the different sulphate concentrations in the samples. While the  $\delta^{34}\text{S}_{\text{SO}_4}$  values remain the same, the floor feeder DC-W-7, the well DW-W-1, and the spring DR-W-1 have a sulphate concentration of 828 mg/L, 717 mg/L, and 626 mg/L, respectively. In Figure 49, this trend is indicated by a dashed, horizontal line. Sodium and chlorine concentrations show a similar trend in the respective water samples. It almost looks like a subsequent dilution with deionised water, which of course, is not a reasonable explanation.

One option is that it is only a spurious correlation. A varying degree of sulphate reduction, sulphide removal and re-oxidation may accidentally lead to the same values and thus mimic a meaningless correlation.

The second option is that water, which infiltrated the recharge area, travelled at different velocities. The longer the contact with Lower Fars Formation, the more gypsum and salt was dissolved. In the aquifer, water may have been transported in different fissures so that the water did not entirely homogenize. However, dissolved sulphate is subject to the same processes, namely bacterial sulphate reduction, followed by precipitation of sulphides and a partial re-oxidation. Also, processes occurred to the same extent, leading to sulphur species with surprisingly similar isotopic compositions. Accordingly, water extracted from the well, the floor feeder, and the spring could point towards a common reservoir, that is not entirely homogenized yet.

The third option involves Sagirma Formation (review Figure 3). Gypsum from this formation is expected to have the same  $\delta^{34}\text{S}$  value as Lower Fars gypsum – a hypothesis that is based on literature values, not on actual measurements. Dissolution of Sagirma gypsum leads to dissolved gypsum with a  $\delta^{34}\text{S}$  value of 22.2 ‰. At some point, this water enters into Pila Spi and Oligocene Formation, where it is subject to the same sulphur transformation processes as sulphate from Lower Fars Formation. As before, the processes must occur to the same extent. Subsequently, the different waters mix and form a reservoir that is not entirely homogenized. Considering that the area is karstified, flow-areas of different velocities may influence the distribution of species.

Another option that must be considered, is that Lower Fars gypsum is less important for the cave than assumed. A third sulphur source with a sulphur isotopic composition of around 25 ‰ is conceivable. The only other formation that is known to be present in the area and to contain considerable amounts of gypsum is Sagirma Formation. Thus, the derived literature value might be wrong. Future studies should therefore include an isotopic analysis of Sagirma gypsum to evaluate the contribution of this source.

Summing up, the reason for the phenomenon could not be entirely resolved. The presented explanations merely offer a starting point for further investigations.

### 5.5.3 The Origin of Sulphate Oxygen

The oxidation of dissolved sulphide or metal sulphides to sulphate involves the incorporation of oxygen. Depending on the mode of oxidation, sulphate oxygen may come from either atmospheric oxygen or from water. While atmospheric oxygen is globally homogeneous (averaging  $\delta^{18}\text{O} = 23.5 \pm 0.3 \text{‰}$ ; Dole *et al.* 1954, Kroopnick and Craig 1972), the water samples in this region had  $\delta^{18}\text{O}$  values between -6.62 and -5.53 ‰. These differences may provide an opportunity to reveal the source and reaction pathway of oxygen in the oxidation of reduced sulphur species. Figure 50 depicts the  $\delta^{18}\text{O}_{\text{SO}_4}$  and  $\delta^{18}\text{O}_{\text{H}_2\text{O}}$  values of corresponding water samples.

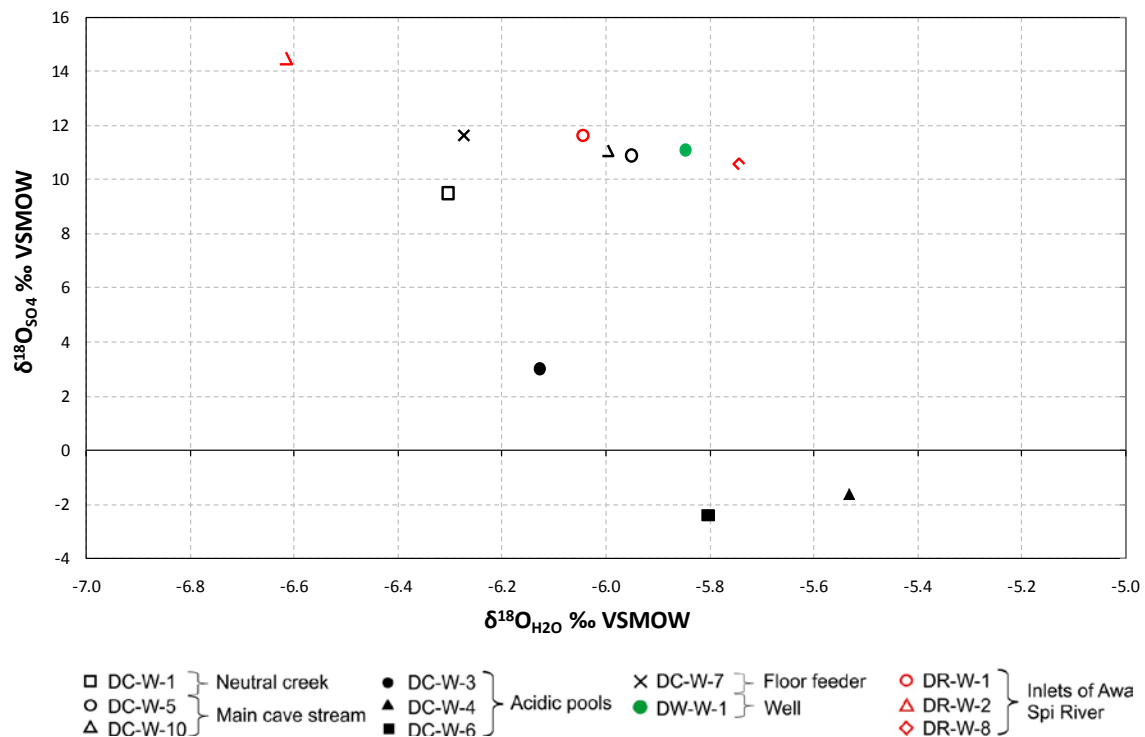


Figure 50: Oxygen isotopic composition of dissolved sulphate and ambient water. Cave waters are depicted with black symbols, springs with red symbols, and well water with a green symbol

#### ➤ Sulphate from Lower Fars Formation

During bacterial sulphate reduction, S-O bonds are broken and a kinetic isotope effect occurs for oxygen isotopes as observed for sulphur (Turchyn *et al.* 2010). However, this process is typically superimposed by an isotope exchange between sulphate oxygen and oxygen in ambient water (Brunner *et al.* 2005, Knöller *et al.* 2006). According to Knöller *et al.* (2006), the oxygen isotope exchange usually leads to an enrichment of heavy oxygen in residual sulphate, until a certain equilibrium value is reached.

Oxygen isotope analyses of three samples from Lower Fars Formation revealed  $\delta^{18}\text{O}$  values ( $\pm 0.6$  ‰) of 12.6 ‰, 13.1 ‰, and 15.2 ‰, respectively. Based on these analyses, only one single sample (spring DR-W-2) shows a minor enrichment of  $^{18}\text{O}$  compared to the source sulphate. Also, there is one group of samples with  $\delta^{18}\text{O}$  values between 10.6 and 11.7 ‰. Considering an overall analytical precision of  $\pm 0.6$  ‰ VSMOW for  $\delta^{18}\text{O}$ , two samples are ultimately identical to source gypsum, while others are slightly depleted in  $^{18}\text{O}$ . This may be ascribed to three possible explanations: Firstly, sulphate reduction rates are very low and the oxygen isotopic composition of residual sulphate is practically retained. Secondly, re-oxidation of sulphides involving the integration of oxygen from ambient water occurred, which lowers the overall oxygen isotopic composition of dissolved sulphate. Thirdly, dissolved sulphate was mixed with dissolved sulphate from another source.

#### ➤ Isolated pools

Arguably the most interesting samples depicted in the graph, are the two isolated pools DC-W-6 and DC-W-4. With  $\delta^{18}\text{O}_{\text{SO}_4}$  of around -2 ‰, sulphate from DC-W-4 and DC-W-6 is not at all related to that of Lower Fars gypsum ( $\delta^{18}\text{O} \approx 13.6$  ‰). Bacterial sulphate reduction would cause a positive shift of  $\delta^{18}\text{O}$  values and not a depletion of around 15 ‰. Instead,  $\text{H}_2\text{S}$  or intermediate sulphide minerals were subsequently oxidized by one or another pathway. The great similarity of  $\delta^{18}\text{O}$  of sulphate and ambient water suggests that almost all oxygen that was incorporated during oxidation, originates from water. This will be evaluated in the following paragraphs.

Depending on the availability of reactive iron ( $\text{Fe}^{2+}$ ), ascending sulphide effluxes will immediately precipitate as  $\text{FeS}$ , and subsequently be converted to  $\text{FeS}_2$ . The first process is known to occur within milliseconds (Rickard 1995) - the latter takes place within days (Rickard 1997). Sediments from the pools DC-W-4 and DC-W-6 have not been analyzed for their mineralogical composition, but sediments of the related pool DC-W-3 did not contain any pyrite. This does not mean that pyrite is unimportant for the system. Instead it is likely, that all pyrite has been oxidized to sulphate already. Pyrite can be oxidized either abiotically or biologically, either by oxygen or by aqueous  $\text{Fe}^{3+}$ .

Biofilms at the acidic cave site 4 were identified to contain *Acidithiobacillus ferrooxidans*, a strictly aerobic, pyrite oxidizing organism. Possibly due to anthropogenic interferences, there was no biofilm on the pool at site 6. However, it is strongly assumed that *A. ferrooxidans* also thrives in the ascending water of DC-W-6.

The content of dissolved oxygen was low at site 4 (0.64 mg/L) and relatively high at site 6 (2.78 mg/L). Water at both sites contained considerable amounts of iron, namely 43.1 mg/L and 33.4 mg/L, respectively. According to photometrical measurements, the relative content of  $\text{Fe}^{2+}$  is relatively low, but modelled with PhreeqC (Heiland 2016),  $\text{Fe}^{2+}$  should be the dominant species. Regardless of the species measured – iron seems to play an important role in the system. Considering that *A. ferrooxidans* utilizes  $\text{Fe}^{2+}$  as energy substrate, iron may be recycled over and over again. The bacterium oxidizes  $\text{Fe}^{2+}$  to  $\text{Fe}^{3+}$ , and during pyrite oxidation,  $\text{Fe}^{3+}$  is reduced back to  $\text{Fe}^{2+}$ . Accordingly, biotic oxidation by *A. ferrooxidans* is thought to be the controlling process at these sites. This is consistent with the observations of other workers. Luther III *et al.* (2011) for example reported that reaction rates of biotic sulphide oxidation are significantly higher than abiotic rates – often several orders of magnitude. As noted above, the content of dissolved oxygen at site 6 was relatively high. Hence, microbial growth of aerophilic and microaerophilic microorganisms would be supported not only in the pool itself, but also further down the conduit. This suggests that microbially mediated dissolution of limestone starts well below the level of the cave floor.

The relative proportion of water-derived oxygen in sulphate was computed using equation [6], the enrichment factors for biological pyrite oxidation reported by Balci *et al.* (2007) (see chapter 3.1.2.3), as well as the isotopic data. Based on these values, 97 % and 101 % of sulphate oxygen in DC-W-4 and DC-W-6 have been supplied from the water.

#### 5.5.4 Formation of Secondary Cave Minerals

In this chapter, the isotopic results concerning secondary gypsum (review Figure 37) and elemental sulphur (review Figure 38) from cave walls will be discussed.

##### ➤ Sulphur isotopic composition

With the exception of one elemental sulphur sample (DC-ES-13c), all remaining samples have a remarkably uniform  $\delta^{34}\text{S}$  value near -10 ‰. Crust samples were taken from different locations in the cave and from different layers of the wall, and still the sulphur isotopic composition points towards one common sulphur source. Since sulphur from crude oil had a  $\delta^{34}\text{S}$  value of around 9 ‰, it seems intuitively right, to propose  $\text{H}_2\text{S}$  affluxes from hydrocarbons as the main source of sulphur in secondary cave minerals. But can this proposal withstand a critical examination? Onac *et al.* (2011) wrote, that minerals (e.g. gypsum) produced via the reaction series given in chapter 3.2, undergo little fractionation between sulphide and sulphate, so they will reflect the original isotopic composition of the source of reduced sulphur. However, this does not necessarily point back to the sulphur isotopic composition of oil, but to that of dissolved sulphide in the cave waters. Imagine the following scenario:  $\text{H}_2\text{S}$  from one or another source ascends through the more oxic groundwater. While one part is oxidized to sulphuric acid by sulphur oxidizing bacteria (e.g. Macalady *et al.* 2006), some of the  $\text{H}_2\text{S}$  gas also diffuses into the cave atmosphere, where it mixes with  $\text{H}_2\text{S}$  affluxes from other cave waters. This  $\text{H}_2\text{S}$  mix may be completely oxidized by  $\text{O}_2$  to sulphuric acid in surficial condensates. The acid reacts with the limestone, which is then replaced with gypsum, reflecting the  $\delta^{34}\text{S}$  value of gaseous  $\text{H}_2\text{S}$  in the cave atmosphere (e.g. Nakai and Jensen 1964, Yonge and Krouse 1987). Considering the uniform  $\delta^{34}\text{S}$  value in secondary minerals, the sulphur isotopic composition of atmospheric  $\text{H}_2\text{S}$  must be relatively uniform over time and space. No atmospheric  $\text{H}_2\text{S}$  was gathered during the fieldwork, but it is expected to have a  $\delta^{34}\text{S}$  value of around -10 ‰. While Figure 33 and Figure 42 display  $\delta^{34}\text{S}$  values of sulphide in water, Figure 35 relates sulphide concentrations in the water to the total concentration of sulphur. DC-W-3, DC-W-5, and DC-W-10, all three of which are thought to be mixtures of different waters, have a  $\delta^{34}\text{S}_{\text{HS}^-}$  value of around -10 ‰. The floor feeders have higher or lower values: Dissolved sulphide from the large cave discharge DC-W-7 has a  $\delta^{34}\text{S}$  value of -7.6 ‰, the small discharges DC-W-4 and DC-W-6 that form isolated pools, have  $\delta^{34}\text{S}_{\text{HS}^-}$  values of around -12.8 and -14.1 ‰, respectively. Hence, the -10 ‰ of gypsum appears to be a more or less balanced mixture of these two sources. While DC-W-6 has the highest concentration of dissolved sulphide (~ 10 mg/L) but a low discharge rate, DC-W-7 has the highest discharge rate and a lower sulphide

concentration. Since the two waters contain sulphur from different endmembers, it also implies that secondary gypsum and elemental sulphur on the walls are composed of sulphur from both endmembers: Gypsum and H<sub>2</sub>S affluxes. Note that this suggestion is entirely based on the assumption, that all involved sulphur transformation processes occur without significant fractionations. If this is not the case, sulphur from hydrocarbon affluxes might be the dominant source after all.

When H<sub>2</sub>S is oxidized to sulphuric acid and reacts with adjacent limestone, gypsum can be formed. Yet, when the limestone is already covered with a sulphate crust, the formation of gypsum crystals on the surface of the wall may be attributed to other processes. One option is that gypsum near the host rock surface dissolves and that the water evaporates, carrying dissolved gypsum to the surface where it re-crystallizes. Since the sulphate molecule itself is not affected by this process, it should not be accompanied by sulphur or oxygen isotopic fractionation. The second option for supply of calcium ions, are calcium-rich aerosols that are caught in the thin film of sulphuric acid on the cave wall. The third option is that calcium carbonate is dissolved somewhere else. A migrating, thin layer of condensed water may carry the Ca<sup>2+</sup> ions over the surface of the wall, where they bind with SO<sub>4</sub><sup>2-</sup> ions to form gypsum. This process could be especially relevant for the enhanced crystal growth in the isolated chamber. The water flowing through this chamber has a very low concentration of hydrogen sulphide (0.32 mg/L) with a δ<sup>34</sup>S value of approximately -21 ‰. Accordingly, it cannot be the source of gypsum on the walls of the chamber. The noticeable draft of fresh air in that room may cause a chimney effect, sucking humid and H<sub>2</sub>S rich air through the connecting passage, into the chamber, where it quickly oxidizes to sulphuric acid and forms gypsum upon contact with calcium ions.

As mentioned in the beginning of this chapter, one sample of elemental sulphur had a markedly different sulphur isotopic composition (δ<sup>34</sup>S = -15.2 ‰). The respective sample was one of the two small sulphur knobs that were collected from the surface of two different gypsum crystals. The gypsum crystals themselves had been embedded into the cave wall. According to Machel (1992), elemental sulphur does not form from reduction of sulphates, but from oxidation of reduced sulphur, especially H<sub>2</sub>S. The oxidation may proceed inorganically or via the action of sulphur oxidizing bacteria. However, due to the low to negligible fractionation effects that are associated with the respective processes, δ<sup>34</sup>S ratios of elemental sulphur cannot be used to discriminate between a biogenic and an inorganic origin of the elemental sulphur (Machel 1992). Accordingly, there is no evidence that the

knobs may have formed via different oxidation mechanisms. Considering the small size of the samples (~ 1 mm in diameter), the isotopic difference of 5 ‰ may simply be attributed to temporal or local inhomogeneities of  $\delta^{34}\text{S}$  in gaseous  $\text{H}_2\text{S}$ .

➤ **Oxygen isotopic composition**

While the sulphur isotopic composition of gypsum is approximately the same in all samples,  $\delta^{18}\text{O}$  values range from -7.0 to +3.3 ‰ (see Figure 37). Oxygen isotopes are very sensible to small, local inhomogeneities. Accordingly, it can happen very easily that  $\delta^{18}\text{O}_{\text{SO}_4}$  values spread more than they should. Still, a total range of 10.3 ‰ is significant, and cannot be ascribed to small variations alone.

Oxygen may be derived from water or atmospheric oxygen. For atmospheric oxygen, the  $\delta^{18}\text{O}$  value is known to be 23.5 ‰ (Kroopnick and Craig 1972), but the  $\delta^{18}\text{O}$  value of water vapour and in condensates on the cave wall can only be approximated. Based on the range in analyzed cave waters, a mean  $\delta^{18}\text{O}_{\text{H}_2\text{O}}$  value of about -6 ‰ can be determined. The temperature in the main cave room was 22° C. Using an enrichment factor of  $\epsilon^{18}\text{O}_{\text{vapour-water}}$  of -9.5 ‰ (at 25° C, approximated for oceans, Clark and Fritz 1997), water vapour in the cave atmosphere would have a  $\delta^{18}\text{O}$  value of -15.7 ‰. Assuming that almost 100 % of water vapour remains in the air, no or only a negligible isotope effect will be observed in thin condensation layers on the wall. Accordingly,  $\delta^{18}\text{O} = -15.7$  ‰ was set as the oxygen isotopic composition of water. Balci *et al.*'s (2007) enrichment factors apply to pyrite oxidation in acidic environments. The system differs significantly from the aqueous-gaseous  $\text{H}_2\text{S}$  system, which is investigated here, so these enrichment factors cannot be applied. Unfortunately, oxidation studies that include the isotope effect on sulphate oxygen seem to focus on the oxidation of metal sulphides, instead of dissolved or gaseous  $\text{H}_2\text{S}$ . The old experiments (bubbling  $\text{O}_2$  through  $\text{Na}_2\text{S}$  solution) and respective enrichment factors of Lloyd (1967) were thought to be the closest approximation for the given system. Lloyd concluded that there is no oxygen isotope selectivity during the incorporation of water oxygen. For the incorporation of  $\text{O}_2$ , he determined a kinetic isotope effect of -8.7 ‰, favouring the lighter isotope. These enrichment factors were used to calculate the proportion of water-derived oxygen in produced gypsum crusts after equation [6]. The computed proportions varied between 38 % and 71 %. Gypsum DC-SG-15 was not sampled in the cave itself, but from the open sinkhole, where the ambient air is hot and dry. It is therefore not surprising that atmospheric oxygen contributed the larger portion (55 %) to the sulphate. Leaving this sample aside, the relative proportions of water-derived oxygen correlate with the layer of the wall, the sample was taken from. First layer gypsum has the highest content of water-derived

oxygen (71, 65, and 61 %). Second layer gypsum and the large gypsum crystals embedded in the wall have a slightly lower content of water-derived oxygen (59, 57, 53, and 51 %). The sample from the layer underneath had the lowest content of water-derived oxygen in gypsum (38 %).

Unfortunately, the mode of gypsum formation is unknown. As described in the previous section about sulphur isotopes, several options are conceivable. Considering the variability of  $\delta^{18}\text{O}$  values, it appears unlikely that re-crystallization of gypsum from deeper layers has occurred. If calcium ions were supplied via aerosols or a stream of thin condensate water, differences may be attributed to temporal differences in the characteristics of the cave atmosphere. Depending on the season, air temperature, humidity, hydrogen sulphide and oxygen concentration in the air, and other factors may vary and influence the dissolution and crystallization processes.

The current dataset is too small to resolve the underlying mechanisms. It is necessary to take several more samples – possibly as undisturbed cores from the outermost layer to the host rock limestone. The presented evaluation is more based on speculations than on real data, but it may present a starting point for further investigations.

## 6 Summary of the Main Results

Darzila cave, an active sulphuric acid cave in Northern Iraq, was subject to microbiological and isotopic investigations. In the following section, a summary of the main results will be given.

### ➤ The microbial community of the cave

The actively forming cave complex hosts a rich, microbial community. Two distinct biofilm morphologies were observed in Darzila cave: Filamentous, rock-attached streamers at the main floor feeder and slimy, floating films at the acidic sites. Bacterial 16S rRNA gene analyses revealed interesting sulphur-oxidizing communities. In the filaments, the dominant members were closely related to *Thiofaba teptiphilia*, *Acidithiobacillus albertensis*, and *Acidithiobacillus thiooxidans*. These bacteria are thought to be the main driving force of sulphide oxidation at the floor feeder. And because they are directly attached to the limestone, they are thought to mediate subaqueous dissolution of the host rock. The floating film was found to be dominated by a variety of *Acidithiobacilli*, including *At. ferrooxidans*. It was hypothesized that this organism plays a decisive role in pyrite oxidation and subaqueous dissolution of limestone at these sites.

Cave sediments were expected to be inhabited by a variety of sulphate reducing bacteria. Instead, they were dominated by typical soil and coliform bacteria. These organisms are not particularly relevant for karstic processes, but point towards anthropogenic input via skin, hairs and the intestinal tract.

### ➤ The origin of the fluids

The main goal of thesis was to trace back the origin of sulphur in Darzila cave. The evaluation of isotopes in dissolved sulphide and sulphate showed, that sulphur originates from at least two sources: H<sub>2</sub>S affluxes from hydrocarbons, gypsum from Lower Fars formation, and possibly also from Sagirma Formation. The endmembers clearly differed in their sulphur isotopic composition. Sulphur in crude oil was found to be strongly depleted in <sup>34</sup>S ( $\delta^{34}\text{S} = -9.05 \text{ ‰}$ ), whereas gypsum from Lower Fars Formation was <sup>34</sup>S enriched ( $\delta^{34}\text{S} = 22.2 \text{ ‰}$ ).

For the main floor feeder DC-W-7, the springs DR-W-1 and DR-W-2, well water DW-W-1, gypsum from Lower Fars Formation could be identified as sulphur source. What these

samples had in common was a comparably low sulphate concentration, a significant sulphur isotopic difference between sulphate and sulphide, and  $\delta^{34}\text{S}$  values above 22.2 ‰. Except for the sulphide rich spring DR-W-2,  $^{34}\text{S}$  enrichments in residual sulphates were smaller than expected from BSR in the aquifer. This indicates that sulphate reduction was followed by several secondary transformation processes. Degassing of produced sulphide, precipitation of metal sulphides, and re-oxidation to elemental sulphur and sulphate were proposed as the main processes affecting the sulphur isotopic composition of the fluids. The oxygen isotopic composition of sulphate appeared to be unaffected by BSR. It was argued, that this could be ascribed to low reduction rates, to a mixture with sulphates from another sources, or to re-oxidation of sulphides.

The isolated pools DC-W-4 and DC-W-6 were clearly influenced by  $\text{H}_2\text{S}$  affluxes. Due to their high sulphate concentration, the small isotopic difference between the dissolved sulphur species, and the strongly  $^{34}\text{S}$  and  $^{18}\text{O}$  depleted sulphate, Lower Fars gypsum cannot be the source of sulphur. The pools might contain sulphur from gypsum too, but the overwhelming hydrocarbon affluxes would mask any other sulphur contribution. Elevated  $\delta^{18}\text{O}$  and  $\delta\text{D}$  values could be ascribed to enhanced dissolution of  $^{34}\text{S}$  enriched host rock and  $^2\text{H}$  exchange with ascending  $\text{H}_2\text{S}$ , respectively. Oxidation of dissolved sulphide and iron sulphides to sulphuric acid was ascribed to excessive microbial activity. All sulphate oxygen was incorporated from oxygen of ambient water.

All other waters were found to be a mixture of waters from different sources. Dissolved sulphur species in the small cave creek showed clear signs of BSR, but the isotopic composition was superimposed by the input of sulphur from another source. The creek itself, influences the isotopic composition of the pool DC-W-3 and of the main stream in the rear part of the cave.

It was proposed in previous studies that there is a hydraulic connection of cave waters and the spring DR-W-1. This subject will need further investigation. It appears that cave water was diluted prior discharge. Interestingly, spring water is more closely related to water from the well and to water of the large floor feeder in the cave. This finding suggests that there is a major subterranean reservoir. Yet, one observation complicated the situation: While the  $\delta^{34}\text{S}$  values of dissolved sulphate in these waters were all 25 ‰ VCDT, the concentration of sulphate clearly varied. This could be attributed to different flow velocities in the aquifer, leading to an inhomogeneous distribution of species. However, it must be considered that there may be a third sulphur source with a  $\delta^{34}\text{S}$  value of around 25 ‰.

➤ **Secondary gypsum**

The cave walls were covered by extensive crusts of gypsum and elemental sulphur. Isotopic analysis of these coatings revealed a remarkably uniform sulphur isotopic composition of around -10 ‰. If it is correct that degassing of sulphide, oxidation to sulphuric acid, dissolution of limestone, and formation of gypsum occur without significant isotopic effects, then sulphur in these coatings presents a more or less balanced mixture of H<sub>2</sub>S affluxes from the main floor feeder and from the isolated pools.

The overwhelming presence of gypsum crystals in the isolated chamber is probably caused by a chimney effect: Humid, H<sub>2</sub>S rich air is sucked into the chamber, where it quickly oxidizes to sulphuric acid and forms gypsum upon contact with calcium ions.

The oxygen isotopic composition of gypsum coatings is not uniform at all.  $\delta^{18}\text{O}$  values clearly drop from the innermost to the outermost layer of the wall. It was argued that it could point towards different  $\delta^{34}\text{S}$  ratios of gaseous H<sub>2</sub>S over time, but further investigations are required to strengthen or disprove this hypothesis.

## 7 Recommendations

During data acquisition and subsequent evaluation it became apparent, that the preparation procedures should be improved. Future studies that involve the extraction of sulphur species for isotopic analysis should consider the following methodological aspects:

- The extraction of dissolved sulphate for isotopic analysis involves precipitation of  $\text{BaSO}_4$  and filtration to remove excess solution. Instead of drying the precipitate immediately, it should be washed with deionised water until the filtrate is free of chlorine. Accordingly, a few mL of 10 %  $\text{AgNO}_3$  solution should be included into the field extraction kit. This way, re-dissolution of precipitates, a second filtration, drying, and labelling step in the laboratory can be avoided.
- If possible, sediment samples should be preserved by flushing the bags with nitrogen and by freezing the samples, to avoid oxidation of reduced sulphur species.
- After Soxhlet extraction of elemental sulphur from sediments, sulphur recovery from the organic solvent may proceed by different methods. If precipitation as  $\text{CuS}$  and subsequent liberation of  $\text{H}_2\text{S}$  and precipitation as  $\text{ZnS}$  is chosen, hot and concentrated  $\text{HNO}_3$  must be used instead of  $\text{HCl}$  to dissolve  $\text{CuS}$ .
- The success and the problems of a sequential extraction of sedimentary sulphur species would be more transparent, if the procedure was conducted together with a standard.

Furthermore, it became apparent, that the understanding of processes relating to Darzila cave has just begun. Every process that could be unravelled led to further questions. Future research might include the following inquiries:

- While most sulphur containing materials in the cave were analyzed for their sulphur isotopic composition, gaseous  $\text{H}_2\text{S}$  in the cave atmosphere still presents a missing link. Its  $\delta^{34}\text{S}$  value is assumed to be around -10 ‰, but this was not experimentally confirmed yet. Gaseous  $\text{H}_2\text{S}$  should be sampled by sucking the air through a solution of  $\text{Zn}$ -acetate. Subsequent sulphur isotopic analyses could help to trace back the origin of sulphur and gypsum coatings on the cave walls.
- Gypsum from Sagirma Formation might influence  $\delta^{34}\text{S}$  values of waters in the study area. Accordingly, samples should be taken and analyzed for their sulphur isotopic composition, in order to evaluate possible contribution.

- 
- The layers of the wall showed a distinct gradient with respect to their oxygen isotopic composition of sulphate. This phenomenon may be investigated further by taking undisturbed cores and by systematically analyzing contained gypsum for its  $\delta^{18}\text{O}$  values.
  - The comparison of sulphide concentrations obtained by photometry and by the precipitation as ZnS gave very different values. Water from the well, the main floor feeder, and from the pool at cave site 6 was especially affected. Measurements of sulphides at these sites should be repeated, possibly with a variety of different methods.
  - So far, all studies of Darzila cave focussed on the dry season. It would be a very valuable extension of the current data set, to collect water and air samples during the rainy season.
  - It is argued whether or not Pila Spi limestone presents the host rock of Darzila cave, so there is need for a thorough investigation of this subject.
  - 16S rRNA gene analyses of sediments did not detect any sulphate reducing bacteria. It is not clear, whether this is due to methodological constraints or if their cell density is extremely low. A specialized test system for counting sulphate reducing bacteria, such as SaniCheck from BIOSAN Laboratories could shed light into the subject.
  - 16S rRNA gene analysis detects the dominant species in the biofilms, but it cannot give any information about their quantities. Now that the relevant species are known, adequate probes can be designed and used for subsequent FISH (fluorescence *in situ* hybridization) analysis. This would allow quantifying the organisms. Depending on the conducted preparation, it may even give information about the architecture of the biofilms.
  - No biofilm was found on the water surface of the acidic site DC-W-6, but it is strongly assumed that there is a rich sulphur-oxidizing community in the water itself. This should be tested by cultivation or gene analysis. A confirmation of the presence of *Acidithiobacillus ferrooxidans* would strengthen the hypothesis, that this organism plays a decisive role in pyrite oxidation and iron cycling at this site.

## 8 References

- Acinas, S. G.; Sarma-Rupavtarm, R.; Klepac-Ceraj, V.; Polz, M. F. (2005): PCR-Induced Sequence Artifacts and Bias: Insights from Comparison of Two 16S rRNA Clone Libraries Constructed from the Same Sample. In: *Applied and Environmental Microbiology* 71 (12), p. 8966–8969.
- Al-Manmi, D. (2012): Personal communication. University of Sulaymaniyah.
- Angert, E.; Northup, D. E.; Reysenbach, A.-L.; Peek, A.; Goebel, B.; Pace, N. (1998): Molecular phylogenetic analysis of a bacterial community in Sulphur River, Parker Cave, Kentucky. In: *American Mineralogist* 83, p. 1583–1592.
- Aziz, M. (2001): Climate of North Iraq, Brief. (unpublished working document of FAO AM SS). FAO documentation Fund. Erbil.
- Bachinski, D. (1969): Bond strength and sulfur isotopic fractionation in coexisting sulfides. In: *Economic Geology* 64, p. 56–65.
- Baer, D.; Paul, J.; Gupta, M.; O'Keefe, A. (2002): Sensitive absorption measurements in the near-infrared region using off-axis integrated-cavity-output spectroscopy. In: *Applied Physics B: Lasers and Optics* 75 (2-3), p. 261–265.
- Balci, N.; Shanks III, W.; Mayer, B.; Mandernack, K. (2007): Oxygen and sulfur isotope systematics of sulfate produced by bacterial and abiotic oxidation of pyrite. In: *Geochimica et Cosmochimica Acta* 71, p. 3796–3811.
- Balci, N.; Mayer, B.; Shanks III, W.; Mandernack, K. (2012): Oxygen and sulfur isotope systematics of sulfate produced during abiotic and bacterial oxidation of sphalerite and elemental sulfur. In: *Geochimica et Cosmochimica Acta* 77, p. 335–351.
- Barton, H.; Luiszer, F. (2005): Microbial metabolic structure in a sulfidic cave hot spring: Potential mechanisms of biospeleogenesis. In: *Journal of Cave and Karst Studies* 67 (1), p. 28–38.
- Beatty, J. T.; Overmann, J.; Lince, M.; Manske, A.; Lang, A.; Blankenship, R. *et al.* (2005): An obligately photosynthetic bacterial anaerobe from a deep-sea hydrothermal vent. In: *Proceedings of the National Academy of Sciences* 102 (26), p. 9306–9310.
- Beaudoin, G.; Taylor, B.; Rumble III, D.; Thiemens, M. (1994): Variations in the sulfur isotope composition of troilite from the Cañon Diablo iron meteorite. In: *Geochimica et Cosmochimica Acta* 58 (19), p. 4253–4255.
- Bell, M.J.; Waltham, T.; Culshaw, M. (2005): Sinkholes and subsidence. Karst and Cavernous Rocks in Engineering and Construction. 1st. Berlin: Springer-Verlag.
- Berglund, M.; Wieser, M. E. (2011): Isotopic compositions of the elements 2009 (IUPAC Technical Report). In: *Pure Appl. Chem* 83 (2), p. 397–410.
- Billon, G.; Boughriet, A.; Oudane, B. (2001): Artefacts in the speciation of sulfides in anoxic sediments. In: *Analyst* 126, p. 1805–1809.
- Bitton, G. (2005): Microbial indicators of fecal contamination: Application to microbial source tracking. Tallahassee, USA: Florida Stormwater Association.
- Bland, J.M.; Altmann, D.G. (1986): Statistical methods for assessing agreement between two methods of clinical measurement. *Lancet*. P. 307-310.
- Boguski, T.K (2008): Understanding Units of Measure: Centre for Hazardous Substance Research (CHSR) at Kansas State University.

- Böttcher, M. E.; Usdowski, E. (1993):  $^{34}\text{S}/^{32}\text{S}$  Ratios of the dissolved Sulphate of River, Well and Spring Waters in a Gypsum-Carbonate Karst Area at the Southwest Edge of the Harz Mountains. In: *Zeitschrift der Deutschen Geologischen Gesellschaft* 144, p. 471–477. Available online at: [http://www.schweizerbart.de/papers/zdgg/detail/144/54649/34S\\_32S\\_Ratios\\_of\\_the\\_dissolved\\_Sulphate\\_of\\_River\\_](http://www.schweizerbart.de/papers/zdgg/detail/144/54649/34S_32S_Ratios_of_the_dissolved_Sulphate_of_River_).
- Böttcher, M. E.; Smock, A.; Cypionka, H. (1998): Sulfur isotope fractionation during experimental precipitation of iron(II) and manganese(II) sulfide at room temperature. In: *Chemical Geology* 146, p. 127–134.
- Bottrel, S.; Raiswell, R. (2000): Sulphur Isotopes and Microbial Sulphur Cycling in Sediments. In: R.E Riding and S.M Awramik (Ed.): *Microbial Sediments*. Berlin-Heidelberg: Springer Verlag.
- Brunner, B.; Bernasconi, S.; Kleikemper, J.; Schroth, M. (2005): A model for oxygen and sulfur isotope fractionation in sulfate during bacterial sulfate reduction processes. In: *Geochimica et Cosmochimica Acta* 69 (20), p. 4773–4785.
- Canfield, D. E. (2001a): Biogeochemistry of Sulfur Isotopes. In: *Reviews in Mineralogy and Geochemistry* 43 (1), p. 607–636.
- Canfield, D. E.; Teske, A. (1996): Late Proterozoic rise in atmospheric oxygen concentration inferred from phylogenetic and sulphur-isotope studies. In: *Nature* 382, p. 127–132.
- Canfield, D. E.; Raiswell, R.; Westrich, J. T.; Reaves, C. M.; Berner, R. A. (1986): The use of chromium reduction in the analysis of reduced inorganic sulfur in sediments and shales. In: *Chemical Geology* 54 (1-2), p. 149–155.
- Carmody, R.W; Plummer, L.N; Busenberg, E.; Coplen, T.B (1998): Methods for collection of dissolved sulfate and sulfide and analysis of their sulfur isotopic composition. Reston, Virginia (97-234).
- Castenholz, R.; Rippka, R.; Herdman, M.; Wilmotte, A. (2001): Subsection III, formerly Oscillatoriales. In: D.r Boone, R.W Castenholz and G.M Garrity (Ed.): *Bergey's Manual of Systematic Bacteriology. The Archaea and the Deeply Branching and Phototrophic Bacteria*. 2. Edition New York, USA: Springer (Vol 1).
- Chernousova, E.; Gridneva, E.; Grabovich, M.; Dubinina, G.; Akimov, V.; Rossetti, S.; Kuever, J. (2009): *Thiothrix caldifontis* sp. nov. and *Thiothrix lacustris* sp. nov., gammaproteobacteria isolated from sulfide springs. In: *International Journal of Systematic and Evolutionary Microbiology*.59 (12), p. 3128–3135.
- Clark, I.D; Fritz, P. (1997): *Environmental Isotopes in Hydrogeology*. New York: Lewis Publishers.
- Claypool, G. E.; Holser, W. T.; Kaplan, I. R.; Sakai, H.; Zak, I. (1980): The age curves of sulfur and oxygen isotopes in marine sulfate and their mutual interpretation. In: *Chemical Geology* 28, p. 199–260.
- Cooper, D. C.; Morse, J. W. (1998): Extractability of Metal Sulfide Minerals in Acidic Solutions: Application to Environmental Studies of Trace Metal Contamination within Anoxic Sediments. In: *Environ. Sci. Technol* 32 (8), p. 1076–1078.
- Coplen, T.B.; Kendall, C.; Hoppo, J. (1983): Comparison of stable isotope reference samples. *Nature* (302), p. 236-238).

- Craig, H. (1961): Isotopic Variations in Meteoric Waters. In: *Science* 133 (3465), p. 1702–1703.
- Das, S. (2005): Genus: Borea. In: D.J Brenner, N.R Krieg, J.T Staley and G.M Garrity (Ed.): *Bergey's Manual of Systematic Bacteriology. The Proteobacteria. Part C: The Alpha-, Beta-, Delta-, and Epsilonproteobacteria. 2. Edition 5 Bände. New York, USA: Springer (Vol 2), p. 459–461.*
- Ding, T. (2001): Calibrated sulfur isotope abundance ratios of three IAEA sulfur isotope reference materials and V-CDT with a reassessment of the atomic weight of sulfur. In: *Geochimica et Cosmochimica Acta* 65 (15), p. 2433–2437.
- Dole, M.; Lane, G.; Rudd, D.; Zaukelies, D. (1954): Isotopic composition of atmospheric oxygen and nitrogen. In: *Geochimica et Cosmochimica Acta* 6, p. 65–78.
- Egemeier, S. (1973): Cavern Development by Thermal Waters with a Possible Bearing on Ore Deposition. PhD. Stanford University.
- Egemeier, S. (1981): Cavern Development by thermal waters. In: *Bulletin of the National Speleological Society* 43, p. 31–51.
- Ehrlich, H L. (2002): Geomicrobiology. 4th ed., rev. and expanded. New York: M. Dekker.
- Engel, A.; Stern, L.; Bennett, P. (2004): Microbial contributions to cave formation: New insights into sulfuric acid speleogenesis. In: *Geology* 32 (5).
- Ercolini, D. (2004): PCR-DGGE fingerprinting: novel strategies for detection of microbes in food. In: *Journal of Microbiological Methods* 56 (3), p. 297–314.
- Farmer III, J.; Brenner, F. (2005): Genus: Yokenella. In: D.J Brenner, N.R Krieg, J.T Staley and G.M Garrity (Ed.): *Bergey's Manual of Systematic Bacteriology. The Proteobacteria, Part B: The Gammaproteobacteria. 2. Edition 5 Bände. New York, USA: Springer (2), p. 848–850.*
- Faure, Gunter (1986): Principles of isotope geology. 2nd. New York: Wiley (51).
- Federal Geographic Data Committee (2006): 37 - Lithologic patterns. FGDC Digital Cartographic Standard for Geologic Map Symbolization (FGDC Document Number FGDC-STD-013-2006).
- Ford, D. (2006): Karst geomorphology, caves and cave deposits: a review of North American contributions during the past half century. In: R. S. Harmon, Carol M. Wicks, Derek Ford and William B. White (Ed.): *Perspectives on Karst geomorphology, hydrology, and geochemistry. A tribute volume to Derek C. Ford and William B. White. Boulder, Colo: Geological Society of America.*
- Friedrich, C. G.; Rother, D.; Bardischewsky, F.; Quentmeier, A.; Fischer, J. (2001): Oxidation of Reduced Inorganic Sulfur Compounds by Bacteria: Emergence of a Common Mechanism? In: *Applied and Environmental Microbiology* 67 (7), p. 2873–2882.
- Fry, B.; Gest, H.; Hayes, J. M. (1988): 34S/32S fractionation in sulfur cycles catalyzed by anaerobic bacteria. In: *Appl. Environ. Microbiol* 54 (1), p. 250–256.
- Galdenzi, S.; Menichetti, M. (1995): Occurrence of hypogenic caves in a karst region: Examples from central Italy. In: *Environmental Geology* 26 (1).
- Galdenzi, S.; Maruoka, T. (2000): Gypsum deposits in the Frasassi Caves, Central Italy. In: *Journal of Cave and Karst Studies* 65 (2).

- Garlick, G. (1969): The stable isotopes of oxygen. In: K.H Wedepohl (Ed.): Handbook of Geochemistry. 8B. Heidelberg, New York: Springer.
- Gat, J.; Carmi, I. (1970): Evolution of the isotopic composition of atmospheric waters in the Mediterranean Sea area. In: *Journal of Geophysical Research* 75, p. 3039–3048.
- Green, S.; Leigh, M.; Neufeld, J. (2010): Denaturing gradient gel electrophoresis (DGGE) for microbial community analysis. In: Kenneth N. Timmis (Ed.): Handbook of Hydrocarbon and Lipid Microbiology. Berlin, Heidelberg: Springer Berlin Heidelberg.
- Groot, P. de (2009): Chapter 8 - Sulfur. In: P. A. De Groot (Ed.): Handbook of Stable Isotope Analytical Techniques: Elsevier B.V. (1).
- Grouven, U.; Bender, R.; Ziegler, A.; Lange, S. (2007): Vergleich von Messmethoden – comparing methods of measurement. *Dtsch Med Wochenschr* (132). P. 69-73.
- Gunn, J. (2004): Encyclopedia of Caves and Karst Science. London: Fitzroy Dearborn.
- Habicht, K.; Canfield, D. (1997a): Sulfur isotope fractionation during bacterial sulfate reduction in organic-rich sediments. In: *Geochimica et Cosmochimica Acta* 61 (24), p. 5351–5361.
- Habicht, K.; Canfield, D. (1997b): Sulfur isotope fractionation during bacterial sulfate reduction in organic-rich sediments. In: *Geochimica et Cosmochimica Acta* 61 (24), p. 5351–5361.
- Haddad, R.; Smoor, P. (1973): Groundwater Survey of Erbil Project Area. In: *IARNR Techn. Bull.* 50.
- Hallberg, K. B.; González-Toril, E.; Johnson, D. B. (2010): *Acidithiobacillus ferrivorans*, sp. nov.; facultatively anaerobic, psychrotolerant iron-, and sulfur-oxidizing acidophiles isolated from metal mine-impacted environments. In: *Extremophiles* 14 (1), p. 9–19.
- Hamamin, D. F.; Ali, S. S. (2012): Hydrodynamic study of karstic and intergranular aquifers using isotope geochemistry in Basara basin, Sulaimani, North-Eastern Iraq. In: *Arab J Geosci*.
- Haubrich, F. (2011): Kurzbeschreibung Präparation von S-haltigen Substanzen für die Analyse der Stabilen Isotope  $\delta^{34}\text{S}$  und  $\delta^{18}\text{O}$ . Unpublished report.
- Haubrich, F. (2012): personal communication.
- Häuselmann, P.; Neumann, A. (1999): Cave Symbols: The Official UIS List. voted by the national delegates. Available online at: [www.uis-speleo.org](http://www.uis-speleo.org), last check at 16.04.2012.
- HAZRA Engineering Company (1963): Hydrogeological Survey of Iraq. Chicago, Bagdad.
- Hearn, R.; Berglund, M.; Ostermann, M.; Pusticek, N.; Taylor, P. (2005): A comparison of high accuracy isotope dilution techniques for the measurement of low level sulfur in gas oils. In: *Analytica Chimica Acta* 532 (1), p. 55–60.
- Heidel, C.; Tichomirowa, M. (2010): The role of dissolved molecular oxygen in abiotic pyrite oxidation under acid pH conditions - Experiments with  $^{18}\text{O}$ -enriched molecular oxygen. In: *Applied Geochemistry* 25, p. 1664–1675.
- Heidel, C.; Tichomirowa, M.; Junghans, M. (2009): The influence of pyrite grain size on the final oxygen isotope difference between sulphate and water in aerobic pyrite oxidation experiments. In: *Isotopes in the Environmental and Health Studies* 45, p. 321–342.
- Heiland, K. (2016): Hydrogeochemical investigation of Darzila karst cave, NE Iraq. In: *Freiberg Online Geology (FOG)* (44), pp 135

- Hill, C. A. (1990): Sulfuric acid speleogenesis of Carlsbad Cavern and its relationship to hydrocarbons, Delaware basin, New Mexico and Texas. In: *AAPG* 74 (11), p. 1685–1694.
- Hoefs, J. (2004): Stable isotope geochemistry. With 18 tables. 5., rev. and updated. Berlin [u.a.]: Springer.
- Hose, L.; Pisarowicz, J. (1999): Cueva de Villa Luz, Tabasco, Mexico- Reconnaissance Study of an Active Sulfur Spring Cave and Ecosystem. In: *Journal of Cave and Karst Studies* 61 (1), p. 13–21.
- Hose, L. D.; Palmer, A. N.; Palmer, M. V.; Northup, D. E.; Boston, P. J.; DuChene, H. R. (2000): Microbiology and geochemistry in a hydrogen-sulphide-rich karst environment. In: *Chemical Geology* 169 (3-4), p. 399–423.
- Iraq: Oil infrastructure (2003): Iraqi oil field map 2.pdf: CIA. Available online at: <http://lib.utexas.edu/maps/iraq.html#country.html>.
- 1999-12: Solid mineral fuels; determination of total sulfur; Eschka method.
- Iurkiewicz, A. A.; Stevanovic, Z. P. (2010): Reconnaissance study of active sulfide springs and cave systems in the southern part of the Sulaimani Governorate (NE Iraq). In: *Carbonates Evaporites* 25 (3), p. 203–216.
- Janssen, A. J.; Lens, P. N.; Stams, A. J.; Plugge, C. M.; Sorokin, D. Y.; Muyzer, G. *et al.* (2009): Application of bacteria involved in the biological sulfur cycle for paper mill effluent purification. In: *Science of The Total Environment* 407 (4), p. 1333–1343.
- Jassim, S.Z; Goff, J.C (Ed.) (2006): Geology of Iraq. Brno, Czech republic: Dolin, Prague and Moravian Museum.
- Jassim, S.; Buday, T. (2006): Units of the Unstable Shelf and the Zagros Suture. Chapter 6. In: S.Z Jassim and J.C Goff (Ed.): Geology of Iraq. Brno, Czech republic: Dolin, Prague and Moravian Museum, p. 71–83.
- Jensen, M.; Nakai, N. (1962): Sulfur isotope meteorite standards, results and recommendations. In: M.L.R Jensen. National Science Foundation (Ed.): Biogeochemistry of sulfur isotopes: proceedings of a National Science Foundation symposium held at Yale University, April 12-14, 1962: Yale University, p. 30–35.
- Kaasalainen, H.; Stefánsson, A. (2011): Sulfur speciation in natural hydrothermal waters, Iceland. In: *Geochimica et Cosmochimica Acta* 75 (10), p. 2777–2791.
- Kampschulte, A.; Bruckschen, P.; Strauss, H. (2001): The sulphur isotopic composition of trace sulphates in Carboniferous brachiopods: implications for coeval seawater, correlation with other geochemical cycles and isotope stratigraphy. In: *Chemical Geology* 175 (1-2), p. 149–173.
- Kanagawa, T. (2003): Bias and artifacts in multitemplate polymerase chain reactions (PCR). In: *J. Biosci. Bioeng* 96 (4), p. 317–323.
- Kaplan, I. R.; Rittenberg, S. C. (1964): Microbiological Fractionation of Sulphur Isotopes. In: *Microbiology* 34 (2), p. 195–212.
- Kelly, D. P.; Wood, A. P. (2000): Reclassification of some species of *Thiobacillus* to the newly designated genera *Acidithiobacillus gen. nov.*, *Halothiobacillus gen. nov.* and *Thermithiobacillus gen. nov.* In: International Journal of Systematic and Evolutionary Microbiology 50 (2), p. 511–516.

- Kester, C. L.; Rye, R. O.; Johnson, C. A.; Schwartz, C.; Holmes, C. (2001): On-line Sulfur Isotope Analysis of Organic Material by Direct Combustion: Preliminary Results and Potential Applications. In: *Isotopes in Environmental and Health Studies* 37 (1), p. 53–65.
- Khanaqa, P.A (2011): Personal communication during fieldwork.
- Khanaqa, P.; Al-Manmi, D. (2011): Hydrogeochemistry and geomicrobiology of Darzila spring in Sangaw, Sulaimaniyah, NE Iraq. In: *Iraqi Bulletin of Geology and Mining* 7 (3), p. 63-79i.
- Kharanjany, S. O. A. (2008): Sedimentary facies of Oligocene rock units in Asdagh mountain -Sangaw district - Kurdistan region - NE Iraq. Master thesis. University of Sulaymaniyah.
- Klimchouk, A. (1996): Gypsum karst of the world – Speleogenesis in gypsum, *International Journal of Speleology* (25), p. 3-4.
- Klimchouk, A. (2007): Hypogene speleogenesis: Hydrogeological and Morphogenetic Perspective. Special Paper no. 1. Carlsbad, NM: National Cave and karst Research Institute.
- Knöller, K. (2012): personal communication, email 14.03. and 08.10.2012, 2012.
- Knöller, K.; Schubert, M. (2010): Interaction of dissolved and sedimentary sulfur compounds in contaminated aquifers. In: *Chemical Geology* 276 (3-4), p. 284–293.
- Knöller, K.; Vogt, C.; Richnow, H.-H.; Weise, S. M. (2006): Sulfur and Oxygen Isotope Fractionation during Benzene, Toluene, Ethyl Benzene, and Xylene Degradation by Sulfate-Reducing Bacteria. In: *Environ. Sci. Technol* 40 (12), p. 3879–3885.
- Korber, D.R.; Wolfaardt, G.M.; Brozel, V.; MacDonald, R.; Niepel, T., (1999). Models for Studying Initial Adhesion and Surface Growth in Biofilm Formation on Surfaces. In: *Methods in Enzymology*, 310. p. 3-13.
- Kroopnick, P.; Craig, H. (1972): Atmospheric oxygen: isotopic composition and solubility fractionation. In: *Science* 175, p. 54–55.
- Lauerwald, F. (2004): Sulfur Geochemistry of Hot Springs at Yellowstone National Park. Diploma thesis. TU Bergakademie Freiberg.
- Lawa, F. (2012): Personal communication. Geologist, specialized in sequence stratigraphy, stratigraphy and paleontology. University of Sulaymaniyah.
- Le Faou, A. (1990): Thiosulfate, polythionates and elemental sulfur assimilation and reduction in the bacterial world. In: *FEMS Microbiology Letters* 75 (4), p. 351–382.
- Levett, P. N. (2005): Reclassification of *Leptospira parva* Hovind-Hougen *et al.* 1982 as *Turneriella parva* *gen. nov.*, *comb. nov.* In: *International Journal of Systematic and Evolutionary Microbiology* 55 (4), p. 1497–1499.
- LGR (2012): Personal communication with the technical support of Los Gatos Research, 24.10.2012
- Lipthay, J. R. de; Enzinger, C.; Johnsen, K.; Aamand, J.; Sørensen, S. J. (2004): Impact of DNA extraction method on bacterial community composition measured by denaturing gradient gel electrophoresis. In: *Soil Biology and Biochemistry* 36 (10), p. 1607–1614.
- Lis, G.; Wassenaar, L. I.; Hendry, M. J. (2008): High-Precision Laser Spectroscopy D/H and  $^{18}\text{O}/^{16}\text{O}$  Measurements of Microliter Natural Water Samples. In: *Anal. Chem* 80 (1), p. 287–293.

- Lloyd, R. (1967): Oxygen-18 composition of oceanic sulphate. In: *Science* 156, p. 1228–1231.
- Ludwig, W.; Strunk, O.; Westram, R.; Richter, L.; Meier, H.; Yadhukumar *et al.* (2004): ARB: a software environment for sequence data (32). In: *Nucleic Acids Research* (4), p. 1363–1371.
- Luther III, G. W.; Findlay, A. J.; MacDonald, D. J.; Owings, S. M.; Hanson, T. E.; Beinart, R. A.; Girguis, P. R. (2011): Thermodynamics and Kinetics of Sulfide Oxidation by Oxygen: A Look at Inorganically Controlled Reactions and Biologically Mediated Processes in the Environment. In: *Front. Microbio* 2.
- Maala, K. (2001): Geological Map of Sulaymaniyah Quadrangles, scale 1:250000. Iraq-Baghdad: State Company of Geological Survey and Mining.
- Macalady, J. L.; Lyon, E. H.; Koffman, B.; Albertson, L. K.; Meyer, K.; Galdenzi, S.; Mariani, S. (2006): Dominant Microbial Populations in Limestone-Corroding Stream Biofilms, Frasassi Cave System, Italy. In: *Applied and Environmental Microbiology* 72 (8), p. 5596–5609.
- Macalady, J. L.; Dattagupta, S.; Schaperdoth, I.; Jones, D. S.; Druschel, G. K.; Eastman, D. (2008): Niche differentiation among sulfur-oxidizing bacterial populations in cave waters. In: *ISME J* 2 (6), p. 590–601.
- Machel, H. (1992): Low-temperature and high-temperature origins of elemental sulphur in diagenetic environments. In: G.R Wessel and B.H Wimberley (Ed.): Native sulphur developments in geology and environment. Littleton, CO, p. 3–22.
- Machel, H. (2001): Bacterial and thermochemical sulfate reduction in diagenetic settings — old and new insights. In: *Sedimentary Geology* 140 (1-2), p. 143–175.
- Madigan, M.T.; Brock, T.D. (2009); Brock biology of microorganisms. 12 edition. San Francisco, CA: Pearson / Benjamin Cummings.
- Mariotti, A.; Germon, J. C.; Hubert, P.; Kaiser, P.; Letolle, R.; Tardieux, A.; Tardieux, P. (1981): Experimental determination of nitrogen kinetic isotope fractionation: Some principles; illustration for the denitrification and nitrification processes. In: *Plant Soil* 62 (3), p. 413–430.
- Mawlood D. (2003): Application of Isotope Hydrology Studies Considering the Specific Climatic, Hydrological and Geological Conditions In Order to Research Underground Water Resources in a Specific Area in the Near East. Dissertation. Technische Universitaet Wien; Fakultae fuer Bauingenieurwesen; Institut fuer Hydraulik, Gewaesserkunde und Wasserwirtschaft.
- Mori, K.; Suzuki, K.-i. (2008): *Thiofaba tepidiphila* gen. nov., sp. nov., a novel obligately chemolithoautotrophic, sulfur-oxidizing bacterium of the Gammaproteobacteria isolated from a hot spring. In: *International Journal of Systematic and Evolutionary Microbiology* 58 (8), p. 1885–1891.
- Muyzer, G. (1999): DGGE/TGGE a method for identifying genes from natural ecosystems. In: *Current Opinion in Microbiology* 2 (3), p. 317–322.
- Muyzer, G.; Stams, A. J. M. (2008): The ecology and biotechnology of sulphate-reducing bacteria. In: *Nat Rev Micro*.
- Nairn, A.E.M; Alsharhan, A.S (1997): Sedimentary Basins and Petroleum Geology of the Middle East: Elsevier Science. Available online at: <http://books.google.de/books?id=0Ug0GdmopWMC>.

- Nakai, N.; JENSEN, M. (1964): The kinetic isotope effect in the bacterial reduction and oxidation of sulfur. In: *Geochimica et Cosmochimica Acta* 28 (12), p. 1893–1912.
- Ohmoto, H.; Rye, R. O. (1979): Isotopes of sulfur and carbon. In: H.L Barnes (Ed.): *Geochemistry of Hydrothermal Ore deposits*: Wiley and Sons, p. 509–567.
- Onac, B. P.; Wynn, J. G.; Sumrall, J. B. (2011): Tracing the sources of cave sulfates: a unique case from Cerna Valley, Romania. In: *Chemical Geology* 288 (3-4), p. 105–114.
- Orr, W. (1974): Changes in Sulfur Content and Isotopic Ratios of Sulfur during Petroleum Maturation--Study of Big Horn Basin Paleozoic Oils. In: *AAPG Bulletin* 58 (11), p. 2295–2318.
- Osseo-Asare, K. (1998): Solution chemistry and separation process in precious and rare metals systems. In: A.E Torma and I.H Gundiler (Ed.): *Precious and Rare Metals Technologies*. Amsterdam: Elsevier.
- Ostermann, M.; Kettisch, P.; Becker, D.; Vogl, J. (2003): Measurements of sulfur in oil using a pressurised wet digestion technique in open vessels and isotope dilution mass spectrometry. In: *Analytical and Bioanalytical Chemistry* 377 (4), p. 779–783.
- Palmer, A. N. (2011): Distinction between epigenic and hypogenic maze caves. In: *Geomorphology* 134 (1-2), p. 9–22.
- Palmer, A. N.; Palmer, M. (2004): Sulfate-carbonate interactions in the development of karst. In: *Northeastern Geology & Environmental Sciences* 26 (1&2), p. 93–106.
- Palmer, A. N.; Hill, C. A. (2012): Sulfuric Acid Caves. In: D.C Culver and W.B White (Ed.): *Encyclopedia of Caves*. 2nd. Waltham, USA: Elsevier, p. 810–819.
- Palmer, A. (1991): Origin and morphology of limestone caves. In: *Geological Society of America Bulletin* 103 (1), p. 113–135.
- Palmer, A.; Palmer, M. (2000): Hydrochemical interpretation of cave patterns in the Guadalupe Mountains, New Mexico. In: *Journal of Cave and Karst Studies* 62 (2), p. 91–108.
- Paytan, A. (2012): Personal communication.
- Paytan, A.; Kastner, M.; Campbell, D.; Thiemens, M. (1998): Sulfur Isotopic Composition of Cenozoic Seawater Sulfate. In: *Science* 282 (5393), p. 1459–1462.
- Peix, A.; Ramírez-Bahena, M.-H.; Velázquez, E. (2009): Historical evolution and current status of the taxonomy of genus *Pseudomonas*. In: *Infection, Genetics and Evolution* 9 (6), p. 1132–1147.
- Poore, R.Z.; Matthews, R.K. (1984). Late Eocene-Oligocene oxygen- and carbon-isotope record from south atlantic ocean, deep sea drilling project site 522.
- Rees, C. (1973): A steady-state model for sulphur isotope fractionation in bacterial reduction processes. In: *Geochimica et Cosmochimica Acta* 37 (5), p. 1141–1162.
- Rees, C. E.; Holt, B. (1991): Chapter 2. The isotopic analysis of sulfur and oxygen. In: H. R. Krouse and V.A Grinenko (Ed.): *Stable Isotopes in the Assessment of Natural and Anthropogenic Sulphur in the Environment*: John Wiley & Sons Ltd, p. 43–64.
- Rickard, D. (1995): Kinetics of FeS precipitation. 1. Competing reaction-mechanisms. In: *Geochimica et Cosmochimica Acta* 59 (21), p. 4367–4379.

- Rickard, D. (1997): Kinetics of pyrite formation by the H<sub>2</sub>S oxidation of iron(II)monosulfide in aqueous solutions between 25 and 125 degrees C: the rate equation. In: *Geochimica et Cosmochimica Acta* 61 (1), p. 115–134.
- Rozanski, K.; Araguás-Araguás, L.; Gonfiantini, R. (1993): Isotopic patterns in modern global precipitation, p. 1–36.
- SafetyDirectory (2004): H<sub>2</sub>S Safety Factsheet. Available online at: [http://www.safetydirectory.com/hazardous\\_substances/hydrogen\\_sulfide/fact\\_sheet.htm](http://www.safetydirectory.com/hazardous_substances/hydrogen_sulfide/fact_sheet.htm), last check at 08.10.2012.
- Sakai, H.; Casadevall, T.; Moore, J. (1982): Chemistry and isotope ratios of sulfur in basalts and volcanic gases at Kilauea volcano, Hawaii. In: *Geochimica et Cosmochimica Acta* 46 (5), p. 729–738.
- Sanger, F. (1977): DNA Sequencing with Chain-Terminating Inhibitors. In: *Proceedings of the National Academy of Sciences* 74 (12), p. 5463–5467.
- Seal, R. R. (2006): Sulfur Isotope Geochemistry of Sulfide Minerals. In: *Reviews in Mineralogy and Geochemistry* 61 (1), p. 633–677.
- Shen, Y.; Buick, R. (2004): The antiquity of microbial sulfate reduction. In: *Earth-Science Reviews* 64 (3-4), p. 243–272.
- Siegfried, R.; Wiberly, J.; Moore, R. (1951): Determination of sulfur after combustion in a small oxygen bomb. Rapid titrimetric method. In: *Anal. Chem* 23, p. 1008–1011.
- Steffens, Heinrich (1819): Vollständiges Handbuch der Oryktognosie. Dritter Theil. Halle, In der Curtschen Buchhandlung.
- Sterky, F.; Lundeberg, J. (2000): Sequence analysis of genes and genomes. In: *Journal of Biotechnology* 76 (1), p. 1–31.
- Studel R. (1998): Chemie der Nichtmetalle: Mit Atombau, Molekülgeometrie und Bindungstheorie. 2. Edition: Walter de Gruyter.
- Studel, R.; Eckert, B. (2003): Aqueous sulfur sols. In: *Top. Curr. Chem.* 230, p. 1–79.
- Stevanovic, Z. P.; Iurkiewicz, A. A.; Maran, A. (2009): New insights into karst and caves of northwestern Zagros (Northern Iraq). In: *Acta Carsologica* 38 (1), p. 83–96.
- Stevanovic, Z. P.; Markovic, M. (Ed.) (2003a): Hydrogeology of Northern Iraq. FAO Northern Iraq Coordination Office. 2nd. Erbil (1. Climate, Hydrogeology, Geomorphology & Geology).
- Stevanovic, Z. P.; Markovic, M. (Ed.) (2003b): Hydrogeology of Northern Iraq. FAO Northern Iraq Coordination Office. Erbil (2. General Hydrogeology and Aquifer Systems).
- Suda, S.; Watanabe, M.; Otsuka, S.; Mahakahant, A.; Yongmanitchai, W.; Nopartnaraporn, N. *et al.* (2002): Taxonomic revision of water-bloom-forming species of oscillatoroid cyanobacteria. In: *International Journal of Systematic and Evolutionary Microbiology* 52 (5), p. 1577–1595.
- Szaran, J. (1996): Experimental investigation of sulphur isotope fractionation between dissolved and gaseous H<sub>2</sub>S. In: *Chemical Geology* 127.
- Tang, K.; Baskaran, V.; Nemati, M. (2009): Bacteria of the sulphur cycle: An overview of microbiology, biokinetics and their role in petroleum and mining industries. In: *Biochemical Engineering Journal* 44 (1), p. 73–94.
- Taylor, B.; Wheeler, M. (1994): Sulfur- and oxygen- isotope geochemistry of acid mine drainage in the western United States: field and experimental studies revisited. In: C.

- Alpers and D. Blowes (Ed.): Environmental Geochemistry of Sulfide Oxidation: American Chemical Society Symposium Series, p. 481–514.
- Thode, H. G. (1991): Sulphur isotopes in Nature and the Environment: An Overview. In: H. R. Krouse and V.A Grinenko (Ed.): Stable Isotopes in the Assessment of Natural and Anthropogenic Sulphur in the Environment: John Wiley & Sons Ltd.
- Thode, H. G.; Monster, J. (1970): Sulfur Isotope Abundances and Genetic Relations of Oil Accumulations in Middle East Basin. In: *The American Association of Petroleum Geologists Bulletin* 54 (4), p. 627–637.
- Thode, H.; Rees, C. (1970): Sulfur isotope geochemistry and Middle East oil studies. In: *Endeavour* 29, p. 24–28.
- Tichomirowa, M. (2012): Personal communication.
- Trüper, H. (1984): Microorganisms and the Sulfur cycle. In: A. Müller and B. Krebs (Ed.): Sulfur. Its significance for chemistry, for the geo-, bio- and cosmosphere and technology: (Bielefeld sulfur meeting; Bielefeld, June 14-16, 1983). Amsterdam a.o: Elsevier.
- Turchyn, A. V.; Brüchert, V.; Lyons, T. W.; Engel, G. S.; Balci, N.; Schrag, D. P.; Brunner, B. (2010): Kinetic oxygen isotope effects during dissimilatory sulfate reduction: A combined theoretical and experimental approach. In: *Geochimica et Cosmochimica Acta* 74 (7), p. 2011–2024.
- Tuttle, M. (1986): An analytical scheme for determining forms of sulphur in oil shales and associated rocks. In: *Talanta* 33 (12), p. 953–961.
- Vredenburg, L.; Cheney, E. (1971): Sulfur and Carbon Isotopic Investigation of Petroleum, Wind River Basin, Wyoming. In: *AAPG Bulletin* 55 (11), p. 1954–1975.
- Whitten, K.W; Davis, R.E; Peck, L.; Stanley, G.G (2009): Chemistry: Cengage Learning (OWL Series). Available online at: <http://books.google.de/books?id=6Zwu9-qT0qQC>.
- Wilkin, R.; Barnes, H. (1996): Pyrite formation by reactions of iron monosulfides with dissolved inorganic and organic sulfur species. In: *Geochimica et Cosmochimica Acta* 60 (21), p. 4167–4179.
- Wimpenny, J. (2000): An overview of biofilms as functional communities. In: D.G Allison, P. Gilbert, H.M Lappin-Scott and M. Wilson (Ed.): Community structure and co-operation in biofilms. Cambridge, UK; New York: Cambridge University Press, p.1–24.
- Worden, R.; Smalley, P. (1996): H<sub>2</sub>S-producing reactions in deep carbonate gas reservoirs: Khuff Formation, Abu Dhabi. In: *Chemical Geology* 133, p. 157–171.
- World Weather Online (2011): Sangaw Weather, Iraq Weather Averages. Online: <http://www.worldweatheronline.com/Sangaw-weather-averages/AsSulaymaniyah/IQ.aspx>.
- Yonge, C.; Krouse, H. R. (1987): The origin of sulphates in Castleguard Cave, Columbia Icefields, Canada. In: *Chemical Geology: Isotope Geoscience section* 65(3-4), p.427–433.
- Zaback, D. A.; Pratt, L. M. (1992): Isotopic composition and speciation of sulfur in the Miocene Monterey Formation: Revaluation of sulfur reactions during early diagenesis in marine environments. In: *Geochimica et Cosmochimica Acta* 56 (2), p. 763–774.

## 9 Appendix

- 9.1 Appendix A - Tables
- 9.2 Appendix B - Figures
- 9.3 Appendix C – Spreadsheet

### List of tables

Table A 1: GPS data and altitude of Darzila cave, Darzila village and water, oil and biofilm sampling points .....	129
Table A 2: GPS data and altitude of rock sampling points .....	129
Table A 3: Standard solutions for the analysis of $\delta\text{D}$ and $\delta^{18}\text{O}$ in water.....	129
Table A 4: Summary of preparation procedures for $\delta^{34}\text{S}$ analysis. Detailed description in chapter 4.3.2.1.....	130
Table A 5: Solutions that are necessary for the preparation of species for sulphur isotopic analysis.....	131
Table A 6: Elemental composition of raw oil (sample DR-O-4) .....	132
Table A 7: International standard materials for $\delta^{34}\text{S}$ and $\delta^{18}\text{O}$ analysis.....	132
Table A 8: List of materials for construction of the work bench. See Figure B 1 for illustration. ....	132
Table A 9: In-situ parameter (corrected EH values; redox conditions: if $\text{EH} \leq 0$ mV then reducing, if $0 < \text{EH} < 400$ mV then partially reducing, if $\text{EH} \geq 400$ mV then oxidising) and on-site photometry (evaluated by Heiland 2016). Calc. = calculated from $\text{Ag}_2\text{S}$ precipitation yields (evaluated in this thesis).....	133
Table A 10: Cations and anions of water samples analysed with ion chromatography (laboratories of the chair for hydrogeology, TU Freiberg; data evaluated by Heiland 2016).....	134
Table A 11: ICP-MS results of water samples, in alphabetical order (laboratories of the chair for hydrogeology, TU Freiberg; data evaluated by Heiland, 2016).....	135
Table A 12: ICP-MS (continuation I).....	136
Table A 13: ICP-MS results (continuation II).....	137
Table A 14: ICP-MS results (continuation III).....	138
Table A 15: Semi-quantitative analysis of minerals in cave sediments. Grey values: When grouped together, Illite, Muscovite and Smectite represent the dioctahedral silicate minerals. The sum of their percentages is a reliable value for the group. However, the percentages of the individual minerals may depart from the listed value. To stress this extra uncertainty, affected data are given in grey. ....	139
Table A 16: XRF results of rock samples (laboratories of the chair for hydrogeology, TU Freiberg).....	140

---

Table A 17: XRF results of rock samples (continuation I).....	141
Table A 18: XRF results of rock samples (continuation II) .....	142
Table A 19: Isotopic composition of H <sub>2</sub> O of water samples.....	143
Table A 20: Sulphur Isotopic Composition of Dissolved Sulphide in Water Samples.....	143
Table A 21: Sulphur and Oxygen Isotopic Composition of Dissolved Sulphate in Water Samples. $\delta^{34}\text{S}$ values were determined at the UFZ as well as the TUBAF. nm = not measured. ....	143
Table A 22: Sulphur and Oxygen Isotopic Analysis of Sedimentary Sulphur Species. ....	144
Table A 23: Sulphur and Sulphate Oxygen Isotopic Composition of Primary Gypsum, Secondary Gypsum, Elemental Sulphur, Carbonate Rock and Crude Oil. nm = not measured.....	145
Table A 24: Comparison of sedimentary sulphur yields from X-ray fluorescence spectroscopy (XRF), X-ray diffraction (XRD), Eschka- and sequential extraction. ....	146
Table A 25: Calculation of fraction f residual sulphate based on an initial value from a well sample in the Chamchamal region, sampled in the dry season (Al-Manmi 2012).....	147

## List of figures

Figure B 1: Work bench design for the distillation unit. The list of materials is given in Table A 8. ....	148
Figure B 2: Nitrogen distribution device of the distillation unit with glass tubes and Teflon valves .....	149

## 9.1 Appendix A - Tables

Table A 1: GPS data and altitude of Darzila cave, Darzila village and water, oil and biofilm sampling points

<b>ID</b>	<b>GPS data</b>	<b>Altitude [m]</b>
Darzila cave	N35 08.779 E45 16.741	688
Darzila village	N35 08.474 E45 17.237	640
DR-W-1	N35 08.632 E45 17.375	664
DR-W-2	N35 08.544 E45 17.372	645
DR-O-4	N35 08.439 E45 17.265	634
DR-B-6	N35 08.424 E45 17.175	632
DR-W-8	N35 08.548 E45 17.029	637
DW-W-1	N35 08.794 E45 16.635	687
Recharge area, well	N35 35.251 E44 51.549	754

Table A 2: GPS data and altitude of rock sampling points

<b>ID</b>	<b>GPS data</b>	<b>Altitude [m]</b>	<b>Geological Formation</b>
<sup>1</sup> DS-PG-2a	N38 08.949 E45 18.286	766	Lower Fars Formation
DS-PG-2b	N35 09.001 E45 18.355	791	Lower Fars Formation
DS-PG-4	N35 26.649 E45 09.062	661	Lower Fars Formation
DS-PL-1	N35 08.803 E45 16.697	691	Oligocene Formation
DC-PL-15	N35 08.779 E45 16.741	688	Oligocene Formation

<sup>1</sup>Sample was collected from loose debris on the hillside instead of the actual formation.

Table A 3: Standard solutions for the analysis of  $\delta\text{D}$  and  $\delta^{18}\text{O}$  in water

<b>LGR standards</b>	<b><math>\delta\text{D}</math> in ‰ vs. VSMOW</b>	<b><math>\delta^{18}\text{O}</math> in ‰ vs. VSMOW</b>
1A	$-154.3 \pm 0.5$	$-19.50 \pm 0.15$
2A	$-123.6 \pm 0.5$	$-16.14 \pm 0.15$
3A	$-96.4 \pm 0.5$	$-13.10 \pm 0.15$
4A	$-51.0 \pm 0.5$	$-7.69 \pm 0.15$
5A	$-9.5 \pm 0.5$	$-2.80 \pm 0.15$

Table A 4: Summary of preparation procedures for  $\delta^{34}\text{S}$  analysis. Detailed description in chapter 4.3.2.1.

Section	Sample type	Sulphur species	Overall procedure
a) and b)	Water	$\text{H}_2\text{S}$	Precipitation as $\text{ZnS}$ Dissolution with $\text{HCl}$ and $\text{CrCl}_2$ solution Distillation Precipitation of $\text{H}_2\text{S}$ as $\text{ZnS}$ Reprecipitation with $\text{AgNO}_3$ as $\text{Ag}_2\text{S}$
		$\text{SO}_4^{2-}$	Acidification with $\text{HCl}$ Precipitation as $\text{BaSO}_4$ Removal of $\text{Cl}^-$
c)	Gypsum	$\text{SO}_4^{2-}$	Pulverization, dissolution with $\text{H}_2\text{O}_{\text{deion.}}$ Filtration, Acidification of filtrate with $\text{HCl}$ Precipitation as $\text{BaSO}_4$ Removal of $\text{Cl}^-$
d)	Carbonate rock	$\text{SO}_4^{2-}$	Pulverization, dissolution with $\text{HCl}$ Filtration Precipitation as $\text{BaSO}_4$ Removal of $\text{Cl}^-$
e)	Elemental sulphur	$\text{S}^0$	Removal of embedded $\text{SO}_4^{2-}$ and $\text{Cl}^-$
f)	Crude oil	$\text{H}_2\text{S}$ , organic S	Digestion with $\text{HNO}_3$ and $\text{H}_2\text{O}_2$ at high temperature Precipitation as $\text{BaSO}_4$
g) and h)	Sediment	$\text{SO}_4^{2-}$	Dissolution with $\text{H}_2\text{O}_{\text{deion.}}$ Filtration, Acidification of filtrate with $\text{HCl}$ Precipitation as $\text{BaSO}_4$ Removal of $\text{Cl}^-$
		$\text{S}^0$	Soxhlet extraction with dichlormethane as solvent $\text{S}^0$ precipitation during solvent regeneration
		$\text{FeS}_2$	Dissolution with $\text{CrCl}_2$ solution Distillation Precipitation of $\text{H}_2\text{S}$ as $\text{ZnS}$ Reprecipitation with $\text{AgNO}_3$ as $\text{Ag}_2\text{S}$
		total S	Addition of Eschka`s mixture Heated to $825^\circ\text{C}$ Dissolution Precipitation as $\text{BaSO}_4$ Removal of $\text{Cl}^-$

Table A 5: Solutions that are necessary for the preparation of species for sulphur isotopic analysis.

<b>Solution / Mixture</b>	<b>Purpose</b>	<b>Materials and preparation</b>
10% AgNO <sub>3</sub> solution	Test solution for the presence of Cl <sup>-</sup>	5 g AgNO <sub>3</sub> (VEB Laborchemie Apolda, p.a.) + 1 mL 65% HNO <sub>3</sub> (ALDRICH, p. a.), filled up to 50 g with deionised water
0.1 M AgNO <sub>3</sub> solution	Re-precipitation of ZnS to Ag <sub>2</sub> S	17 g AgNO <sub>3</sub> (VEB Laborchemie Apolda, p.a.) filled up to 1000 g with deionised water
1.5 M BaCl <sub>2</sub> ·2 H <sub>2</sub> O solution	Precipitation of BaSO <sub>4</sub>	17 g BaCl <sub>2</sub> ·2 H <sub>2</sub> O (Isocomerz, p. a.), filled up to 50 mL with deionised water
3% ammonia zinc-acetate solution	Precipitation of ZnS	300 mL of 25 % ammonia (Prolabo VWR) and 71.8 g Zn(CO <sub>3</sub> COO) <sub>2</sub> ·2 H <sub>2</sub> O were dissolved in 1700 mL deionised water
Bromine water (saturated)	Oxidation of sulphur species	Saturated bromine water was prepared by carefully adding liquid bromine (FISHER CHEMICAL, extra pure) in a glass bottle containing deionised water. The addition of bromine was continued until a little excess of bromine remained undissolved.
0.25 M Mercury(II) chloride solution	Formation of a thin amalgam layer on zinc granules	17.8 g of HgCl <sub>2</sub> (NQR GmbH, p.a.) were dissolved in 300 mL of deionised water. An ultrasonic bath was necessary to dissolve the powder completely.
1 M CrCl <sub>2</sub> solution	Reduction of chromium reducible sulphur species	Chromium-(II) solution was prepared on the basis of the procedures described in Canfield <i>et al.</i> (1986) and Tuttle (1986) and on the lab routine of the <i>Stable Isotope Geochemistry Laboratory</i> of the TUBAF. See chapter 4.3.2.1 (Sample preparation, paragraph g) for a detailed description.
Eschka`s mixture	Extraction of all sulphur species from sediment	Two parts MgO (Fluka Chemie GmbH, p.a.) and one part anhydrous Na <sub>2</sub> CO <sub>3</sub> (Merck, p.a.) by weight

Table A 6: Elemental composition of raw oil (sample DR-O-4)

Aliquot	N (%)	C (%)	H (%)	S (%)
<b>a</b>	ca. 0.2	83.55	11.73	0.13
<b>b</b>	ca. 0.2	84.58	11.59	0.14
<b>c</b>	ca. 0.2	81.21	11.14	0.14
<b>Ø-value</b>	ca. 0.2	83.11	11.49	0.14

Table A 7: International standard materials for  $\delta^{34}\text{S}$  and  $\delta^{18}\text{O}$  analysis

	Description	$\delta^{34}\text{S}$ in ‰ VCDT	$\delta^{18}\text{O}$ in ‰ VSMOW	UFZ	TUBAF
IAEA - SO-05	BaSO <sub>4</sub>	0.5	12.7 ± 0.2	x	x
IAEA - SO-06	BaSO <sub>4</sub>	-34.1	-11.0	x	x
IAEA-NBS-127	BaSO <sub>4</sub>	20.3 ± 0.4	9.3 ± 0.4	-	x
IAEA - S - 1	Ag <sub>2</sub> S	-0.3		x	-
IAEA - S - 2	Ag <sub>2</sub> S	22.7		x	-
IAEA - S - 3	Ag <sub>2</sub> S	-32.3		x	-

Table A 8: List of materials for construction of the work bench. See Figure B 1 for illustration.

Pos.	Quantity or length	Structural element	Number
1	2	Cap 30x30	Bosch Rexroth: 3 842 501 232
2	6294 mm	Profile 30 x 30	Bosch Rexroth: 3 842 990 720
3	3	Rod	12-0026-3-6 - 0_2
4	6	Inwards hexagon skrew	ISO 4762 - M5 x 10
5	6	Sliding block N8	Bosch Rexroth: 3 842 514 930
6	6	Thumb skrew	DIN 316 - M6 x 8
7	6	Angle bracket	12-0026-3-6 - 0_1
8	8	Sliding block N8 M6 with spring	Bosch Rexroth: 3 842 529 296
9	8	Inwards hexagon skrew with counter sunk	ISO 10642 - M6 x 12
10	1	Bench	12-0026-3-6 - 0_5
11	18	Angle bracket: 30x30	Bosch Rexroth: 3 842 523 528
12	4	Hinged foot	Bosch Rexroth: 3 842 502 257
13	1	Floor	12-0026-3-6 - 0_4

Table A 9: In-situ parameter (corrected EH values; redox conditions: if  $EH \leq 0$  mV then reducing, if  $0 < EH < 400$  mV then partially reducing, if  $EH \geq 400$  mV then oxidising) and on-site photometry (evaluated by Heiland 2016). Calc. = calculated from  $Ag_2S$  precipitation yields (evaluated in this thesis).

Sample ID	Date	pH	EC	DO	T	Turbidity	$E_H$	Redox conditions	$NH_4^+$	* $NH_4^+$	** $Fe_{total}$	** $Fe^{2+}$	$NO_2^-$	$PO_4$	$HS^-/H_2S/S^{2-}$	$HS^-/H_2S/S^{2-}$ calc.
			$\mu S/cm$	mg/L	$^{\circ}C$	NTU	mV		mg/L	mg/L	mg/L	mg/L	mg/L	mg/L	mg/L	mg/L
									$\pm 0.02$	$\pm 0.02$	$\pm 0.017$	$\pm 0.017$	$\pm 0.001$	$\pm 0.05$	$\pm 0.02$	
DC-W-1	15.09.2011	7.3	1583	4.2	22.8	1	109	partially reducing	0.09		0.09	0.25	0.02	0.11	0.06	0.32
DC-W-2	15.09.2011	7.0	1730	2.3	26.0	106	-76	reducing	2.40		< 0.03	0.06	0.03	1.86	0.12	
DC-W-3	15.09.2011	3.3	2840	0.8	21.4	38	-84	reducing	1.56	3.10	7.12	6.76	0.01	1.78	3.36	3.02
DC-W-4	19.09.2011	1.6	13340	0.7	21.6	18	263	partially reducing	0.02	4.80	15.04	9.88	0.03	4.60	3.92	4.04
DC-W-5	15.09.2011	7.7	1710	2.8	25.3	26	1	partially reducing	0.12		< 0.03	0.17	0.02	0.52	6.32	4.53
DC-W-6	22.09.2011	1.0	42700	2.9	21.4	57	249	partially reducing	0.29	56.00	n.d.	0.04	0.03	6.68	0.05	10.09
DC-W-7	19.09.2011	6.6	1725	0.5	26.2	56	-132	reducing	0.70		n.d.	0.09	0.03	2.30	0.07	4.79
DC-W-8	19.09.2011	6.8	1740	1.8	26.1	36	-79	reducing	0.74		n.d.	0.06	0.02	2.07	0.11	
DC-W-9	27.09.2011	7.3	1589	3.1	23.0	5	239	partially reducing	0.11		n.d.	< 0.03	0.01	0.18	< 0.01	
DC-W-10	27.09.2011	8.0	1707	3.3	25.3	255	7	partially reducing	0.47		n.d.	0.04	0.02	1.20	4.32	5.56
DC-W-11	27.09.2011	8.1	1702	2.9	24.9	379	24	partially reducing	< 0.02		n.d.	0.05	< 0.005	1.46	1.30	
DR-W-1	29.09.2011	7.5	1395	2.7	24.0	128	150	partially reducing	< 0.02		n.d.	< 0.03	< 0.005	0.11	0.09	0.22
DR-W-2	29.09.2011	7.2	850	0.9	22.1	107	-51	reducing	0.64		n.d.	< 0.03	0.02	1.96	7.84	10.48
DR-W-3	29.09.2011	7.4	892	0.5	22.8	67	-32	reducing	0.57		n.d.	< 0.03	0.04	1.29	6.40	
DR-W-6	06.10.2011	7.7	931	0.4	21.6	123	-73	reducing	0.67		n.d.	< 0.03	0.01	1.35	4.24	
DR-W-7	12.10.2011	7.9	2092	8.0	17.3	2	313	partially reducing	0.30		n.d.	0.17	0.03	3.48	< 0.01	
DR-W-8	06.10.2011	7.3	1656	1.4	25.2	15	1	partially reducing	0.27		n.d.	0.11	0.01	0.07	0.02	0.69
DR-W-9	06.10.2011	7.7	981	1.4	21.0	95	-16	reducing	0.24		n.d.	< 0.03	0.01	0.46	5.12	
DW-W-1	06.10.2011	6.8	1605	1.6	26.6	39	-107	reducing	1.32		n.d.	0.17	< 0.005	3.60	49.92	11.90

n.d. – not determined; \*\*calculation:  $\text{conc.}(S_2O_3^{2-} \text{cyanolysed}(+ \text{KCN stabilisation})) - \text{conc.}(S_2O_3^{2-} \text{uncyanolysed})$ ; \*repeated measurement also showed wrong results:  $\text{SnO}_6^{2-} = -0.062 \text{ mg/L}$  ( $0.006 - 0.068 = -0.062$ )

Table A 10: Cations and anions of water samples analysed with ion chromatography (laboratories of the chair for hydrogeology, TU Freiberg; data evaluated by Heiland 2016)

Sample ID	Li <sup>+</sup>	Na <sup>+</sup>	NH <sub>4</sub> <sup>+</sup>	K <sup>+</sup>	Mn <sup>2+</sup>	Ca <sup>2+</sup>	Mg <sup>2+</sup>	F <sup>-</sup>	Cl <sup>-</sup>	Br <sup>-</sup>	NO <sub>3</sub> <sup>-</sup>	PO <sub>4</sub>	SO <sub>4</sub> <sup>2-</sup>	SO <sub>3</sub> <sup>2-</sup>	S <sub>2</sub> O <sub>3</sub> <sup>2-</sup>	**S <sub>n</sub> O <sub>6</sub> <sup>2-</sup>	[SCN] <sup>-</sup>
	mg/L	mg/L	mg/L	mg/L	mg/L	mg/L	mg/L	mg/L	mg/L	mg/L	mg/L	mg/L	mg/L	mg/L	mg/L	mg/L	mg/L
DC-W-1	0.009	11.91		1.88		276	62.7	0.81	11.41	0.068	0.197	0.024	797	0.014	0.021	0.062	0.00
DC-W-2	0.013	13.80		1.79		302	74.4	1.10	15.69	0.066	0.056	0.019	889	0.010	0.145	0.096	0.00
DC-W-3	0.017	12.63	2.79	3.72	0.160	533	81.1	1.32	12.37	0.075	0.203	0.321	1783	0.000	0.162	0.147	0.00
DC-W-4	0.044	16.31	5.57	11.60	0.550	551	94.6	1.32	16.53	0.029	0.037	4.001	4840	0.015	0.070	-0.056	0.00
DC-W-5	0.013	14.02		1.75		278	74.3	0.98	15.48	0.084	0.025	0.027	863	0.008	1.171	0.850	0.00
DC-W-6	0.058	29.44	63.71	33.47	0.810	593	122.6	1.15	28.22	0.000	0.000	6.011	13210	0.059	0.060	0.019	0.00
DC-W-7	0.011	14.20	0.07	1.88		299	74.6	1.03	16.11	0.075	0.047	0.018	828	0.008	0.050	0.075	0.00
DC-W-8	0.011	14.07		1.85		301	76.3	1.09	15.94	0.082	0.048	0.015	888	0.000	0.071	0.085	0.00
DC-W-9	0.007	10.80		1.55		292	64.1	0.88	11.52	0.060	0.226	0.013	790	0.009	0.006	0.002	0.00
DC-W-10	0.015	14.18		1.91		306	70.7	1.06	15.76	0.061	0.080	0.014	855	0.000	1.719	0.710	0.00
DC-W-11	0.012	14.08		1.68		306	74.3	1.09	15.83	0.069	0.084	0.014	830	0.008	3.036	0.703	0.00
DR-W-1	0.007	10.50		1.42		240	62.9	1.06	10.95	0.062	0.090	0.009	627	0.012	n.d.	n.d.	0.00
DR-W-2	0.005	8.79		1.01		127	37.5	0.63	10.02	0.057	0.053	0.002	264	0.030	n.d.	n.d.	0.00
DR-W-3	0.008	9.05		0.97		132	39.1	0.66	10.39	0.051	0.033	0.003	285	0.000	n.d.	n.d.	0.00
DR-W-6	0.007	10.17		1.19		141	41.3	0.67	11.76	0.048	0.160	0.003	289	0.000	n.d.	n.d.	0.00
DR-W-7	0.019	136.53		2.05		297	38.3	0.19	230.42	0.282	0.141	0.011	657	0.000	n.d.	n.d.	0.00
DR-W-8	0.008	14.11	0.04	1.88		311	75.8	1.07	15.70	0.074	0.134	0.015	868	0.005	n.d.	n.d.	0.00
DR-W-9	0.007	10.89		1.18		150	42.3	0.69	13.12	0.059	0.074	0.001	317	0.309	n.d.	n.d.	0.00
DW-W-1	0.011	11.19	0.05	2.10		266	81.0	1.48	11.52	0.064	0.095	0.007	717	0.396	n.d.	n.d.	0.00

n.d. – not determined; \*\*calculation:  $\text{conc.}(\text{S}_2\text{O}_3^{2-} \text{cyanolysed} (+ \text{KCN stabilisation})) - \text{conc.}(\text{S}_2\text{O}_3^{2-} \text{uncyanolysed})$ ; \*repeated measurement also showed wrong results:  $\text{SnO}_6^{2-} = -0.062 \text{ mg/L}$  ( $0.006 - 0.068 = -0.062$ )

Table A 11: ICP-MS results of water samples, in alphabetical order (laboratories of the chair for hydrogeology, TU Freiberg; data evaluated by Heiland, 2016)

Element		Ag	Al	As	B	Ba	Be	Bi	Br	Ca	Cd	Ce	Co	Cr	Cs	Cu	Dy
Mode		2V		2V							2V		2V	2V		2V	
Unit		µg/L	mg/L	µg/L	µg/L	µg/L	µg/L	µg/L	µg/L	mg/L	µg/L	µg/L	µg/L	µg/L	µg/L	µg/L	µg/L
<b>Detection limit</b>	1:1	0.005	0.001	0.200	1.0	0.1	0.01	0.002	2.0	0.0	0.01	0.001	0.01	0.1	0.001	1.0	0.001
<b>Detection limit</b>	1:5	0.025	0.005	1.000	5.0	0.3	0.05	0.010	10.0	0.1	0.05	0.005	0.05	0.5	0.005	5.0	0.005
<b>Detection limit</b>	1:10	0.050	0.010	2.000	10.0	0.5	0.10	0.020	20.0	0.2	0.10	0.010	0.10	1.0	0.010	10.0	0.010
DC-W-1	1:1	0.005	0.01	0.536	70.1	27.7	< 0.01	0.034	67.2	309.8	0.09	4.60	0.16	< 0.1	0.034	< 1.0	0.008
DC-W-2	1:1	< 0.005	0.01	< 0.200	86.5	24.3	< 0.01	0.016	86.3	319.9	< 0.01	0.59	0.02	< 0.1	0.041	< 1.0	0.007
DC-W-3	1:1	< 0.005	5.53	0.605	72.7	30.3	0.19	0.010	74.6	533.8	0.07	8.20	1.49	14.6	0.172	< 1.0	0.653
DC-W-4	1:5	< 0.025	40.01	1.594	118.3	31.8	1.09	0.027	99.5	564.7	0.55	31.63	11.58	120.4	1.281	< 5.0	2.883
DC-W-5	1:1	< 0.005	0.14	< 0.200	85.3	23.1	< 0.01	0.004	84.7	316.7	< 0.01	2.34	0.06	0.3	0.035	< 1.0	0.015
DC-W-6	1:10	< 0.050	32.61	3.113	177.7	30.1	1.05	0.038	160.0	576.1	1.22	11.83	11.56	98.2	3.491	10.7	1.700
DC-W-7	1:1	< 0.005	0.00	< 0.200	91.3	22.9	< 0.01	0.002	81.6	315.4	< 0.01	0.04	0.02	< 0.1	0.034	< 1.0	0.006
DC-W-8	1:1	< 0.005	0.01	< 0.200	93.3	23.2	< 0.01	0.001	82.0	322.4	< 0.01	0.05	0.02	< 0.1	0.033	< 1.0	0.007
DC-W-9	1:1	< 0.005	0.01	0.564	73.7	25.9	< 0.01	< 0.002	64.3	300.6	0.01	0.03	0.15	< 0.1	0.013	< 1.0	0.005
DC-W-10	1:1	< 0.005	0.03	< 0.200	91.5	23.5	< 0.01	< 0.002	85.3	321.7	< 0.01	0.08	0.04	< 0.1	0.026	< 1.0	0.008
DC-W-11	1:1	< 0.005	0.04	< 0.200	88.4	23.2	< 0.01	< 0.002	82.3	314.1	< 0.01	0.06	0.05	0.1	0.030	< 1.0	0.008
DR-W-1	1:1	< 0.005	0.13	0.661	71.0	32.0	< 0.01	< 0.002	67.4	238.7	< 0.01	0.13	0.06	< 0.1	0.030	< 1.0	0.012
DR-W-2	1:1	< 0.005	0.03	< 0.200	48.5	48.8	< 0.01	< 0.002	55.9	127.5	< 0.01	0.03	0.02	< 0.1	0.009	< 1.0	0.003
DR-W-3	1:1	< 0.005	0.03	< 0.200	49.6	46.8	< 0.01	< 0.002	57.6	132.2	< 0.01	0.03	0.03	< 0.1	0.009	< 1.0	0.003
DR-W-6	1:1	< 0.005	0.03	< 0.200	51.5	45.4	< 0.01	< 0.002	59.4	139.6	< 0.01	0.03	0.01	< 0.1	0.009	< 1.0	0.003
DR-W-7	1:1	< 0.005	0.01	0.790	116.3	49.2	< 0.01	< 0.002	325.4	308.2	< 0.01	0.01	0.08	< 0.1	0.007	< 1.0	0.001
DR-W-8	1:1	< 0.005	0.04	0.534	90.5	29.7	< 0.01	< 0.002	84.0	320.4	< 0.01	0.21	0.15	0.1	0.009	< 1.0	0.019
DR-W-9	1:1	0.043	0.03	0.227	53.8	44.8	< 0.01	0.006	62.1	146.5	< 0.01	0.02	0.02	< 0.1	0.008	< 1.0	0.002
DW-W-1	1:1	< 0.005	0.00	< 0.200	76.3	20.9	< 0.01	< 0.002	66.9	274.1	< 0.01	0.02	0.02	0.2	0.001	< 1.0	0.001

Table A 12: ICP-MS (continuation I)

Element		Er	Eu	Fe	Ga	Gd	Ho	I	In	K	La	Li	Lu	Mg	Mn	Mo	Nd
Mode		3V					2V					2V	2V				
Unit		µg/L	µg/L	mg/L	µg/L	µg/L	µg/L	µg/L	µg/L	mg/L	µg/L	µg/L	µg/L	mg/L	µg/L	µg/L	µg/L
<b>Detection limit</b>	1:1	0.001	0.001	0.001	0.010	0.001	0.001	0.05	0.001	0.02	0.001	0.10	0.001	0.001	0.05	0.01	0.001
<b>Detection limit</b>	1:5	0.005	0.005	0.005	0.050	0.005	0.005	0.25	0.005	0.10	0.005	0.50	0.005	0.005	0.25	0.05	0.005
<b>Detection limit</b>	1:10	0.010	0.010	0.010	0.100	0.010	0.010	0.50	0.010	0.20	0.010	1.00	0.010	0.010	0.50	0.10	0.010
DC-W-1	1:1	0.005	0.009	0.03	0.048	0.036	0.002	9.20	0.022	3.04	10.250	8.61	0.001	61.0	19.4	12.25	0.040
DC-W-2	1:1	0.004	0.008	0.01	0.028	0.012	0.002	9.36	0.008	6.38	1.232	9.71	< 0.001	72.7	9.7	0.26	0.035
DC-W-3	1:1	0.349	0.217	7.41	0.216	0.970	0.131	8.65	0.007	6.18	5.424	11.84	0.034	67.3	109.0	3.33	3.995
DC-W-4	1:5	1.548	0.947	43.14	8.835	3.954	0.565	15.02	0.024	15.85	18.990	39.63	0.187	85.1	555.3	0.94	16.210
DC-W-5	1:1	0.008	0.011	0.16	0.042	0.033	0.003	9.08	0.003	24.43	4.746	9.71	0.001	70.4	12.2	0.37	0.091
DC-W-6	1:10	1.078	0.389	33.40	7.390	1.863	0.364	18.40	0.038	32.18	6.522	48.34	0.150	108.1	609.7	1.07	5.881
DC-W-7	1:1	0.003	0.008	0.01	0.021	0.006	0.001	9.59	< 0.001	1.99	0.024	10.02	< 0.001	73.3	9.4	0.65	0.022
DC-W-8	1:1	0.004	0.009	0.01	0.020	0.009	0.001	9.61	< 0.001	1.98	0.027	10.36	< 0.001	75.0	9.6	0.59	0.027
DC-W-9	1:1	0.003	0.009	0.02	0.024	0.006	0.001	7.62	< 0.001	1.74	0.020	8.80	< 0.001	61.0	19.3	11.32	0.019
DC-W-10	1:1	0.005	0.009	0.03	0.024	0.010	0.002	9.74	< 0.001	1.98	0.039	10.29	0.001	74.3	12.4	0.82	0.037
DC-W-11	1:1	0.005	0.009	0.03	0.026	0.009	0.002	9.63	< 0.001	2.14	0.035	9.84	< 0.001	72.3	21.6	1.11	0.035
DR-W-1	1:1	0.007	0.013	0.09	0.072	0.019	0.002	8.08	0.001	1.47	0.076	7.84	0.001	60.8	13.7	5.64	0.068
DR-W-2	1:1	0.002	0.014	0.01	0.026	0.005	0.001	7.40	< 0.001	1.00	0.018	5.77	< 0.001	35.8	4.2	0.28	0.018
DR-W-3	1:1	0.002	0.014	0.02	0.025	0.005	0.001	7.36	< 0.001	1.07	0.015	5.86	< 0.001	36.3	5.6	0.35	0.014
DR-W-6	1:1	0.002	0.014	0.02	0.028	0.005	0.001	7.37	< 0.001	1.00	0.015	6.06	< 0.001	38.2	5.8	0.61	0.016
DR-W-7	1:1	0.001	0.015	0.01	< 0.010	0.003	< 0.001	3.34	0.001	2.26	0.004	18.38	< 0.001	35.7	5.4	1.61	0.007
DR-W-8	1:1	0.010	0.015	0.15	0.020	0.028	0.004	10.08	< 0.001	2.11	0.106	10.06	0.001	74.2	31.4	3.86	0.107
DR-W-9	1:1	0.001	0.014	0.02	0.028	0.003	0.001	7.53	< 0.001	1.08	0.008	6.33	< 0.001	39.7	6.5	0.60	0.009
DW-W-1	1:1	0.001	0.006	0.27	0.012	0.001	< 0.001	7.76	< 0.001	2.03	0.005	9.29	< 0.001	80.4	51.4	0.07	0.007

Table A 13: ICP-MS results (continuation II)

Element		Ni	P	Pb	Pr	Rb	S	Sb	Sc	Se	Si	Sm	Sn	Sr	Tb	Te
Mode		2V	2V				2V		2V	1V	2V					
Unit		µg/L	µg/L	µg/L	µg/L	µg/L	mg/L	µg/L	µg/L	µg/L	mg/L	µg/L	µg/L	mg/L	µg/L	µg/L
<b>Detection limit</b>	1:1	0.10	10.00	0.01	0.001	0.005	0.5	0.010	0.10	0.5	0.10	0.001	0.05	0.00002	0.001	0.010
<b>Detection limit</b>	1:5	0.50	50.00	0.05	0.005	0.025	2.5	0.050	0.50	2.5	0.50	0.005	0.25	0.00010	0.005	0.050
<b>Detection limit</b>	1:10	1.00	100.00	0.10	0.010	0.050	5.0	0.100	1.00	5.0	1.00	0.010	0.50	0.00020	0.010	0.100
DC-W-1	1:1	1.65	28.96	0.49	0.010	1.81	304.7	0.217	0.22	< 0.5	8.34	0.009	< 0.05	4.33	0.002	< 0.010
DC-W-2	1:1	0.24	17.30	< 0.01	0.008	2.01	351.2	< 0.010	0.25	< 0.5	8.58	0.009	< 0.05	5.20	0.001	< 0.010
DC-W-3	1:1	25.18	347.10	0.27	0.973	5.51	610.3	0.095	0.47	< 0.5	14.80	0.873	0.11	4.64	0.121	< 0.010
DC-W-4	1:5	101.30	2489.00	6.07	3.919	40.40	1468.0	0.832	1.42	< 2.5	59.01	3.841	< 0.25	4.39	0.534	< 0.050
DC-W-5	1:1	0.76	39.29	0.02	0.022	2.35	333.9	< 0.010	0.26	< 0.5	9.07	0.019	< 0.05	4.82	0.003	< 0.010
DC-W-6	1:10	107.70	5393.00	5.79	1.462	61.23	3805.0	0.539	2.68	< 5.0	50.43	1.428	< 0.50	4.22	0.292	< 0.100
DC-W-7	1:1	0.21	24.67	< 0.01	0.005	1.84	437.9	< 0.010	0.27	< 0.5	9.14	0.005	< 0.05	4.94	0.001	< 0.010
DC-W-8	1:1	0.22	17.28	< 0.01	0.006	1.88	436.4	< 0.010	0.28	< 0.5	9.33	0.006	< 0.05	5.06	0.001	< 0.010
DC-W-9	1:1	1.49	16.78	< 0.01	0.004	1.72	313.4	0.367	0.23	< 0.5	8.97	0.005	< 0.05	4.09	0.001	< 0.010
DC-W-10	1:1	0.38	21.02	< 0.01	0.008	1.88	340.4	< 0.010	0.29	< 0.5	9.47	0.008	< 0.05	4.99	0.001	< 0.010
DC-W-11	1:1	0.74	23.25	< 0.01	0.008	1.94	330.8	0.134	0.26	< 0.5	9.31	0.008	< 0.05	4.84	0.001	< 0.010
DR-W-1	1:1	0.37	23.40	< 0.01	0.016	1.47	249.3	0.049	0.26	< 0.5	8.66	0.016	< 0.05	3.72	0.002	< 0.010
DR-W-2	1:1	0.15	< 10.00	< 0.01	0.004	0.75	242.8	0.011	0.15	< 0.5	6.81	0.004	< 0.05	2.69	0.001	< 0.010
DR-W-3	1:1	0.24	14.64	< 0.01	0.003	0.80	169.3	0.059	0.15	< 0.5	6.82	0.004	< 0.05	2.72	< 0.001	< 0.010
DR-W-6	1:1	0.10	13.62	< 0.01	0.003	0.80	129.5	< 0.010	0.16	< 0.5	6.99	0.004	< 0.05	2.79	< 0.001	< 0.010
DR-W-7	1:1	0.69	21.34	< 0.01	0.001	0.56	266.8	0.797	0.29	< 0.5	9.95	0.002	< 0.05	4.37	< 0.001	0.019
DR-W-8	1:1	0.51	33.07	< 0.01	0.024	1.71	355.5	0.305	0.30	< 0.5	10.00	0.024	< 0.05	4.88	0.003	< 0.010
DR-W-9	1:1	0.15	14.61	< 0.01	0.002	0.85	142.6	< 0.010	0.15	< 0.5	7.24	0.002	< 0.05	2.90	< 0.001	< 0.010
DW-W-1	1:1	0.16	22.87	< 0.01	0.001	1.77	473.1	< 0.010	0.25	< 0.5	11.34	0.002	< 0.05	4.56	< 0.001	< 0.010

Table A 14: ICP-MS results (continuation III)

Element		Th	Tl	Tm	U	V	Y	Yb	Zn
Mode		2V							
Unit		µg/L	µg/L	µg/L	µg/L	µg/L	µg/L	µg/L	µg/L
<b>Detection limit</b>	1:1	0.001	0.001	0.001	0.001	0.10	0.001	0.001	1.00
<b>Detection limit</b>	1:5	0.005	0.005	0.005	0.005	0.50	0.005	0.005	5.00
<b>Detection limit</b>	1:10	0.010	0.010	0.010	0.010	1.00	0.010	0.010	10.00
DC-W-1	1:1	0.001	0.196	0.001	4.841	1.65	0.11	0.004	22.72
DC-W-2	1:1	< 0.001	0.041	< 0.001	1.908	0.65	0.10	0.003	22.50
DC-W-3	1:1	0.014	0.081	0.041	3.088	7.42	4.61	0.241	68.56
DC-W-4	1:5	0.251	0.112	0.199	1.188	63.60	16.03	1.285	173.90
DC-W-5	1:1	0.001	0.076	0.001	2.110	0.93	0.14	0.006	17.91
DC-W-6	1:10	0.700	0.129	0.149	1.117	83.42	11.82	0.969	292.70
DC-W-7	1:1	< 0.001	0.002	< 0.001	1.821	0.61	0.09	0.003	48.80
DC-W-8	1:1	< 0.001	0.002	0.001	1.873	0.72	0.10	0.003	44.56
DC-W-9	1:1	< 0.001	0.004	< 0.001	4.660	1.51	0.08	0.003	81.91
DC-W-10	1:1	< 0.001	0.002	< 0.001	2.082	0.92	0.10	0.004	27.69
DC-W-11	1:1	0.001	0.002	0.001	1.962	1.02	0.09	0.003	17.62
DR-W-1	1:1	0.002	0.002	0.001	1.379	0.90	0.11	0.005	48.44
DR-W-2	1:1	< 0.001	< 0.001	< 0.001	0.514	0.60	0.04	0.002	27.95
DR-W-3	1:1	< 0.001	< 0.001	< 0.001	0.552	0.56	0.04	0.001	21.59
DR-W-6	1:1	< 0.001	< 0.001	< 0.001	0.610	0.51	0.04	0.001	19.26
DR-W-7	1:1	< 0.001	0.003	< 0.001	0.868	1.54	0.03	0.001	137.10
DR-W-8	1:1	0.004	0.002	0.001	1.801	0.73	0.17	0.008	31.22
DR-W-9	1:1	< 0.001	0.001	< 0.001	0.643	0.50	0.03	0.001	16.99
DW-W-1	1:1	< 0.001	< 0.001	< 0.001	0.261	< 0.1	0.03	< 0.001	58.98

Table A 15: Semi-quantitative analysis of minerals in cave sediments. Grey values: When grouped together, Illite, Muscovite and Smectite represent the dioctahedral silicate minerals. The sum of their percentages is a reliable value for the group. However, the percentages of the individual minerals may depart from the listed value. To stress this extra uncertainty, affected data are given in grey.

	DC-S-1		DC-S-2		DC-S-3		DC-S-5		DC-S-9	
	wt%	± wt%								
Actinolite	-	-	-	-	-	-	1.75	0.39	1.04	0.39
Anatase	0.82	0.13	-	-	-	-	-	-	-	-
Anhydrite	-	-	-	-	16.94	0.51	-	-	-	-
Ankerite Fe <sub>0.54</sub>	-	-	-	-	-	-	1.31	0.33	-	-
Bassanite	-	-	-	-	11.21	0.39	-	-	-	-
Calcite	12.08	0.39	6.49	0.84	-	-	19.35	0.48	15.93	0.42
Chlorite Ib-2	4.81	0.87	-	-	-	-	2.84	0.57	3.89	0.72
Dolomite	-	-	0.89	0.25	-	-	-	-	-	-
Gypsum	4.64	0.36	-	-	60.39	0.66	3.56	0.30	3.44	0.36
Illite 1 Mt	-	-	5.38	1.11	-	-	5.89	0.99	5.37	0.87
Kaolinite	6.98	1.50	5.19	1.20	-	-	3.43	1.05	4.78	0.99
Microcline, maximum	-	-	4.07	0.66	-	-	3.66	0.51	3.88	0.45
Muscovite 2M1	12.25	0.84	7.1	0.93	-	-	6.64	0.69	9.55	0.75
Orthoclase	1.34	0.39	-	-	-	-	-	-	-	-
Plagioclase Albite	5.31	0.39	5.81	0.48	-	-	5.68	0.39	5.44	0.39
Pyrite	1.8	0.15	2.12	0.30	-	-	1.54	0.13	0.85	0.13
Quartz	25.56	0.75	25.1	3.30	7.41	0.54	25.64	0.69	17.37	17.37
Smectite 2wCa	24.42	2.28	15.14	2.22	-	-	12.25	1.80	27.75	1.68
Sulphur alpha	-	-	21.94	2.37	4.05	0.39	6.22	0.42	-	-
Vermiculite 2M Bailey	-	-	0.75	0.36	-	-	0.24	0.20	0.71	0.45

Table A 16: XRF results of rock samples (laboratories of the chair for hydrogeology, TU Freiberg)

Sample ID	Ca	S	Mg	Si	Fe	Ag	Al	As	Ba	Bi	Br	Cd	Ce	Cl	Co	Cr	Cs
	g/kg	g/kg	g/kg	g/kg	g/kg	g/kg	g/kg	g/kg	g/kg	g/kg	g/kg	g/kg	g/kg	g/kg	g/kg	g/kg	g/kg
DS-PL-1	393	0.069	1.182	0.5281	0.0795	0.0155	<0.02	<0.0005	<0.002	<0.001	0.0014	<0.002	<0.002	0.0247	<0.003	<0.001	<0.004
DS-PL-3	359.9	0.8164	6.414	22.29	4.111	0.00018	6.902	0.0034	0.1285	<0.001	0.0016	<0.002	0.113	0.1215	<0.003	<0.001	<0.004
DS-PG-2b	292.8	209.3	19.18	2.806	0.5171	<0.002	<0.02	<0.0003	<0.002	<0.001	0.0012	<0.002	<0.002	0.2191	<0.003	<0.001	<0.004
DS-PG-4	247.1	178.2	17.47	3.913	0.7975	0.0085	<0.02	<0.0005	0.0403	<0.001	0.0005	<0.002	<0.002	0.2436	<0.003	<0.001	<0.004
DS-PL-5	368.5	0.5715	7.101	12.88	1.118	<0.002	3.14	<0.0004	0.2865	<0.001	0.0217	<0.002	<0.002	0.1003	<0.003	<0.001	<0.004
DC-SG-1	242.7	180.8	18.98	1.638	<0.001	<0.002	<0.02	<0.0005	0.0339	<0.001	0.0012	<0.002	<0.002	0.2177	<0.003	<0.001	<0.004
DC-SG-9a	239.6	178.6	18.06	2.768	<0.001	<0.0029	<0.02	<0.0005	0.0398	<0.001	0.0009	<0.002	<0.002	0.2435	<0.003	<0.001	<0.004
DC-SG-9c	293.6	212.8	17.59	5.134	<0.001	0.0106	<0.02	<0.0005	0.0245	<0.001	0.0009	<0.002	<0.002	0.2154	<0.003	<0.001	<0.004
DC-SG-9b	283.4	219.3	19.05	1.962	0.0031	0.0088	<0.02	<0.0005	<0.002	<0.001	0.0013	<0.002	<0.002	0.1724	<0.003	<0.001	<0.004
DC-SG-9e	295.3	220.2	19.76	3.234	<0.001	0.0071	<0.02	<0.0005	0.0452	<0.001	0.0013	<0.002	<0.002	0.144	<0.003	<0.001	<0.004
DC-SG-14b	242.6	176.2	16.25	2.472	<0.001	<0.002	<0.02	<0.0005	0.0476	<0.001	0.0011	<0.002	<0.002	0.1699	<0.003	<0.001	<0.004
DC-SG-14c	240.5	180.8	18.44	2.182	<0.001	0.0146	<0.02	<0.0005	0.0343	<0.001	0.001	<0.002	<0.002	0.1676	<0.003	<0.001	<0.004
DC-SG-13a	121.4	154.4	7.35	245.6	0.3234	<0.002	<0.02	<0.0005	0.4716	<0.001	0.001	<0.002	<0.002	0.1341	<0.003	0.2078	<0.004
DC-SG-13b	213.2	178.1	11.97	120.2	0.1764	<0.002	<0.02	<0.0005	0.1767	<0.001	0.0011	<0.002	<0.002	0.141	<0.003	0.0991	<0.004
DC-SG-13c	288.7	209.8	16.91	25.16	0.9004	0.0095	<0.02	<0.0005	0.0449	<0.001	0.0008	<0.002	<0.002	0.1459	<0.003	<0.001	<0.004
DC-SG-15	244.5	182.7	18.02	4.796	<0.001	0.0056	<0.02	<0.0005	<0.002	<0.001	0.0011	<0.002	<0.002	0.2219	<0.003	<0.001	<0.004
DC-PL-15	393.1	1.765	1.341	1.476	0.4318	0.0038	0.3404	<0.0005	0.0368	<0.001	0.0009	<0.002	<0.002	0.0235	<0.003	<0.001	<0.004
DC-PL-16	389.2	4.967	1.535	2.196	8.361	<0.002	0.756	0.0035	<0.002	<0.001	0.0013	<0.002	<0.002	0.0539	<0.003	0.0053	<0.004

Table A 17: XRF results of rock samples (continuation I)

Sample ID	Cu	Ga	Ge	Hf	Hg	I	K	La	Mn	Mo	Nb	Ni	P	Pb	Rb	Sb
	g/kg	g/kg	g/kg	g/kg	g/kg	g/kg	g/kg	g/kg	g/kg	g/kg	g/kg	g/kg	g/kg	g/kg	g/kg	g/kg
DS-PL-1	<0.0004	0.0024	<0.0005	<0.001	<0.001	0.0102	<0.01	0.0263	0.0395	0.0134	<0.001	<0.0005	<0.003	0.0034	0.001	0.0115
DS-PL-3	0.0054	0.0035	<0.0005	<0.001	<0.001	0.0162	1.99	0.0618	0.1565	0.0107	<0.001	<0.0005	0.0687	0.0039	0.0094	0.0121
DS-PG-2b	<0.0011	<0.0005	<0.0005	<0.0016	<0.001	0.0231	0.63	<0.002	0.0068	0.0107	<0.001	0.0065	<0.03	0.0045	0.0024	0.0177
DS-PG-4	<0.0001	0.0011	<0.0005	<0.001	<0.001	<0.003	0.902	<0.002	0.0108	0.0113	<0.001	0.0025	<0.03	0.0019	0.0021	0.0112
DS-PL-5	0.0025	0.0017	<0.0005	<0.001	<0.001	0.0161	0.783	0.0965	0.2152	0.0113	<0.001	<0.0005	0.0984	0.0027	0.0037	0.0153
DC-SG-1	<0.0005	0.0011	<0.0003	<0.001	<0.001	0.0113	0.407	<0.002	<0.001	0.0125	<0.001	0.0026	<0.03	0.0016	0.001	0.0062
DC-SG-9a	<0.0005	0.0012	<0.0005	<0.001	<0.001	0.0133	0.557	<0.002	<0.001	0.0092	<0.001	0.0028	<0.03	0.001	0.0009	0.0139
DC-SG-9c	<0.0005	<0.0005	<0.0005	<0.001	<0.0006	0.0228	0.303	<0.002	<0.0005	0.0123	<0.001	0.0027	<0.03	0.0032	0.0014	0.0165
DC-SG-9b	<0.0005	<0.0005	<0.0005	<0.0015	<0.001	0.0188	0.506	<0.002	<0.001	0.0117	<0.001	0.0043	<0.03	0.0035	0.0016	0.0158
DC-SG-9e	<0.0009	0.0021	<0.0005	<0.001	<0.001	0.0218	0.524	<0.002	<0.0015	0.0119	<0.001	0.0028	<0.03	0.0035	0.0012	0.0193
DC-SG-14b	<0.0002	0.0013	<0.0005	<0.001	<0.001	0.0131	0.51	<0.002	<0.0015	0.0141	<0.001	0.0036	<0.03	0.003	0.0011	0.0125
DC-SG-14c	<0.0005	<0.0005	<0.0005	<0.0013	<0.001	0.0103	0.552	<0.002	<0.001	0.0144	<0.001	0.004	<0.03	0.0021	0.0008	0.0049
DC-SG-13a	0.0025	0.0016	<0.0005	0.0059	<0.001	0.0032	0.263	<0.002	0.0134	0.0088	0.0096	0.0125	<0.03	0.0126	0.0014	0.0078
DC-SG-13b	<0.0013	0.0014	<0.0005	0.0012	<0.001	0.0137	0.372	0.0816	<0.001	0.0108	0.0025	0.0055	<0.03	0.0059	0.001	0.0139
DC-SG-13c	<0.0005	<0.0009	<0.0005	<0.001	<0.001	0.019	0.353	0.0592	0.0095	0.0116	<0.001	0.0033	<0.03	0.0027	0.0013	0.0147
DC-SG-15	<0.0005	0.0013	<0.0005	<0.001	<0.001	0.0179	0.39	<0.002	<0.0019	0.0135	<0.001	0.0015	<0.03	0.0024	0.001	0.011
DC-PL-15	<0.0012	0.0014	<0.0005	<0.001	<0.001	0.0186	<0.01	<0.002	0.0553	0.0119	<0.001	<0.0005	0.0272	0.0035	0.0013	0.0157
DC-PL-16	<0.0005	0.0014	<0.0005	<0.001	<0.001	0.0209	<0.01	<0.002	0.098	0.0466	<0.001	0.0319	0.0582	0.0027	0.0016	0.0162

Table A 18: XRF results of rock samples (continuation II)

Sample ID	Se	Sn	Sr	Ta	Te	Th	Ti	Tl	U	V	W	Y	Zn	Zr
	g/kg	g/kg	g/kg	g/kg	g/kg	g/kg	g/kg	g/kg	g/kg	g/kg	g/kg	g/kg	g/kg	g/kg
DS-PL-1	<0.0005	0.0075	0.1337	0.064	0.0086	0.0029	<0.002	<0.001	<0.001	<0.031	0.0012	0.001	0.007	<0.001
DS-PL-3	<0.0005	0.0087	0.3681	0.0609	0.0082	0.0017	0.474	<0.0004	<0.001	<0.018	0.0009	0.0028	0.0215	0.0103
DS-PG-2b	<0.0005	0.0168	1.005	0.0779	0.0164	0.0021	0.08	0.0016	<0.0007	<0.035	<0.0012	0.0016	0.0118	<0.001
DS-PG-4	<0.0005	0.0034	1.1	0.0722	0.0036	<0.0004	0.0555	0.0005	<0.001	<0.021	<0.001	0.0009	0.0075	<0.001
DS-PL-5	<0.0005	0.0143	0.7159	0.0654	0.0159	0.002	0.273	<0.0002	<0.001	0.0995	<0.001	0.0026	0.0098	<0.0103
DC-SG-1	<0.0005	0.006	0.0515	0.0622	0.0118	0.0033	<0.002	0.0009	<0.001	<0.023	<0.001	0.0008	0.0068	<0.001
DC-SG-9a	<0.0005	0.0089	0.0614	0.0634	0.0118	0.0031	<0.002	0.0008	<0.001	<0.021	0.0015	<0.0005	0.0066	<0.001
DC-SG-9c	<0.0005	0.0129	0.0714	0.0716	0.017	0.0034	<0.002	0.0015	<0.001	<0.027	0.0021	0.0009	0.008	<0.001
DC-SG-9b	<0.0005	0.012	0.1405	0.0714	0.015	0.0036	0.0251	0.0018	<0.001	<0.043	0.0025	0.0019	0.008	<0.001
DC-SG-9e	<0.0005	0.0173	0.0829	0.0648	0.0195	0.0033	0.0334	0.0016	<0.001	<0.030	<0.001	0.0011	0.0083	0.00003
DC-SG-14b	<0.0005	0.0093	0.0431	0.0628	0.0038	0.0027	0.0279	0.0013	<0.001	<0.020	0.0011	0.0008	0.0066	<0.001
DC-SG-14c	<0.0005	0.0042	0.0386	0.0656	0.007	0.0027	0.022	0.0012	<0.001	<0.022	0.0023	0.0009	0.0067	<0.0002
DC-SG-13a	<0.0005	0.0053	0.1093	0.0629	0.0063	0.0042	3.667	0.0011	0.0007	<0.0066	0.0036	0.0095	0.0089	0.2022
DC-SG-13b	<0.0005	0.0109	0.1019	0.0632	0.0098	0.0034	1.454	0.001	<0.001	<0.014	0.0012	0.0046	0.0103	0.0593
DC-SG-13c	<0.0005	0.0109	0.1173	0.0691	0.0099	0.0027	0.266	0.0008	<0.001	<0.024	<0.001	0.0025	0.0073	0.007
DC-SG-15	<0.0005	0.0029	0.3544	0.0703	0.0094	0.0025	<0.0035	0.0013	<0.001	<0.029	0.0011	0.0009	0.0067	<0.001
DC-PL-15	<0.0005	0.0145	0.1309	0.0667	0.0123	0.0025	<0.002	0.0011	<0.001	<0.024	0.001	0.0015	0.007	<0.001
DC-PL-16	0.0097	0.0125	0.1554	0.063	0.0173	0.0019	<0.018	<0.001	<0.001	<0.031	<0.0013	0.0018	0.0236	<0.001

Table A 19: Isotopic composition of H<sub>2</sub>O of water samples.

Sample ID	$\delta D$	Std.-dev.	$\delta^{18}O$	Std.-dev.
	‰ VSMOW		‰ VSMOW	
DC-W-1	<b>-28.52</b>	0.12	<b>-6.30</b>	0.03
DC-W-3	<b>-27.92</b>	0.10	<b>-6.13</b>	0.05
DC-W-4	<b>-25.59</b>	0.21	<b>-5.53</b>	0.04
DC-W-5	<b>-29.34</b>	0.18	<b>-5.95</b>	0.03
DC-W-6	<b>-24.77</b>	0.15	<b>-5.80</b>	0.03
DC-W-7	<b>-29.01</b>	0.16	<b>-6.27</b>	0.07
DC-W-8	<b>-30.15</b>	0.12	<b>-6.12</b>	0.03
DC-W-10	<b>-29.62</b>	0.13	<b>-6.00</b>	0.03
DR-W-1	<b>-29.61</b>	0.14	<b>-6.05</b>	0.03
DR-W-2	<b>-31.85</b>	0.09	<b>-6.62</b>	0.07
DR-W-8	<b>-28.04</b>	0.11	<b>-5.74</b>	0.03
DW-W-1	<b>-28.39</b>	0.10	<b>-5.85</b>	0.04

Table A 20: Sulphur Isotopic Composition of Dissolved Sulphide in Water Samples.

Sample ID	Sampling	Volume	Ag <sub>2</sub> S Precipitate	ID <sub>UFZ</sub>	$\delta^{34}S_{UFZ}$
		L	g		‰ ± 0.4 VCDT
DC-W-1	27.09.2011	10	0.025	5	<b>-20.7</b>
DC-W-3	27.09.2011	6	0.140	6	<b>-10.9</b>
DC-W-4	27.09.2011	6	0.188	7	<b>-12.8</b>
DC-W-5	24.09.2011	10	0.350	8	<b>-9.3</b>
DC-W-6	17.10.2011	10	0.780	9	<b>-14.1</b>
DC-W-7	24.09.2011	10	0.370	10	<b>-7.6</b>
DC-W-10	27.09.2011	10	0.430	11	<b>-10.1</b>
DR-W-1	29.09.2011	10	0.017	12	<b>-10.8</b>
DR-W-2	29.09.2011	10	0.810	13	<b>9.6</b>
DR-W-8	07.10.2011	10	0.053	14	<b>-8.3</b>
DW-W-1	06.10.2011	10	0.920	15	<b>-6.5</b>

Table A 21: Sulphur and Oxygen Isotopic Composition of Dissolved Sulphate in Water Samples.  $\delta^{34}S$  values were determined at the UFZ as well as the TUBAF. nm = not measured.

Sample ID	BaSO <sub>4</sub> Precipitate	ID <sub>UFZ</sub>	$\delta^{34}S_{UFZ}$	$\delta^{18}O_{UFZ}$	$\delta^{34}S_{TUBAF}$
	g		‰ ± 0.4 VCDT	‰ ± 0.6 VSMOW	‰ ± 0.3 VCDT
DC-W-1	nm	33	<b>17.1</b>	<b>9.5</b>	<b>18.0</b>
DC-W-3	nm	34	<b>4.9</b>	<b>3.0</b>	<b>5.2</b>
DC-W-4	nm	35	<b>-4.8</b>	<b>-1.6</b>	<b>-4.5</b>
DC-W-5	nm	36	<b>24.4</b>	<b>10.9</b>	<b>25.2</b>
DC-W-6	nm	37	<b>-9.1</b>	<b>-2.4</b>	<b>-8.0</b>
DC-W-7	nm	38	<b>25.3</b>	<b>11.7</b>	<b>26.3</b>
DC-W-10	nm	39	<b>23.6</b>	<b>11.1</b>	<b>25.2</b>
DR-W-1	nm	40	<b>25.3</b>	<b>11.7</b>	<b>26.4</b>
DR-W-2	nm	41	<b>32.6</b>	<b>14.5</b>	<b>34.1</b>
DR-W-8	nm	42	<b>21.8</b>	<b>10.6</b>	<b>22.5</b>
DW-W-1	nm	43	<b>24.9</b>	<b>11.1</b>	<b>26.1</b>

Table A 22: Sulphur and Oxygen Isotopic Analysis of Sedimentary Sulphur Species.

Sample ID	Sample Size	Extracted Species	Product	Mass of Product	ID <sub>UFZ</sub>	$\delta^{34}\text{S}_{\text{UFZ}}$	$\delta^{18}\text{O}_{\text{UFZ}}$
	g			mg		‰ $\pm$ 0.4* VCDT	‰ $\pm$ 0.6 VSMOW
DC-S-1	10	SO <sub>4</sub> <sup>2-</sup>	BaSO <sub>4</sub>	970	19	-11.9	1.4
DC-S-2	10	SO <sub>4</sub> <sup>2-</sup>	BaSO <sub>4</sub>	260	20	-6.8	2.6
DC-S-3	10	SO <sub>4</sub> <sup>2-</sup>	BaSO <sub>4</sub>	800	21	-10.3	-1.8
DC-S-5	10	SO <sub>4</sub> <sup>2-</sup>	BaSO <sub>4</sub>	703	22	4.12 $\pm$ 2.1	5.4
DC-S-9	10	SO <sub>4</sub> <sup>2-</sup>	BaSO <sub>4</sub>	160	23	-9.3	6.7
DC-S-2	10	S <sup>0</sup>	S <sup>0</sup>	273	62	-7.5	-
DC-S-3	10	S <sup>0</sup>	S <sup>0</sup>	381	63	-11.4	-
DC-S-5	10	S <sup>0</sup>	S <sup>0</sup>	274	64	-9.2	-
DC-S-1	10	FeS <sub>2</sub>	Ag <sub>2</sub> S	420	1	-22.9	-
DC-S-2	10	FeS <sub>2</sub>	Ag <sub>2</sub> S	436	2	-15.3	-
DC-S-5	10	FeS <sub>2</sub>	Ag <sub>2</sub> S	888	3	-11.8	-
DC-S-9	10	FeS <sub>2</sub>	Ag <sub>2</sub> S	92	4	-22.9 $\pm$ 2.2	-
DC-S-1	2	Total	BaSO <sub>4</sub>	306	24	-14.3	-
DC-S-2	2	Total	BaSO <sub>4</sub>	602	25	-8.3	-
DC-S-3	2	Total	BaSO <sub>4</sub>	782	26	-10.2	-
DC-S-5	2	Total	BaSO <sub>4</sub>	774	27	-7.78**	-
DC-S-9	2	Total	BaSO <sub>4</sub>	84	28	-13.9	-

\*If not stated otherwise. \*\*Value from one single measurement.

Table A 23: Sulphur and Sulphate Oxygen Isotopic Composition of Primary Gypsum, Secondary Gypsum, Elemental Sulphur, Carbonate Rock and Crude Oil. nm = not measured.

Sample Type	Sample ID	Sampling	Sample Size	Extracted Species	Product	Mass of Product	ID <sub>UFZ</sub>	$\delta^{34}\text{S}_{\text{UFZ}}$	$\delta^{18}\text{O}_{\text{UFZ}}$	$\delta^{34}\text{S}_{\text{TUBAF}}$
						g		‰ ± 0.4 VCDT	‰ ± 0.6 VSMOW	‰ ± 0.3 VCDT
Primary gypsum	DS-PG-2a	29.09.2011	143 mg	SO <sub>4</sub> <sup>2-</sup>	BaSO <sub>4</sub>	0.190	46	22.1	13.1	23.2
	DS-PG-2b	07.10.2011	135 mg	SO <sub>4</sub> <sup>2-</sup>	BaSO <sub>4</sub>	0.176	47	22.5	15.2	23.5
	DS-PG-4	07.10.2011	151 mg	SO <sub>4</sub> <sup>2-</sup>	BaSO <sub>4</sub>	0.195	48	22.0	12.6	23.2
Secondary gypsum	DC-SG-9a	24.09.2011	137 mg	SO <sub>4</sub> <sup>2-</sup>	BaSO <sub>4</sub>	0.181	49	-10.1	-3.5	-9.7
	DC-SG-9b	24.09.2011	134 mg	SO <sub>4</sub> <sup>2-</sup>	BaSO <sub>4</sub>	0.176	50	-10.2	-1.5	-9.9
	DC-SG-9c	24.09.2011	127 mg	SO <sub>4</sub> <sup>2-</sup>	BaSO <sub>4</sub>	0.166	51	-10.0	-4.9	-9.9
	DC-SG-13a	24.09.2011	100 mg	SO <sub>4</sub> <sup>2-</sup>	BaSO <sub>4</sub>	0.077	52	-9.9	-3.2	-9.6
	DC-SG-13b	24.09.2011	105 mg	SO <sub>4</sub> <sup>2-</sup>	BaSO <sub>4</sub>	0.098	53	-9.6	3.3	-9.2
	DC-SG-13c	27.09.2011	52 mg	SO <sub>4</sub> <sup>2-</sup>	BaSO <sub>4</sub>	0.068	54	-10.9	-0.9	-10.8
	DC-SG-13d	27.09.2011	48 mg	SO <sub>4</sub> <sup>2-</sup>	BaSO <sub>4</sub>	0.064	55	-10.0	-2.7	-9.7
	DC-SG-15	22.09.2011	150 mg	SO <sub>4</sub> <sup>2-</sup>	BaSO <sub>4</sub>	0.198	56	-10.2	1.1	-10.1
	DC-SG-14a	24.09.2011	107 mg	SO <sub>4</sub> <sup>2-</sup>	BaSO <sub>4</sub>	0.137	45	-10.5	-7.0	-
Elemental sulphur	DC-ES-1	24.09.2011	nm	S <sup>0</sup>	S <sup>0</sup>	nm	60	-10.7	-	-10.3
	DC-ES-13a	24.09.2011	nm	S <sup>0</sup>	S <sup>0</sup>	nm	61	-11.3	-	-10.9
	DC-ES-13c	27.09.2011	nm	S <sup>0</sup>	S <sup>0</sup>	nm	-	-	-	-15.2
	DC-ES-13d	27.09.2011	nm	S <sup>0</sup>	S <sup>0</sup>	nm	-	-	-	-10.1
Carbonate rock	DS-PL-1	07.10.2011	25 g	SO <sub>4</sub> <sup>2-</sup>	BaSO <sub>4</sub>	<b>0.0</b>	-	-	-	-
	DC-PL-15	07.10.2011	3 g	SO <sub>4</sub> <sup>2-</sup>	BaSO <sub>4</sub>	0.03	29	-13.7	1.3	-
	DC-PL-16	27.09.2011	2.5 g	SO <sub>4</sub> <sup>2-</sup>	BaSO <sub>4</sub>	0.0075	32	-3.7	1.4	-
Crude oil	DR-O-1	29.09.2011	1.65 g	H <sub>2</sub> S, S-org	BaSO <sub>4</sub>	nm	59	-9.1	-	-

Table A 24: Comparison of sedimentary sulphur yields from X-ray fluorescence spectroscopy (XRF), X-ray diffraction (XRD), Eschka- and sequential extraction.

Method		Unit	Measured (m) / Calculated (c)	DC-S-1	DC-S-9	DC-S-2	DC-S-3	DC-S-5
<b>XRF</b>	Total S	mg/g	m	30.53	6.03	144.20	203.30	73.35
<b>XRD</b>	Total S	mg/g	c	21.26	12.98	231.57	205.26	79.43
	SO <sub>4</sub> -S	mg/g	c	10.93	8.10	0.00	164.76	8.39
	FeS <sub>2</sub> -S $\triangleq$ Ag <sub>2</sub> S-S	mg/g	c	9.62	4.54	11.33	0.00	8.23
	S <sup>0</sup> -S	mg/g	c	0	0	219.40	40.50	62.20
<b>Eschka-Extraction</b>	Sediment weight	g	m	2	2	2	2	2
	BaSO <sub>4</sub>	mg	m	305.60	83.90	601.50	782.30	774.40
	Total S	mg/g	c	20.99	5.76	41.32	53.74	53.20
	$\delta^{34}\text{S}$	‰ vs VCDT	m	-14.27 $\pm$ 0.4	-13.92 $\pm$ 0.4	-8.34 $\pm$ 0.4	-10.17 $\pm$ 0.4	* -7.78
<b>Sequential extraction</b>	Sediment weight	g	m	10	10	10	10	10
	BaSO <sub>4</sub>	BaSO <sub>4</sub> weight	mg	970	160	260	800	703
	S content	mg S/g	c	13.33	2.20	3.57	10.99	9.66
	$\delta^{34}\text{S}$	‰ vs VCDT	m	-11.9 $\pm$ 0.4	-9.28 $\pm$ 0.4	-6.76 $\pm$ 0.4	-10.32 $\pm$ 0.4	4.12 $\pm$ 2.1
	S <sup>0</sup>	S <sup>0</sup> weight	mg	0	0	273	381	274
	S content	S content	c	0	0	27.3	38.1	27.4
	$\delta^{34}\text{S}$	$\delta^{34}\text{S}$	m	nm	nm	-7.51 $\pm$ 0.4	-11.37 $\pm$ 0.4	-9.23 $\pm$ 0.4
	Ag <sub>s</sub> S	Ag <sub>s</sub> S weight	mg	420	92	436	0	888
	S content	S content	c	5.43	1.19	5.64	0	11.49
	$\delta^{34}\text{S}$	$\delta^{34}\text{S}$	m	-22.94 $\pm$ 0.4	-22.9 $\pm$ 2.2	-15.29 $\pm$ 0.4	nm	-11.84 $\pm$ 0.4
	Total S	S content	c	18.76	3.39	36.51	49.09	48.55
	$\delta^{34}\text{S}$ : $\Sigma$ of S <sub>species</sub>	‰ vs VCDT	c	-15.10 $\pm$ 0.3	-14.06 $\pm$ 0.8	-8.64 $\pm$ 0.3	-11.13 $\pm$ 0.3	-7.19 $\pm$ 0.6

Nm= not measured; \* from singular measurement

Table A 25: Calculation of fraction f residual sulphate based on an initial value from a well sample in the Chamchamal region, sampled in the dry season (Al-Manmi 2012).

<b>Sample</b>	<b>SO<sub>4</sub><sup>2-</sup></b>	<b>Fraction f residual sulphate (C/C<sub>0</sub>)</b>
	[mg/L]	
Initial (C <sub>0</sub> )	2002	1.00
DC-W-1	797	0.40
DC-W-3	1783	0.89
DC-W-4	4840	2.42
DC-W-5	863	0.43
DC-W-6	13210	6.60
DC-W-7	828	0.41
DC-W-10	855	0.43
DR-W-1	627	0.31
DR-W-2	264	0.13
DR-W-8	868	0.43
DW-W-1	717	0.36

## 9.2 Appendix B - Figures

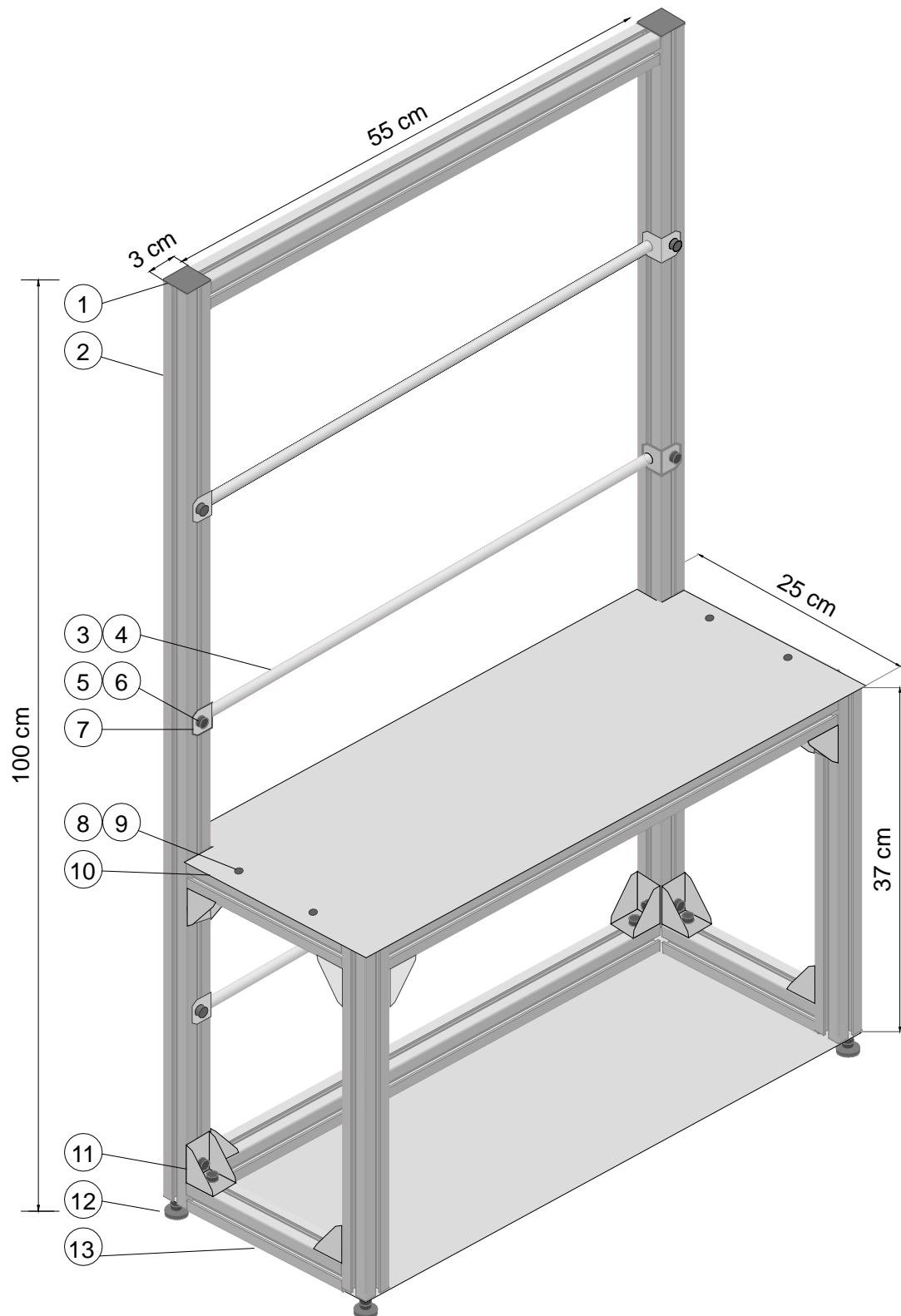


Figure B 1: Work bench design for the distillation unit. The list of materials is given in Table A 8.

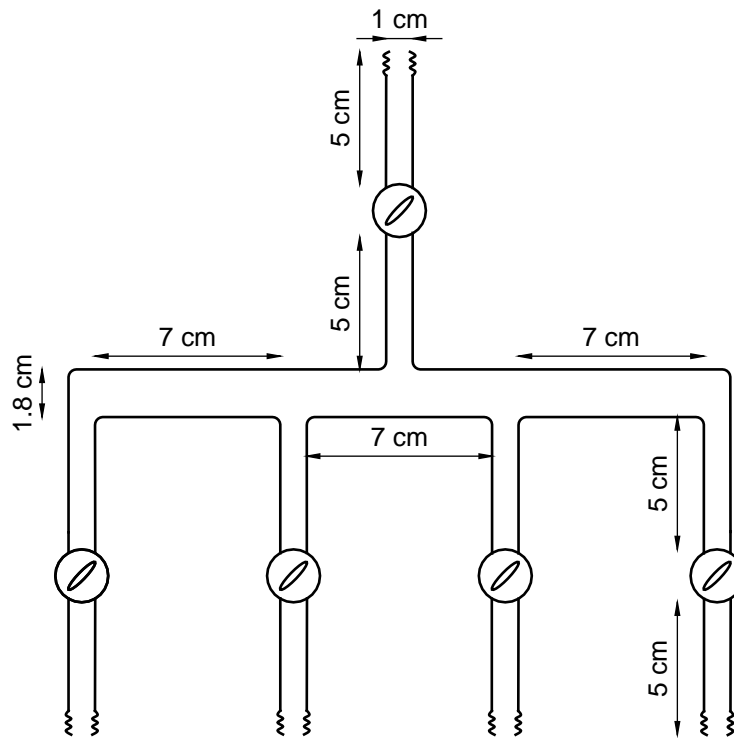


Figure B 2: Nitrogen distribution device of the distillation unit with glass tubes and Teflon valves

### **9.3 Appendix C – Spreadsheet**

- Digital version of the tables in Appendix A
- Distance matrix: 16S rRNA gene sequence similarities between sediment / biofilm extracts and approved sequences from related species